

16977361

EXPERIMENTAL TESTING ON THE COMPRESSIVE STRENGTH OF SOLID STEEL ROUND BARS

BY

**Marwan Saliba, B. Eng
Ryerson University, Toronto, 2002**

**A Thesis
Presented to Ryerson University
In partial fulfillment of the
Requirement for the degree of
Master of Applied Science
In the program of
Civil Engineering
Toronto, Ontario, Canada, 2005
Marwan Saliba 2005©**

**PROPERTY OF
RYERSON UNIVERSITY LIBRARY**

UMI Number: EC53762

INFORMATION TO USERS

The quality of this reproduction is dependent upon the quality of the copy submitted. Broken or indistinct print, colored or poor quality illustrations and photographs, print bleed-through, substandard margins, and improper alignment can adversely affect reproduction.

In the unlikely event that the author did not send a complete manuscript and there are missing pages, these will be noted. Also, if unauthorized copyright material had to be removed, a note will indicate the deletion.



UMI Microform EC53762
Copyright 2009 by ProQuest LLC
All rights reserved. This microform edition is protected against
unauthorized copying under Title 17, United States Code.

ProQuest LLC
789 East Eisenhower Parkway
P.O. Box 1346
Ann Arbor, MI 48106-1346

Author's Declaration

I hereby declare that I am the sole author of this thesis.

I authorize Ryerson to lend this document to other institutions or individuals for the purpose of scholarly research.

Marwan Saliba

I further authorize Ryerson University to reproduce the document by photocopying or by other means, in total or part, at the request of other institutions or individuals for the purpose of scholarly research.

Marwan Saliba

Ryerson University requires the signatures of all persons using or photocopying this thesis.

Please sign below, and give address and date.

[illegible]

ABSTRACT

EXPERIMENTAL TESTING ON THE COMPRESSIVE STRENGTH OF SOLID STEEL ROUND BARS

**MARWAN SALIBA, M.A.SC. THESIS, CIVIL ENGINEERING DEPARTMENT,
RYERSON UNIVERSITY, TORONTO, 2005**

Solid steel round bars are used as legs, diagonals and horizontal members of a communication tower. The Canadian Standards, CAN/CSA-S16.1-94, AISC-LRFD Specifications of 1993, and the European Standard, Eurocode 3, provide the factored compressive resistance of structural steel members other than solid rounds. While, the Current Canadian Standard, CAN/CSA-S37-01 of 2001, for Antenna towers and Antenna Supporting Structures specifies empirical expressions for the compressive strength of solid rounds based on the SSRC column curves for non-solid-round bars and the results from experimental investigation on the compressive resistance of solid rounds carried out back to 1965. This thesis provides a summary of the available literature on the compressive strength of solid rounds as well as the results of recently tested large solid round bars. Correlation between the results from these tests and the current practice for the design of solid rounds is investigated. Recommendations to update the available code equations are drawn.

ACKNOWLEDGEMENTS

I wish to express my deep appreciation to my advisor Dr. K. Sennah at Ryerson University, for his constant support and valuable supervision during the development of this research. Dr. Sennah devoted his time and effort to make this study a success. His most helpful guidance is greatly appreciated.

The author wishes to acknowledge the companies that donated the steel material and provided financial support to this research work. These companies are Radian Communication Systems Corp. of Oakville, Ontario, Sabre Communications Corp. of Sioux City, IA, U.S.A., and ERI, Electronics Research Inc. of Chandler, Indiana, U.S.A. The author also acknowledges the financial support of the Structural Steel Education Foundation of the Canadian Institute of Steel Construction.

The author wishes to thank N. Jaalouk for his assistance in the experimental work. The author is also very grateful to his parents and brothers for their great support and encouragement during the course of this study.

TO MY FAMILY

TABLE OF CONTENTS

ABSTRACT.....	iv
ACKNOWLEDGEMENTS.....	v
TABLE OF CONTENTS	vii
NOTATIONS.....	ix
LIST OF TABLE	xi
LIST OF FIGURES	xii
INTRODUCTION.....	1
1.1 General.....	1
1.2 Need for Investigation.....	3
1.3 Objectives of the Thesis.....	4
1.4 Outline of the Thesis.....	4
LITERATURE REVIEW	5
2.1 General.....	5
2.2 Critical-load Theory.....	5
2.3 Inelastic Buckling of Column.....	6
2.4 Imperfect Column.....	8
2.5 Compressive Resistance of Steel Columns.....	8
2.5.1 Influence of Residual Stresses.....	10
2.5.2 Influence of Out-of-Straightness.....	12
2.5.3 Effect of Cold-Straightening.....	13
2.6 Structural Stability Research Council (SSRC) Column Strength Curves..	15
2.7 Canadian Standards.....	17
2.8 AISC (LRFD) Specifications.....	18
2.9 European Standard.....	19

EXPERIMENTAL STUDY	23
3.1 General.....	23
3.2 Description of the Test Specimens.....	23
3.2.1 Testing Centrally Loaded Columns made of Stress-Relieved Steel.....	23
3.2.2 Testing Centrally Loaded Columns made of Non-Stress-Relieved Steel.....	23
3.2.3 Stub Column Test.....	24
3.3 Test Set-Up.....	25
3.4 Instrumentations.....	26
3.4.1 Strain Gauges.....	26
3.4.2 Mechanical Dial Gauges.....	27
3.4.3 Automatic Strain Indicator.....	27
3.5 Test Procedure.....	27
3.6 Material Property.....	28
3.7 Determination of Yield Strength from Tension Coupons.....	28
ANALYSIS AND DISCUSSION OF RESULTS	33
4.1 General.....	33
4.2 Results from Tension Coupon	34
4.3 Results from Testing Centrally Loaded Columns Made of Stress-Relieved Steel	35
4.4 Correlation between the Experimental Failure Load of Stress-Relieved Steel Bars and the Compressive Resistance as Obtained from Design Standards.....	37
4.5 Results from Testing Centrally Loaded Columns Made of Non-Stress-Relieved Steel.....	39
4.6 Correlation between the Experimental Failure Load of Non-Stress-Relieved Steel Bars and the Compressive Resistance as Obtained from Design Standards.....	41
4.7 Results from Testing Stub Columns.....	43
CONCLUSIONS AND RECOMMENDATIONS	45
5.1 General.....	45
5.2 Conclusions.....	46
5.3 Recommendations for Future Research.....	47
REFERENCES.....	48

NOTATIONS

A	Cross-sectional area of member
C_r	Compressive resistance of a member
E	Modulus of elasticity
E_{eff}	Effective modulus
EI	Elastic stiffness
E_r	Reduced modulus
E_t	Tangent modulus
F_y	Yield stress
\overline{F}_y	Average value of equivalent yield strengths
I	Moment of inertia of a section
K	Effective buckling length factor, or Characteristic value of a parameter
K_s	Coefficient of variation modification factor for steel
L	Unbraced length of the solid round bar
N	Design value of axial compressive force
P	Column axial load
P_E	Euler buckling load
P_r	Reduced modulus load
P_t	Tangent modulus load
r	Governing radius of gyration about the plane of buckling
v	Column displacement
V_s	Coefficient of variation of equivalent yield strengths
w	Column displacement

y_0	Initial out-of-straightness
σ	Compressive strength, or Standard deviation
λ	Non-dimensional slenderness parameter
$\bar{\lambda}_M$	Non-dimensional slenderness in bending
ϕ	Resistance factor for compression
δ	Total deflection at mid height of solid round bar
ϑ	Rotation
ε	Strain
Δ	Displacement
α	Imperfection factor
χ	Reduction factor according to the standard and buckling curves as used in Europe

LIST OF TABLE

<u>Table</u>	<u>Pages</u>
Table 2.1 Ultimate limit state analysis.....	52
Table 2.2 Parameters α for calculation of reduction factor x	52
Table 3.1 Details of Test Specimens: 20 Stress Relieved Specimens.....	52
Table 3.2 Details of Test Specimens: 25 Non-Stress Relieved Specimens.....	53
Table 3.3 Details of Test Specimens: 8 Non-Stress Relieved Specimens.....	53
Table 3.4 Details of Test Specimens: 7 Stub Columns for Non-Stress Relieved Specimens.....	54
Table 3.5 Coefficient of Variation Modification Factor for Steel, K_s	54
Table 4.1 Results of coupon testing for stress-relieved bars.....	55
Table 4.2 Results of coupon testing for non-stress-relieved bars.....	55
Table 4.3 Results of testing to-collapse 20 stress-relieved steel solid rounds.....	56
Table 4.4 Comparison between the experimental finding and available Code equations For 20 stress-relieved steel bars using theoretical buckling length.....	57
Table 4.5 Comparison between the experimental finding and available Code equations For 20 stress-relieved steel bars using the practical buckling length.....	58
Table 4.6 Results of testing to-collapse 25 non-stress-relieved steel solid rounds.....	59
Table 4.7 Comparison between the experimental finding and available Code equations For 25 non-stress-relieved steel bars using theoretical buckling length.....	60
Table 4.8 Comparison between the experimental finding and available Code equations For 25 non-stress-relieved steel bars using practical buckling length.....	61
Table 4.9 Results of testing to-collapse 8 non-stress-relieved steel solid rounds.....	62
Table 4.10 Comparison between the experimental finding and available Code Equations for 8 non-stress-relieved steel bars using the theoretical buckling length.....	63
Table 4.11 Comparison between the experimental finding and available Code Equations for 8 non-stress-relieved steel bars using practical buckling Length.....	64
Table 4.12 Stub column test results for non-stress-relieved steel solid rounds.....	64

LIST OF FIGURES

<u>Figure</u>	<u>Page</u>
Figure 1.1 Views of communication towers.....	65
Figure 1.2 Close-up view of tower segment.....	66
Figure 2.1 Behavior of perfect and imperfect columns (Galambos, 1998).....	66
Figure 2.2 General stress-strain relationship (Galambos, 1998).....	67
Figure 2.3 Column curve.....	67
Figure 2.4 Initially bent column.....	68
Figure 2.5 Effective length factor (CAN/CSA S16-01, 2003).....	69
Figure 2.6 SSRC column strength curve 1 for structural steel (Bjordhovde, 1972), (Based on maximum strength and initial out-of-straightness of L/1000).....	70
Figure 2.7 SSRC column strength curve 2 for structural steel (Bjordhovde, 1972), (Based on maximum strength and initial out-of-straightness of L/1000).....	70
Figure 2.8 SSRC column strength curve 3 for structural steel (Bjordhovde, 1972), (Based on maximum strength and initial out-of-straightness of L/500).....	71
Figure 2.9 Buckling curves (Eurocode 3, 2003).....	71
Figure 3.1 View of the MTS machine.....	72
Figure 3.2 Schematic diagram of the specimen setup and strain gauge locations.....	73
Figure 3.3 Test set-ups for axial resistance of solid rounds.....	74
Figure 3.4 Test set up for tension coupon before and after failure.....	74
Figure 4.1 Views of coupon sample preparation procedure.....	75
Figure 4.2 Stress-strain curve for the coupon sample of SR 38-mm bar.....	76
Figure 4.3 Initial part of the stress-strain curve for the coupon sample of SR 51-mm bar.....	76
Figure 4.4 Stress-strain curve for the coupon sample of SR 64-mm bar.....	77
Figure 4.5 Stress-strain curve for the coupon sample of SR 76-mm bar.....	77
Figure 4.6 Stress-strain curve for the coupon sample of SR 89-mm bar.....	78
Figure 4.7 Stress-strain curve for the coupon sample of SR 102-mm bar.....	78
Figure 4.8 Stress-strain curve for the coupon sample of SR 128-mm bar.....	79
Figure 4.9 Views of the coupon sample for 38-mm bar before and after testing.....	79
Figure 4.10 Initial portion of the stress-strain curve for the coupon sample of NSR 38-mm bar.....	80
Figure 4.11 Views of the coupon sample for 51-mm bar before and after testing.....	80
Figure 4.12 Initial part of the stress-strain curve for the coupon sample of NSR 51-mm bar.....	81
Figure 4.13 Views of the coupon sample for 64-mm bar before and after testing.....	81
Figure 4.14 Initial part of the stress-strain curve for the coupon sample of NSR 64-mm bar.....	82
Figure 4.15 Views of the coupon sample for 76-mm bar before and after testing.....	82
Figure 4.16 Initial portion of the stress-strain curve for the coupon sample of NSR 76-mm bar.....	83
Figure 4.17 Views of the coupon sample for 89-mm bar before and after testing.....	83
Figure 4.18 Initial part of the stress-strain curve for the coupon sample of NSR 89-mm bar.....	84

Figure 4.19 Views of the coupon sample for 102-mm bar before and after testing.....	84
Figure 4.20 Initial portion of the stress-strain curve for the coupon sample of NSR 102-mm bar.....	85
Figure 4.21 Views of the coupon sample for 114-mm bar before and after testing.....	85
Figure 4.22 Initial part of the stress-strain curve for the coupon sample of NSR 114-mm bar.....	86
Figure 4.23 Views of specimen SR-1 before and after testing.....	87
Figure 4.24 Axial load-strain relationships for specimen SR-1.....	87
Figure 4.25 Load-lateral deflection curves for specimen SR-1.....	88
Figure 4.26 Views of specimen SR-2 before and after testing.....	88
Figure 4.27 Axial load-strain relationships for specimen SR-2.....	89
Figure 4.28 Load-lateral deflection curves for specimen SR-2.....	89
Figure 4.29 Load versus overall shortening curve for specimen SR-2.....	90
Figure 4.30 Views of specimen SR-3 before and after testing.....	90
Figure 4.31 Axial load-strain relationships for specimen SR-3.....	91
Figure 4.32 Load-lateral deflection curves for specimen SR-3.....	91
Figure 4.33 Load versus overall shortening curve for specimen SR-3.....	92
Figure 4.34 Views of specimen SR-4 before and after testing.....	92
Figure 4.35 Axial load-strain relationships for specimen SR-4.....	93
Figure 4.36 Load-lateral deflection curves for specimen SR-4.....	93
Figure 4.37 Load versus overall shortening curve for specimen SR-4.....	94
Figure 4.38 Views of specimen SR-5 before and after testing.....	94
Figure 4.39 Axial load-strain relationships for specimen SR-5.....	95
Figure 4.40 Load-lateral deflection curves for specimen SR-5.....	95
Figure 4.41 Load versus overall shortening curve for specimen SR-5.....	96
Figure 4.42 Views of specimen SR-6 before and after testing.....	96
Figure 4.43 Axial load-strain relationships for specimen SR-6.....	97
Figure 4.44 Load-lateral deflection curves for specimen SR-6.....	97
Figure 4.45 Load versus overall shortening curve for specimen SR-6.....	98
Figure 4.46 Views of specimen SR-7 before and after testing.....	98
Figure 4.47 Axial load-strain relationships for specimen SR-7.....	99
Figure 4.48 Load-lateral deflection curves for specimen SR-7.....	99
Figure 4.48 Load versus overall shortening curve for specimen SR-7.....	100
Figure 4.49 Views of specimen SR-8 before and after testing.....	100
Figure 4.50 Axial load-strain relationships for specimen SR-8.....	101
Figure 4.51 Load-lateral deflection curves for specimen SR-8.....	101
Figure 4.52 Load versus overall shortening curve for specimen SR-8.....	102
Figure 4.53 Views of specimen SR-9 before and after testing.....	102
Figure 4.54 Axial load-strain relationships for specimen SR-9.....	103
Figure 4.55 Load versus overall shortening curve for specimen SR-9.....	103
Figure 4.56 Views of specimen SR-10 before and after testing.....	104
Figure 4.57 Axial load-strain relationships for specimen SR-10.....	104
Figure 4.58 Load-lateral deflection curves for specimen SR-10.....	105
Figure 4.59 Load versus overall shortening curve for specimen SR-10.....	105
Figure 4.60 Views of specimen SR-11 before and after testing.....	106
Figure 4.61 Axial load-strain relationships for specimen SR-11.....	106

Figure 4.62 Load-lateral deflection curves for specimen SR-11.....	107
Figure 4.63 Load versus overall shortening curve for specimen SR-11.....	107
Figure 4.64 Views of specimen SR-12 before and after testing.....	108
Figure 4.65 Axial load-strain relationships for specimen SR-12.....	108
Figure 4.66 Load-lateral deflection curves for specimen SR-12.....	109
Figure 4.67 Load versus overall shortening curve for specimen SR-12.....	109
Figure 4.68 Views of specimen SR-13 before and after testing.....	110
Figure 4.69 Axial load-strain relationships for specimen SR-13.....	110
Figure 4.70 Load-lateral deflection curves for specimen SR-13.....	111
Figure 4.71 Load versus overall shortening curve for specimen SR-13.....	111
Figure 4.72 Views of specimen SR-14 before and after testing.....	112
Figure 4.73 Axial load-strain relationships for specimen SR-14.....	112
Figure 4.74 Load-lateral deflection curves for specimen SR-14.....	113
Figure 4.75 Load versus overall shortening curve for specimen SR-14.....	113
Figure 4.76 Views of specimen SR-15 before and after testing.....	114
Figure 4.77 Axial load-strain relationships for specimen SR-15.....	114
Figure 4.78 Load-lateral deflection curves for specimen SR-15.....	115
Figure 4.79 Load versus overall shortening curve for specimen SR-15.....	115
Figure 4.80 Views of specimen SR-16 before and after testing.....	116
Figure 4.81 Axial load-strain relationships for specimen SR-16.....	116
Figure 4.82 Load-lateral deflection curves for specimen SR-16.....	117
Figure 4.83 Load versus overall shortening curve for specimen SR-16.....	117
Figure 4.84 Views of specimen SR-17 before and after testing.....	118
Figure 4.85 Axial load-strain relationships for specimen SR-17.....	118
Figure 4.86 Load-lateral deflection curves for specimen SR-17.....	119
Figure 4.87 Load versus overall shortening curve for specimen SR-17.....	119
Figure 4.88 Views of specimen SR-18 before and after testing.....	120
Figure 4.89 Axial load-strain relationships for specimen SR-18.....	120
Figure 4.90 Load-lateral deflection curves for specimen SR-18.....	121
Figure 4.91 Load versus overall shortening curve for specimen SR-18.....	121
Figure 4.92 Views of specimen SR-19 before and after testing.....	122
Figure 4.93 Axial load-strain relationship for specimen SR-19.....	122
Figure 4.94 Load-lateral deflection curves for specimen SR-19.....	123
Figure 4.95 Load versus overall shortening curve for specimen SR-19.....	123
Figure 4.96 Views of specimen SR-20 before and after testing.....	124
Figure 4.97 Axial load-strain relationships for specimen SR-20.....	124
Figure 4.98 Load versus overall shortening curve for specimen SR-20.....	125
Figure 4.99 Load versus overall shortening curve for specimen SR-20.....	125
Figure 4.100 Views of specimen NSR-1 before and after testing.....	126
Figure 4.101 Views of specimen NSR-2 before and after testing.....	126
Figure 4.102 Axial load-strain relationships for specimen NSR-2.....	127
Figure 4.103 Load-lateral deflection curves for specimen NSR-2.....	127
Figure 4.104 Load versus overall shortening curve for specimen NSR-2.....	128
Figure 4.105 Views of specimen NSR-3 before and after testing.....	128
Figure 4.106 Axial load-strain relationships for specimen NSR-3.....	129
Figure 4.107 Load-lateral deflection curves for specimen NSR-3.....	129

Figure 4.108 Load versus overall shortening curve for specimen NSR-3.....	130
Figure 4.109 Views of specimen NSR-4 before and after testing.....	130
Figure 4.110 Axial load-strain relationships for specimen NSR-4.....	131
Figure 4.111 Load-lateral deflection curves for specimen NSR-4.....	131
Figure 4.112 Load versus overall shortening curve for specimen NSR-4.....	132
Figure 4.113 Views of specimen NSR-5 before and after testing.....	132
Figure 4.114 Axial load-strain relationships for specimen NSR-5.....	133
Figure 4.115 Load-lateral deflection curves for specimen NSR-5.....	133
Figure 4.116 Load versus overall shortening curve for specimen NSR-5.....	134
Figure 4.117 Views of specimen NSR-6 before and after testing.....	134
Figure 4.118 Axial load-strain relationships for specimen NSR-6.....	135
Figure 4.119 Load-lateral deflection curves for specimen NSR-6.....	135
Figure 4.120 Load versus overall shortening curve for specimen NSR-6.....	136
Figure 4.121 Views of specimen NSR-7 before and after testing.....	136
Figure 4.122 Axial load-strain relationships for specimen NSR-7.....	137
Figure 4.123 Load-lateral deflection curves for specimen NSR-7.....	137
Figure 4.124 Load versus overall shortening curve for specimen NSR-7.....	138
Figure 4.125 Views of specimen NSR-8 before and after testing.....	138
Figure 4.126 Axial load-strain relationships for specimen NSR-8.....	139
Figure 4.127 Load-lateral deflection curves for specimen NSR-8.....	139
Figure 4.128 Load versus overall shortening curve for specimen NSR-8.....	140
Figure 4.129 Views of specimen NSR-9 before and after testing.....	140
Figure 4.130 Axial load-strain relationships for specimen NSR-9.....	141
Figure 4.131 Load-lateral deflection curves for specimen NSR-9.....	141
Figure 4.132 Load versus overall shortening curve for specimen NSR-9.....	142
Figure 4.133 Views of specimen NSR-10 before and after testing.....	142
Figure 4.134 Axial load-strain relationships for specimen NSR-10.....	143
Figure 4.135 Load-lateral deflection curves for specimen NSR-10.....	143
Figure 4.136 Load versus overall shortening curve for specimen NSR-10.....	144
Figure 4.137 Views of specimen NSR-11 before and after testing.....	144
Figure 4.138 Axial load-strain relationships for specimen NSR-11.....	145
Figure 4.139 Load versus overall shortening curve for specimen NSR-11.....	145
Figure 4.140 Views of specimen NSR-12 before and after testing.....	146
Figure 4.141 Axial load-strain relationships for specimen NSR-12.....	146
Figure 4.142 Load-lateral deflection curves for specimen NSR-12.....	147
Figure 4.143 Load versus overall shortening curve for specimen NSR-12.....	147
Figure 4.144 Views of specimen NSR-13 before and after testing.....	148
Figure 4.145 Axial load-strain relationships for specimen NSR-13.....	148
Figure 4.146 Load-lateral deflection curves for specimen NSR-13.....	149
Figure 4.147 Load versus overall shortening curve for specimen NSR-13.....	149
Figure 4.148 Views of specimen NSR-14 before and after testing.....	150
Figure 4.149 Axial load-strain relationships for specimen NSR-14.....	150
Figure 4.150 Load-lateral deflection curves for specimen NSR-14.....	151
Figure 4.151 Load versus overall shortening curve for specimen NSR-14.....	151
Figure 4.152 Views of specimen NSR-15 before and after testing.....	152
Figure 4.153 Axial load-strain relationships for specimen NSR-15.....	152

Figure 4.154 Load-lateral deflection curves for specimen NSR-15.....	153
Figure 4.155 Load versus overall shortening curve for specimen NSR-15.....	153
Figure 4.156 Views of specimen NSR-16 before and after testing.....	154
Figure 4.157 Axial load-strain relationships for specimen NSR-16.....	154
Figure 4.158 Load-lateral deflection curves for specimen NSR-16.....	155
Figure 4.159 Load versus overall shortening curve for specimen NSR-16.....	155
Figure 4.160 Views of specimen NSR-17 before and after testing.....	156
Figure 4.161 Axial load-strain relationships for specimen NSR-17.....	156
Figure 4.162 Load-lateral deflection curves for specimen NSR-17.....	157
Figure 4.163 Load versus overall shortening curve for specimen NSR-17.....	157
Figure 4.164 Views of specimen NSR-18 before and after testing.....	158
Figure 4.165 Axial load-strain relationships for specimen NSR-18.....	158
Figure 4.166 Load-lateral deflection curves for specimen NSR-18.....	159
Figure 4.167 Load versus overall shortening curve for specimen NSR-18.....	159
Figure 4.168 Views of specimen NSR-19 before and after testing.....	160
Figure 4.169 Axial load-strain relationships for specimen NSR-19.....	160
Figure 4.170 Load-lateral deflection curves for specimen NSR-19.....	161
Figure 4.171 Load versus overall shortening curve for specimen NSR-19.....	161
Figure 4.172 Views of specimen NSR-20 before and after testing.....	162
Figure 4.173 Axial load-strain relationships for specimen NSR-20.....	162
Figure 4.174 Load versus overall shortening curve for specimen NSR-20.....	163
Figure 4.175 Load versus overall shortening curve for specimen NSR-20.....	163
Figure 4.176 Views of specimen NSR-21 before and after testing.....	164
Figure 4.177 Axial load-strain relationships for specimen NSR-21.....	164
Figure 4.178 Load-lateral deflection curves for specimen NSR-21.....	165
Figure 4.179 Load versus overall shortening curve for specimen NSR-21.....	165
Figure 4.180 Views of specimen NSR-22 before and after testing.....	166
Figure 4.181 Axial load-strain relationships for specimen NSR-22.....	166
Figure 4.182 Load-lateral deflection curves for specimen NSR-22.....	167
Figure 4.183 Load versus overall shortening curve for specimen NSR-22.....	167
Figure 4.184 Views of specimen NSR-23 before and after testing.....	168
Figure 4.185 Axial load-strain relationships for specimen NSR-23.....	168
Figure 4.186 Load-lateral deflection curves for specimen NSR-23.....	169
Figure 4.187 Load versus overall shortening curve for specimen NSR-23.....	169
Figure 4.188 Views of specimen NSR-24 before and after testing.....	170
Figure 4.189 Axial load-strain relationships for specimen NSR-24.....	170
Figure 4.190 Load-lateral deflection curves for specimen NSR-24.....	171
Figure 4.191 Load versus overall shortening curve for specimen NSR-24.....	171
Figure 4.192 Views of specimen NSR-25 before and after testing.....	172
Figure 4.193 Axial load-strain relationships for specimen NSR-25.....	172
Figure 4.194 Load-lateral deflection curves for specimen NSR-25.....	173
Figure 4.195 Load versus overall shortening curve for specimen NSR-25.....	173
Figure 4.196 Views of the NSR tested specimens.....	174
Figure 4.197 Views of specimen NSR-26 before and after testing.....	174
Figure 4.198 Axial load-strain relationships for specimen NSR-26.....	175
Figure 4.199 Views of specimen NSR-27 before and after testing.....	175

Figure 4.200 Axial load-strain relationships for specimen NSR-27.....	176
Figure 4.201 Load versus overall shortening curve for specimen NSR-27.....	176
Figure 4.202 Views of specimen NSR-28 before and after testing.....	177
Figure 4.203 Axial load-strain relationships for specimen NSR-28.....	177
Figure 4.204 Load versus overall shortening curve for specimen NSR-28.....	178
Figure 4.205 Views of specimen NSR-29 before and after testing.....	178
Figure 4.206 Axial load-strain relationships for specimen NSR-29.....	179
Figure 4.207 Load versus overall shortening curve for specimen NSR-29.....	179
Figure 4.208 Views of specimen NSR-30 before and after testing.....	180
Figure 4.209 Axial load-strain relationships for specimen NSR-30.....	180
Figure 4.210 Load versus overall shortening curve for specimen NSR-30.....	181
Figure 4.211 Views of specimen NSR-31 before and after testing.....	181
Figure 4.212 Axial load-strain relationships for specimen NSR-31.....	182
Figure 4.213 Load versus overall shortening curve for specimen NSR-31.....	182
Figure 4.214 Views of specimen NSR-32 before and after testing.....	183
Figure 4.215 Axial load-strain relationships for specimen NSR-32.....	183
Figure 4.216 Load versus overall shortening curve for NSR-32.....	184
Figure 4.217 Views of specimen NSR-33 before and after testing.....	184
Figure 4.218 Axial load-strain relationships for specimen NSR-33.....	185
Figure 4.219 Load versus overall shortening for specimen NSR-33.....	185
Figure 4.220 Views of specimen SC-1 before and after testing.....	186
Figure 4.221 Axial load-strain relationships for specimen SC-1.....	186
Figure 4.222 Load versus overall shortening curve for specimen SC-1.....	187
Figure 4.223 Views of specimen SC-2 before and after testing.....	187
Figure 4.224 Axial load-strain relationships for specimen SC-2.....	188
Figure 4.225 Load versus overall shortening curve for specimen SC-2.....	188
Figure 4.226 Views of specimen SC-3 before and after testing.....	189
Figure 4.227 Axial load-strain relationships for specimen SC-3.....	189
Figure 4.228 Load versus overall shortening curve for specimen SC-3.....	190
Figure 4.229 Views of specimen SC-4 before and after testing.....	190
Figure 4.230 Axial load-strain relationships for specimen SC-4.....	191
Figure 4.231 Load versus overall shortening curve for specimen SC-4.....	191
Figure 4.232 Views of specimen SC-5 before and after testing.....	192
Figure 4.233 Axial load-strain relationships for specimen SC-5.....	192
Figure 4.234 Load versus overall shortening curve for specimen SC-5.....	193
Figure 4.235 Views of specimen SC-6 before and after testing.....	193
Figure 4.236 Axial load-strain relationships for specimen SC-6.....	194
Figure 4.237 Load versus overall shortening curve for specimen SC-6.....	194
Figure 4.238 Views of specimen SC-7 before and after testing.....	195
Figure 4.239 Axial load-strain relationships for specimen SC-7.....	195
Figure 4.240 Load versus overall shortening curve for specimen SC-7.....	196

CHAPTER I

INTRODUCTION

1.1 General

In the information industry, satellites, antenna towers and cables are used to transmit the signal from communication tools. Some of these communication tools are mobile phones and pagers. Antenna towers are the best choice because they are relatively economical and effective for remote transmission, especially in North America where land area is large and distances among the cities and towns are great. Antenna tower transmission of signals is the best medium, which is widely used not only in Canada but also in USA and Europe. These kinds of steel towers have their own characteristic. They are tall and slender. They can be classified into three types as shown in Figure 1.1, namely: (a) monopoles with heights up to 70 m; (b) self-supporting towers with heights up to 120 m; and (c) guyed towers with heights up to 620 m. The environmental factors like the land-use classification of the property and whether the surrounding area is residential, industrial or agricultural play an essential part in determining the height of the tower. The telecommunication towers used in Canada are either square based self-supporting towers or triangular towers supported by guy cables, depending upon various factors, such as the space available at the site for its installation and the height of the tower. The most popular cross-section of the tower is the triangular shape. Legs, diagonals and horizontals are made of solid round steel bars with varying diameters and with all the joints welded or bolted. View of tower segment is shown in Figure 1.2. Solid round steel bars are widely used in the industry as compression members. For example, with increasing needs in information industry for transmitting communication signals, antenna towers made of solid round steel bars are frequently used

around the world for their economy and effectiveness. It should be noted, however, that the residual stresses in the material, which may occur during rolling, heat treatment, rotary straightening or other processes, may have significant influence on the behaviour of the these members.

The towers are subjected to self-weight, snow, wind loads and also earthquake loads in seismic areas. Although the behaviour of the entire tower is rather complicated when subjected to these loads, the resultant forces in the members are mainly axial tension or compression. Hence, the behaviour of the tower members under axial forces is the most important consideration in the tower design. For this reason, the properties of the members with the residual stresses must be studied in order to obtain an optimized design while satisfying the safety requirements. Design loads during fabrication, erection and service can be classified as two categories, vertical loads and transverse loads. Leg members (chords) bear vertical loads and bending moments caused by transverse loads. But most of the shear force is borne by cross-brace diagonals, one in compression and the other in tension. In designing these members, not only the strength and stiffness but also the stability problems should be considered. The advancement of knowledge and technology has always resulted in an improvement in the specifications and the underlying philosophy through which various structures are designed. Since antenna towers are made of steel, the progress in the specifications concerning the design of steel structures generally, and the antenna towers specially, should be studied.

1.2 Need for Investigation

The behavior of members in tension is very simple compared with that of those in compression. The mostly used philosophy for steel tower design at the present time is based on the ultimate strength of the members. There are many factors affecting the behavior of compression members, for example, the properties of steel, the slenderness of the member, the end constraints, cross-section of the member, initial out-of-straightness of the column, etc. The effect of end restraints, an important consideration in column stability analysis, is generally represented by the effective length factor. Residual stress is another factor influencing the compression behavior of the steel members and a lot of work on this topic has been done. But unfortunately, most of the work was on wide-flange shapes. Few research results are available on solid round steel. For members in compression, because of the existence of residual stresses, early localized yielding occurs at some part of the cross section when the loading increases and the ultimate strength is appreciably reduced. Also, the fatigue life will be shortened due to the residual stresses when the tower is subjected to dynamic loads such as wind load. The superseded Canadian Standards of 1994, CAN/CSA-S16.1-94, AISC-LRFD Specifications of 1993, and the European Standard, Eurocode 3, provide the factored compressive resistance of structural steel members other than solid rounds. While, the Current Canadian Standard, CAN/CSA-S37-01 of 2001, for Antenna towers and Antenna Supporting Structures specifies empirical expressions for the compressive strength of solid rounds based on the well-known Structural Stability Research Council (SSRC) column curves for non-solid-round members as well as the results from experimental investigation on the compressive resistance of solid rounds carried out back to 1965. As a result, there is an urgent need for

experimental data on the load carrying capacity of solid rounds made of stress-relieved or non-stress-relieved steel so that the code equation can be easily updated. This will reflect on considerable savings to owners of communication towers and other structures that use solid rounds as primary members.

1.3 Objectives of the study

The objectives of the study are:

- i) To experimentally determine the compressive resistance of solid round steel members made of stress-relieved or non-stress-relieved steel.
- ii) To compare the experimental failure loads with the compressive resistance of solid rounds obtained from the available codes and specifications.
- iii) To recommend modification factors to the available code equations for the compressive resistance of solid rounds based on the experimental results obtained in this thesis.

1.4 Outline of the Thesis

The thesis begins with an introduction to communication towers, followed by the need and objectives of the present investigation. The relevant literature is reviewed in Chapter 2. In chapter 3, details of experimental test set-up, geometric properties of the tested solid round steel members, support assembly and loading conditions are presented. Experimental results are presented and analyzed in Chapter 4. Finally, the conclusions and recommendations for further study are presented in Chapter 5.

CHAPTER II

LITERATURE REVIEW

2.1 General

This chapter summarizes the literature pertained to the compressive strength of axially loaded steel members with emphasis on solid steel rounds. The literature review includes the critical-load theory, inelastic buckling of columns, imperfect column, compressive resistance of columns, influence of residual stresses, influence of out-of-straightness, effect of cold-straightening, American specification, Canadian Standard, and European Code pertained to compressive resistance of columns

2.2 Critical-Load Theory

The strength of a perfectly straight prismatic column with perfect central loading and well-defined end restraints is the Euler load, P_E , as long as the material is still elastic when buckling occurs (Galambos, 1998):

$$P_E = \frac{\pi^2 EI}{(KL)^2} \quad (2-1)$$

where,

EI is the elastic stiffness,

L is the length of the column

K is the effective length factor (1.0 for perfectly frictionless pins).

When the axial load attains P_E , a stable equilibrium configuration is possible even in the presence of lateral deflection (Figure 2.1a), while the load remains essentially constant (Figure 2.1b, path OAB). Even if an initial deflection, and/or an initial load eccentricity is present, the maximum load will approach the Euler load asymptotically as long as the material remains elastic (curve C in Figure 2.1b)

2.3 Inelastic Buckling of Column

Many practical columns are in a range of slenderness where at buckling portions of the columns are no longer elastic. The stiffness of the column is reduced by yielding, which may be a result of the nonlinearity in the material itself or it may be due to partial yielding of the cross section at points of compressive residual stress. The post-buckling behaviour of such a column is radically different from the elastic column. Bifurcation buckling occurs at the tangent modulus load, point D in Figure 2.1 (c) (Galambos 1998):

$$P_t = \frac{\pi^2 E_t I}{(KL)^2} \quad (2-2)$$

where, E_t is the tangent modulus. The tangent modulus E_t is the slope of the stress-strain curve at a load level (Figure 2-2) when the material is non-linear.

Further lateral deflection is possible only if the load increases. If there were no further changes in stiffness due to yielding, the load would asymptotically approach the reduced modulus load as the deflection becomes large, (Point E in Figure 2-1c)(Galambos 1998):

$$P_r = \frac{\pi^2 E_r I}{(KL)^2} \quad (2-3)$$

where, E_r is the reduced modulus.

In presence of residual stress, E_r and E_t depend on the shape of the cross-section. Since increased loading beyond the tangent modulus load results in further yielding, stiffness continues to be reduced and the load-deflection curve achieves a peak, (P_{max}) point F in Figure 2-1(c) beyond which it falls off. Thus, a perfect inelastic column will begin to deflect laterally when $P = P_t$ and $P_t < P_{max} < P_r$ (Galambos 1998).

In linear analysis of columns, it is assumed that the material behaves according to Hooke's law and the stresses in the member must remain below the proportional limit of the material for this postulation to be valid. From Figure 2-3 it can be seen that for slender columns, the applied load reaches Euler's load before the axial stress exceeds the proportional limit. The Euler load represents the correct buckling load of such members and the linear elastic analysis is therefore valid for slender columns. For stocky columns, the axial stress will exceed the proportional limit of the material before the applied load reaches the Euler load. Therefore, the results of the elastic analysis are not valid for stocky columns, and the buckling load of stocky columns must be determined by taking inelastic behaviour into account. This type of buckling is known as inelastic buckling. For columns that buckle inelastically, some of the fibres in the cross-section have been yielded before buckling occurs. Consequently, only the fibres that remain elastic are effective in resisting the additional applied force. Since only a small portion of the cross-section is effective in resisting the axial force at buckling, the elastic modulus E is replaced by an effective modulus, E_{eff} , to describe the behaviour of the inelastic column.

2.4 Imperfect Column

In Euler theory, the member is assumed to be perfectly straight and the loading is assumed to be concentric at every cross-section of the member. However, in actual structures, perfect members do not exist; minor imperfections of shape and small eccentricities of loading are present. For studying the behavior of an imperfect column, consider a member whose centroidal axis is initially bent and assume that the material obeys Hooke's law and that the deformations are small.

The initial deflection is assumed to be of the form (Figure 2.4):

$$y_o = a \sin\left(\frac{\pi x}{L}\right) \quad (2-4)$$

Due to the axially applied load P , the resulting bending moment in the column is given by

$$M = P (y_o + y) \quad (2-5)$$

And the total deflection at mid-height is given by

$$\delta = \frac{a}{1 - (P / P_E)} \quad (2-6)$$

Where, y_o is the initial out-of-straightness of the column, L is the column length, y is the lateral deflection at distance x from the column end.

2.5 Compressive Resistance of Steel Columns

Steel columns are conventionally classified as short, intermediate, or long members, and each category has an associated characteristic type of behavior. A short column is one, which can resist a load equal to the yield load. A long column fails by elastic buckling on which the maximum load depends only on the bending stiffness (EI)

and length of the member. Columns in the intermediate range are most common in steel structures (Figure 2.3). Failure is characterized by inelastic buckling and is greatly influenced by the magnitude and pattern of residual stresses that are present and the magnitude, shape of the initial imperfections or out-of-straightness and the end restraint.

These effects lessen for both shorter and longer columns. To take into account these effects, a computerized maximum strength analysis was performed (Bjorhovde 1972) first on basic data available from carefully constructed column tests performed at Lehigh University on W-shaped and hollow column sections. Next, a set of 112 column curves was generated for members from whom measured residual-stress distributions were available, assuming an initial crookedness of 1/1000 of the column length and zero end restraint. Bjorhovde grouped the whole spectrum of column behavior to three column curves known as Structural Stability Research Council (SSRC) Column Strength Curves 1, 2 and 3 (Galampos 1998).

In a pilot investigation conducted from 1954 to 1956, the behavior of 70-mm diameter stress-relieved bars was studied experimentally (Fujita and Driscoll 1962). Three stub-column tests, nine axially loaded column tests (eight "T-1" steel bars and one structural carbon-steel bar), and two eccentrically loaded column tests were performed. The slenderness ratios of these bars ranged from 30 to 73. Comparison with the tangent modulus concept for axially loaded columns, and with an inelastic strength theory for the eccentrically loaded columns, showed that the ultimate strength of solid round columns might be predicted adequately by theory.

Latter, (Galambos and Yoda, 1962) reported testing four axially loaded solid round bars of 190.5 mm diameter and slenderness ratios of 52, 61, 66 and 67, respectively. Then, Galambos (1965) added the results of the experimental ultimate axial compressive strength of fourteen bars with diameter 70 mm slenderness ratios ranging from 30 to 62. The effects of residual stress and initial crookedness on column strength were also considered. The initial out-of-straightness (also refereed as initial crookedness or initial curvature) also affects the primary column strength. The analysis of the strength of inelastic, initially curved columns has either made use of assumed values and shapes of the initial out-of-straightness, or can use actually measured data. The former is the most common, mostly because the measurements that are available for columns are rare. This applies in particular to the magnitude of the maximum out-of-straightness, normally assumed to occur at the mid-height of the member. The latter is usually thought to be that of a half-sine wave (Bjorhovde 1972).

★ 2.5.1. Influence Of Residual Stresses

Residual stresses in structural steel shapes and plates result primarily from uneven cooling after rolling of hot-rolled steel columns. The quick cooling parts of sections when solidified resist further shortening, while those parts that are still hot tend to shorten further as they cool. The net result is that the area that cooled more quickly has residual compressive stresses, while the slower cooling areas have residual tensile stresses. In the elastic region, residual stresses and initial crookedness have a significant influence on the strength of solid round bars. These stresses are of particular importance for columns with slenderness ratio varying from approximately 40 to 120, a range that includes a very large

percentage of real-world columns. The influence of the initial crookedness is predominant if only small residual stresses are present. For materials, which are quenched without stress relieving, the effect of residual stresses and initial crookedness is significant (Galambos 1965). Few researchers (among them: Hetenyi, 1957; Watanabe et al., 1955; Bühler, 1954) measured experimentally the residual stresses in cylindrical steel bars by the boring-out technique. According to the study by Nitta and Thürlimann (1962b) on the effect of thermal residual stresses and initial deflections on solid round steel bars, members containing high residual stress caused by water quenching, for example, carry approximately a 10 to 20% lower load than air-cooled or stress-relieved steel columns, provided that the generalized slenderness ratio and initial deflections are the same. Few authors utilized analytical and numerical simulation techniques, such as the finite-element method, to predict residual stresses produced by the manufacturing process (Jahanian, 1995; Toparli and Aksoy, 1991; Kamamoto et al., 1985; Weiner and Huddleston, 1959). Recently, Weiner and Huddleston showed a solution of the phase-transformation stresses from the standpoint of the flow theory of plasticity. Since the process for obtaining a general solution is very involved it seems almost inevitable to introduce simplifying assumptions when performing numerical calculations. Hence certain constant values of the material properties are used as a common value for the whole cooling instead of taking the true values corresponding to the variable temperatures. By including the effect of the residual stresses in steel columns a reasonable approach to the solution of the buckling load was suggested by Osgood, Yang and others.

Fujita and Driscoll (1962) solved graphically the ultimate strength of H-shape and built-up columns including the effect of residual stresses due to welding. Since these

particular solutions are not applicable to any other cross sectional shapes in which the magnitude and the distribution pattern of residual stresses are different, further studies are necessary in order to visualize the true column behavior until failure occurs. Most recently, Ding (2000) used the classical boring-out method to determine the residual stresses on fourteen samples of hot-rolled solid round steel bars. The diameter of the specimens ranged from 38.1 to 152.4 mm, with yield strength of 456 MPa. It should be noted that the residual stresses are an unavoidable consequence of the manufacturing process. Hence, the measurement of them is needed in order to assess the performance of columns under combined effect.

The results obtained by the studies of Batterman and Johnston (1967) showed that the separate effects of residual stresses and initial curvature cannot be added to give a good approximation of the combined effects on the maximum column strength. Residual stresses have little effect on the maximum strength of very slender columns, either straight or initially crooked, which have strengths approaching the Euler load. However, such columns made of higher-strength steels can tolerate much greater lateral deflection before yield or before becoming unstable. The differences in column strength, caused by variations in the shape of the residual stress pattern, are smaller for initially curved columns than for initially straight columns.

2.5.2. Influence Of Out-of-Straightness

The initial out-of-straightness (also referred to as initial crookedness or initial curvature) also affects the primary column strength. The analysis of the strength of inelastic,

initially curved columns has either made use of assumed values and shapes of the initial out-of-straightness, or can use actually measured data. The former is the most common, mostly because the measurements that are available for columns are rare. This applies in particular to the magnitude of the maximum out-of-straightness, normally assumed to occur at mid-height of the member. The latter is usually thought to be that of half-sine wave (Batterman and Johnston, 1967; Bjorhovde and Tall, 1971).

2.5.3. Effect of Cold-Straightening

The strength of cold-straightened columns is, in general, greater than that of the corresponding as-rolled members because of the improved straightness and redistribution of residual stress (Alpsten 1970). According to the study by Nitta and Thürlimann (1962a) on the effect of cold straightening on the ultimate strength of circular columns, the tangent modulus concept cannot be used for predication of cold-straightening columns, as there exists no bifurcation point in the load-deflection curve of cold-straightened column, which contains ant-symmetric residual stress. The strength depends upon the magnitude of the cold-straightening residual stresses and the out-of-straightness remaining after cold-straightening operation. The load carrying capacity of such column can be determined by ultimate load analysis.

Fujita and Deiscoll (1962) tested nine axially loaded bars and two eccentrically loaded bars (eight USS "T-1" constructional alloy steel bars and one structural carbon steel bar). The bars were of 70 mm in diameter, with slenderness ratio (KL/r) ranging from 30 to 73. The bars were cold straightened and subsequently stress-relieved, followed

by air-cooling. Comparison with the theory based on the 'tangent modulus' concept for axially loaded columns, and with an inelastic-strength theory for the eccentrically loaded columns shows that the ultimate strength of solid round columns may be predicated adequately by the tangent modulus concept.

Recently, Mull (1999) experimentally determined the compressive resistance of forty steel solid round specimens for five different diameters of specimens ranging from 31.75 mm to 57.15 mm. The effective slenderness ratios of the specimens varied from 59 to 117. The specimens were tested as pinned-end columns loaded concentrically. From the measured strain data, it was determined that only sixteen of the forty specimens had load eccentricities less than or equal to $1/500^{\text{th}}$ of the effective length of the specimen. For these sixteen specimens, the ratio of the resistance computed from the Canadian Standard "*Limit States Design of Steel Structures*", CAN/CSA-S16.1-94, to the experimental failure loads ranged from 0.98 to 0.79, and, for resistances computed from AISC-LRFD Specification (1993), the ratios ranged from 1.10 to 0.89. So, more tests need to be carried out of wide range of solid rounds, especially of large diameters, to reach recommendations that may provide considerable savings in the design and evaluation of solid round bars. Previous studies on the effective length factors of solid round bars used as bracing diagonals (Jaboo, 1998; Sun, 1999, Chen, 2000; Lim, 2000) and as chord members (Qureshi, 1999). General effective length factors for structural steel members are specified in CAN/CSA-S16-01, Figure 2.5.

2.6 Structural Stability Research Council (SSRC) Column Strength Curves

In a major study, Bjorhovde (1972) examined the deterministic and probabilistic characteristics of column strength in general and developed an extensive database for the maximum strengths of centrally loaded compression members, covering the full practical range of shapes, steel grades, and manufacturing methods. This study resulted in a collection of 112 maximum-strength column curves. Then, these curves were subdivided into groups of curves with a mean or similar curve for each group. The latter defines the *multiple column curve concept* (Bjorhovde and Tall, 1971; Bjorhovde, 1972; Bjorhovde and Birkemoe, 1979). This results in three curves known as *SSRC column strength curves 1, 2 and 3*, and they are reproduced as shown in Figures 2.6, 2.7 and 2.8, respectively. Algebraic representations of the three column strength curves were obtained by curve fitting, and the resulting equations are as follows:

SSRC curve 1:

- | | | |
|----|----------------------------------|---|
| 1. | For $0 \leq \lambda \leq 0.15$ | $\sigma_\mu = \sigma_y$ |
| 2. | For $0.15 \leq \lambda \leq 1.2$ | $\sigma_\mu = \sigma_y (0.990 + 0.122\lambda - 0.367\lambda^2)$ |
| 3. | For $1.2 \leq \lambda \leq 1.8$ | $\sigma_\mu = \sigma_y (0.051 + 0.801\lambda^{-2})$ |
| 4. | For $1.8 \leq \lambda \leq 2.8$ | $\sigma_\mu = \sigma_y (0.008 + 0.942\lambda^{-2})$ |
| 5. | For $\lambda \geq 2.8$ | $\sigma_\mu = \sigma_y \lambda^{-2}$ (Euler Load) |

SSRC curve 2:

- | | | |
|----|----------------------------------|--|
| 1. | For $0 \leq \lambda \leq 0.15$ | $\sigma_\mu = \sigma_y$ |
| 2. | For $0.15 \leq \lambda \leq 1.0$ | $\sigma_\mu = \sigma_y (1.035 - 0.202\lambda - 0.222\lambda^2)$ |
| 3. | For $1.0 \leq \lambda \leq 2.0$ | $\sigma_\mu = \sigma_y (-0.111 + 0.636\lambda^{-1} + 0.087\lambda^{-2})$ |
| 4. | For $2.0 \leq \lambda \leq 3.6$ | $\sigma_\mu = \sigma_y (0.009 + 0.877\lambda^{-2})$ |
| 5. | For $\lambda \geq 3.6$ | $\sigma_\mu = \sigma_y \lambda^{-2}$ (Euler Load) |

SSRC curve 3:

- | | | |
|----|----------------------------------|--|
| 1. | For $0 \leq \lambda \leq 0.15$ | $\sigma_\mu = \sigma_y$ |
| 2. | For $0.15 \leq \lambda \leq 0.8$ | $\sigma_\mu = \sigma_y (1.093 - 0.622\lambda)$ |
| 3. | For $0.8 \leq \lambda \leq 2.2$ | $\sigma_\mu = \sigma_y (-0.128 + 0.707\lambda^{-1} - 0.102\lambda^{-2})$ |
| 4. | For $2.2 \leq \lambda \leq 5.0$ | $\sigma_\mu = \sigma_y (0.008 + 0.792\lambda^{-2})$ |
| 5. | For $\lambda \geq 5.0$ | $\sigma_\mu = \sigma_y \lambda^{-2}$ (Euler Load) |

2.7 Canadian Standards

The experimental investigation on the compressive resistance of solid rounds carried out was as far back as to 1965 on structural carbon and construction alloy steel (Galambos and Ueda, 1962; Galambos, 1965). Since there is no other literature on the compressive resistance of solid rounds, the superseded version of the Canadian Standard for Antennas, Towers, and Antenna-Supporting Structures, CAN/CSA-S37-94, assumed the applicability of Column Strength Curve 2 of the Structural Stability Research Council (Galambos, 1998) to hot rolled solid round bars 51 mm in diameter and less and to hot-rolled solid round bars greater than 51 mm in diameter that are stress-relieved to manufacturer's recommendations after initial cold-straightening at the mill. It should be noted that the resulting equations of the SSRC Column Strength curve 2, equations 1 to 5 listed below, were obtained for W-shapes and hollow structural sections.

$$0 \leq \lambda \leq 0.15 \quad C_r = \phi A F_y \quad (2.7)$$

$$0.15 < \lambda \leq 1.0 \quad C_r = \phi A F_y [1.035 - 0.202\lambda - 0.222\lambda^2] \quad (2.8)$$

$$1.0 < \lambda \leq 2.0 \quad C_r = \phi A F_y [-0.111 + 0.636\lambda^{-1} + 0.087\lambda^{-2}] \quad (2.9)$$

$$2.0 < \lambda \leq 3.6 \quad C_r = \phi A F_y [0.009 + 0.877\lambda^{-2}] \quad (2.10)$$

$$3.6 < \lambda \leq 5.0 \quad C_r = \phi A F_y [\lambda^{-2}] \quad (2.11)$$

where:

$\lambda = \frac{KL}{r} \sqrt{\frac{F_y}{\pi^2 E}}$; F_y = yield stress; ϕ = resistance factor; A = cross-sectional area; λ = slenderness function; L = length of member; r = radius of gyration; K = effective length factor; E = modulus of elasticity.

Also, the CAN/CSA-S37-94 presented expressions of the compressive resistance of solid round bars greater than 51 mm in diameter and not stress-relieved after cold straightening, based on Column Strength Curve 3 of the Structural Stability Research Council (Galambos 1998).

$$0 < \lambda \leq 0.8 \quad C_r = \phi \cdot A \cdot F_y [1.093 - 0.622\lambda] \quad (2.12)$$

$$0.8 < \lambda \leq 2.3 \quad C_r = \phi \cdot A \cdot F_y [-0.128 + 0.707\lambda^{-1} - 0.102\lambda^{-2}] \quad (2.13)$$

$$2.3 < \lambda \leq 5.0 \quad C_r = \phi \cdot A \cdot F_y [0.008 + 0.792\lambda^{-2}] \quad (2.14)$$

Most recently, the Canadian Standard for Antenna towers and Antenna Supporting Structures, CAN/CSA-S37-01, was released to the public, with some modifications to the expressions found in the superseded version of 1994 for compressive strength of solid rounds. These modifications were based on results of testing a limited number of solid rounds back to 1965. The factored axial compressive resistance, C_r , of a member is determined by the following formula:

$$C_r = \phi \frac{AF_y}{[1 + \lambda^{2n}]^{1/n}} \quad (2.15)$$

where:

$n = 1.34$ for hot rolled round bars 51 mm in diameter and less; hot rolled solid round bars greater than 51 mm in diameter and stress relieved to manufacturer's recommendations after initial cold straightening at the mill.
 $= 0.93$ for hot-rolled solid round bars greater than 51 mm in diameter and not stress relieved after cold straightening.

It should be noted that earlier versions of the Canadian Standard "*Limit States Design of Steel Structures*" adopted Equations 2.7 to 2.14 for solid round bars till 1994 version of the standard. However, the current standard "CAN/CSA-S16-01" (2003) omitted these equations for the insufficient data in the literature that supports them. It adopts equation 2.15 for shapes other than solid rounds.

In summary, there is a lack of available literature that would assist code writers to specify more economical and safe expressions for the compressive strength of stress-relieved and non-stress-relieved solid round steel bars. Also, as manufacturing methods have advanced considerably since the current equations were formulated, there is a need to revisit this issue.

2.8 AISC (LRFD) Specifications

According to the AISC-LRFD, "Load and Resistance Factor Design Specifications for Structural Steel Buildings", [American Institute of Steel Construction Inc. 1993], the compressive resistance of structural steel members of different shapes is given by:

$$C_r = \phi.A.F_{cr} \quad (2.16)$$

Where,

$$F_{cr} = [0.658^{\lambda^2}]F_y \quad \text{for } \lambda \leq 1.5, \text{ and} \quad (2.17)$$

$$F_{cr} = \left[\frac{0.877}{\lambda^2} \right] F_y \quad \text{for } \lambda > 1.5 \quad (2.18)$$

It should be noted that equations 2.17 and 2.18 represent SSRC column strength curve 2 and apply for structural steel shapes other than solid rounds.

2.9 European Standard

This European Standard for the design of steel structures, Eurocode 3, (CEN, 2003) specifies rules relating to ultimate limit state analysis of the buckling resistance of steel linear members and frames susceptible to loss of stability. Buckling is a phenomenon in which displacement, v or w , of a member occurs, or rotation, ϑ , occurs about its major axis, or both occur in combination. A distinction is conventionally made between lateral buckling and lateral torsional buckling. Lateral buckling is a phenomenon in which displacements, v or w , of a member occurs, or both occur in conjunction, any rotation, ϑ , about its major axis being neglected. Lateral torsional buckling is a phenomenon in which displacements, v and w , of a member occur in combination with rotation, ϑ , about its major axis, consideration of the latter being obligatory.

Eurocode 3 specifies that the analysis shall take the form of one of the methods given in Table 2.1 shown below, taking into account the following factors:

- Plastic capacity of materials

- Imperfections
- Internal forces and moments
- The effects of deformations
- Slip
- The structural contribution of cross sections
- Deductions in cross-sectional area for holes

As a simplification, lateral buckling and lateral torsional buckling may be checked separately, first carrying out the analysis for lateral buckling and then that for lateral torsional buckling whereby, in the latter case, members shall be notionally singled out of the structural system and subjected to the internal forces and moments acting at the member ends (when considering the system as a whole) and to those acting on the member considered in isolation. Details on whether first or second order theory is to be applied are given together with the relevant method of analysis

The materials used shall be of sufficient plastic capacity. Calculations may be based on assumptions of linear elastic-perfectly plastic stress-strain behavior instead of actual behavior. Reasonable assumptions shall be made in order to take into account the effects of geometrical and structural imperfections. Typical geometrical imperfections are accidental load eccentricity and deviations from design geometry. Typical structural imperfections would be residual stresses. The internal forces and moments occurring at significant points in the members shall be calculated on the basis of the design actions. Calculations of internal forces and moments usually make allowance for deformation effects on equilibrium, using as the design stiffness values the characteristic stiffness

obtained by dividing the nominal characteristics of cross section and the elastic characteristic and shear moduli by a partial safety factor γ_M equal to 1.1. The effect of deformations resulting from stresses due to shear forces may normally be ignored.

Members notionally singled out of the system and considered in isolation shall be analyzed for lateral torsional buckling. Their end moments may require to be determined by second order theory. The moments in the span may then be calculated by first order theory using these end moments.

An analysis of lateral torsional buckling is not required for the following:

- Hollow sections
- Members with sufficient lateral or torsional restraint
- Members designed to be in bending, provided that their non-dimensional slenderness in bending, $\bar{\lambda}_M$, is not more than 0.4

The ultimate limit state analysis shall be made for the direction in which buckling will take place, using equation 2-19

$$\frac{N}{x \cdot N_{pl,d}} \leq 1 \quad (2-19)$$

Where N is design value of the compressive force, $N_{pl,d}$ is the design buckling resistance of the compression member, x is a reduction factor according to the standard and buckling curved as used in Europe.

$$\text{If } \bar{\lambda}_K \leq 0.2; \chi = 1$$

$$\text{If } \bar{\lambda}_K > 0.2; \chi = \frac{1}{k + \sqrt{k^2 - \bar{\lambda}_K^2}}$$

$$\text{where } k = 0.5[1 + \alpha(\bar{\lambda}_k - 0.2) + \bar{\lambda}_k^2]$$

As a simplification, in cases where $\bar{\lambda}_K > 3.0$:

$$x = \frac{1}{\bar{\lambda}_k(\bar{\lambda}_k + \alpha)}$$

Where α is the imperfection factor being taken from Table 2.2 for curve c.

In lieu of the above equations, χ can be obtained from curve c in Figure 2.9.

Chapter III

EXPERIMENTAL STUDY

3.1 General

Axially loaded column strength tests were conducted at the structural laboratory of Ryerson University on 20 stress-relieved steel solid rounds and 35 non-stress-relieved steel solid rounds on different diameter and length. Also, a set of 7 stub columns was tested to collapse. This chapter reports the sizes of the tested specimens as well as the test set-up used to conduct each type of testing.

3.2 Description of the test specimens

3.2.1 Testing Centrally Loaded Columns made of Stress-Relieved Steel

To minimize initial geometric imperfections of the specimen, the column specimen is cut from a straight portion of the stock. Both ends of the specimen are milled. 20 solid rounds made of stress-relieved steel were cut to size per the dimensions shown in Table 3.1. This type of specimens was supplied by Radian Communications Systems Inc. of Oakville, Ontario, Canada. The diameter of the columns ranged from 38 to 128 mm, with slenderness ratios ranging from 10 to 70. It should be noted that the common slenderness ratios for existing tower members range from 40 to 70. However, the inclusion of smaller slenderness ratios was considered as a result of the considerable high compressive forces in the tower legs in high seismic regions. Table 3.1 summarizes the details of these specimens. The results of these tests would be in the form of

lateral deflection of the column at mid-height, axial strains, column shortening and mode of failure.

3.2.2 Testing Centrally Loaded Columns made of Non-Stress-Relieved Steel

Two sets of solid rounds made of non-stress-relieved steel were supplied by *ERI, Electronics Research Inc. of Chandler, Indiana, U.S.A.* The first set included 25 solid rounds with diameter ranging from 38 mm to 114 mm and slenderness ratios ranging from 20 to 75, as shown in Table 3.2. The other set has longer length, with slenderness ratios ranging from 25 to 91. Table 3.3 summarizes the details of these specimens. These tests were intended to stand on the level of the effect of residual stresses arising from the manufacturing process on the column compressive resistance.

3.2.3. Stub Column Tests:

Stub column tests were made of short bars to determine the average compressive stress-strain characteristics of the solid round when instability effects are excluded. This information will be used in a subsequent study for the determination of the tangent-modulus curved needed for the theoretical predication of the critical load of the axially loaded columns and to stand on the percentage reduction in strength when using longer length of columns. SSRC Guidelines (Galambos, 1998) recommend the length of the hot-rolled stub columns to be $2d + 250$ mm or $3d$, whichever is the smaller, where d is the diameter of the bar.

Seven stub columns were supplied by *ERI, Electronics Research Inc. of Chandler, Indiana, U.S.A.* Table 3.4 summarizes the details of the tested stub columns. The length-to-diameter ratio of the stub was maintained at 4. The diameter of the stubs ranged from 38 mm to

114 mm, maintaining a slenderness ratio of 16. These specimens were cold-sawed from the stock and the ends of the columns were milled plane and perpendicular to the longitudinal axis of the column. Stub column tests are expected to provide Young's modulus of elasticity, proportional limit stress, yield strength, elastic range, elastic-plastic range, onset of strain hardening, strain-hardening range, and strain-hardening modulus.

3.3 Test Set-Up

The specimens were tested in the Structural Laboratory of Ryerson University. Two test set-ups were used to conduct the columns strength tests as well as stud column tests. The first test set-up utilized the available 4500-kN compression testing (MTS) machine, shown in Figure 3.1. The clear head of between the upper and lower end plates can accommodate specimens of maximum length of 1118 mm. As a result, all specimens shown in Tables 3.1 to 3.4 were tested using the MTS machine except specimen NSR-26 shown in Table 3.3. This specimen was tested in a set-up prepared to accommodate specimen height of 1219 mm.

The second set up was installed between the upper and lower steel beams of the available self-contained 3D structural steel testing facility in the structural laboratory. A hydraulic jack having a capacity of 900 kN was used for the application of the load. The jack was mounted on a W-shape monorail beam supported by a rigid portal frame as shown in Figure 3.3-b. A universal flat load cell, of 900 kN capacity, was used to measure the applied loads on bridge models. While Figure 3.3 shows the two test setups mentioned herein.

Three types of end conditions were applied to the columns tested in the MTS machine, namely, hinged-hinged (H-H), hinged-fixed (H-F) and fixed-fixed (F-F). A hemispherical bearing block at the upper and/or lower end of the machine provided a uniform distribution of applied stress in the test specimen and ensured the pinned-end restraints of the specimen while flat-ended conditions were considered at the lower end and/or upper end of the specimen ensuring fixed-end constraints. Figure 3.2 shows schematic diagram of the specimens in a test set-up with hinged-fixed conditions.

3.4 Instrumentations

3.4.1 Strain Gauges

Electric resistance strain gauges, manufactured by Kyowa, Japan, type KFG-5-120-C1-11, with a gauge length of 5 mm and a gauge factor of 2.12 were used to measure the axial strain in the test specimen. Four strain gauges were attached in North, East, South and West directions, as shown in Figure 3.2 to measure the axial strain in the specimen at its mid-height. For the application of strain gauges, the surface was properly polished with a 50 mm air grinder using a brush, grit size-50, for roughening and grit size-180 for finishing; and then cleaned with acetone, followed by application of M-Prep conditioner-A and M-prep Neutralizer-5A. Conditioner-A (non-flammable phosphoric acid) was water based acidic surface cleaner, and M-prep Neutralizer-5A (non-flammable ammonia water) was a water based alkaline surface cleaner. After polishing and cleaning the surfaces, Fastac accelerator-H, Sicomet-7000 (for use with cyanacrylate adhesives), was applied on the polished and cleaned surface, followed by the application of the strain gauge adhesive (alkyl cyanoacrylate ester), along with the strain gauge.

3.4.2 Mechanical Dial Gauges

Mechanical dial having travel sensitivity 0.01 mm were used to measure the lateral deflection in the north and east directions at the mid-height of the column. The dial gauge readings were manually taken at specific increments of the loading throughout the test. In some specimens, Linear Variable Displacement Transducers, LVDT's, were used to measure lateral deflection in two perpendicular directions.

3.4.3 Automatic Strain Indicator

Daytronics system 10 data acquisition unit was used to capture the strain reading from rebar strain gauges. This unit consists of balancing unit having quarter, half and full bridge connections of the circuit and data acquisition system which was connected to the computer. Data from the acquisition system was captured using Visual Designer software from Intelligent Instrumentation.

3.5 Test Procedure

Initial dimensions (length, diameter and out-of-straightness) of each specimen were recorded. Then, each specimen was aligned centrally within the testing machine. Dial gauges were installed at the north and east sides of the column at its mid-height. Strain gauge wires were connected to the automatic strain indicator. When using the MTS machine, the load was applied at a rate of 6.9 MPa/min (Galambos, 1998). The converted load rate for each specimen is listed in the last column of Tables 3.1 to 3.4. The MTS machine software recorded the applied load per second as well as the overall shortening of the column with the applied load till failure. At a specified load increment, the readings from the strain gauges and the dial gauges were recorded.

3.6 Material Property

The tensile yield strength is the key mechanical property required by codes and design practice. Because of its standard usage, it is the most accepted value for analyzing and comparing test data. Since the tensile testing is sensitive to the rate of straining, stability test data can easily be shifted by more than 20% if care is not exercised in conducting the tension test and in reporting the test method employed and its results.

Seven tensile coupons for stress relieved steel columns as well as seven tensile coupons taken from non-stress-relieved steel specimens were tested, corresponding to each bar size. The tensile coupons were prepared in accordance with ASTM Standards. The total length of the specimens was 200 mm, with a gauge length of 50 mm and diameter of 12.5 mm. Figure 3.5 shows the test set-up for tension coupon test before and after failure, respectively. Typical load-elongation curve for the tensile coupons are given in the following chapter. The values of yield stress, tensile strength and percent elongation for each specimen are presented in the following chapter.

3.7 Determination of Yield Strength from Tension Coupons

Kennedy and Gad (1980; CSA, 2000) provided guidance to determine representative material strength for use in the evaluation of existing bridges from the test of material samples taken from the bridge. The analysis and interpretation of test data may often be made difficult by presence of spurious high or low observations in the data set. A test observation can be ignored if reasons for its extreme value can be identified and its exclusion from the analysis can be justified. However, such justification may be difficult if there are less than 6 samples in total.

The yield strength for evaluation, F_y , is determined from Eq. (3-1) (CSA, 2000). In this equation, it is assumed that the difference between yield strength observed during a coupon test and static yield strength is 28 MPa.

$$F_y = (\overline{F_y} - 28) e^{-1.3K_s V_s} \quad (3-1)$$

where,

$$\overline{F_y} = \text{Average value of equivalent yield strengths from the tests} = \frac{1}{n} \sum_{i=1}^n F_{yi}$$

K_s = coefficient of variation modification factor for steel from Table 3.5. Coefficient K_s is a measure of confidence in strength data and reflects effect of sample size on the uncertainty of the mean value; higher value of K_s means a greater uncertainty and hence a lower degree of confidence. This confidence in data improves as the number of sample increases. The equivalent yield strength of each coupon is its reported yield strength from the test, except of a coupon is obtained from the flange of a rolled member, the equivalent yield strength of that coupon may be taken as 1.05 times the reported yield strength from the test.

n = number of strength tests

V_s = coefficient of variation of equivalent yield strengths from the tests. It is dimensionless and is defined as the standard deviation divided by the mean $r = \frac{\sigma}{\overline{F_y}}$.

As a general case, the mean value of x is denoted by μ_x . For a continuous random variable, the mean value is defined as

$$\mu_x = \int_{-\infty}^{+\infty} x f_x(x) dx \quad (3-2)$$

For a discrete random variable, the mean value is defined as

$$\mu_x = \sum_{all x_i} x_i p_x(x_i) \quad (3-3)$$

The expected value of X is commonly denoted by E(X) and is equal to the mean value of the variable as defined above:

$$E(X) = \mu_x \quad (3-4)$$

It is also possible to determine the expected value of X^n . This expected value is called the nth moment of X and is defined for continuous variables as

$$E(X^n) = \int_{-\infty}^{+\infty} x^n f_x(x) dx \quad (3-5)$$

$$E(X^n) = \sum_{all x_i} x_i^n p_x(x_i) \quad (3-6)$$

The variance of X, commonly denoted as σ_x^2 , is defined as the expected value of $(X - \mu_x)^2$ and is equal to

$$\sigma_x^2 = \int_{-\infty}^{+\infty} (x - \mu_x)^2 f_x(x) dx \quad (\text{Continuous random variable}) \quad (3-7)$$

$$\sigma_x^2 = \sum_{all x_i} (x_i - \mu_x)^2 p_x(x_i) \quad (\text{Discrete random variable}) \quad (3-8)$$

An important relationship exists among the mean, variance, and second moment of a random variable X:

$$\sigma_x^2 = E(X^2) - \mu_x^2 \quad (3-9)$$

The standard deviation of X is defined as the positive square root of the variance:

$$\sigma_x = \sqrt{\sigma_x^2} \quad (3-10)$$

The nondimensional coefficient of variation, V_x , is defined as the standard deviation divided by the mean:

$$V_x = \frac{\sigma_x}{\mu_x} \quad (3-11)$$

This parameter is always taken to be positive by convention even though the mean may be negative. In many practical applications, the true distribution is not known, and one needs to estimate parameters using test data. If a set of n observations $\{x_1, x_2, \dots, x_n\}$ are obtained for a particular random variable X , then the true mean μ_x can be approximated by the sample mean \bar{x} and the true standard deviation σ_x can be approximated by the sample standard deviation S_x

The sample mean is calculated as

$$\bar{x} = \frac{1}{n} \sum_{i=1}^n x_i \quad (3-12)$$

σ = standard deviation is calculated as follows = S_x

$$= \sqrt{\frac{\sum_{i=1}^n (X_i - \bar{X})^2}{n-1}} \quad (3-13)$$

This method provides the specified yield strength in the structural drawings that can be used in calculating the ultimate load carrying capacity of the column. This value is usually less than the

average yield strength obtained from tests. In this study, it was decided to use the actual yield strength as obtained experimentally for each coupon to obtain the ultimate strength of the respective specimen. This approach will make the comparison more realistic than using a lower value of yield strength or the commercial yield strength of Grade 50 steel.

CHAPTER IV

ANALYSIS AND DISCUSSION OF RESULTS

4.1 General

The results from testing to-collapse 20 solid round bars made of stress-relieved steel and 33 solid round bars made of non-stress-relieved steel, under increasing monotonic axial compressive load, are reported in this chapter. Also, the results from testing 7 stub columns are reported in this chapter. Moreover, results from tensile testing of 7 coupons made of stress-relieved steel and other 7 coupons made of non-stress-relieved steel are reported for different bar diameters. The applied load, the measured axial strain at the mid-height of the column specimen, the lateral deflection at the mid-height and the machine crosshead movement were recorded using a data acquisition system.

The compressive resistance obtained from testing were then compared with the compressive resistances computed based on the Canadian Standard (CAN/CSA-S37-01), the American Specifications (AISC-LRFD) and the European Standard (Euro code 3). The comparison between the experimental findings and the available Code equations for the steel bars was performed using the theoretical buckling length as well as the recommended practical buckling length specified in the Canadian Standard CAN/CSA-S16-01.

4.2 Results from Tension Coupons

Seven tensile coupons for stress relieved steel columns as well as seven tensile coupons taken from non-stress-relieved steel specimens were tested. Columns 1 and 2 of Tables 4.1 and 4.2 summarize the column diameters from which the coupon was machined towards their centroids. The tensile coupons were prepared in accordance with ASTM Standards. The total length of the specimens was 200 mm, with a gauge length of 50 mm and diameter of 12.5 mm. Figure 4.1 shows views of coupon samples during and after the fabrication process. While Figure 3.5 shows the test set-up for tension coupon test before and after failure, respectively.

Results from tensile testing the coupons made of stress-relieved steel and non-stress-relieved steel are presented in Table 4.1 and 4.2, respectively. Each table provides the average of three measurements for the diameter of each tension coupon, area of the tension coupon, peak load and stress, modulus of elasticity, the yield stress, percentage elongation at break and reduction of cross-sectional area after failure. It should be noted that the yield stress was calculated based on the 0.2%-offset method when recorded stress-strain curve did not show the flat-yield plateaux at the end of the elastic stage and before entering the plastic stage.

Figures 4.2 to 4.8 show the recorded axial stress-strain relationship for each tested bar diameter shown in Table 4.1. Some of these curves show distinct upper yield point and flat-yield plateaux before entering the non-linear stage. While others show no yield point before at the end of the elastic stage. Each of the tensile coupons failed in a ductile

manner as indicated in the calculated percentage elongations at break and reduction in cross-sectional area. Each coupon failed in a form of cup and cone. Figures 4.9 and 4.10 show the failure mode and the initial portion of the stress-strain curve of a coupon taken from a 38-mm diameter bar made of non-stress-relieved steel (NSR). Figures 4.11 and 4.12 show similar graphs for 51-mm diameter bar. Also, Figures 4.13 to 4.22 show similar graphs for coupons taken from NSR bars of diameters 64, 76, 89, 102 and 114 mm.

4.2 Results from Testing Centrally Loaded Columns Made of Stress-Relieved Steel

Tests to-collapse on 20 solid round bars made of stress-relieved steel were performed to check the accuracy of the compressive resistance equations specified in steel Standards, Specifications and Codes, when applied to solid rounds. The experimental failure load, as well as other pertinent information, such as diameter, length, end conditions, load rate and slenderness ratio, are given in Table 4.3. Three end conditions were considered while testing, namely: hinged-hinged (H-H), hinged-fixed (H-F), and fixed-fixed (F-F) conditions as listed in Table 4.3 for each tested column. Increasing axial load was applied to each column and readings from strains gauges for axial strains, and from LVDT's for column lateral deflection at its height, were recorded. The MTS machine recorded the crosshead movement with time as during the test. It should be noted that crosshead movement gives an indication of the average shortening over the column length. It should be noted that columns SR-18, SR-19 and SR-20 of 128

mm diameter did not fail because the applied axial load reached the specified capacity of the MTS machine of 4500 KN.

Figures 4.23 to 4.99 show the results from testing the 20 solid rounds made of stress-relieved steel. They include views of each specimen before and after failure. As an example, Figure 4.23 shows views of specimens SR-1 of 38 mm diameter and 660 mm length before and after failure. It can be observed that buckling is the dominant mode of failure for all specimens. Also, these figures include the measured axial strain at each load level. For example, Figure 4.65 shows the relationship between the applied axial load and the axial strains recorded at four points at the mid-height of the column. Two of these points represent the axial strains at the column surface along a line parallel to the machine head (north-south direction), while the other two points represent the axial strains at the column surface along a line perpendicular to the machine head (east-west direction). It can be observed that the strain readings at the four points are very close to each other which prove that there was almost no eccentricity on the application of the load. However, some columns show uneven distribution of axial strains along the perimeter of the columns at its mid-height. It should be noted that care was given at the first few increments of load at the start of each test to locate the column centrally as much as possible. Then, the test was continued till failure. It should be noted that the plane of buckling failure differ from one column to the other. This is why in some figures, such as Figure 4.65, it can be observed that buckling occurred about the east-west axis. While in Figure 4.31, failure occurred at the axis located between the south and west directions.

Some of Figures 4.23 to 4.99 provide the lateral deflection of tested column at its mid-height with increase in axial load. For example, Figure 4.25 shows LVDT readings in the east and north direction of the specimen. It should be noted that the two readings are not interrelated. However, they may give an indication of load level at which buckling started (usually when deflection deviates from the straight line relationship with load). One may observe that in ideal column (the one that has no initial out-of-straightness), the lateral deflection is almost zero till the column buckles laterally. However, this situation did not exist in many of the tested column since there is a small initial imperfection (crookedness) before applying the axial load. Some of Figures 4.23 to 4.99 provide the movement of the sensitive crosshead relative to the fixed crosshead using a built in LVDT, as automatically recorded by the MTS machine, with increase in applied axial load. For example, Figure 4.37 shows the change in the average shortening of column SR-4 of 51 m diameter and 661 mm length, along its length.

4.3 Correlation between the Experimental Failure Load of Stress-Relieved Steel Bars and the Compressive Resistance as Obtained from Design Standards.

The compressive resistances of the tested columns made of stress-relieved steel were computed based on the available empirical expressions specified in the Canadian Standard (CAN/CSA-S37-01), the American Specifications (AISC-LRFD) and the European Standard (Euro code 3). A resistance factor, ϕ , of 1.0 was considered to take into account the actual failure load obtained experimentally. Then, the obtained compressive resistance for each column was correlated with the results from tests.

It should be noted that three end conditions were considered while testing, namely: hinged-hinged (H-H), hinged-fixed (H-F), and fixed-fixed (F-F) conditions. For theoretical calculations of the slenderness factor, λ , the effective buckling length, k , was taken as 1 in case of H-H condition, 0.707 in case of H-F condition and 0.5 in case of F-F condition, as specified in CSA-S16-01 (see Figure 2.5). In testing columns under full fixed-end condition, the full restraint may not exist throughout the test. Therefore, the effective length factor of the tested column may not be constant with increase in the applied load. This may be partly attributed to the indeterminate nature of the stress distribution at the column end, particularly in the load range in which the material yields. As a result, an increase in the effective length factor, K , is expected in case of fixed end condition tested experimentally. In case of H-H condition, this problem does not exist because the critical condition exists at the mid-height of the column. In actual structures, the condition of full-fixity is approached only when the column is anchored securely to a foundation for which rotation is negligible, or when the column is framed integrally to a girder many times more rigid than itself. As a result, CAN/CSA-S16-01 recommends a design value for k as a modification to the ideal value, taking into account the fact that neither perfect fixity nor perfect flexibility is attained in practice. Figure 2.5 summarizes these values as 0.8 for H-F columns and 0.65 for F-F columns.

Table 4.4 shows the comparison between the experimental ultimate load and the compressive resistance of solid rounds made of stress-relieved steel as obtained from CSA-S37-01, AISC-LRFD and Euro code 3, based on the theoretical buckling length factors. While, Table 4.5 presents similar comparison but based on the recommended

practical buckling length factor shown in Figure 2.5. As it can be observed that the experimental failure load is always more or equal to the theoretical ultimate resistance. The following table summarizes the minimum, maximum and average value of the ratio between the experimental failure load the theoretical compressive resistance as obtained from the code equations. The standard deviation and the coefficient of variation are also presented in the table.

Effective length factor, k		Mini	Max.	Average	Standard deviation	Coefficient of variation
Theoretical	AISC-LRFD	1.00	1.52	1.24	0.161	12.9%
	CSA-S37-01	1.00	1.68	1.27	0.189	14.9%
	EURO Code	1.02	1.85	1.34	0.222	16.5%
Practical	AISC-LRFD	1.00	1.62	1.29	0.161	12.4%
	CSA-S37-01	1.00	1.78	1.33	0.201	15.1%
	EURO Code	1.02	1.96	1.42	0.243	17.0%

One may notice that the average ratios of the experimental failure load to that obtained from available code equations are always more than 1. As an example, CSA-37-01 underestimates the compressive resistance by about 27% and 33% when using the theoretical or practical effective buckling length factor, respectively. Considering the variation in results, the ratio between the experimental failure load and the compressive resistance as obtained from S37-01 equations is 1.08 in case of stress-relieved steel bars.

4.4 Results from Testing Centrally Loaded Columns Made of Non-Stress-Relieved Steel

Tests to-collapse on 33 solid round bars made of non-stress-relieved steel were performed to check the accuracy of the compressive resistance equations specified in

steel Standards, Specifications and Codes, when applied to solid rounds. The experimental failure load, as well as other pertinent information, such as diameter, length, end conditions, load rate and slenderness ratio, are given in Table 4.6 and 4.9. In this case, two end conditions were considered while testing, namely: hinged-hinged (H-H), and hinged-fixed (H-F). Increasing axial load was applied to each column and readings from strains gauges for axial strains, and from LVDT's for column lateral deflection at its height, were recorded. The MTS machine recorded the crosshead movement with time as during the test. It should be noted that columns NSR-22, NSR-23 and NSR-24, NSR-25 and NSR-33 of 114 mm diameter did not fail because the applied axial load reached the specified capacity of the MTS machine of 4500 KN.

Figures 4.100 to 4.219 show the results from testing the 33 solid rounds made of non-stress-relieved steel. They include views of each specimen before and after failure. As an example, Figure 4.100 shows views of specimens NSR-1 of 38 mm diameter and 508 mm length before and after failure. It can be observed that buckling is the dominant mode of failure for all specimens. Also, these figures include the measured axial strain at each load level. For example, Figure 4.106 shows the relationship between the applied axial load and the axial strains recorded at four points at the mid-height of the column. It can be observed that the strain readings at the four points are very close to each other which prove that there was almost no eccentricity on the application of the load. However, some columns show uneven distribution of axial strains along the perimeter of the columns at its mid-height. It should be noted that care was given at the first few

increments of load at the start of each test to locate the column centrally as much as possible. Then, the test was continued till failure.

Some of Figures 4.100 to 4.219 provide the lateral deflection of tested column at its mid-height with increase in axial load. For example, Figure 4.107 shows LVDT readings in the east and north direction of column NSR-3 OF 38 mm diameter and 914 mm length. Some of Figures 4.100 to 4.219 provide the movement of the sensitive crosshead relative to the fixed crosshead using a built-in LVDT, as automatically recorded by the MTS machine, with increase in applied axial load. For example, Figure 4.128 shows the change in the average shortening of column NSR-8 of 64 m diameter and 771 mm length, along its length.

4.5 Correlation between the Experimental Failure Load of Non-Stress-Relieved Steel Bars and the Compressive Resistance as Obtained from Design Standards.

The compressive resistances of the tested columns made of non-stress-relieved steel were computed based on the based on the available empirical expressions specified in the Canadian Standard (CAN/CSA-S37-01), the American Specifications (AISC-LRFD) and the European Standard (Euro code 3). A resistance factor, ϕ , of 1.0 was considered to take into account the actual failure load obtained experimentally. Then, the obtained compressive resistance for each column was correlated with the results from tests.

It should be noted that two end conditions were considered while testing, namely: hinged-hinged (H-H) and hinged-fixed (H-F) conditions. For theoretical calculations of

the slenderness factor, λ , the effective buckling length, k , was taken as 1 in case of H-H condition and 0.707 in case of H-F condition, as specified in CSA-S16-01 (see Figure 2.5). However, the compressive resistance of the tested columns was also calculated using the recommended practical effective buckling length factor per Figure 2.5, that is 0.8 for H-F columns.

Tables 4.7 and 4.10 show the comparison between the experimental ultimate load and the compressive resistance of solid rounds made of non-stress-relieved steel as obtained from CSA-S37-01, AISC-LRFD and Euro code 3, based on the theoretical buckling length factors. While, Tables 4.8 and 4.11 present similar comparison but based on the recommended practical buckling length factor shown in Figure 2.5. As it can be observed that the experimental failure load is always more or equal to the theoretical ultimate resistance. The following table summarizes the minimum, maximum and average value of the ration between the experimental failure load the theoretical compressive resistance as obtained from the code equations. The standard deviation and the coefficient of variation are also presented in the table.

Effective length factor, k		Mini	Max.	Average	Standard deviation	Coefficient of variation
Theoretical	AISC-LRFD	1.00	1.41	1.19	0.095	8.0%
	CSA-S37-01	1.07	1.54	1.33	0.118	8.9%
	EURO Code	1.09	1.69	1.31	0.121	9.0%
Practical	AISC-LRFD	1.03	1.41	1.22	0.080	6.5%
	CSA-S37-01	1.12	1.65	1.37	0.120	8.8%
	EURO Code	1.09	1.69	1.35	0.128	9.5%

One may notice that the average ratios of the experimental failure load to that obtained from available code equations are always more than 1. As an example, CSA-S37-01 underestimates the compressive resistance by about 33% and 37% when using the theoretical or practical effective buckling length factor, respectively. Considering the variation in results, the ratio between the experimental failure load and the compressive resistance as obtained from S37-01 equations is 1.22 in case of non-stress-relieved steel bars. It can be observed that the inclusion of the practical effective buckling length factor in compressive resistance calculations provides conservative results when designing a compression member. However, for the sake of revising the available code expressions, it is advisable to use the theoretical effective buckling length factor in compressive resistance calculations so that it can be very close to the experimental failure load.

4.6 Results from Testing Stub Columns

Stub column tests were made of short bars to determine the average compressive stress-strain characteristics of the solid round when instability effects are excluded. One stub column test was performed for each bar size listed in Table 3.4. Axially symmetric residual stresses are introduced in the bars by non-uniform cooling of the member after rolling or heat treatment. In case of stud column (SC-1) listed in Table 3.4, the specimen was carefully centered in the MTS machine. Then, two LVDT's were placed at the mid-height of the specimen to measure the lateral deflection which was observed to be insignificant. Also four strain gauges are used to measure axial strains around the stub cross-section at its mid-height. Figure 4.222 show the stub column SC-1 before and after testing. Figure 4.221 show the relationship between the axial load and the corresponding

axial strain at the mid-height of the stub. While, Figure 4.222 show the relationship between the applied axial load and the corresponding cross-head movement. A linear relation was observed with increase in applied axial load up to a certain load increment when residual stress effect started to force the stub cross-section to behave non-linearly. At failure, the stub buckled laterally as shown in Figure 4.222.

The yield stress of the stub column can simply be obtained at 0.2% offset of strain. Also, modulus of elasticity of the stub column can be obtained as the slope of the straight line portion of the stress-strain curve. However, the maximum compressive residual stress can be obtained by subtracting the stress at which deviation from linearity was first observed in the stub column test from the yield stress. Figures 4.223 to 4.240 show views of the stub column before and after testing, the axial load-strain relationship and the axial load-crosshead movement relationship for stub columns SC-2 to SC-7. Also, Table 4.12 lists the size, end conditions, load rate and experimental failure load for each stub column tested at the structural laboratory. These results will be used in a further research to verify the finite element modelling to be used to obtain the compressive resistance of non-stress-relieved solid round bars.

CHAPTER V

CONCLUSIONS AND RECOMMENDATIONS

5.1 General

The need for information on the compressive resistance of solid round bars made of stress-relieved or non-stress-relieved steel arose from the increased use of these bars in communication towers. Solid steel round bars are used as leg members, diagonal members and horizontal members of a communication tower. The superseded Canadian Standards of 1994, CAN/CSA-S16.1-94, AISC-LRFD Specifications of 1993, and the European Standard, Euro code 3, provide the factored compressive resistance of structural steel members other than solid rounds. While, the Current Canadian Standard, CAN/CSA-S37-01 of 2001, for Antenna towers and Antenna Supporting Structures specifies empirical expressions for the compressive strength of solid rounds based on the well-known Structural Stability Research Council (SSRC) column curves for non-solid-round members as well as the results from experimental investigation on the compressive resistance of solid rounds carried out back to 1965. This thesis provides a summary of the results of tests on 20 stress-relieved steel solid rounds, 33 non-stress-relieved steel solid rounds on different diameter and length and

7 stub columns. Correlation between the results from these tests and the current practice for the design of solid rounds is investigated. The following section summarizes the conclusions deduced from this research.

5.2 Conclusions

Based on the findings of this research, the following conclusions are drawn:

1- For slenderness ratios ranging from 18 to 70, CAN/CSA-S37-01 provides an ultimate compressive resistance of solid round bars made of stress-relieved steel that is about an average of 27% less than that obtained experimentally. While AISC-LRFD provides a conservative compressive resistance of an average of 24%. Euro Code 3 provides the highest conservative value of an average of 34%.

2- For slenderness ratios ranging from 20 to 91, CAN/CSA-S37-01 provides an ultimate compressive resistance of solid round bars made of non-stress-relieved steel that is 33% less than that obtained experimentally. While AISC-LRFD and Euro Code 3 provide conservative compressive resistance of 19% and 31%, respectively, more than that obtained experimentally.

3- Based on the results from the current study, code writers may update the available expression in CSA-S37-01 by multiplying the available code expressions for the compressive strength of solid round bars by a magnification factor of 1.08 in case of stress-relieved steel bars and 1.22 in case of non-stress-relieved steel bars for economical design, considering the practical effective buckling length factor. Also, this increase in compressive resistance of solid rounds would assist the practicing engineers in the evaluation of the load-carrying capacity of existing antenna towers since even a small

increase in strength for live load can make the difference between demolishing a tower or leaving it in service.

4- Results from experimental testing shows that the compressive resistance bars made of stress-relieved steel is greater than that for bars made of non-stress-relieved steel.

5.3 Recommendations for Future Research

Based on the findings from the current research, the following points of search need further investigations:

- 1- Finite Element modelling, including geometric and material nonlinearity, for buckling behaviour of axially loaded solid steel round bars made of stress-relieved steel or non-stress-relieved steel. In the latter, the actual distribution of residual stresses in bar cross-section should be incorporated in the modelling.
- 2- More experiments to-collapse on bars of slenderness ratios between 100 and 140 to widen the scope of application of the proposed expressions of the compressive resistance of solid rounds.
- 3- Conduct testing on short bars to determine the state of residual stresses in non-stress-relieved steel due to the manufacturing process as well as cold straightening.

REFERENCES

- Alpsten, G. (1970). **Residual Stresses and Strength of Cold-Straightened Wide-Flange Shapes**. Jernkontorets Ann., Vol. 154.
- American Institute of Steel Construction, Inc. (1993). **Load and Resistance Factor Design Specification for Structural Steel Buildings, AISC-LRFD**. Chicago, Illinois, USA.
- Batterman, R., and Johanston, B. (1967). **Behaviour and Maximum Strength of Metal Columns**. Journal of the Structural Division, ASCE, Vol. 93, No. ST2, pp. 205-230.
- Bjorhovde, R. (1972). **Deterministic and Probabilistic Approaches to the Strength of Steel Columns**. Ph.D. Dissertation, Lehigh University, Bethlehem, Pa.
- Bjorhovde, R. and Birkemoe, P. C. (1979). **Limit States Design of HSS Columns**. Canadian Journal of Civil Engineering, 6(2): ??-??.
- Bjorhovde, R., and Tall, L. (1971). **Maximum Column Strength and the Multiple Column Curve Concept**. Report No. 337.29, Lehigh University, Fritz Eng. Lab, Bethlehem, PA.
- Bühler, H. (1954). **Complete Determination of the State of Residual Stress in Solid and Hollow Metal Cylinders, Residual Stresses, Residual Stresses in Metals and Metal Construction**. Edited by W. R. Osgood, Reinhold Publishing Corporation, New York, N. Y., PP. 305-329.
- Canadian Standards Association. (1994). **Antennas, Towers, and Antenna-Supporting Structures**. CAN/CSA-S37-94, Rexdale, Ontario, Canada.
- Canadian Standards Association. (2003). **Limit States Design of Steel Structures**. CAN/CSA-S16-01, Rexdale, Ontario, Canada.

- Canadian Standards Association. (2001). **Antennas, Towers, and Antenna-Supporting Structures**. CAN/CSA-S37-01, Rexdale, Ontario, Canada.
- CEN. (2003). Eurocode 3 part 1.1: **General Rules and Rules for Steel Buildings**. CEN, European Committee for Standardization, Brussels, Belgium.
- Chen, Z. (2000). **Theoretical Effective Length Factors for Cross-Braced Solid Round Diagonals**. M.Sc. Thesis, Civil and Environmental Engineering, University of Windsor, Windsor, Ontario, Canada.
- Ding, Y. (2000). **Residual Stresses in Hot-Rolled Solid Round Steel Bars and their Effect on the Compressive Resistance of Members**. M.A.Sc. Thesis, Civil and Environmental Engineering, University of Windsor, Windsor, Ontario, Canada.
- Fujita, Y, and Driscoll, G. (1962). **Strength of Round Columns**. Journal of the Structural Division, ASCE, Vol. 88, No. ST2, pp. 43-59.
- Galambos, T. V. (1998). **Guide to Stability Design Criteria for Metal Structures**, 5th Edition. Structural Stability Research Council, John Wiley & Sons Inc., New York, N.Y.
- Galambos, T. V. (1965). **Strength of Round Steel Columns**. ASCE Journal of the Structural Division, 91(ST1): 121-140.
- Galambos, T. V., and Ueda, Yukio. (1962). **Column tests on 7 ½ in. Round Solid Bars**. ASCE, Journal of the Structural Division, 88(ST4):1-17.
- Hetenyi, M. (1957). **Handbook of Experimental Stress Analysis**. Third Edition, John Wiley & Sons Inc., New York, N.Y.

- Jaboo, K. S. (1998). **Effective Length Factors for Solid Round Diagonal Bracing Members in Latticed Towers**. M.Sc. Thesis, Civil and Environmental Engineering, University of Windsor, Windsor, Ontario, Canada.
- Jahanian, S. (1995). **Residual and Thermo-elasto-plastic Stress Distributions in a Heat Treated Solid Cylinder**. *Materials at High Temperatures*, 13(2):103-110.
- Kamamoto, S., Nihimori T., and Kinoshita, S. (1985). **Analysis of Residual Stress and Distortion Resulting from Quenching in Large Low-Alloy Steel Shafts**. *Journal of Material Science and Technology*, 1:798-804.
- Kennedy, D.J.L., and Gad, A.M. (1980). **Limit States Design of Steel Structures Performance Factors**. *Canadian Journal of Civil Engineering* 7(1): 45-47.
- Lim, H. L. (2000). **Effective Length Factors for Solid Round Members in K-Braced and Z-Braced Antenna Towers**. M.Sc. Thesis, Civil and Environmental Engineering, University of Windsor, Windsor, Ontario, Canada.
- Mull, N. C. (1999). **Compressive Resistance of Solid Rounds**. M.Sc. Thesis, Civil & Environmental Engineering, University of Windsor, Windsor, Ontario, Canada.
- Nitta, A. and Thürlimann, B. (1962a). **Ultimate Strength of High Yield Strength Constructional-Alloy Circular Columns – Effect of Cold-Straightening**. Publication, IABSE, 22: 265-288.
- Nitta, A. and Thürlimann, B. (1962b). **Ultimate Strength of High Yield Strength Constructional-Alloy Circular Columns – Effect of Thermal Residual Stresses**. Publication, IABSE, 22: 231-264.

- Qureshi, A. K. (1999). **Effective Length Factors for Solid Round Chord Members of Guyed Towers**. M.Sc. Thesis, Civil and Environmental Engineering, University of Windsor, Windsor, Ontario, Canada.
- Sun, Y. (1999). **Effective Length Factors for Solid Round Diagonal Members in Guyed Communication Towers**. M.Sc. Thesis, Civil and Environmental Engineering, University of Windsor, Windsor, Ontario, Canada.
- Toparli, M. and Aksoy, T. (1991). **Calculation of Residual Stresses in Cylindrical Steel Bars Quenched in Water from 600°C**. Proceedings of AMSE Conference, New Delhi, India, 4:93- 104.
- Watanabe, M., Sato, K., and Goda, S. (1955). **Thermal and Residual Stresses of Circular Cylinders Suddenly Cooled From the Uniformly Heated Conditions**. Journal of the Society of Naval Architects of Japan, 88: 155-164.
- Weiner, J. H. and Huddleston, J. V. 1959. **Transient and Residual Stresses in Heat-Treated Cylinders**. Journal of Applied Mechanics, 26E(1): 31-39.

Table 2.1 Ultimate limit state analysis

	Method	Calculation of	
		Internal forces and moments	Resistances
		According to	
1	Elastic-elastic	Elastic theory	Elastic theory
2	Elastic-plastic	Elastic theory	Plastic theory
3	Plastic-plastic	Plastic hinge theory	Plastic theory

Table 2.2 Parameters α for calculation of reduction factor x

Buckling Curve	a	b	c	d
α	0.21	0.34	0.49	0.76

Table 3.1 Details of Test Specimens: 20 Stress Relieved Specimens

Specimen number	Diameter (mm)	Length (mm)	End condition	KL/r	Load rate (KN/sec.)
SR-1	38	660	H-H	70.0	0.13
SR-2	38	813	H-F	60.4	0.13
SR-3	38	1143	F-F	60.0	0.13
SR-4	51	661	H-H	52.0	0.23
SR-5	51	812	H-F	45.2	0.23
SR-6	51	1143	F-F	44.8	0.23
SR-7	64	660	H-H	41.2	0.37
SR-8	64	813	H-F	50.8	0.37
SR-9	64	1143	F-F	35.6	0.37
SR-10	76	660	H-H	34.8	0.52
SR-11	76	1140	F-F	30.0	0.52
SR-12	89	661	H-H	29.6	0.73
SR-13	89	813	H-F	26.0	0.73
SR-14	89	1142	F-F	25.6	0.73
SR-15	102	661	H-H	26.0	0.94
SR-16	102	813	H-F	22.4	0.94
SR-17	102	1143	F-F	22.4	0.94
SR-18	128	660	H-H	20.6	1.5
SR-19	128	813	H-F	18.0	1.5
SR-20	128	1143	F-F	18.0	1.5

Table 3.2 Details of Test Specimens: 25 Non-Stress Relieved Specimens

Specimen number	Diameter (mm)	Length (mm)	End condition	KL/r	Load rate (KN/sec.)
NSR-1	38	508	H-H	53.5	0.13
NSR-2	38	711	H-H	74.8	0.10
NSR-3	38	914	H-F	68.0	0.11
NSR-4	51	508	H-H	39.8	0.23
NSR-5	51	711	H-H	55.8	0.20
NSR-6	51	914	H-F	47.0	0.21
NSR-7	64	508	H-H	31.8	0.32
NSR-8	64	711	H-H	44.4	0.28
NSR-9	64	914	H-F	40.0	0.29
NSR-10	76	610	H-H	32.1	0.45
NSR-11	76	711	H-H	37.4	0.43
NSR-12	76	813	H-F	30.3	0.46
NSR-13	76	914	H-F	34.0	0.44
NSR-14	89	610	H-H	27.4	0.64
NSR-15	89	711	H-H	32.0	0.61
NSR-16	89	813	H-F	25.8	0.65
NSR-17	89	914	H-F	29.0	0.63
NSR-18	100	610	H-H	24.4	0.82
NSR-19	100	711	H-H	28.4	0.78
NSR-20	100	813	H-F	23.0	0.82
NSR-21	100	914	H-F	25.8	0.80
NSR-22	114	610	H-H	21.4	1.10
NSR-23	114	711	H-H	24.9	1.06
NSR-24	114	813	H-F	20.1	1.10
NSR-25	114	914	H-F	22.33	1.08

Table 3.3 Details of Test Specimens: 8 Non-Stress Relieved Specimens

Specimen number	Diameter (mm)	Length (mm)	End condition	KL/r	Load rate (KN/sec.)
NSR-26	38	1219	H-F	91	0.13
NSR-27	38	1118	H-F	83	0.13
NSR-28	51	1118	H-F	62	0.24
NSR-29	64	1118	H-F	49	0.38
NSR-30	76	1016	H-F	38	0.53
NSR-31	89	1016	H-F	32	0.73
NSR-32	102	1016	H-F	28	0.95
NSR-33	114	1016	H-F	25	1.19

Table 3.4 Details of Test Specimens: 7 Stub Columns for Non-Stress Relieved Specimens

Specimen number	Diameter (mm)	Length (mm)	End condition	KL/r	Load rate (KN/sec.)
SC-1	38	152	H-H	16	0.13
SC-2	51	203	H-H	16	0.24
SC-3	64	254	H-H	16	0.38
SC-4	76	305	H-H	16	0.53
SC-5	89	356	H-H	16	0.73
SC-6	102	406	H-H	16	0.95
SC-7	114	457	H-H	16	1.19

Table 3.5 Coefficient of Variation Modification Factor for Steel, K_s

n	3	4	5	6	8	10	12	16	20	25	30 or more
K_s	3.46	2.34	1.92	1.69	1.45	1.32	1.24	1.14	1.08	1.03	1.00

Table 4.1 Results of coupon testing for stress-relieved bars

Specimen	Diameter (mm)	Length (mm)	Coupon diameter (mm)	Coupon cross-sectional area (mm ²)	Peak load (N)	Peak stress (MPa)	Modulus of Elasticity (MPa)	Yield stress @ 0.2% offset (MPa)	Auto Elong. @ break	Reduction of area
38-mm bar	38	200	12.75	127.68	70,723	565	193,032	390	30%	63%
51-mm bar	51	200	12.75	127.68	60,048	476	196,479	282	36%	72%
64-mm bar	64	200	12.75	127.68	69,389	552	202,894	369	30%	62%
76-mm bar	76	200	12.65	125.68	76,506	610	199,926	364	27%	54%
89-mm bar	89	200	12.75	127.68	74,726	596	213,714	390	29%	62%
102-mm bar	102	200	12.73	127.16	70,723	569	203,373	365	28%	64%
114-mm bar	128	200	12.65	124.65	71,612	576	199,926	383	29%	55%

Table 4.2 Results of coupon testing for non-stress-relieved bars

Specimen	Diameter (mm)	Length (mm)	Coupon diameter (mm)	Coupon cross-sectional area (mm ²)	Peak load (N)	Peak stress (MPa)	Modulus of Elasticity (MPa)	Yield stress @ 0.2% offset (MPa)	Man. Elong. @ break	Reduction of area
38-mm bar	38	200	12.75	127.68	68440	540	216,330	342	34.05%	67.77%
51-mm bar	51	200	12.75	127.68	71810	566	212,218	381	29.93%	67.72%
64-mm bar	64	200	12.75	127.68	75340	594	197,952	380	29.50%	65.23%
76-mm bar	76	200	12.65	125.68	66960	537	197,583	320	29.6%	52.84%
89-mm bar	89	200	12.75	127.68	75940	599	188,048	367	27.15%	57.57%
102-mm bar	102	200	12.73	127.16	75470	598	201,176	390	28.28%	63.18%
114-mm bar	114	200	12.65	125.68	76970	617	208,713	502	25.67%	59.48%

Table 4.3 Results of testing to-collapse 20 stress-relieved steel solid rounds

Bar number	Diameter (mm)	Length (mm)	End condition	Load rate (kN/sec)	KL/r	Experimental failure load (kN)
SR-1	38	660	H-H	0.13	70.0	444.85
SR-2	38	813	H-F	0.13	60.4	479.12
SR-3	38	1143	F-F	0.13	60.0	327.37
SR-4	51	661	H-H	0.23	52.0	669.92
SR-5	51	812	H-F	0.23	45.2	576.78
SR-6	51	1143	F-F	0.23	44.8	714.62
SR-7	64	660	H-H	0.37	41.2	1254.1
SR-8	64	813	H-F	0.37	50.8	1249.2
SR-9	64	1143	F-F	0.37	35.6	1215.4
SR-10	76	660	H-H	0.52	34.8	2180.26
SR-11	76	1140	F-F	0.52	30.0	1833.4
SR-12	89	661	H-H	0.73	29.6	3141.29
SR-13	89	813	H-F	0.73	26.0	2797
SR-14	89	1142	F-F	0.73	25.6	2557.2
SR-15	102	661	H-H	0.94	26.0	2823.6
SR-16	102	813	H-F	0.94	22.4	3508.7
SR-17	102	1143	F-F	0.94	22.4	3386.2
SR-18	128	660	H-H	1.5	20.6	N/A*
SR-19	128	813	H-F	1.5	18.0	N/A*
SR-20	128	1143	F-F	1.5	18.0	N/A*

* The load reached the capacity of the MTS machine (4500 kN).

Table 4.4 Comparison between the experimental finding and available Code equations for 20 stress-relieved steel bars using theoretical buckling length

Bar number	Diameter (mm)	Length (mm)	End condition	λ	Experimental failure load (kN)	Theoretical failure load (kN)			Experimental failure load /theoretical failure load ratio		
						AISC-LRFD	CSA-S37-01	Euro	AISC-LRFD	CSA-S37-01	Euro
SR-1	38	660	H-H	0.984	444.85	292	265	240	1.52	1.68	1.85
SR-2	38	813	H-F	0.849	479.12	323	300	275	1.48	1.60	1.74
SR-3	38	1143	F-F	0.843	327.37	324	302	276	1.01	1.08	1.19
SR-4	51	661	H-H	0.627	669.92	489	478	444	1.37	1.40	1.51
SR-5	51	812	H-F	0.545	576.78	509	504	472	1.13	1.14	1.22
SR-6	51	1143	F-F	0.540	714.62	510	505	472	1.40	1.42	1.51
SR-7	64	660	H-H	0.560	1254.1	1041	1029	960	1.20	1.22	1.31
SR-8	64	813	H-F	0.488	1249.2	1074	1072	1009	1.16	1.17	1.24
SR-9	64	1143	F-F	0.485	1215.4	1076	1074	1011	1.13	1.13	1.20
SR-10	76	660	H-H	0.472	2180.26	1504	1504	1418	1.45	1.45	1.54
SR-11	76	1140	F-F	0.407	1833.4	1540	1548	1475	1.19	1.18	1.24
SR-12	89	661	H-H	0.404	3141.29	2266	2278	2172	1.39	1.38	1.45
SR-13	89	813	H-F	0.351	2797	2304	2322	2239	1.21	1.20	1.25
SR-14	89	1142	F-F	0.349	2557.2	2324	2306	2242	1.10	1.11	1.14
SR-15	102	661	H-H	0.350	2823.6	2833	2856	2755	1.00	1.00	1.02
SR-16	102	813	H-F	0.304	3508.7	2869	2894	2825	1.22	1.21	1.24
SR-17	102	1143	F-F	0.302	3386.2	2871	2895	2827	1.18	1.17	1.20
SR-18	128	660	H-H	0.287	N/A*	4761	4802	4709	N/A	N/A	N/A
SR-19	128	813	H-F	0.250	N/A*	4801	4840	4802	N/A	N/A	N/A
SR-20	128	1143	F-F	0.249	N/A*	4802	4842	4806	N/A	N/A	N/A

* The load reached the capacity of the MTS machine (4500 kN).

Table 4.5 Comparison between the experimental finding and available Code equations for 20 stress-relieved steel bars using the practical buckling length

Bar number	Diameter (mm)	Length (mm)	End condition	λ	Experimental failure load (kN)	Theoretical failure load (kN)			Experimental failure load /theoretical failure load ratio		
						AISC-LRFD	CSA-S37-01	Euro	AISC-LRFD	CSA-S37-01	Euro
SR-1	38	660	H-H	0.984	444.85	292	265	240	1.52	1.68	1.85
SR-2	38	813	H-F	0.980	479.12	296	269	244	1.62	1.78	1.96
SR-3	38	1143	F-F	1.12	327.37	262	234	210	1.25	1.40	1.56
SR-4	51	661	H-H	0.627	669.92	489	478	444	1.37	1.40	1.51
SR-5	51	812	H-F	0.614	576.78	492	482	448	1.17	1.20	1.29
SR-6	51	1143	F-F	0.702	714.62	469	451	416	1.52	1.58	1.72
SR-7	64	660	H-H	0.560	1254.1	1041	1029	960	1.20	1.22	1.31
SR-8	64	813	H-F	0.552	1249.2	1045	1034	966	1.20	1.21	1.29
SR-9	64	1143	F-F	0.630	1215.4	1005	981	911	1.21	1.24	1.33
SR-10	76	660	H-H	0.472	2180.26	1504	1504	1418	1.45	1.45	1.54
SR-11	76	1140	F-F	0.530	1833.4	1468	1457	1364	1.25	1.26	1.34
SR-12	89	661	H-H	0.404	3141.29	2266	2278	2172	1.39	1.38	1.45
SR-13	89	813	H-F	0.400	2797	2271	2284	2180	1.23	1.22	1.28
SR-14	89	1142	F-F	0.454	2557.2	2226	2229	2107	1.15	1.16	1.21
SR-15	102	661	H-H	0.350	2823.6	2833	2856	2755	1.00	1.00	1.02
SR-16	102	813	H-F	0.344	3508.7	2838	2861	2763	1.24	1.23	1.27
SR-17	102	1143	F-F	0.393	3386.2	2796	2812	2687	1.21	1.20	1.26
SR-18	128	660	H-H	0.287	N/A*	4761	4802	4709	N/A	N/A	N/A
SR-19	128	813	H-F	0.280	N/A*	4766	4807	4720	N/A	N/A	N/A
SR-20	128	1143	F-F	0.323	N/A*	4717	4757	4618	N/A	N/A	N/A

* The load reached the capacity of the MTS machine (4500 kN).

Table 4.6 Results of testing to-collapse 25 non-stress-relieved steel solid rounds

Specimen number	Diameter (mm)	Length (mm)	End condition	Load rate (kN/sec.)	KL/r	Experimental failure load (kN)
NSR-1	38	508	H-H	0.13	53.5	406
NSR-2	38	711	H-H	0.10	74.8	376
NSR-3	38	914	H-F	0.11	68.0	364
NSR-4	51	508	H-H	0.23	39.8	835
NSR-5	51	711	H-H	0.20	55.8	767
NSR-6	51	914	H-F	0.21	47.0	745
NSR-7	64	508	H-H	0.32	31.8	1165
NSR-8	64	711	H-H	0.28	44.4	1281
NSR-9	64	914	H-F	0.29	40.0	1276
NSR-10	76	610	H-H	0.45	32.1	1714
NSR-11	76	711	H-H	0.43	37.4	1590
NSR-12	76	813	H-F	0.46	30.3	1631
NSR-13	76	914	H-F	0.44	34.0	1582
NSR-14	89	610	H-H	0.64	27.4	2584
NSR-15	89	711	H-H	0.61	32.0	2592
NSR-16	89	813	H-F	0.65	25.8	2601
NSR-17	89	914	H-F	0.63	29.0	2443
NSR-18	100	610	H-H	0.82	24.4	4063
NSR-19	100	711	H-H	0.78	28.4	3690
NSR-20	100	813	H-F	0.82	23.0	3785
NSR-21	100	914	H-F	0.80	25.8	3460
NSR-22	114	610	H-H	1.10	21.4	N/A*
NSR-23	114	711	H-H	1.06	24.9	N/A*
NSR-24	114	813	H-F	1.10	20.1	N/A*
NSR-25	114	914	H-F	1.08	22.33	N/A*

* The load reached the capacity of the MTS machine (4500 kN).

Table 4.7 Comparison between the experimental finding and available Code equations for 25 non-stress-relieved steel bars using theoretical buckling length

Specimen number	Diameter (mm)	Length (mm)	End condition	λ	Experimental failure load (kN)	Theoretical failure load (kN)			Experimental failure /theoretical failure load ratio		
						AISC-LRFD	CSA-S37-01	Euro	AISC-LRFD	CSA-S37-01	Euro
NSR-1	38	508	H-H	0.677	406	320	310	287	1.27	1.31	1.41
NSR-2	38	711	H-H	0.947	376	266	244	222	1.41	1.54	1.69
NSR-3	38	914	H-F	0.861	364	284	265	242	1.28	1.37	1.50
NSR-4	51	508	H-H	0.537	835	690	684	639	1.21	1.22	1.31
NSR-5	51	711	H-H	0.752	767	614	585	539	1.25	1.31	1.42
NSR-6	51	914	H-F	0.684	745	640	618	572	1.16	1.21	1.30
NSR-7	64	508	H-H	0.445	1165	1126	987	1068	1.03	1.18	1.09
NSR-8	64	711	H-H	0.620	1281	1041	844	946	1.23	1.52	1.35
NSR-9	64	914	H-F	0.563	1276	1070	890	986	1.19	1.43	1.40
NSR-10	76	610	H-H	0.411	1714	1352	1202	1294	1.27	1.43	1.32
NSR-11	76	711	H-H	0.479	1590	1318	1137	1240	1.21	1.40	1.28
NSR-12	76	813	H-F	0.388	1631	1363	1224	1312	1.20	1.33	1.24
NSR-13	76	914	H-F	0.436	1582	1341	1179	1275	1.18	1.34	1.24
NSR-14	89	610	H-H	0.386	2584	2145	1929	2066	1.20	1.34	1.25
NSR-15	89	711	H-H	0.449	2592	2098	1834	1988	1.24	1.41	1.30
NSR-16	89	813	H-F	0.363	2601	2160	1961	2093	1.20	1.33	1.24
NSR-17	89	914	H-F	0.408	2443	2129	1895	2038	1.15	1.29	1.20
NSR-18	100	610	H-H	0.335	4063	3040	2792	2841	1.34	1.46	1.43
NSR-19	100	711	H-H	0.391	3690	2989	2681	2751	1.23	1.38	1.34
NSR-20	100	813	H-F	0.316	3785	3056	2828	2872	1.24	1.34	1.32
NSR-21	100	914	H-F	0.355	3460	3023	2753	2809	1.14	1.26	1.23
NSR-22	114	610	H-H	0.334	N/A*	4889	4492	4782	N/A*	N/A*	N/A*
NSR-23	114	711	H-H	0.389	N/A*	4809	4316	4634	N/A*	N/A*	N/A*
NSR-24	114	813	H-F	0.315	N/A*	4916	4551	4833	N/A*	N/A*	N/A*
NSR-25	114	914	H-F	0.354	N/A*	4862	4430	4730	N/A*	N/A*	N/A*

* The load reached the capacity of the MTS machine (4500 kN).

Table 4.8 Comparison between the experimental finding and available Code equations for 25 non-stress-relieved steel bars using practical buckling length

Specimen number	Diameter (mm)	Length (mm)	End condition	λ	Experimental failure load (kN)	Theoretical failure load (kN)			Experimental failure /theoretical failure load ratio		
						AISC-LRFD	CSA-S37-01	Euro	AISC-LRFD	CSA-S37-01	Euro
NSR-1	38	508	H-H	0.677	406	320	310	287	1.27	1.31	1.41
NSR-2	38	711	H-H	0.947	376	266	244	222	1.41	1.54	1.69
NSR-3	38	914	H-F	0.974	364	261	237	215	1.40	1.54	1.69
NSR-4	51	508	H-H	0.537	835	690	684	639	1.21	1.22	1.31
NSR-5	51	711	H-H	0.752	767	614	585	539	1.25	1.31	1.42
NSR-6	51	914	H-F	0.774	745	606	574	528	1.23	1.30	1.41
NSR-7	64	508	H-H	0.445	1165	1126	987	1068	1.03	1.18	1.09
NSR-8	64	711	H-H	0.620	1281	1041	844	946	1.23	1.52	1.35
NSR-9	64	914	H-F	0.637	1276	1031	830	933	1.24	1.54	1.37
NSR-10	76	610	H-H	0.411	1714	1352	1202	1294	1.27	1.43	1.32
NSR-11	76	711	H-H	0.479	1590	1318	1137	1240	1.21	1.40	1.28
NSR-12	76	813	H-F	0.439	1631	1339	1177	1273	1.22	1.39	1.28
NSR-13	76	914	H-F	0.493	1582	1311	1124	1229	1.21	1.41	1.29
NSR-14	89	610	H-H	0.386	2584	2145	1929	2066	1.20	1.34	1.25
NSR-15	89	711	H-H	0.449	2592	2098	1834	1988	1.24	1.41	1.30
NSR-16	89	813	H-F	0.411	2601	2127	1891	2035	1.22	1.12	1.28
NSR-17	89	914	H-F	0.462	2443	2087	1815	1972	1.17	1.35	1.24
NSR-18	100	610	H-H	0.335	4063	3040	2792	2841	1.34	1.46	1.43
NSR-19	100	711	H-H	0.391	3690	2989	2681	2751	1.23	1.38	1.34
NSR-20	100	813	H-F	0.357	3785	3021	2748	2805	1.25	1.38	1.35
NSR-21	100	914	H-F	0.402	3460	2978	2659	2732	1.16	1.30	1.27
NSR-22	114	610	H-H	0.334	N/A*	4889	4492	4782	N/A*	N/A*	N/A*
NSR-23*	114	711	H-H	0.389	N/A*	4809	4316	4634	N/A*	N/A*	N/A*
NSR-24*	114	813	H-F	0.356	N/A*	4859	4422	4723	N/A*	N/A*	N/A*
NSR-25*	114	914	H-F	0.401	N/A*	4791	4279	4604	N/A*	N/A*	N/A*

* The load reached the capacity of the MTS machine (4500 kN).

Table 4.9 Results of testing to-collapse 8 non-stress-relieved steel solid rounds

Specimen number	Diameter (mm)	Length (mm)	End condition	Load rate (kN/sec.)	KL/r	Experimental failure load (kN)
NSR-26	38	1219	H-F	0.13	91	225
NSR-27	38	1118	H-F	0.13	83	245
NSR-28	51	1118	H-F	0.24	62	580
NSR-29	64	1118	H-F	0.38	49	1191
NSR-30	76	1016	H-F	0.53	38	1531
NSR-31	89	1016	H-F	0.73	32	2363
NSR-32	102	1016	H-F	0.95	28	3372
NSR-33	114	1016	H-F	1.19	25	N/A*

* The load reached the capacity of the MTS machine (4500 kN).

Table 4.10 Comparison between the experimental finding and available Code equations for 8 non-stress-relieved steel bars using the theoretical buckling length

Specimen number	Diameter (mm)	Length (mm)	End condition	λ	Experimental failure load (kN)	Theoretical failure load (kN)				Experimental failure /theoretical failure load ratio		
						AISC-LRFD	CSA-S37-01	Euro		AISC-LRFD	CSA-S37-01	Euro
NSR-26	38	1219	H-F	1.15	225	223	199	178		1.01	1.13	1.43
NSR-27	38	1118	H-F	1.05	245	243	219	197		1.01	1.12	1.24
NSR-28	51	1118	H-F	0.836	580	580	543	498		1.00	1.07	1.16
NSR-29	64	1118	H-F	0.689	1191	1002	790	894		1.19	1.50	1.33
NSR-30	76	1016	H-F	0.484	1531	1316	1132	1236		1.16	1.35	1.24
NSR-31	89	1016	H-F	0.453	2363	2094	1827	1982		1.13	1.29	1.19
NSR-32	102	1016	H-F	0.395	3372	2985	2673	2870		1.13	1.26	1.17
NSR-33	114	1016	H-F	0.393	N/A*	4802	4302	4615		N/A	N/A	N/A

* The load reached the capacity of the MTS machine (4500 kN).

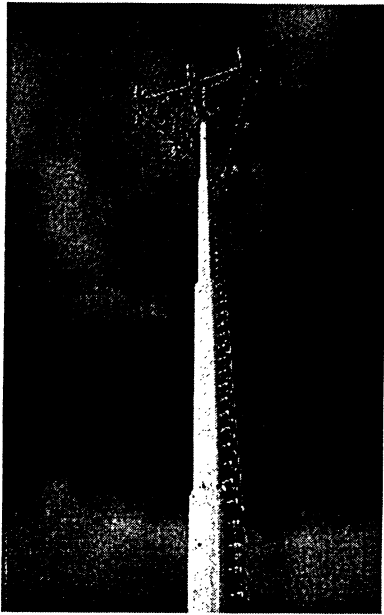
Table 4.11 Comparison between the experimental finding and available Code equations for 8 non-stress-relieved steel bars using practical buckling length

Specimen number	Diameter (mm)	Length (mm)	End condition	KL/r	Experimental failure load (kN)	Theoretical failure load (kN)			Experimental failure /theoretical failure load ratio		
						AISC-LRFD	CSA-S37-01	Euro	AISC-LRFD	CSA-S37-01	Euro
NSR-26	38	1219	H-F	1.300	225	191	170	151	1.18	1.32	1.49
NSR-27	38	1118	H-F	1.192	245	214	190	170	1.14	1.29	1.44
NSR-28	51	1118	H-F	0.946	580	535	489	445	1.08	1.19	1.30
NSR-29	64	1118	H-F	0.780	1191	948	723	825	1.26	1.65	1.44
NSR-30	76	1016	H-F	0.548	1531	1280	1071	1184	1.20	1.43	1.29
NSR-31	89	1016	H-F	0.514	2363	2044	1737	1907	1.16	1.36	1.24
NSR-32	102	1016	H-F	0.447	3372	2931	2566	2780	1.15	1.31	1.21
NSR-33	114	1016	H-F	0.445	N/A*	4716	4130	4474	N/A	N/A	N/A

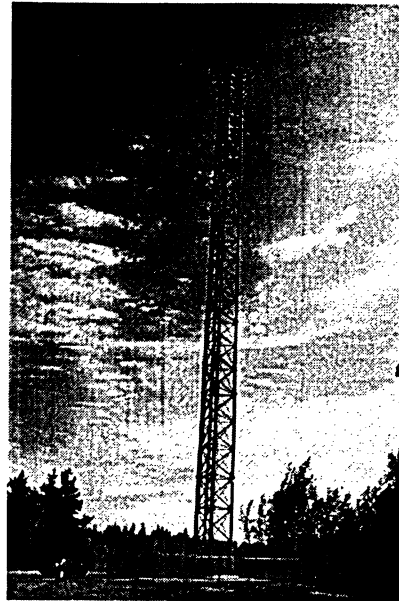
* The load reached the capacity of the MTS machine (4500 kN).

Table 4.12 Stub column test results for non-stress-relieved steel solid rounds

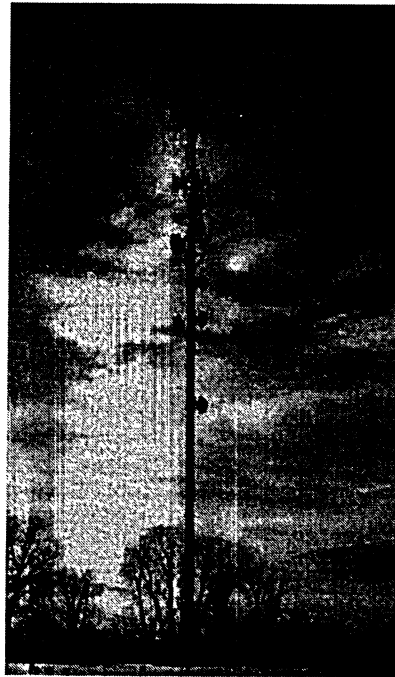
Specimen number	Diameter (mm)	Length (mm)	End condition	Load rate (kN/sec.)	KL/r	Experimental failure load (kN)
SC-1	38	152	H-H	0.13	16	813
SC-2	51	203	H-H	0.24	16	1377
SC-3	64	254	H-H	0.38	16	1754
SC-4	76	305	H-H	0.53	16	2549
SC-5	89	356	H-H	0.73	16	4112
SC-6	102	406	H-H	0.95	16	3873
SC-7	114	457	H-H	1.19	16	4500



a- Monopoles (up to 70 m)



b- Self-supporting towers (up to 120 m)



c- Guyed towers (up to 620 m)

Figure 1.1 Views of communication towers



Figure 1.2 Close-up view of tower segment

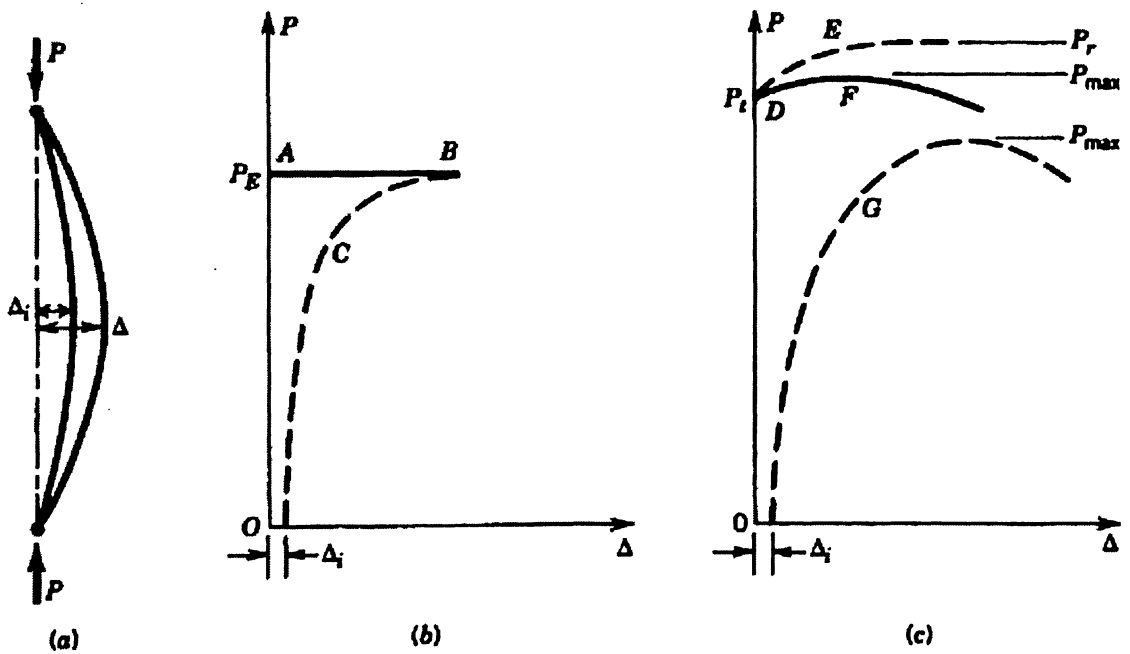


Figure 2.1 Behavior of perfect and imperfect columns (Galambos, 1998)

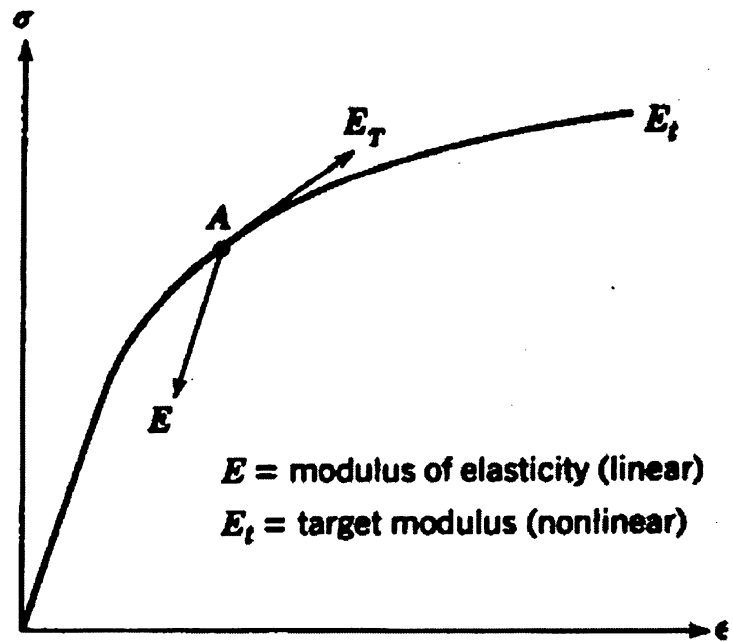


Figure 2.2 General stress-strain relationship (Galambos, 1998)

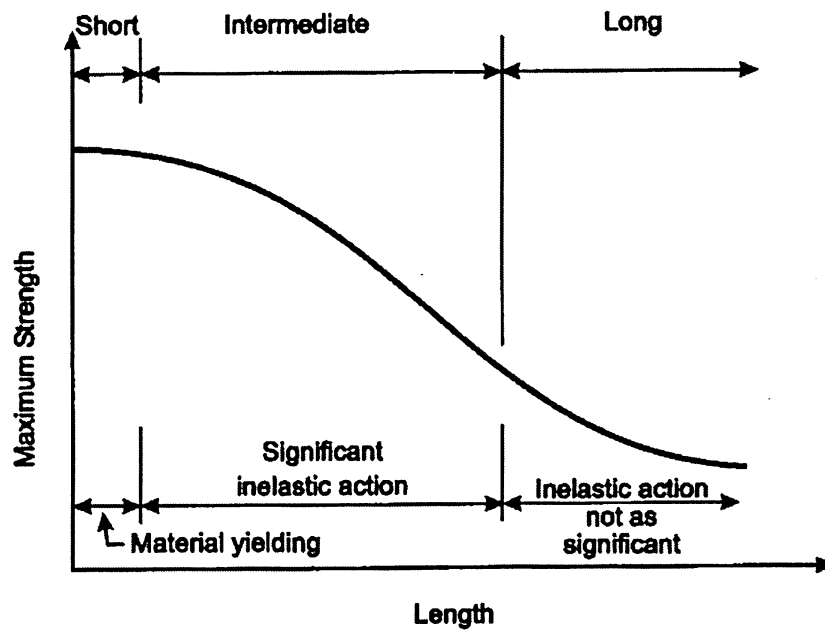


Figure 2.3 Column curve

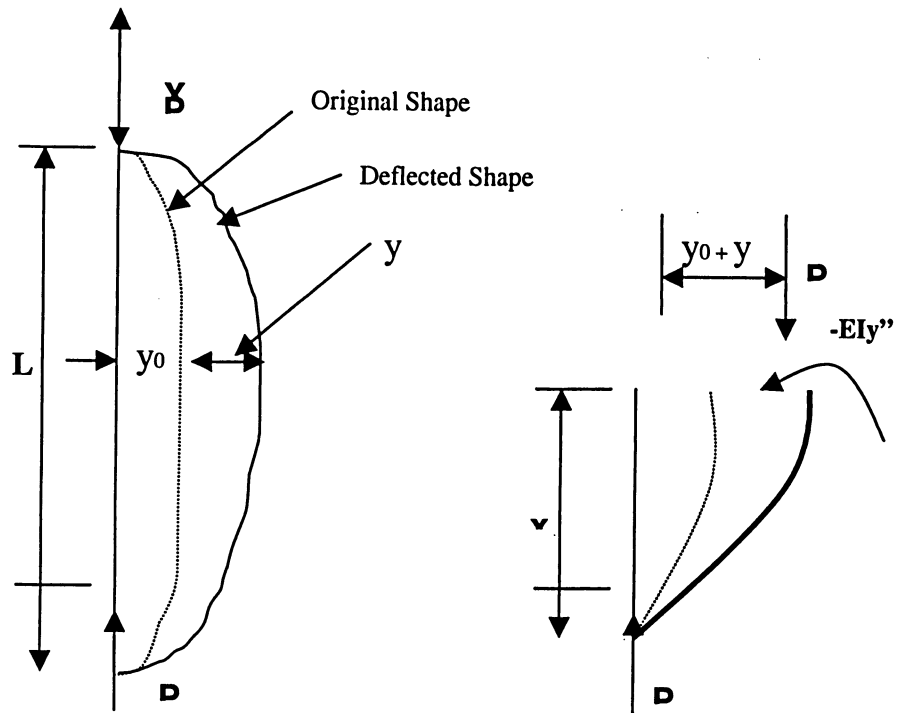

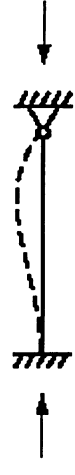
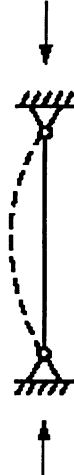
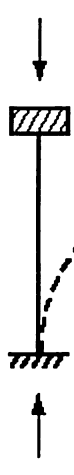
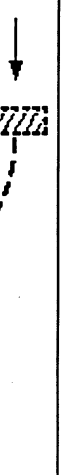



Figure 2.4 Initially bent column

Buckled shape of column is shown by dashed line	(a)	(b)	(c)	(d)	(e)	(f)
						
	0.5	0.7	1.0	1.0	2.0	2.0
Recommended design value when ideal conditions are approximated	0.65	0.80	1.0	1.2	2.0	2.0





End condition code		Rotation fixed, translation fixed
		Rotation free, translation fixed
		Rotation fixed, translation free
		Rotation free, translation free

Figure 2.5 Effective length factor (CAN/CSA S16-01, 2003)

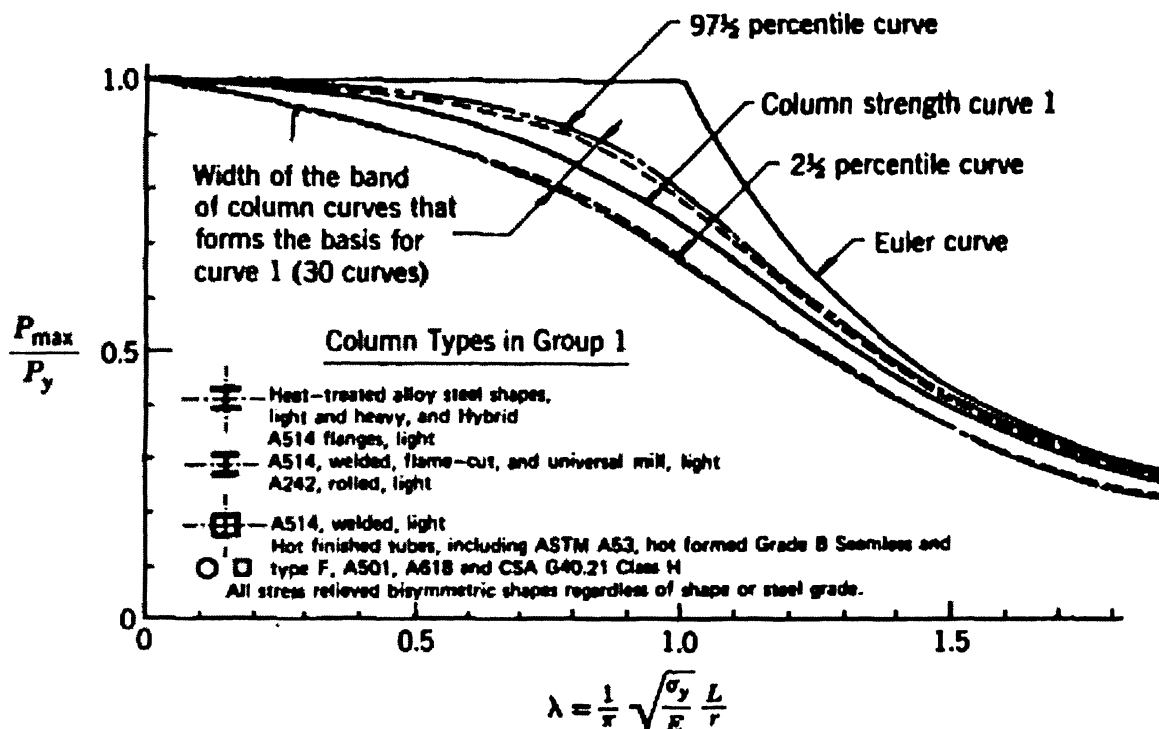


Figure 2.6 SSRC column strength curve 1 for structural steel (Bjordhovde, 1972), (Based on maximum strength and initial out-of-straightness of $L/1000$)

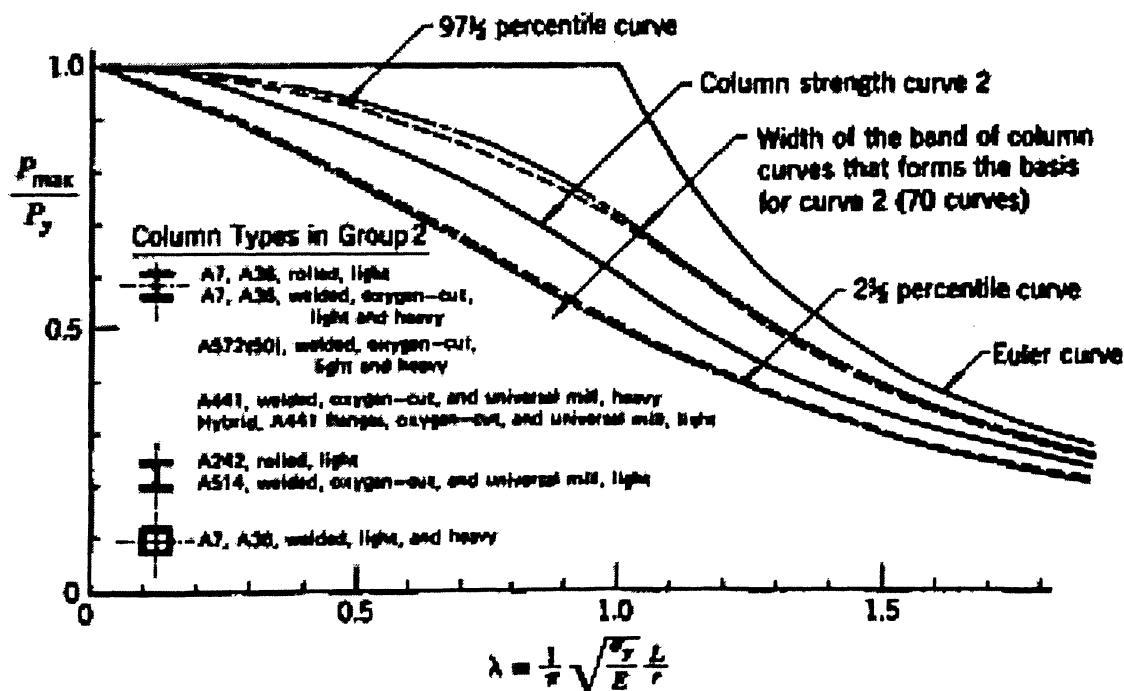


Figure 2.7 SSRC column strength curve 2 for structural steel (Bjordhovde, 1972), (Based on maximum strength and initial out-of-straightness of $L/1000$)

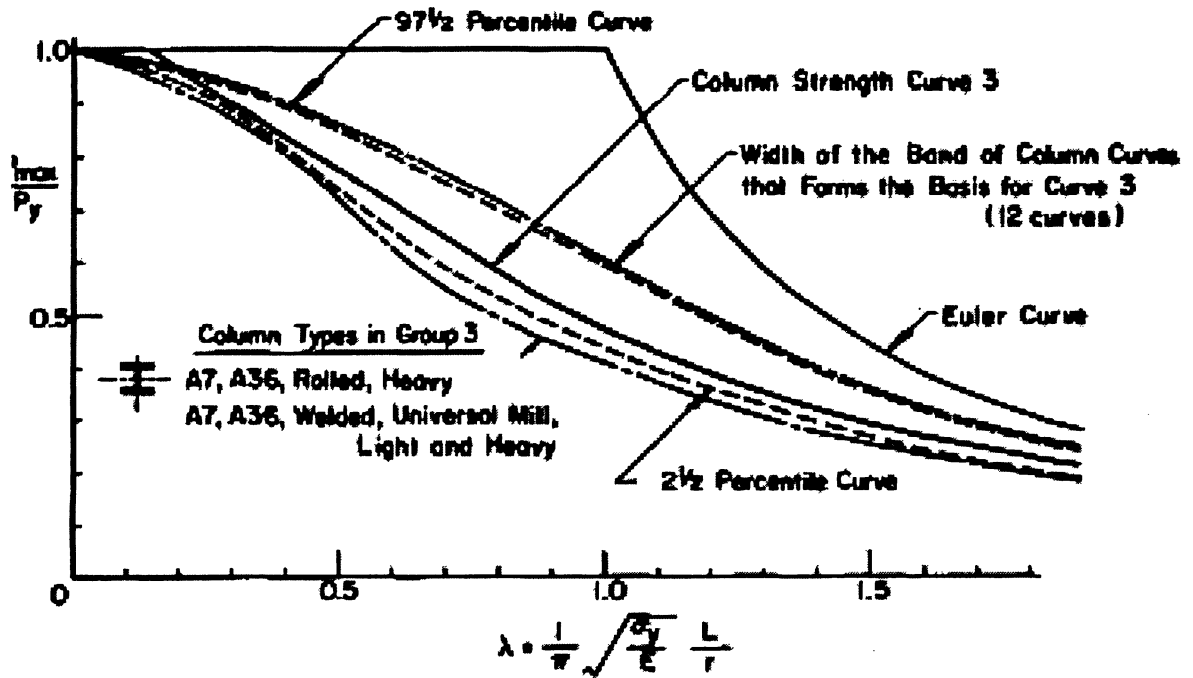


Figure 2.8 SSRC column strength curve 3 for structural steel (Bjordhovde, 1972), (Based on maximum strength and initial out-of-straightness of $L/500$)

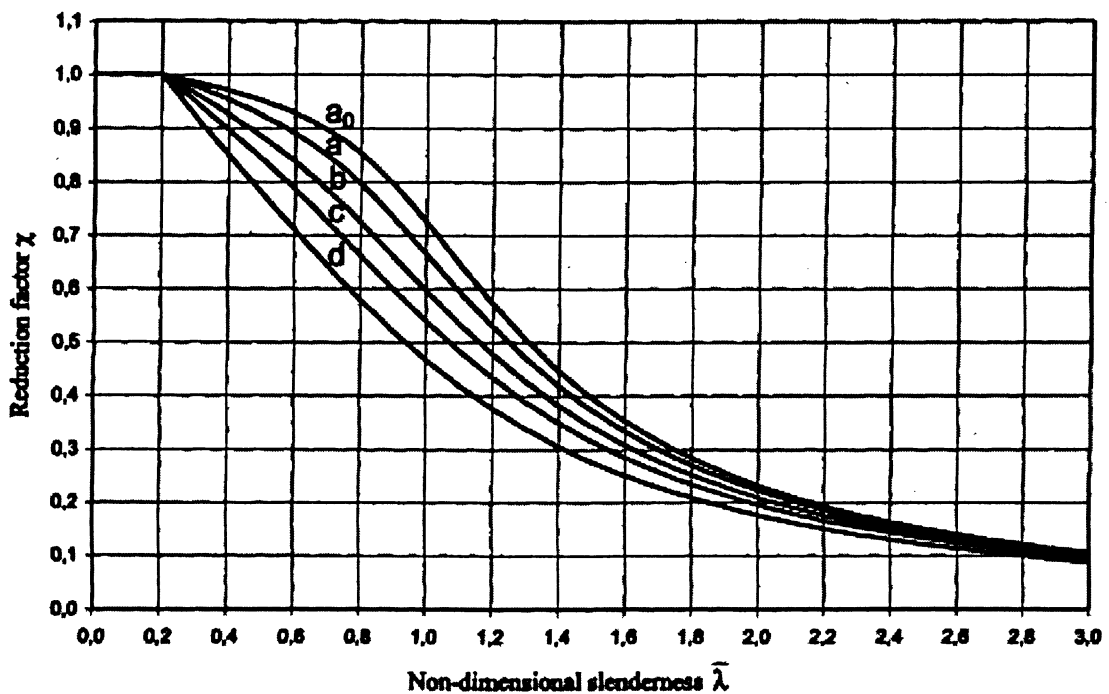


Figure 2.9 Buckling curves (Eurocode 3, 2003)



Figure 3.1 View of the MTS machine

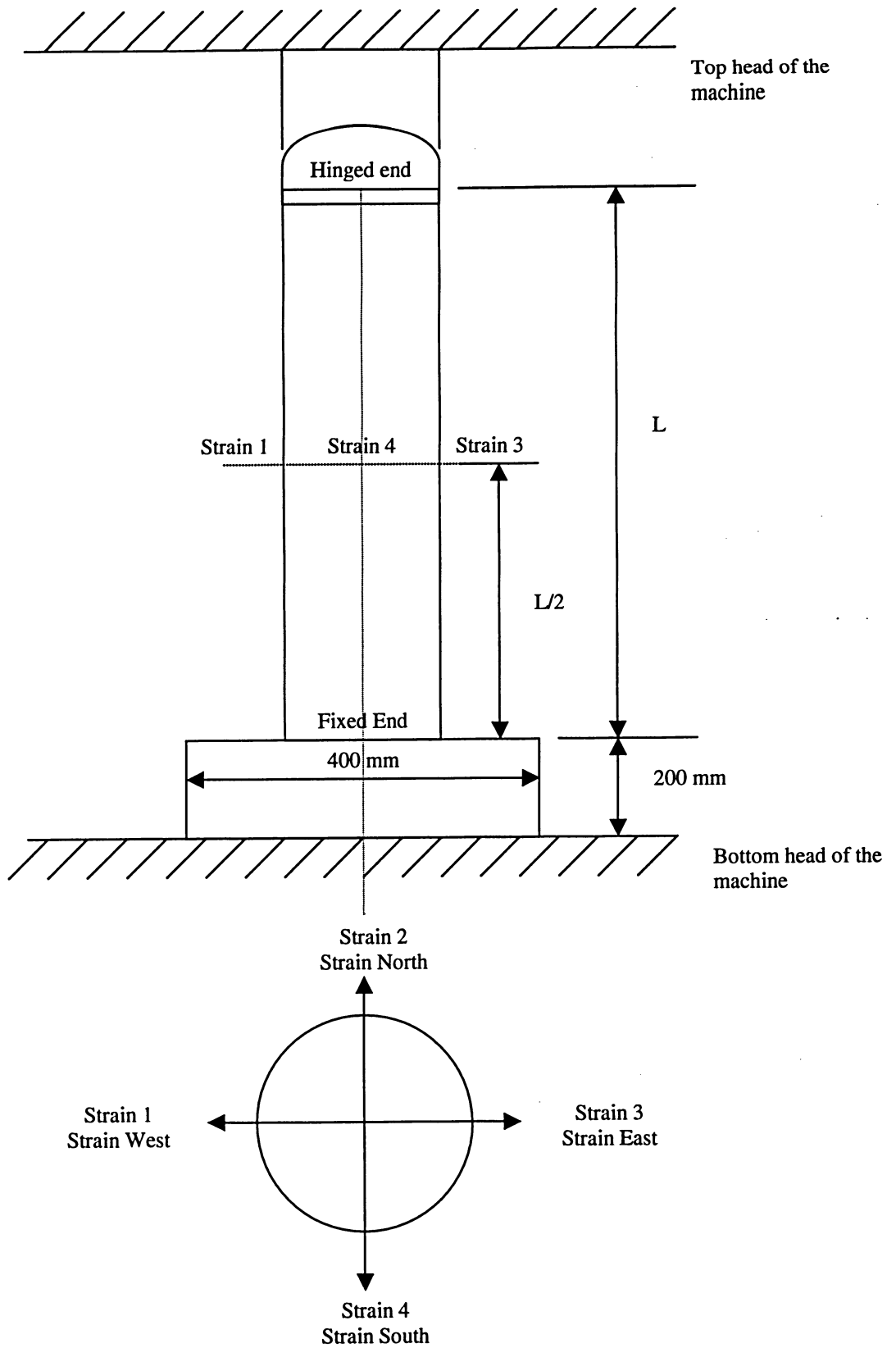
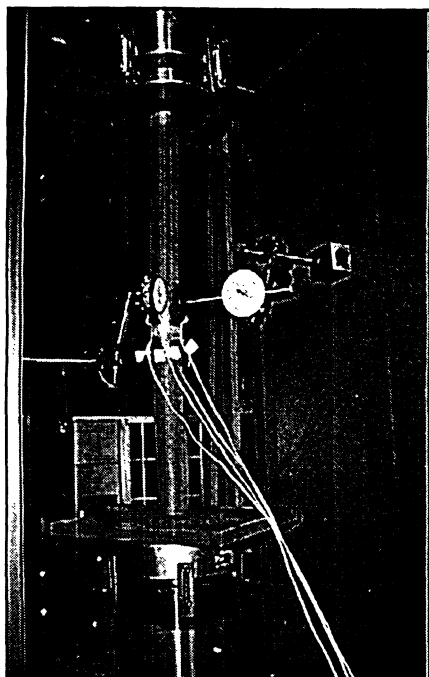
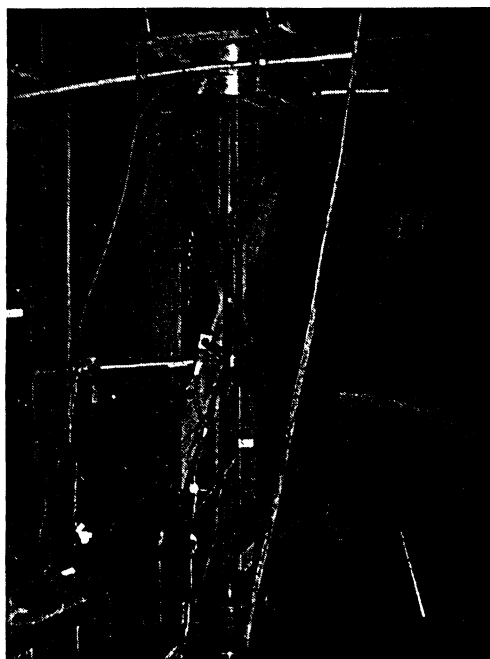


Figure 3.2 Schematic diagram of the specimen setup and strain gauge locations



(a)



(b)

Figure 3.3 Test set-ups for axial resistance of solid rounds

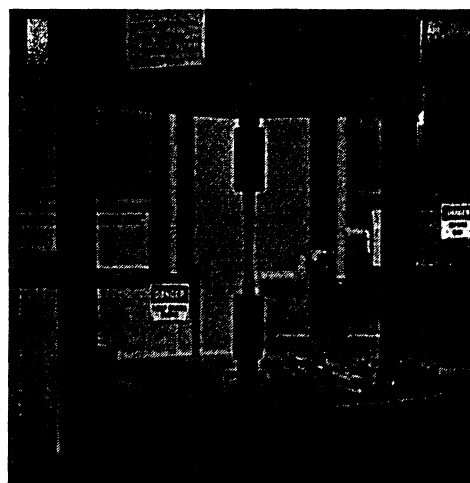
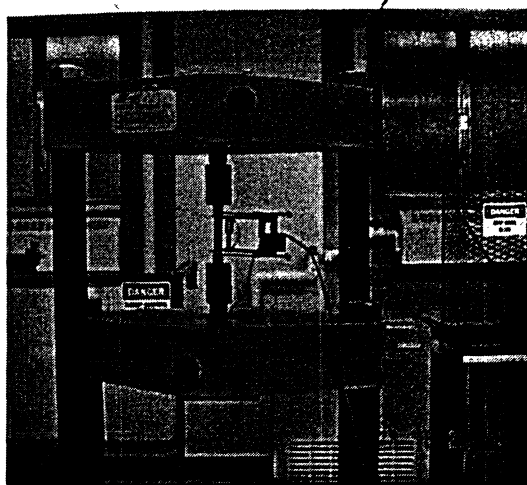


Figure 3.4 Test set up for tension coupon before and after failure

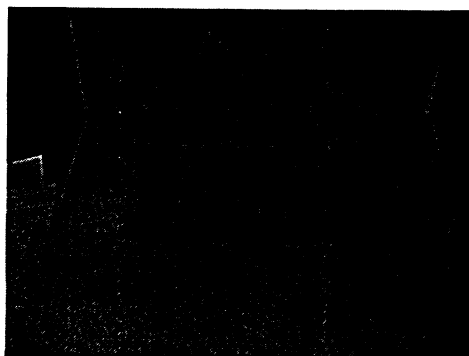
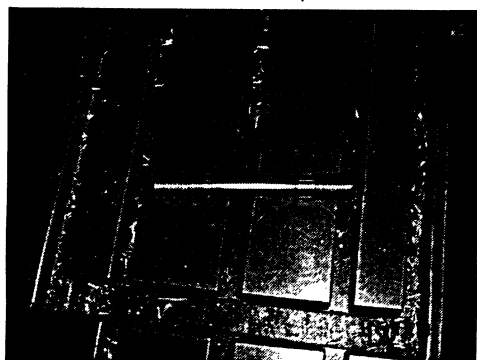
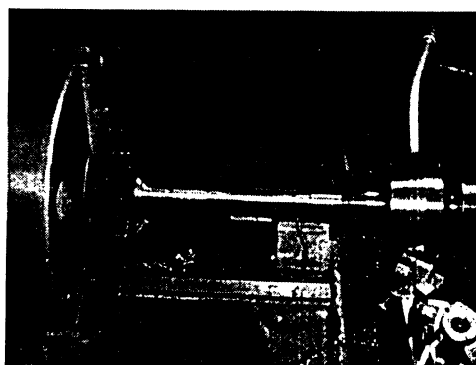
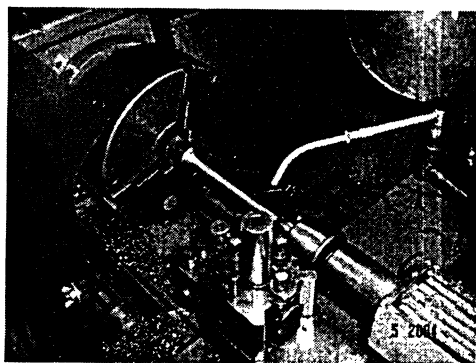
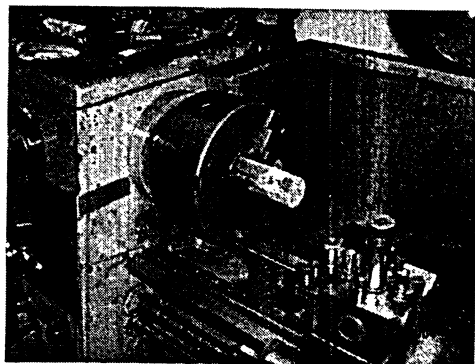


Figure 4.1 Views of coupon sample preparation procedure

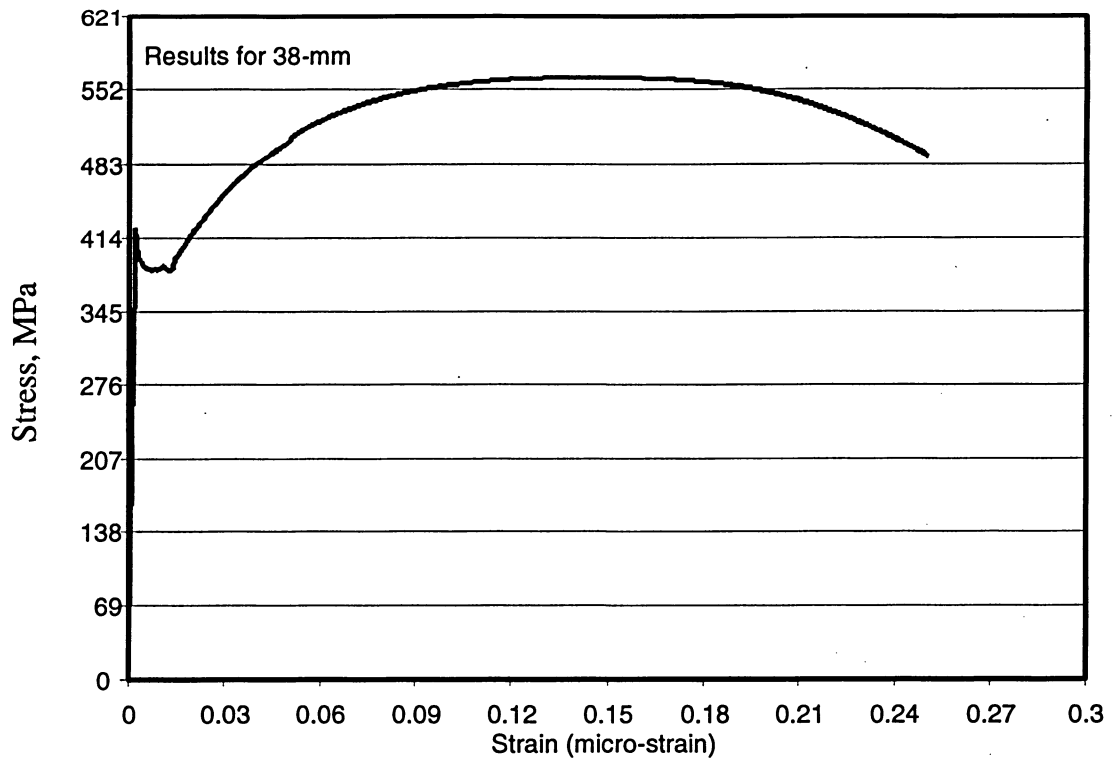


Figure 4.2 Stress-strain curve for the coupon sample of SR 38-mm bar

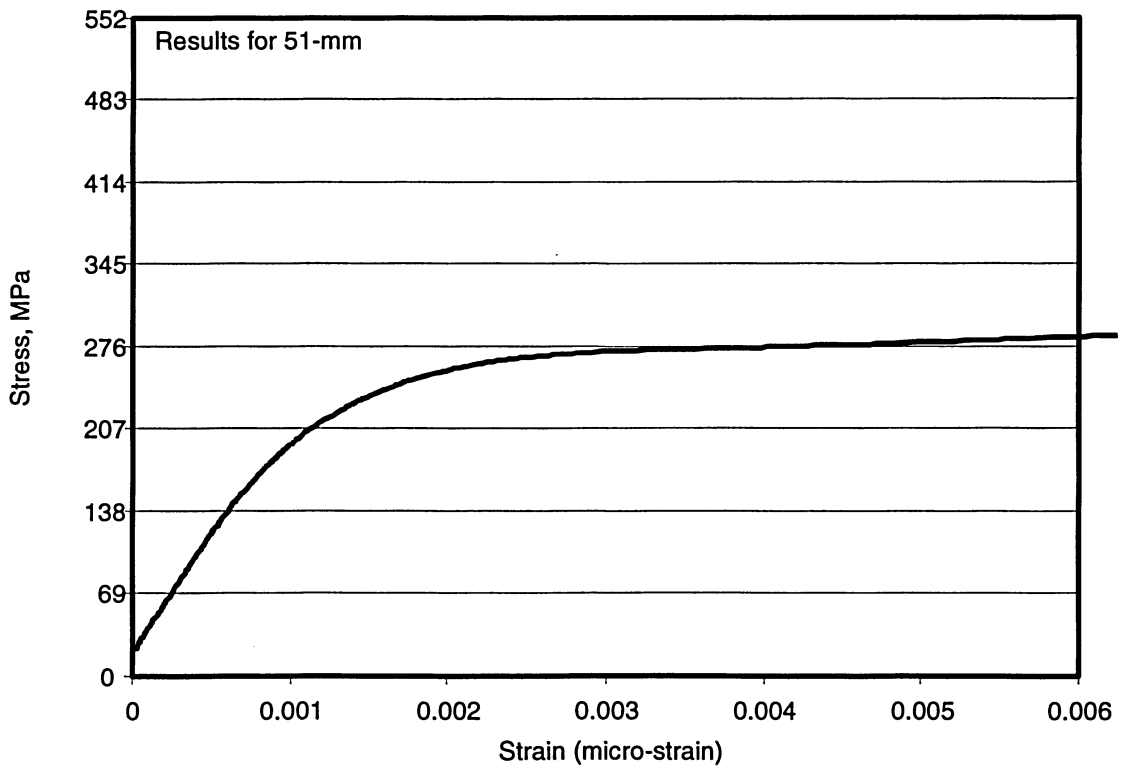


Figure 4.3 Initial part of the stress-strain curve for the coupon sample of SR 51-mm bar

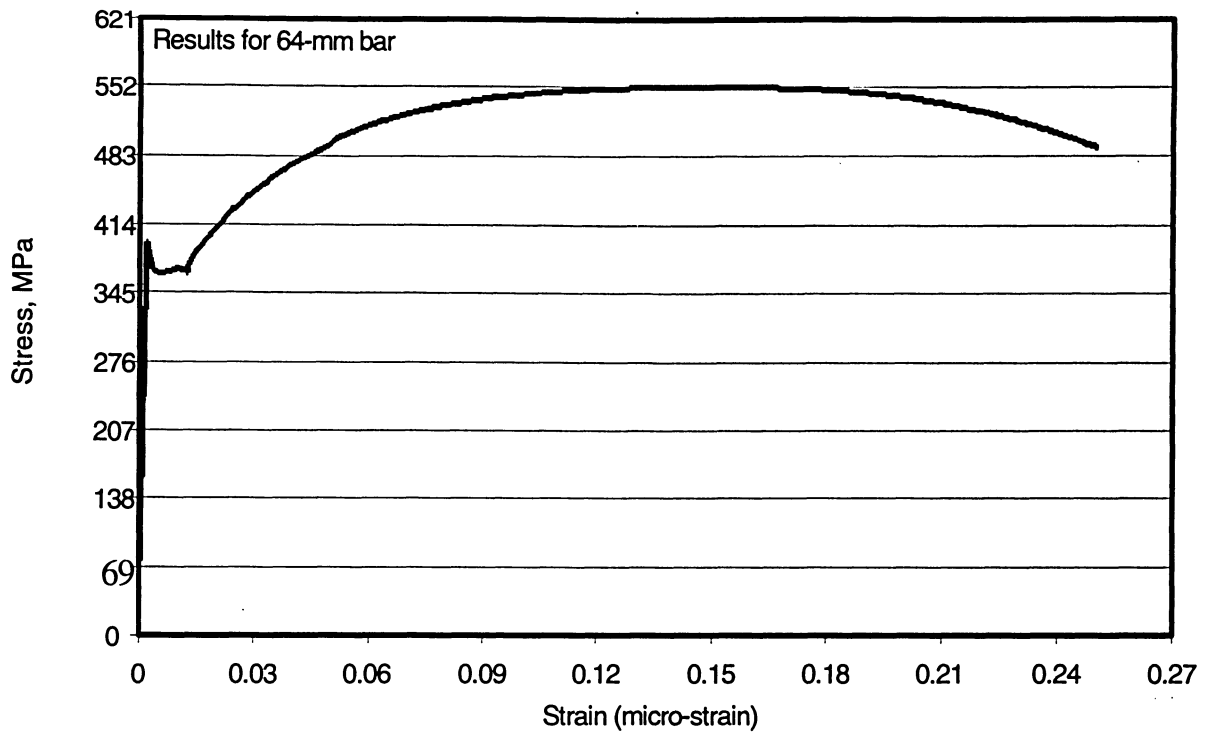


Figure 4.4 Stress-strain curve for the coupon sample of SR 64-mm bar

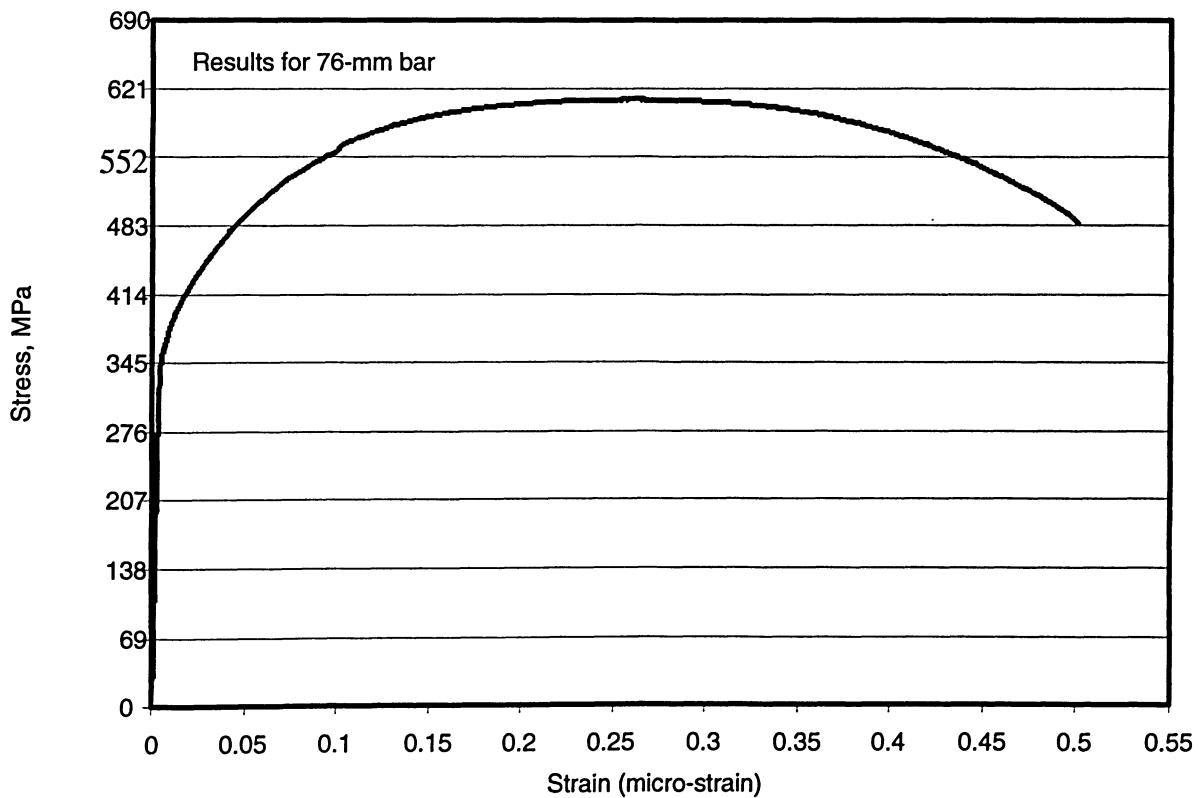


Figure 4.5 Stress-strain curve for the coupon sample of SR 76-mm bar

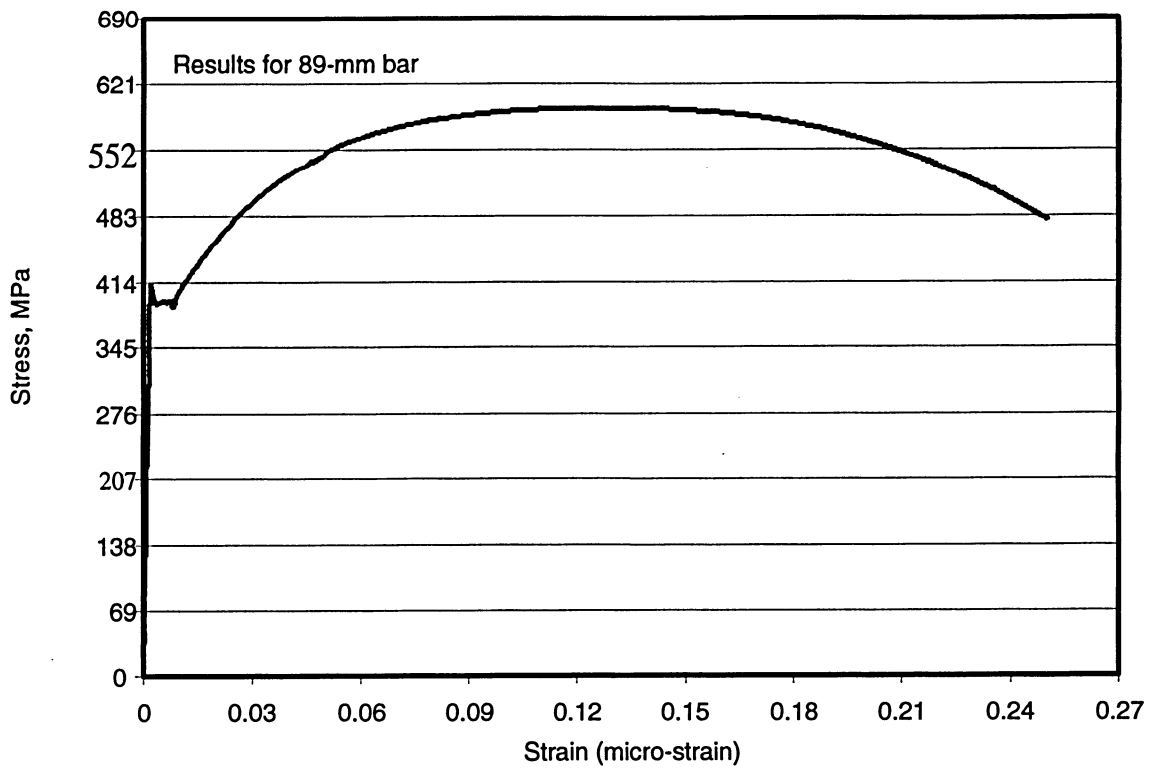


Figure 4.6 Stress-strain curve for the coupon sample of SR 89-mm bar

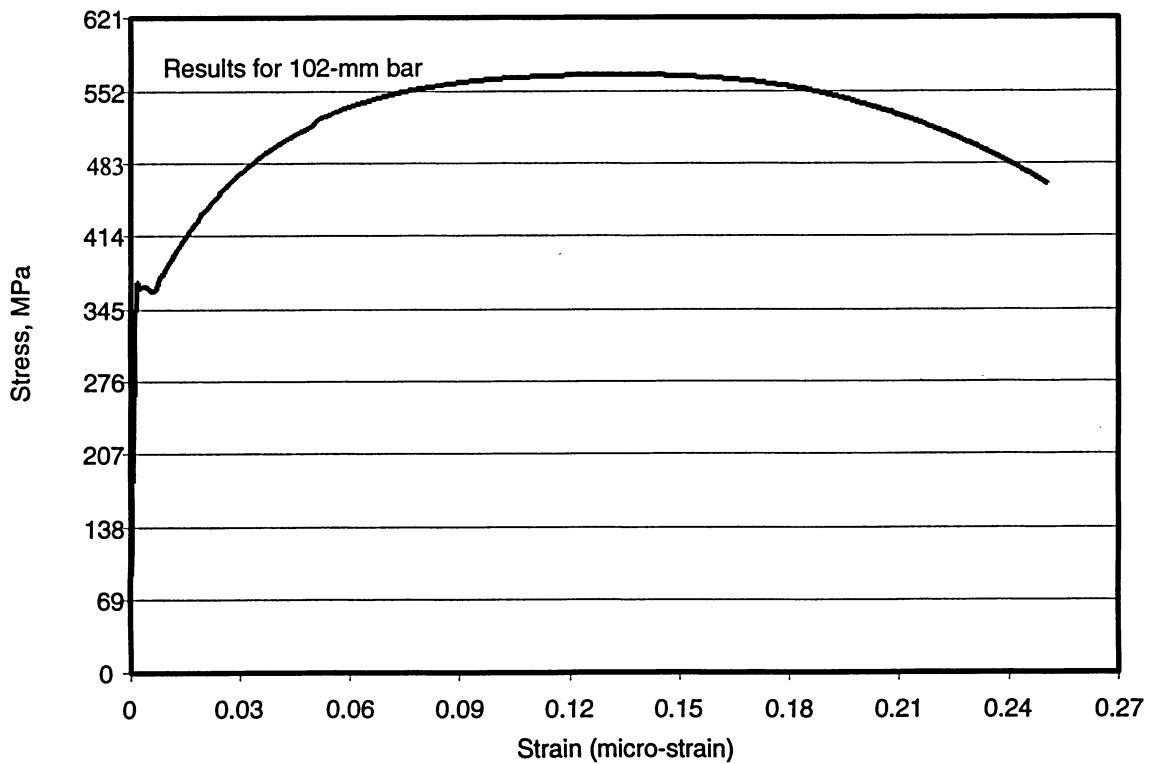


Figure 4.7 Stress-strain curve for the coupon sample of SR 102-mm bar

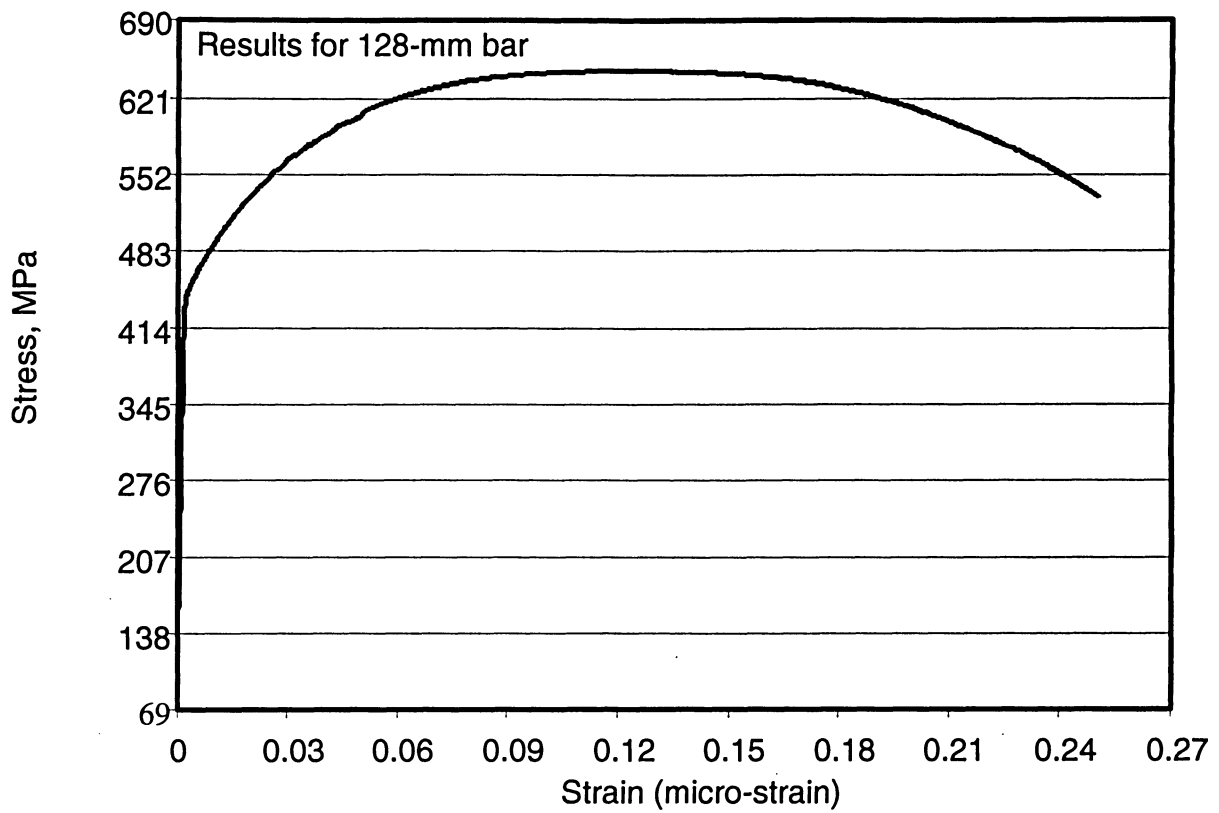


Figure 4.8 Stress-strain curve for the coupon sample of SR 128-mm bar

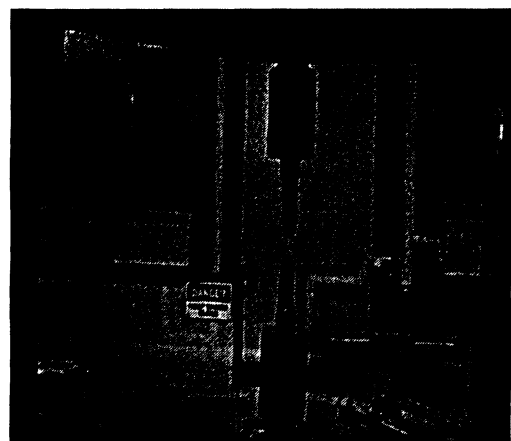
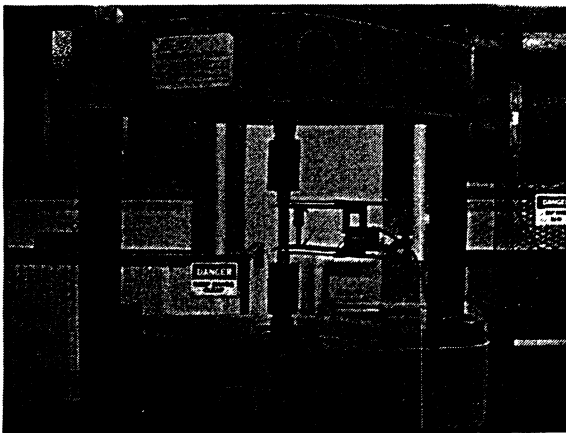


Figure 4.9 Views of the coupon sample for 38-mm bar before and after testing

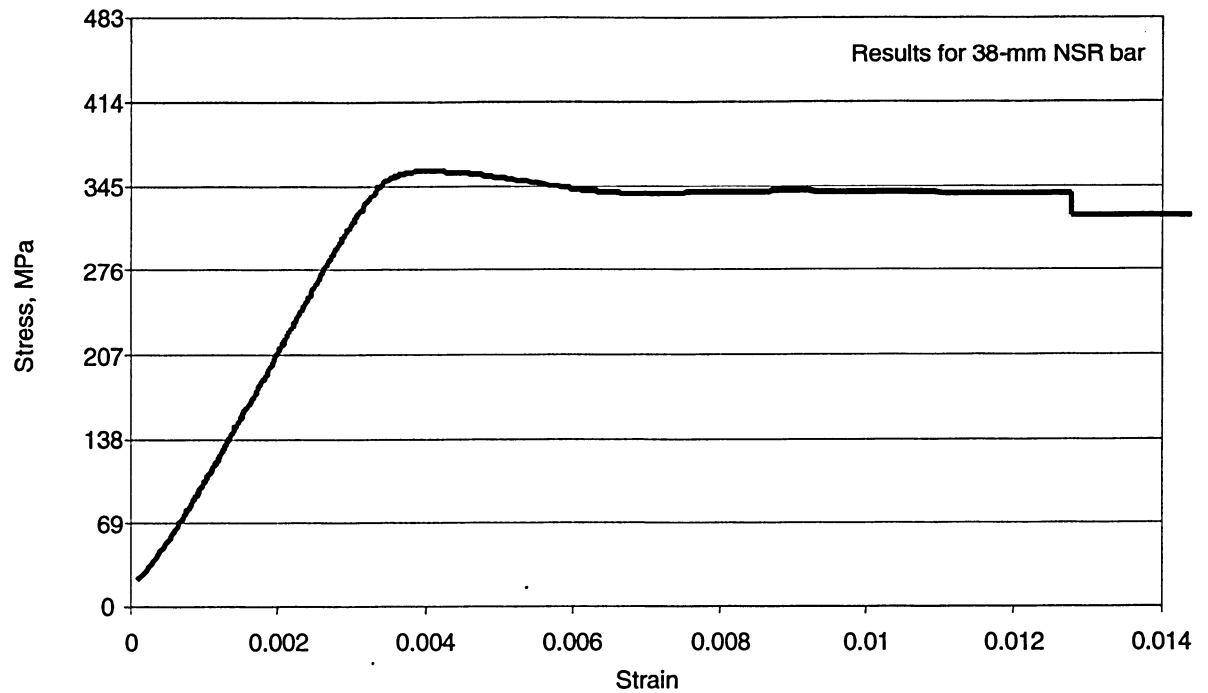


Figure 4.10 Initial portion of the stress-strain curve for the coupon sample of NSR 38-mm bar

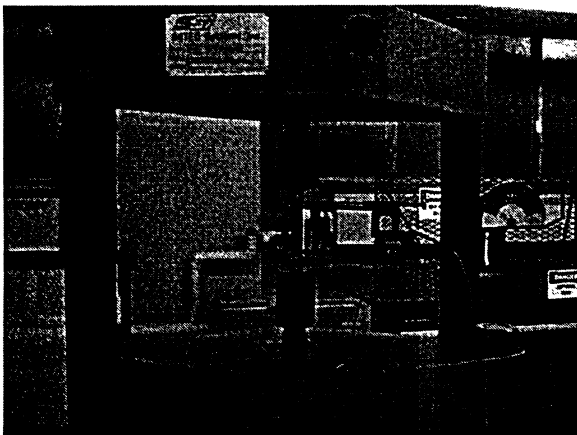


Figure 4.11 Views of the coupon sample for 51-mm bar before and after testing

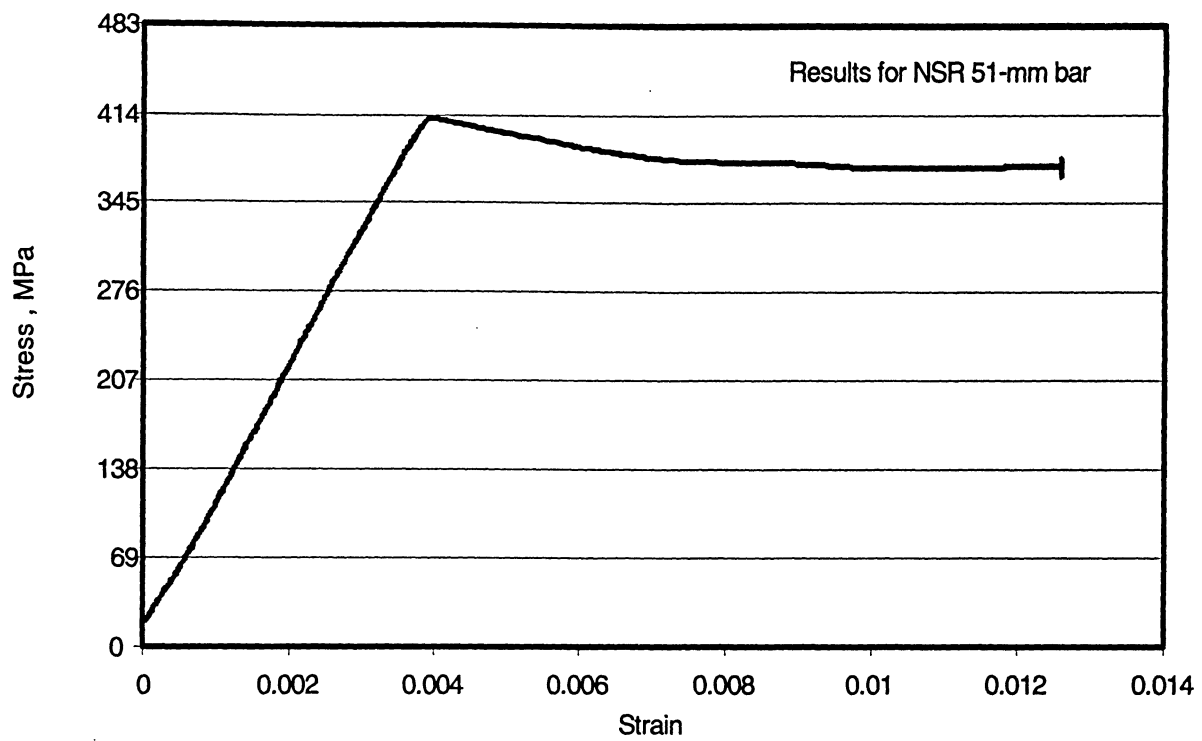


Figure 4.12 Initial part of the stress-strain curve for the coupon sample of NSR 51-mm bar

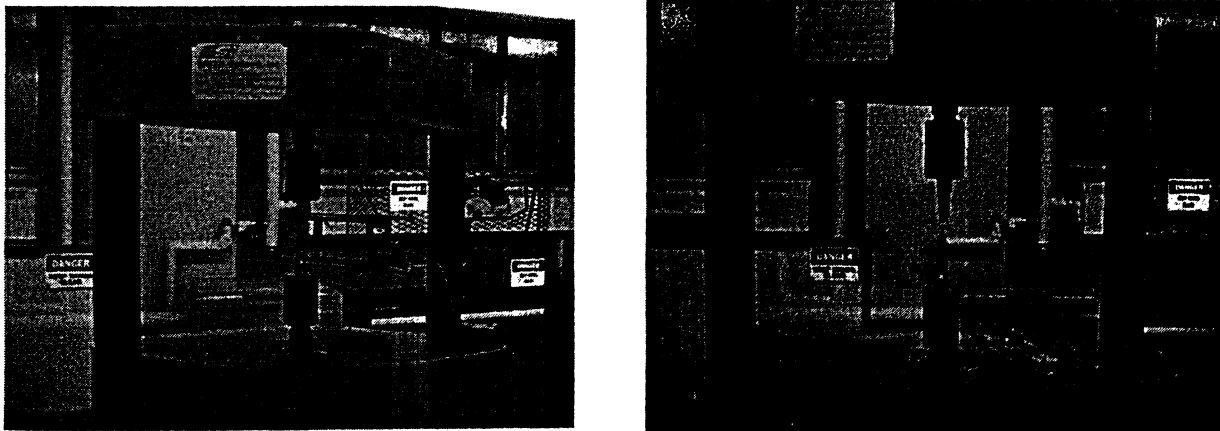


Figure 4.13 Views of the coupon sample for 64-mm bar before and after testing

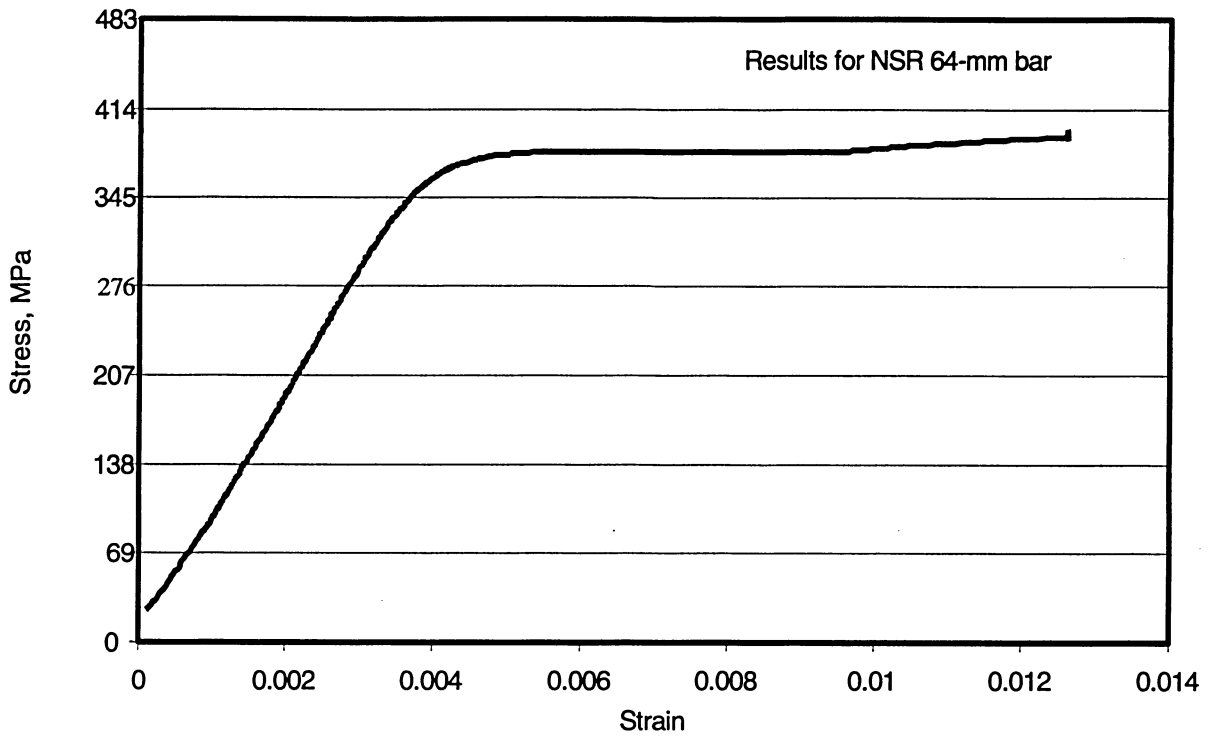


Figure 4.14 Initial part of the stress-strain curve for the coupon sample of NSR 64-mm bar

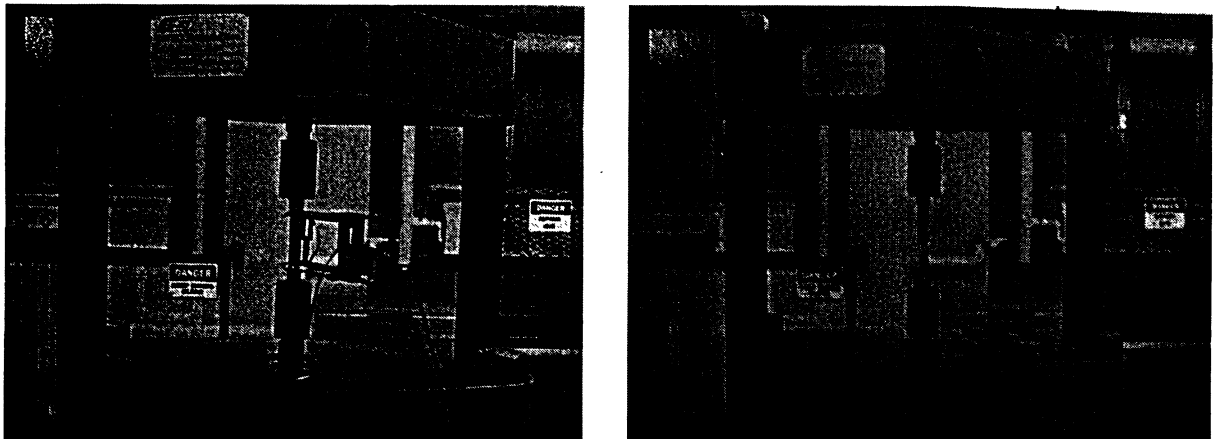


Figure 4.15 Views of the coupon sample for 76-mm bar before and after testing

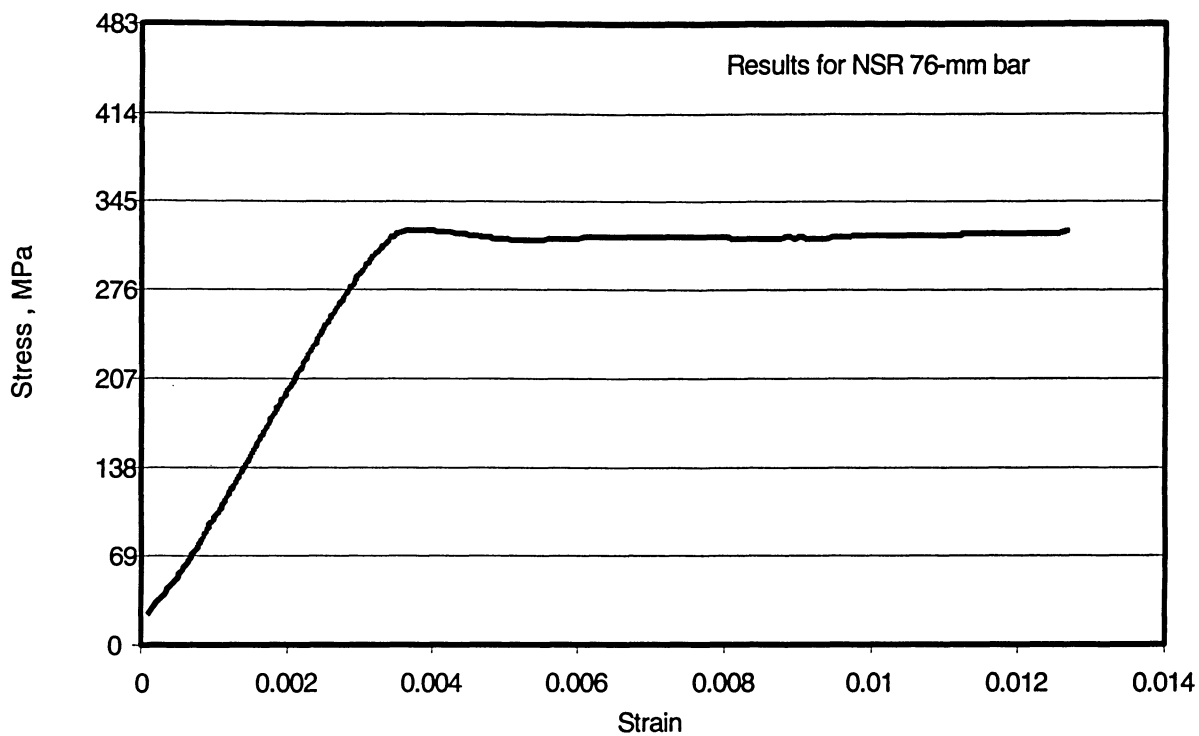


Figure 4.16 Initial portion of the stress-strain curve for the coupon sample of NSR 76-mm bar

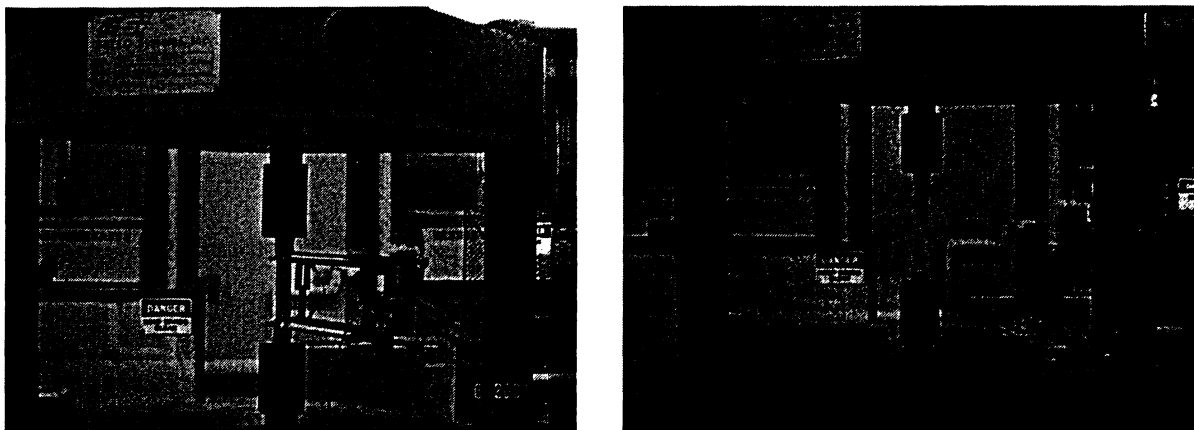


Figure 4.17 Views of the coupon sample for 89-mm bar before and after testing

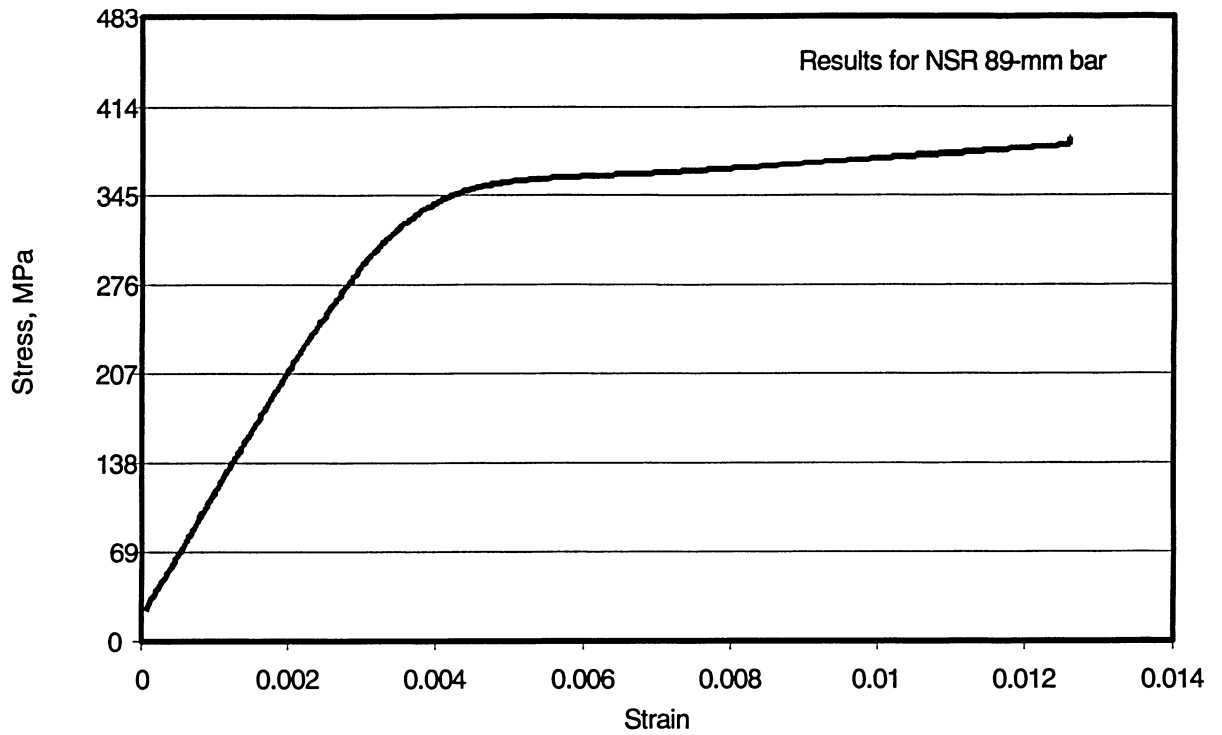


Figure 4.18 Initial part of the stress-strain curve for the coupon sample of NSR 89-mm bar

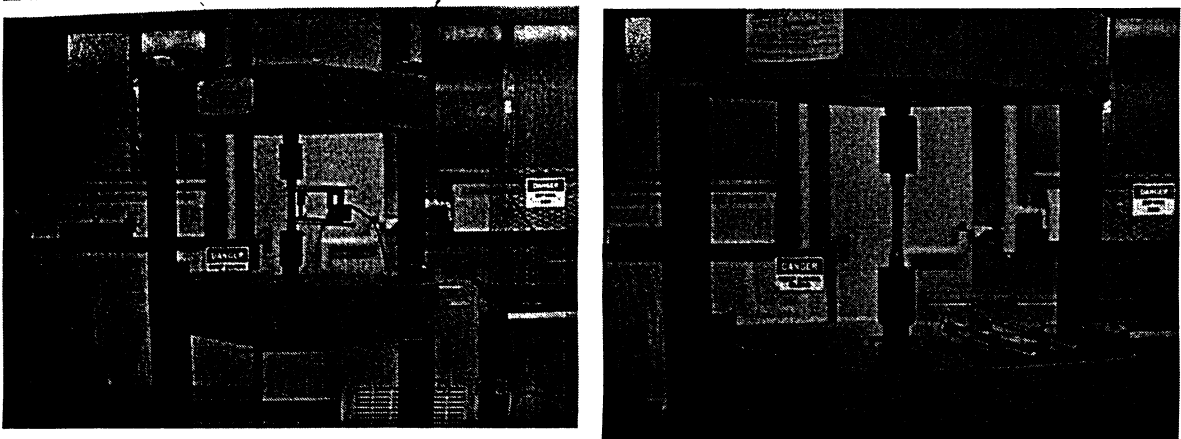


Figure 4.19 Views of the coupon sample for 102-mm bar before and after testing

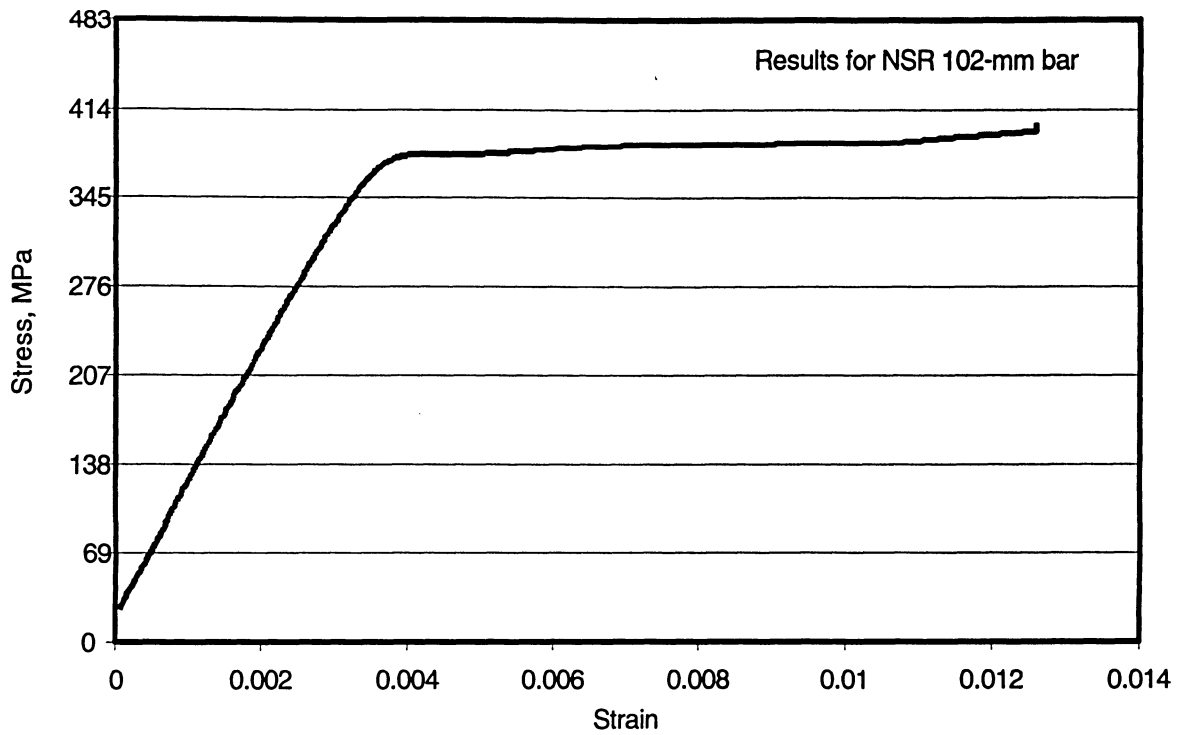
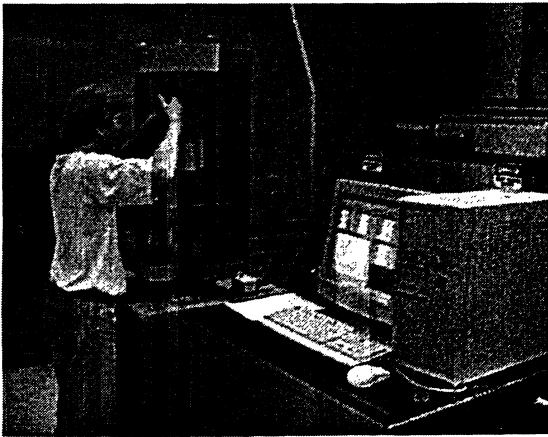


Figure 4.20 Initial portion of the stress-strain curve for the coupon sample of NSR 102-mm bar



114-mm bar before and after testing



Figure 4.21 Views of the coupon sample for

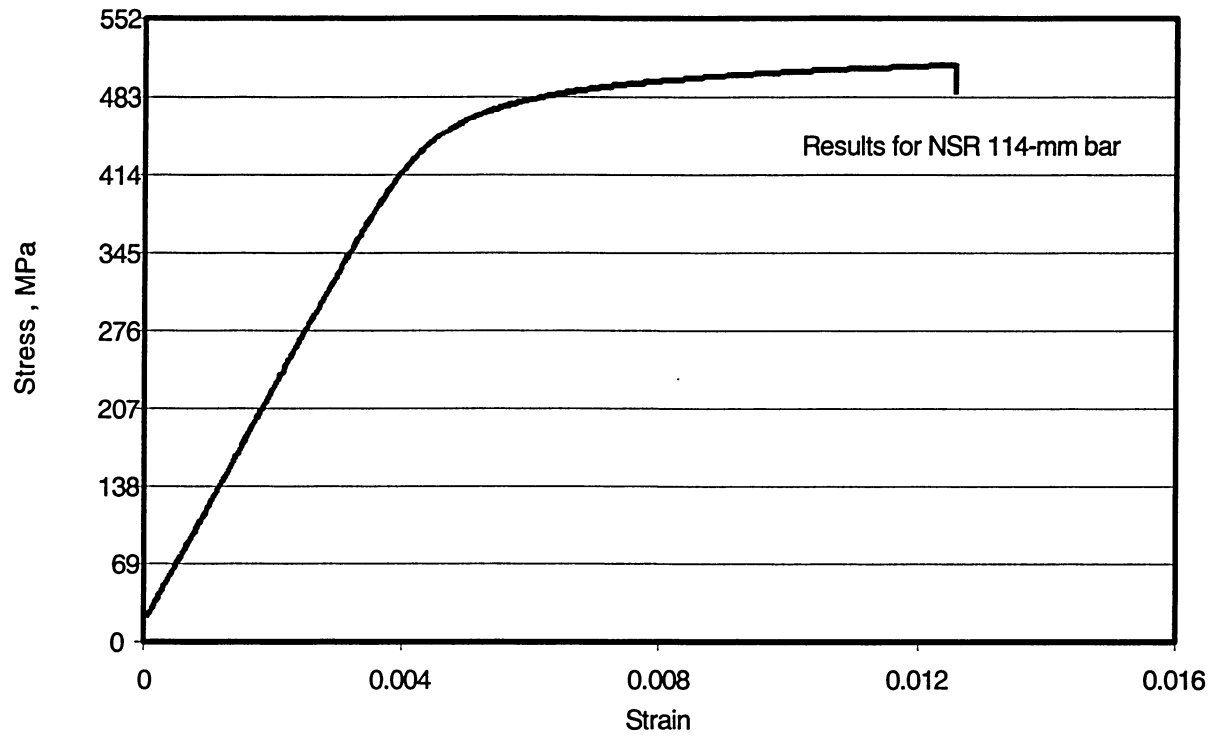


Figure 4.22 Initial part of the stress-strain curve for the coupon sample of NSR 114-mm bar

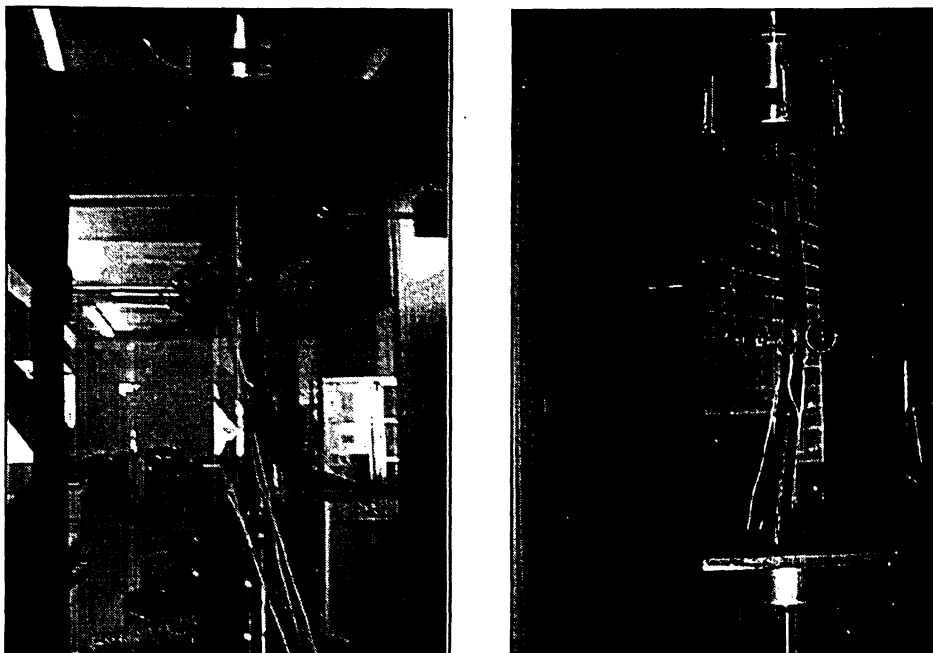


Figure 4.23 Views of specimen SR-1 before and after testing

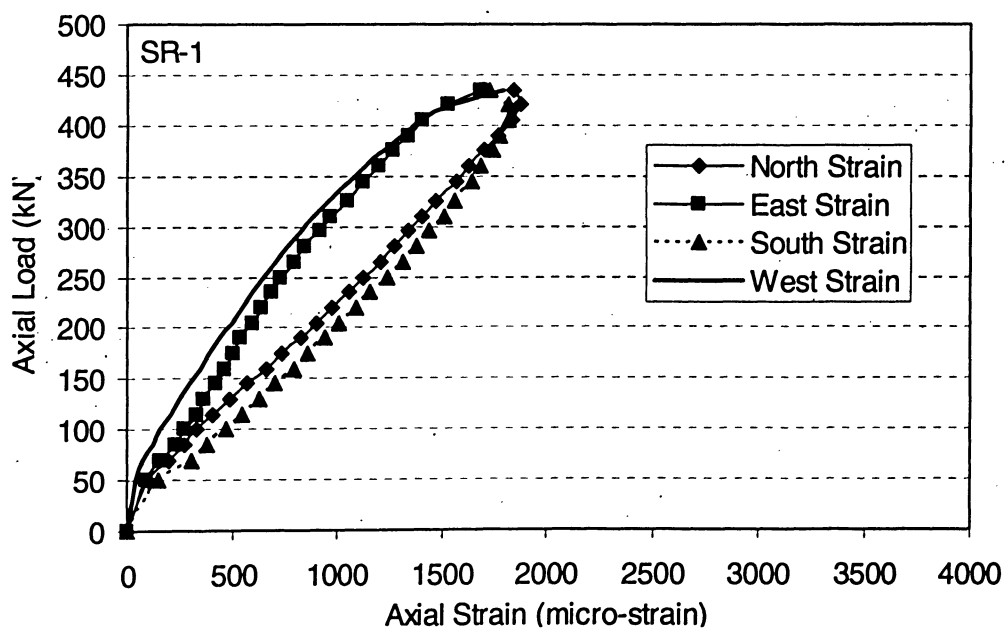


Figure 4.24 Axial load-strain relationships for specimen SR-1

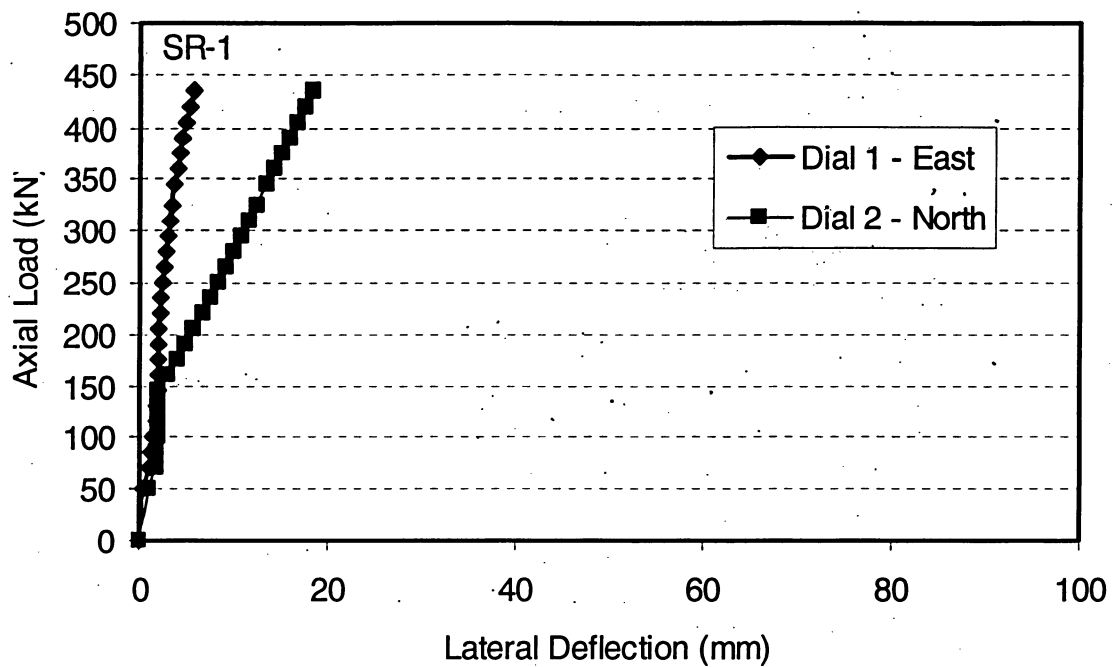


Figure 4.25 Load-lateral deflection curves for specimen SR-1

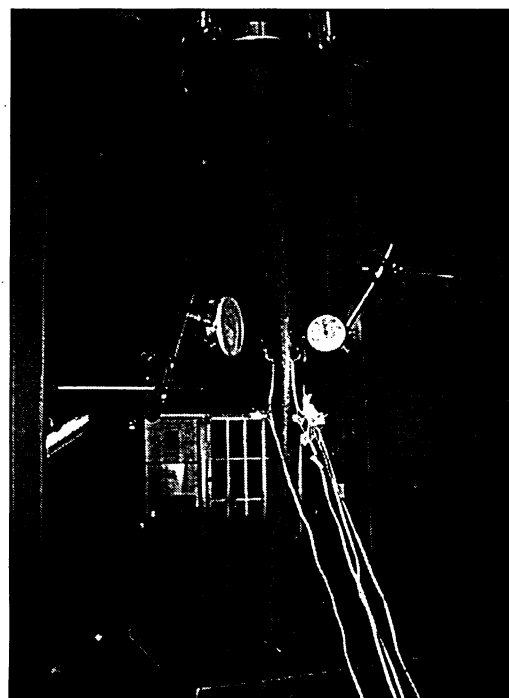
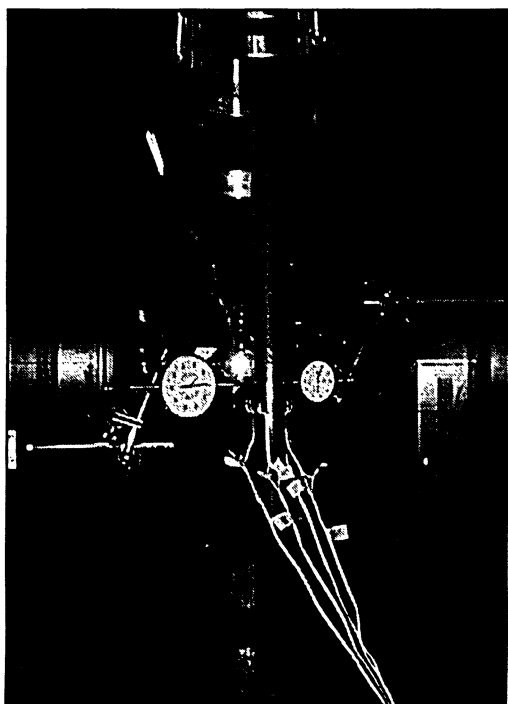


Figure 4.26 Views of specimen SR-2 before and after testing

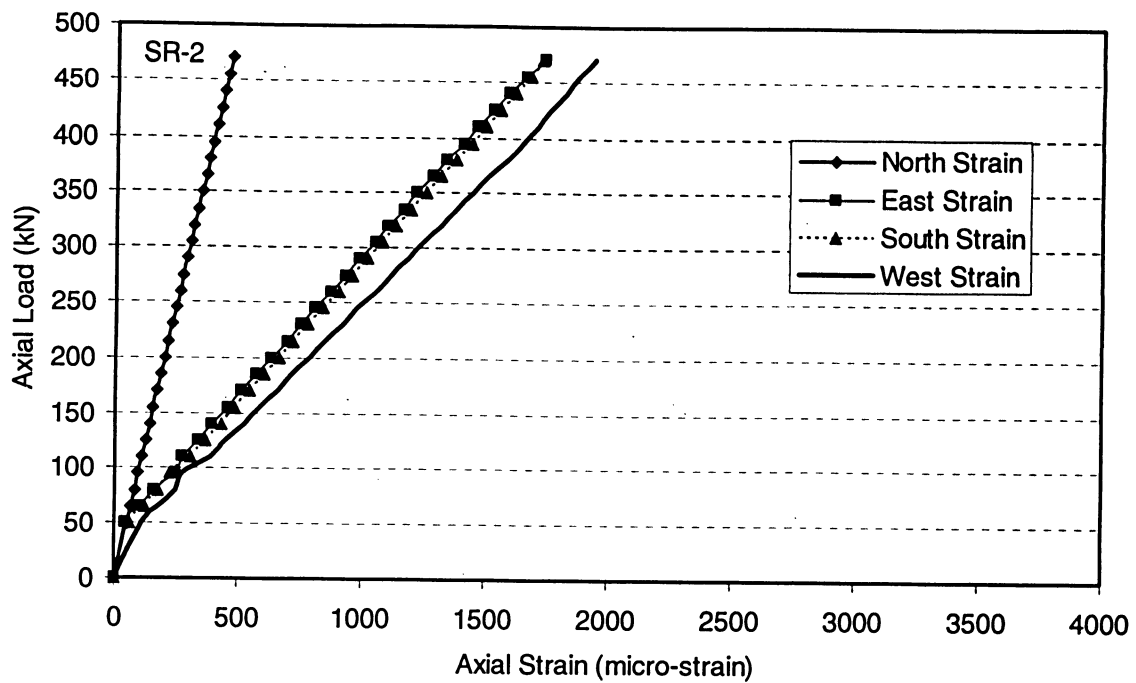


Figure 4.27 Axial load-strain relationships for specimen SR-2

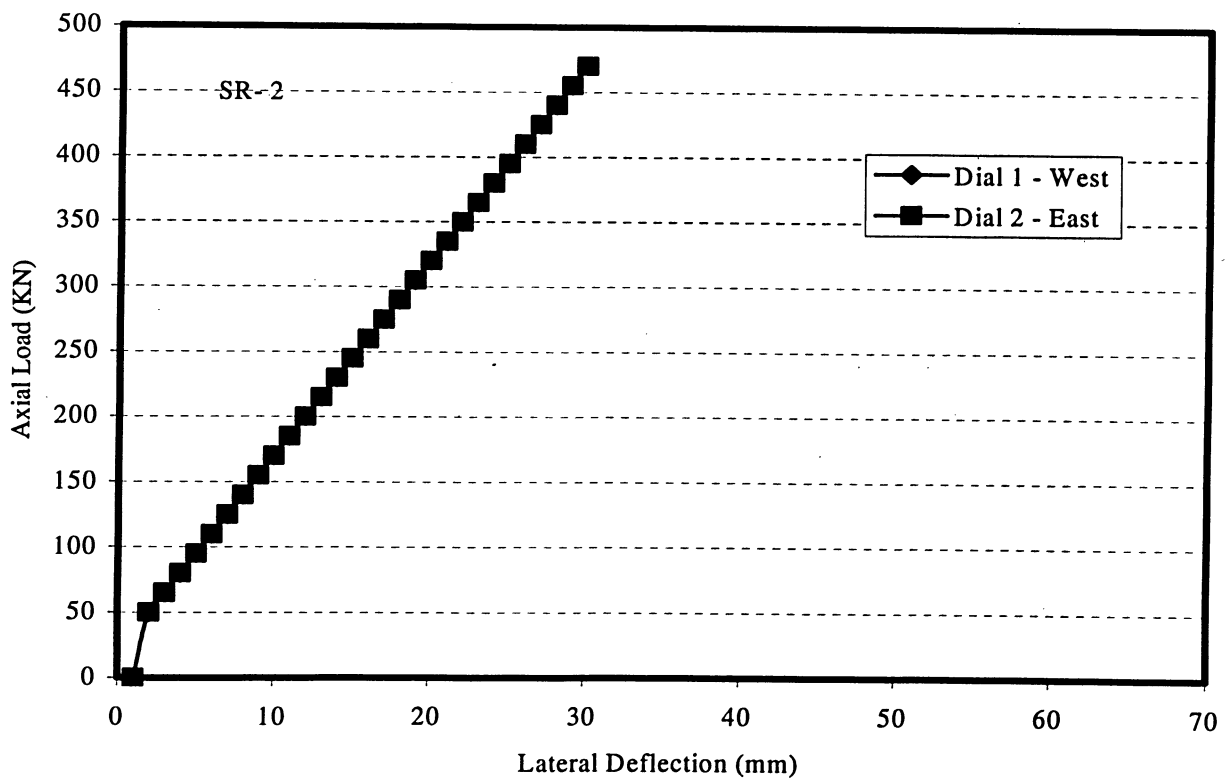


Figure 4.28 Load-lateral deflection curves for specimen SR-2

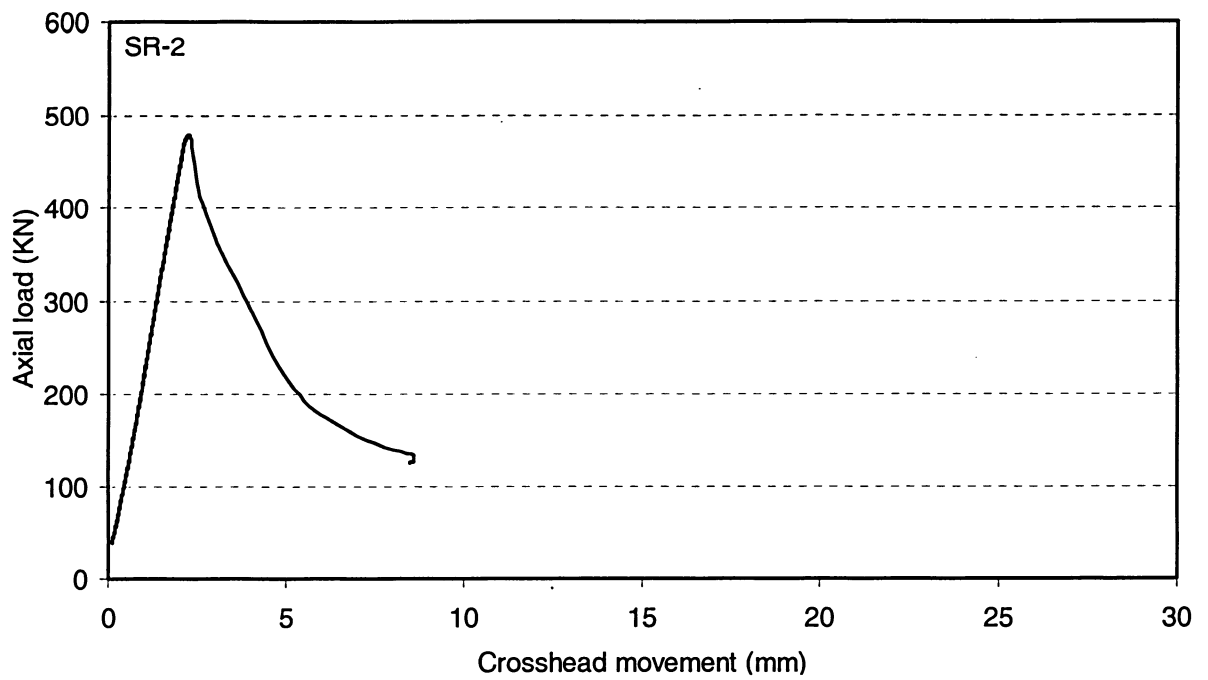


Figure 4.29 Load versus overall shortening curve for specimen SR-2

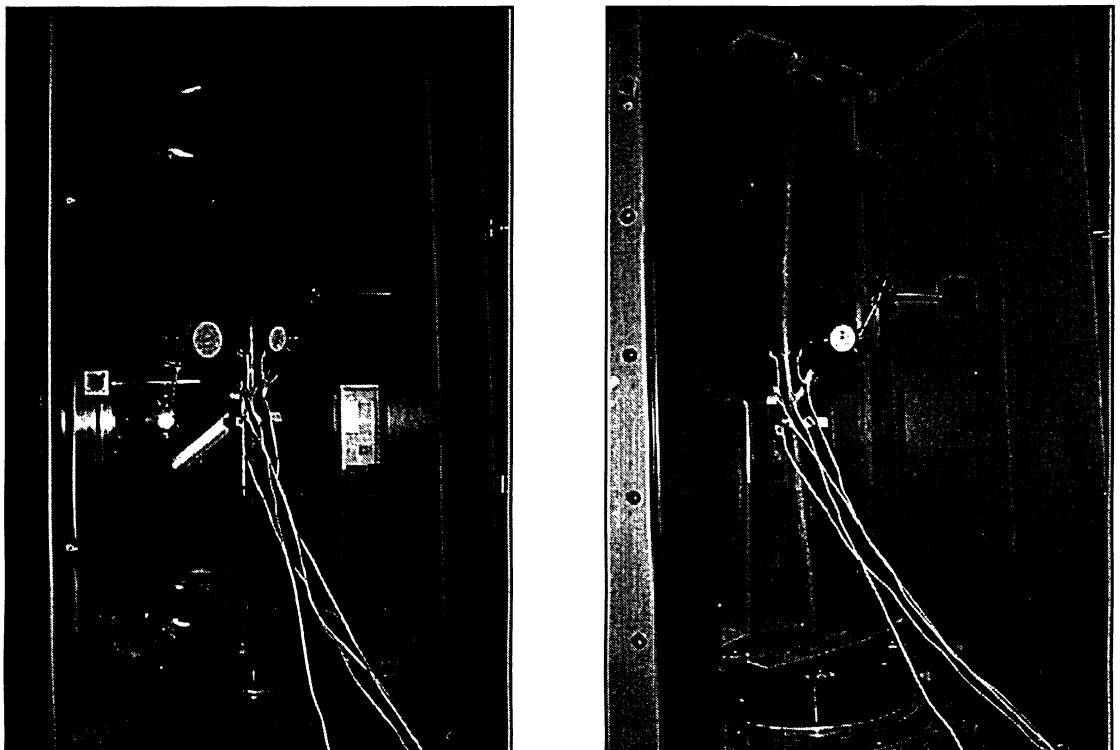


Figure 4.30 Views of specimen SR-3 before and after testing

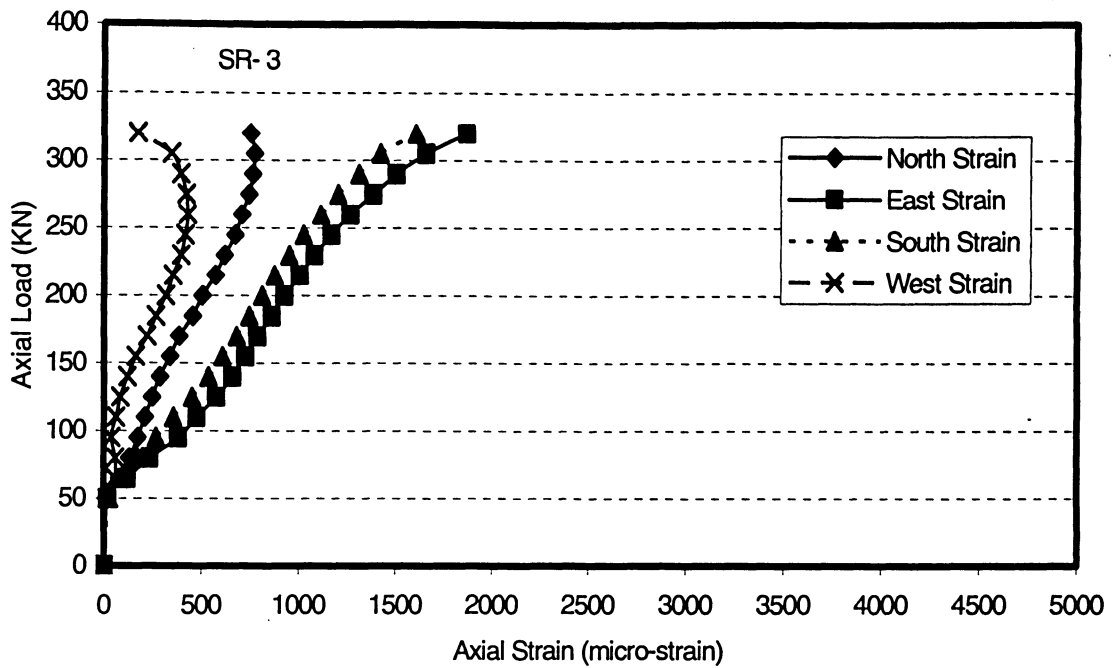


Figure 4.31 Axial load-strain relationships for specimen SR-3

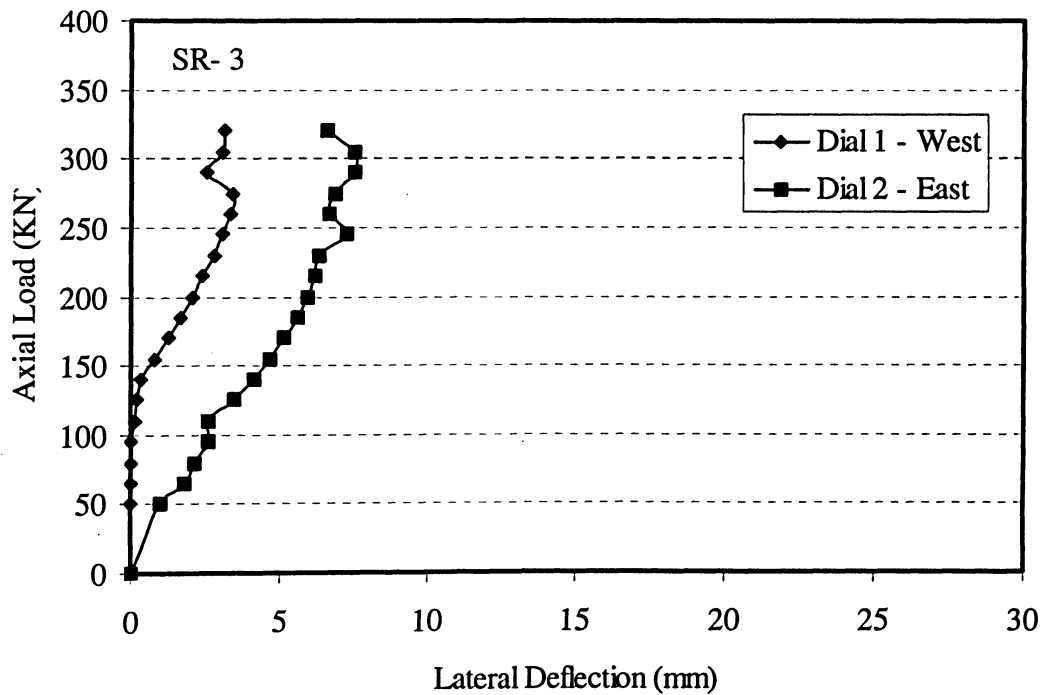


Figure 4.32 Load-lateral deflection curves for specimen SR-3

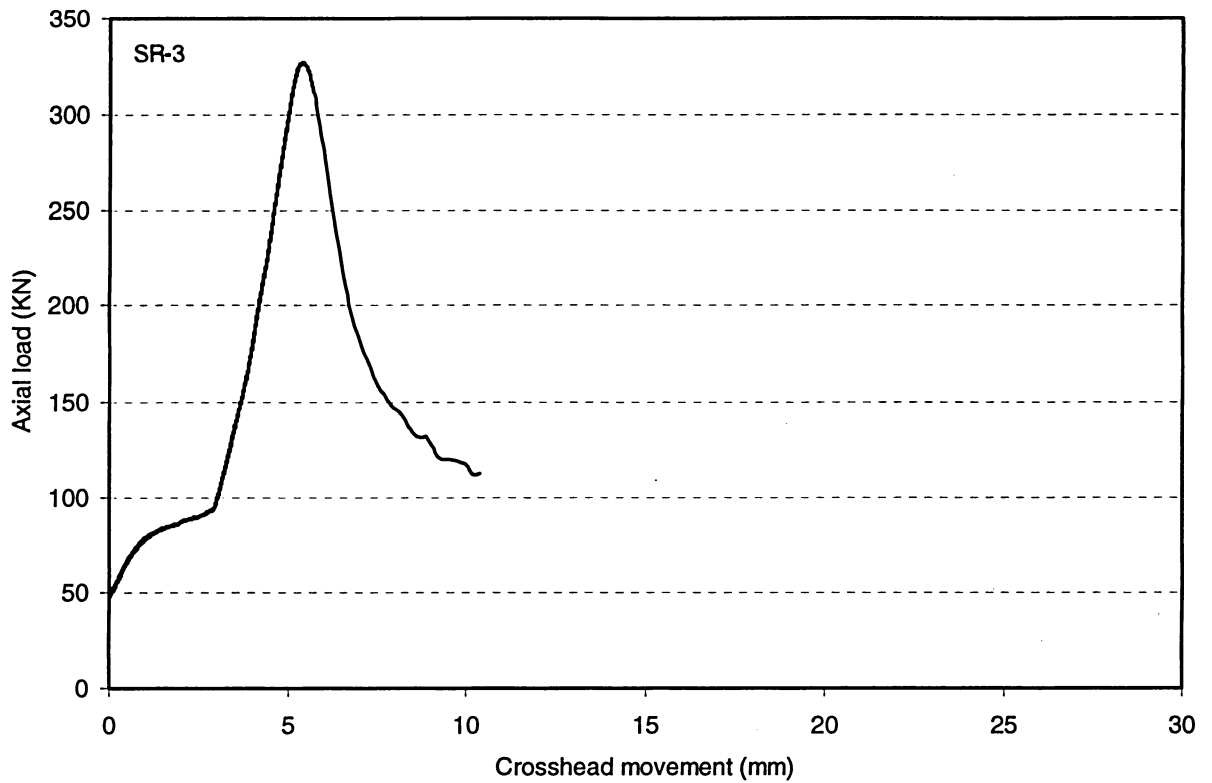


Figure 4.33 Load versus overall shortening curve for specimen SR-3

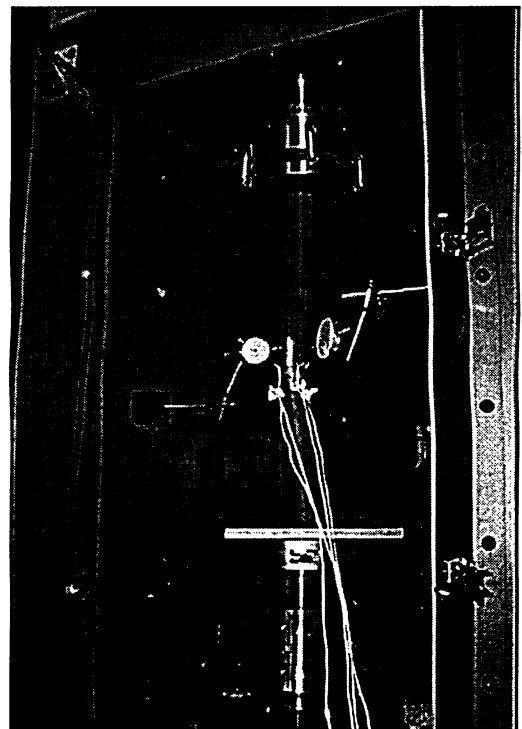
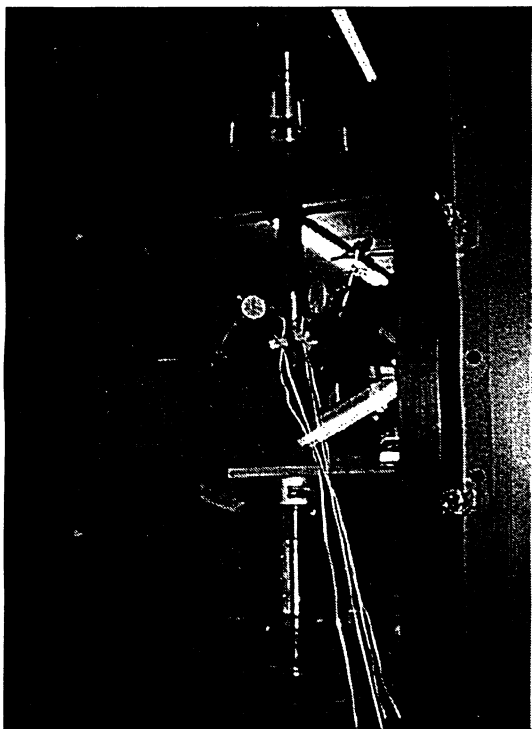


Figure 4.34 Views of specimen SR-4 before and after testing

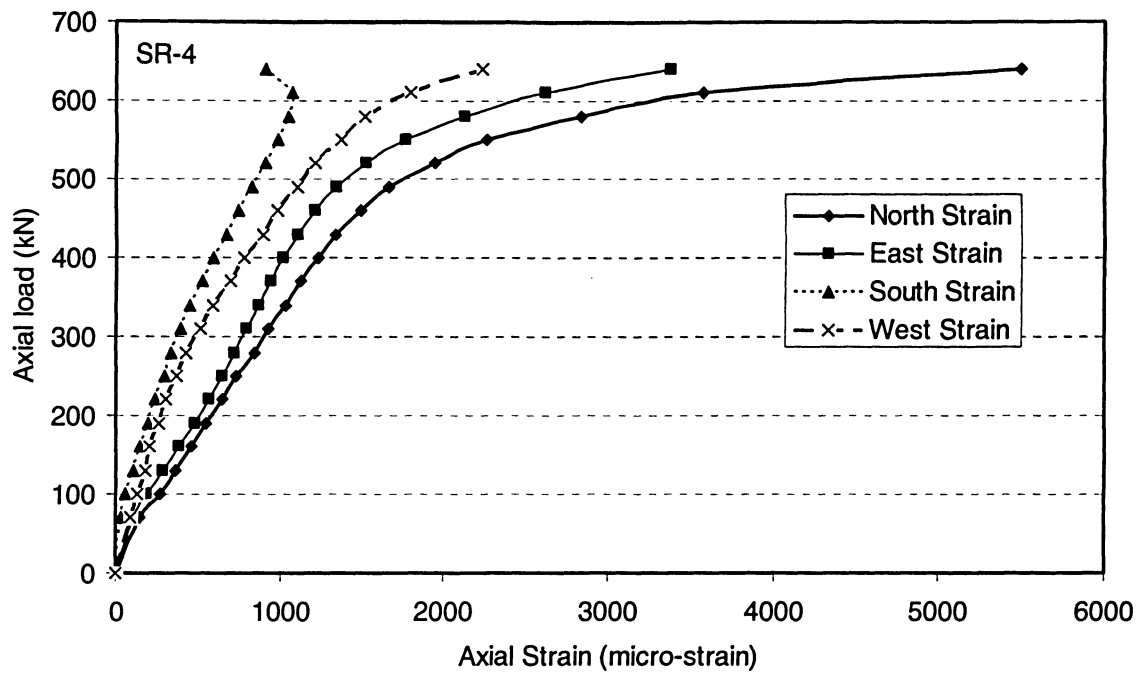


Figure 4.35 Axial load-strain relationships for specimen SR-4

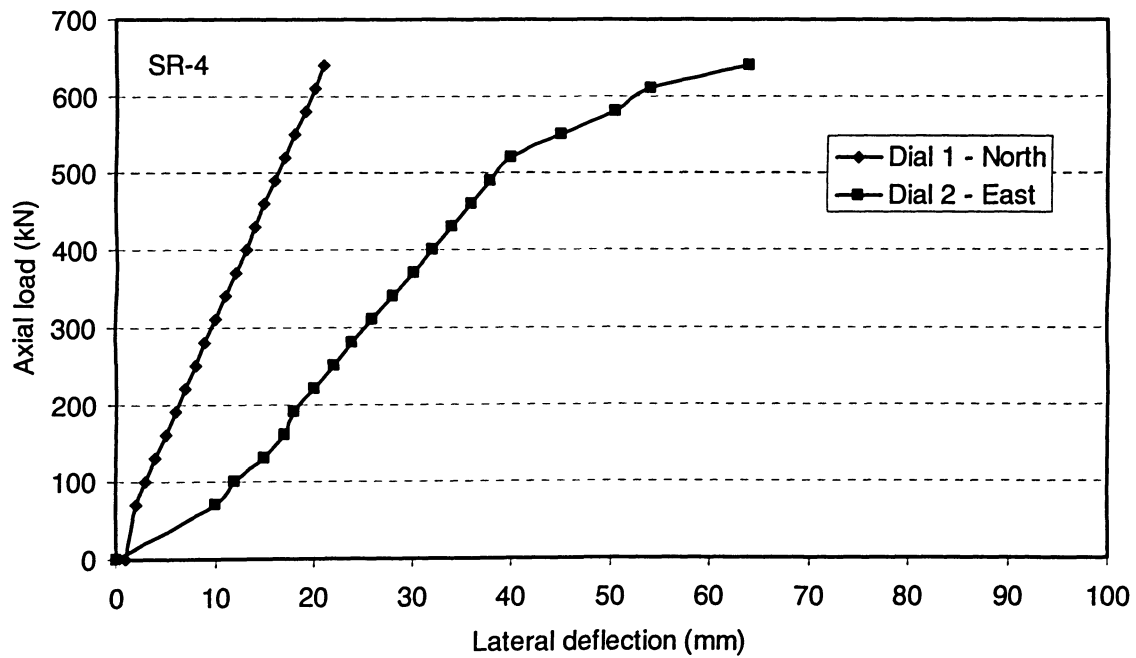


Figure 4.36 Load-lateral deflection curves for specimen SR-4

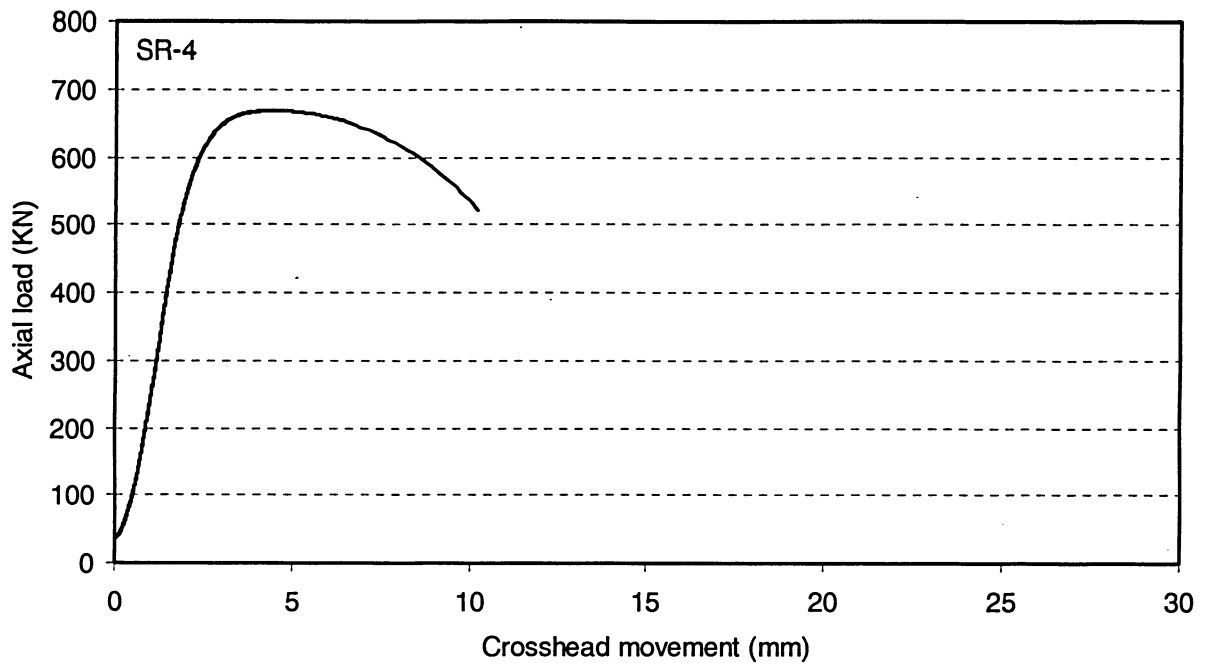


Figure 4.37 Load versus overall shortening curve for specimen SR-4

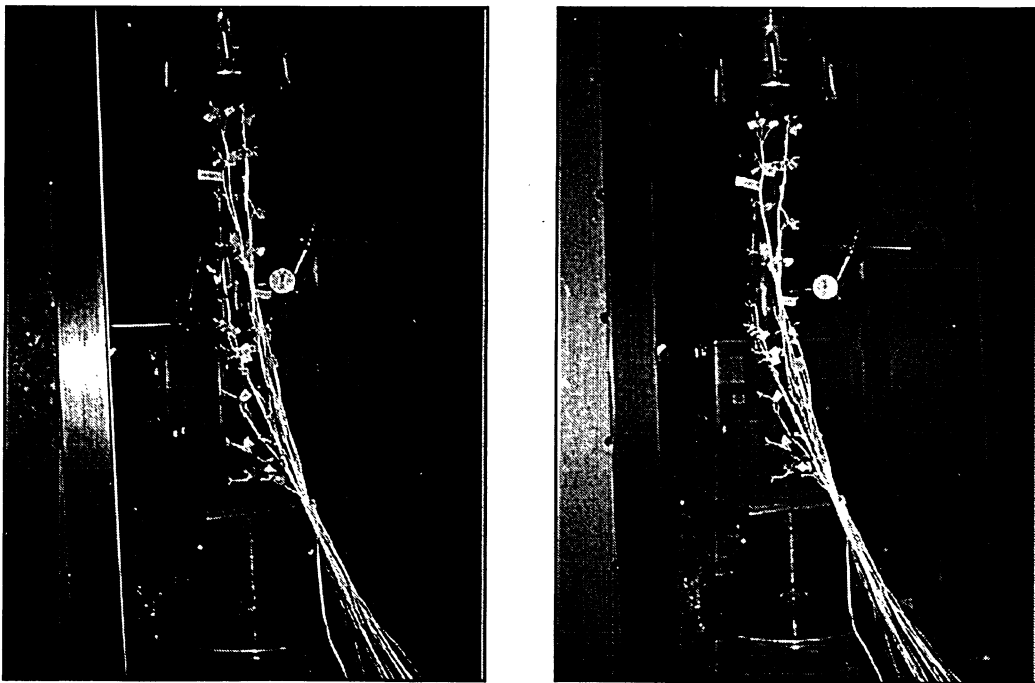


Figure 4.38 Views of specimen SR-5 before and after testing

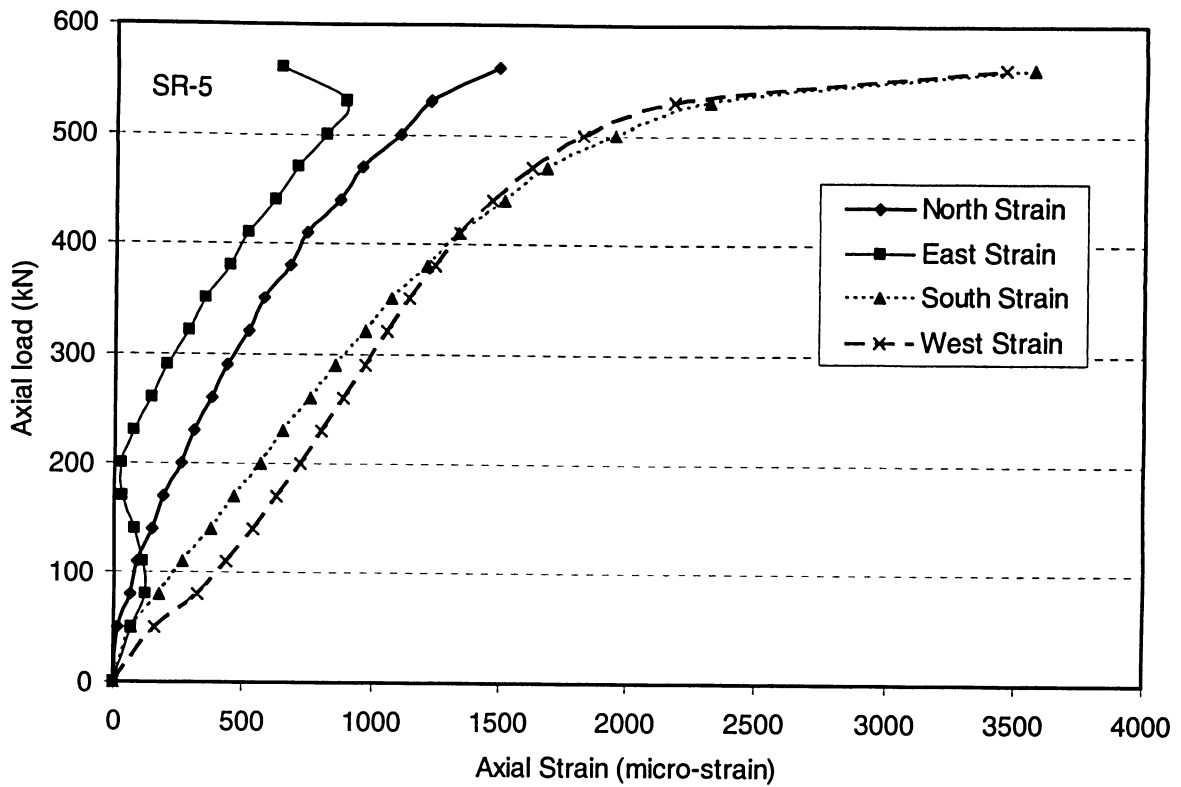


Figure 4.39 Axial load-strain relationships for specimen SR-5

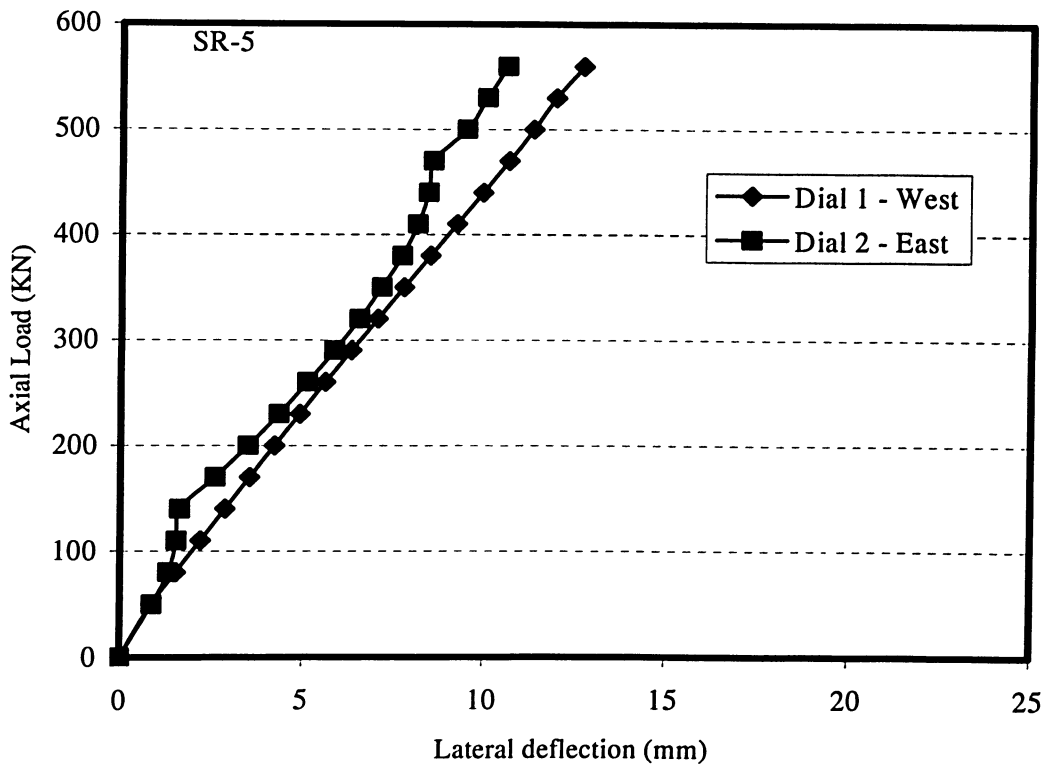


Figure 4.40 Load-lateral deflection curves for specimen SR-5

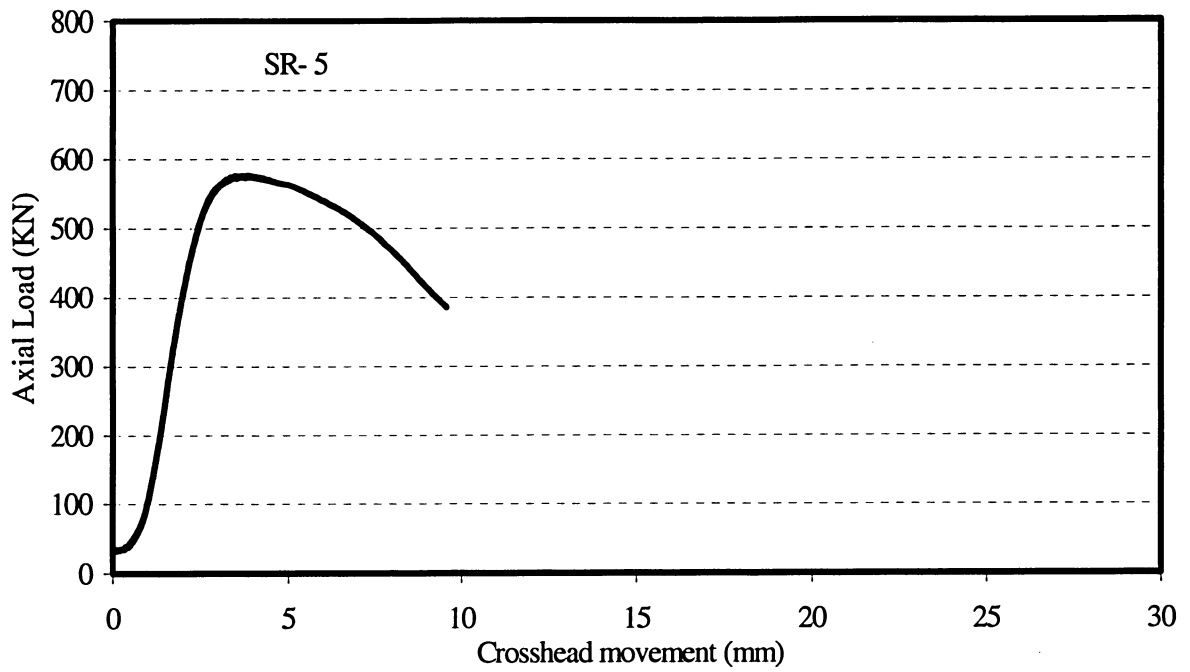


Figure 4.41 Load versus overall shortening curve for specimen SR-5

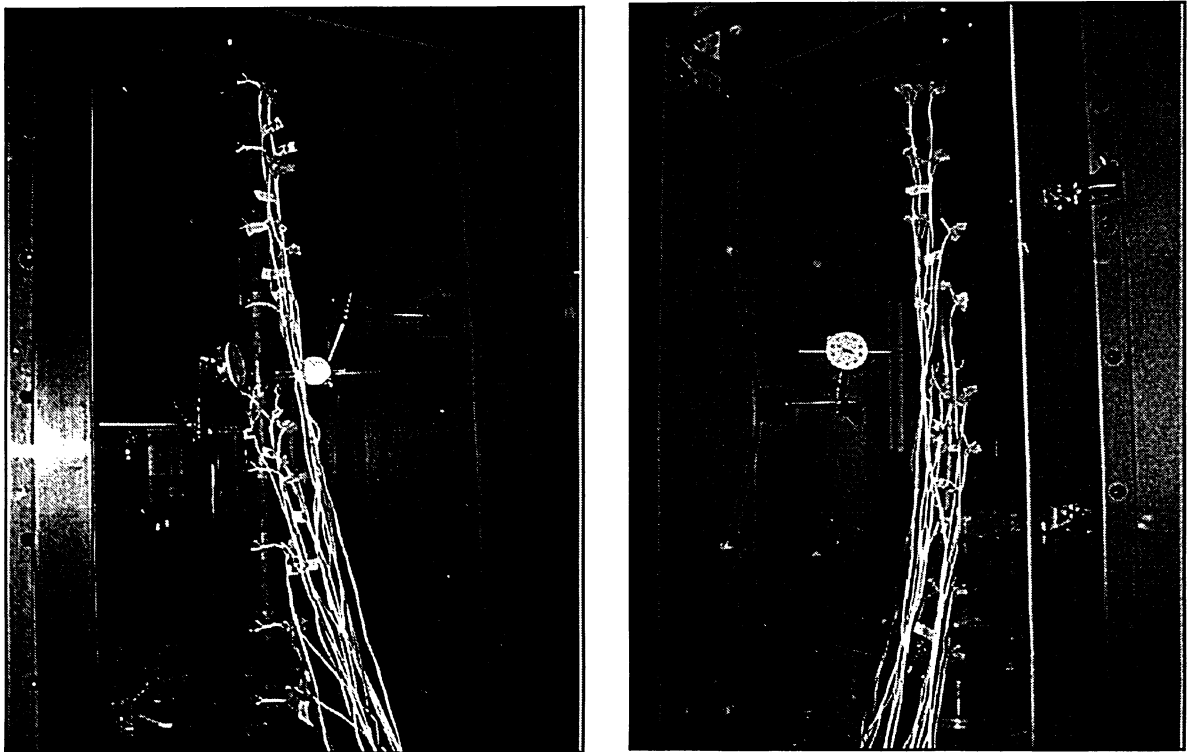


Figure 4.42 Views of specimen SR-6 before and after testing

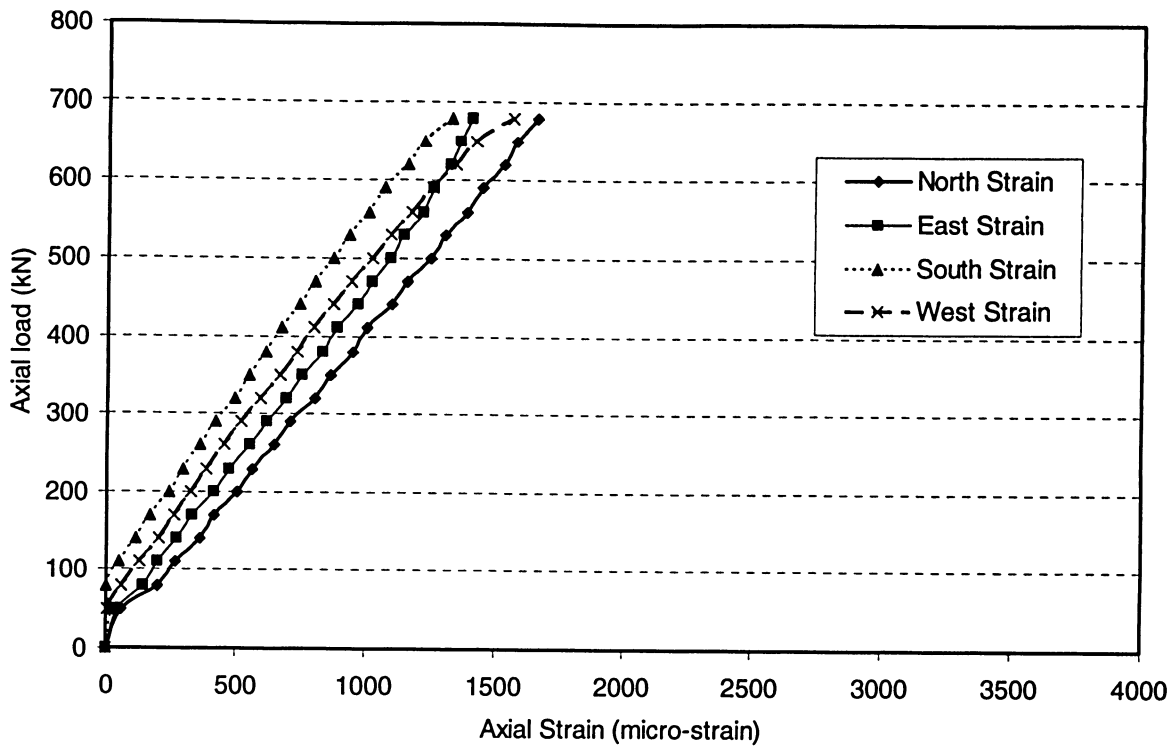


Figure 4.43 Axial load-strain relationships for specimen SR-6

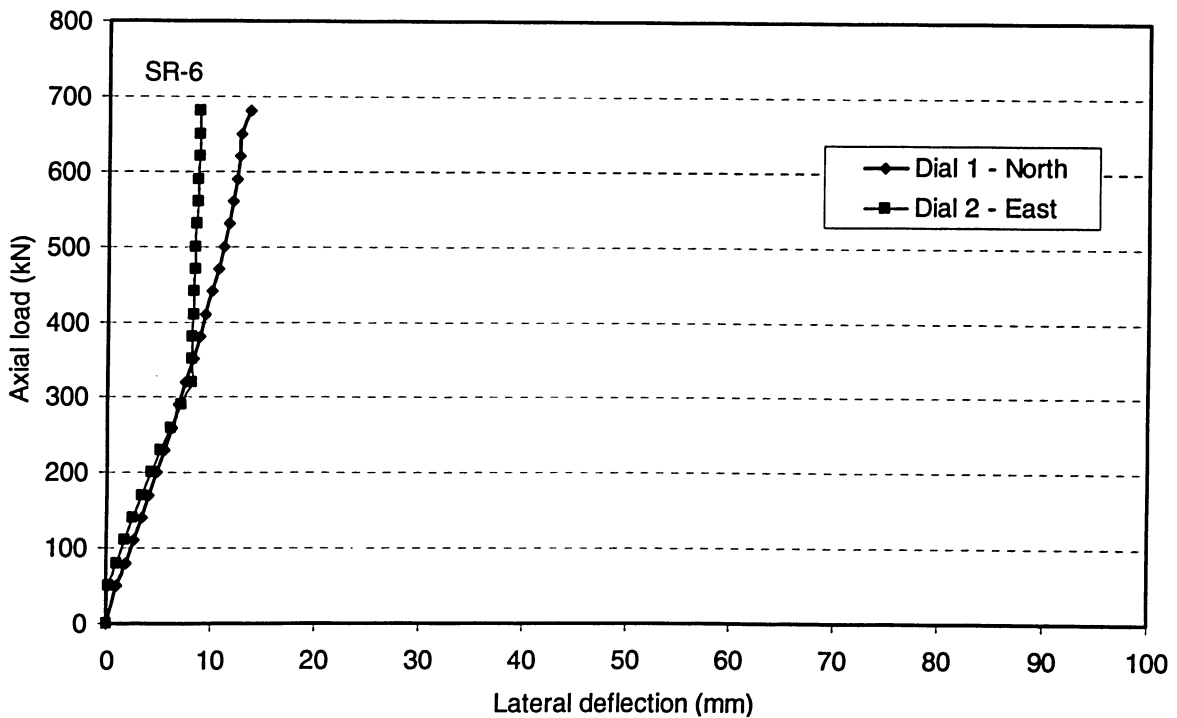


Figure 4.44 Load-lateral deflection curves for specimen SR-6

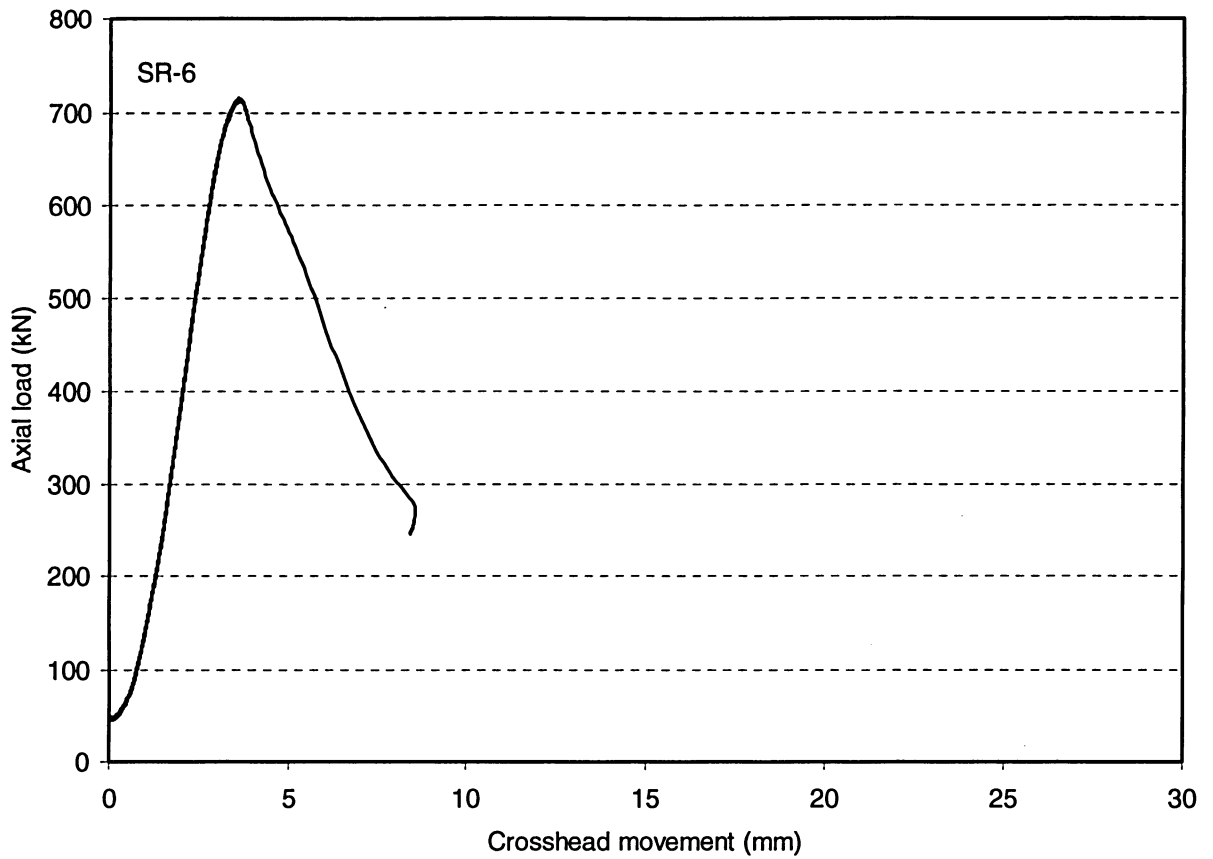


Figure 4.45 Load versus overall shortening curve for specimen SR-6

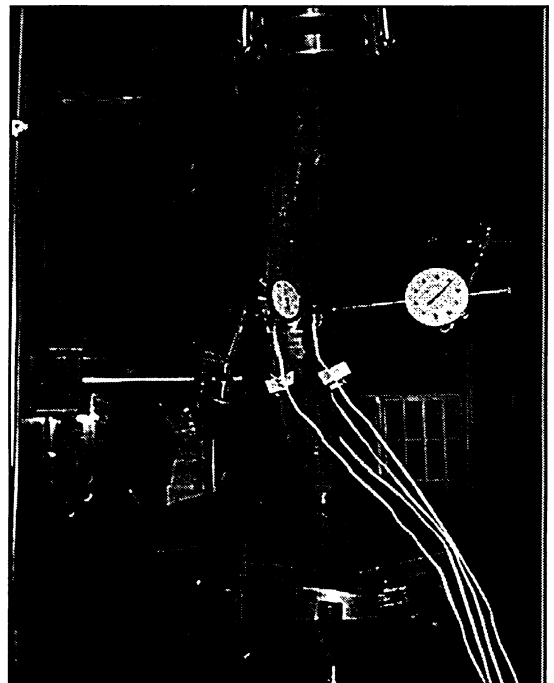
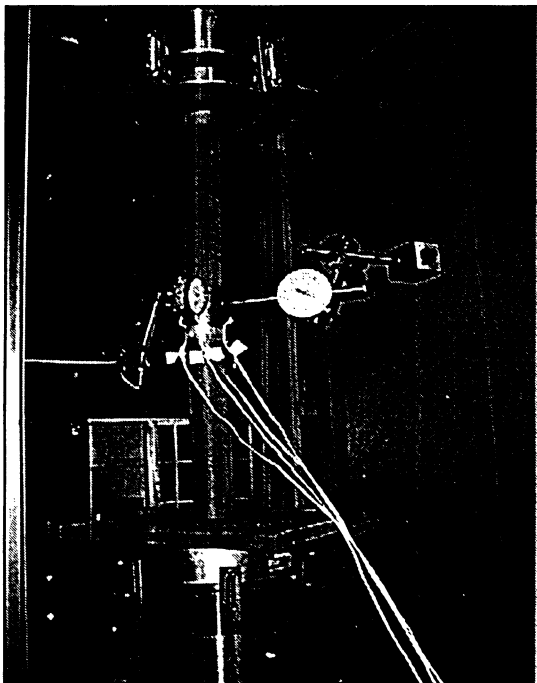


Figure 4.46 Views of specimen SR-7 before and after testing

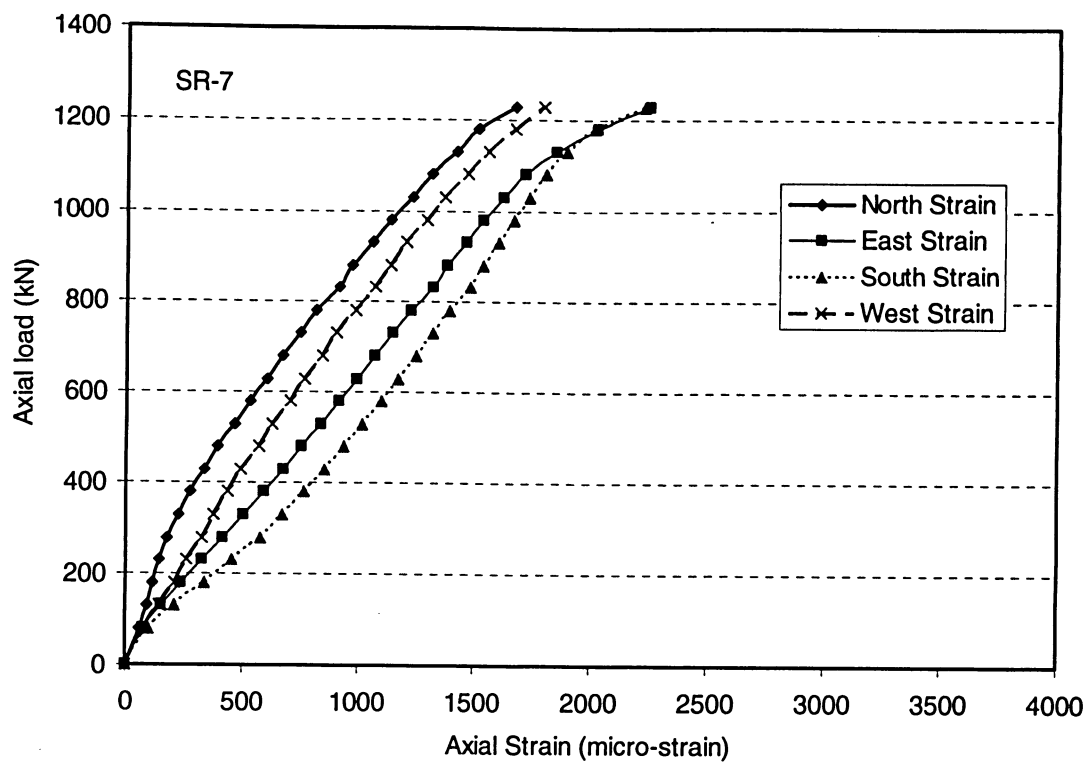


Figure 4.47 Axial load-strain relationships for specimen SR-7

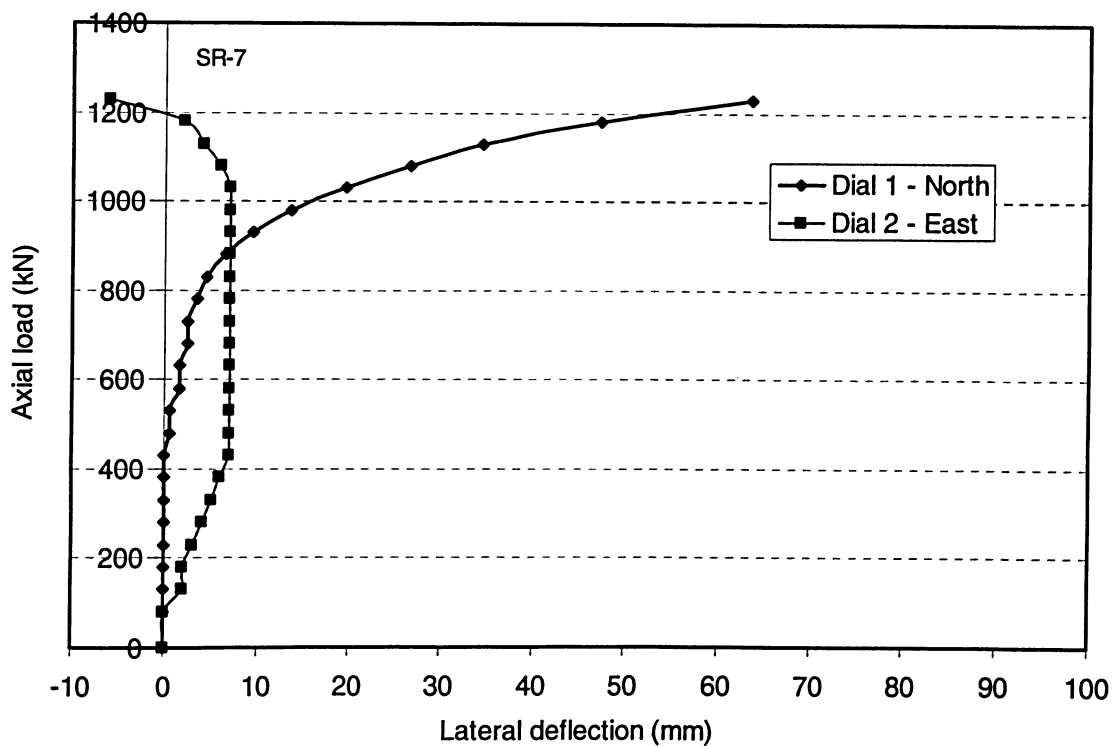


Figure 4.48 Load-lateral deflection curves for specimen SR-7

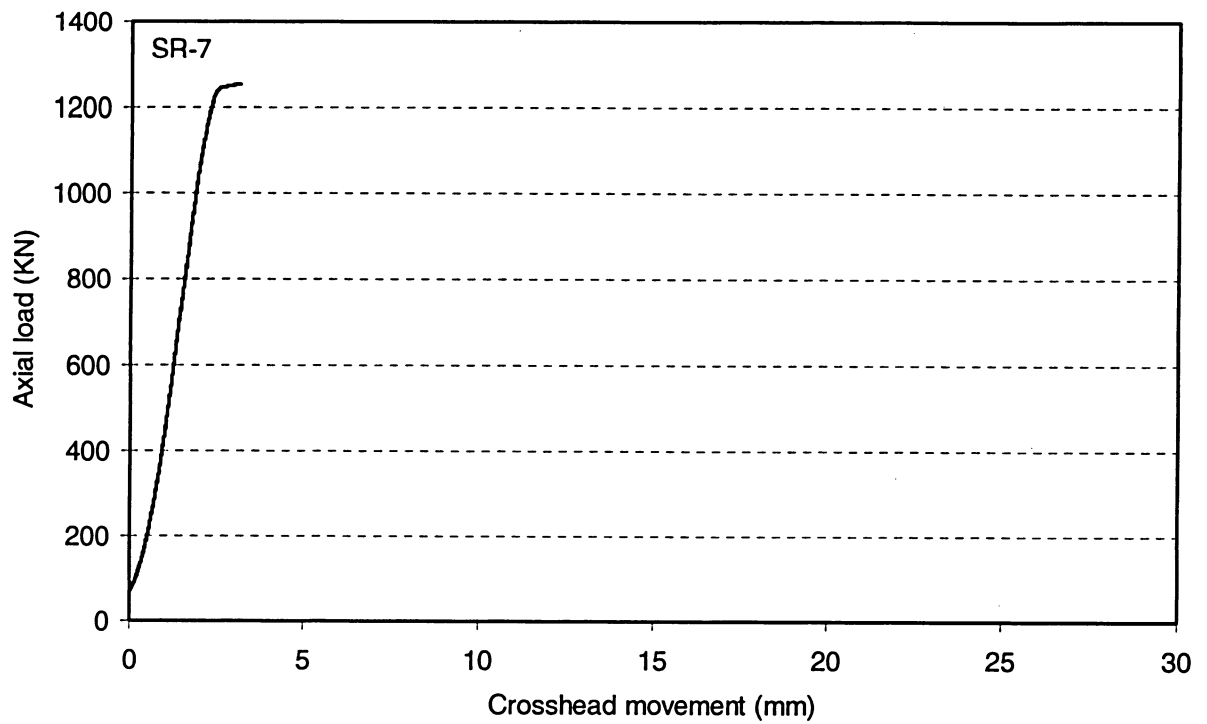


Figure 4.48 Load versus overall shortening curve for specimen SR-7

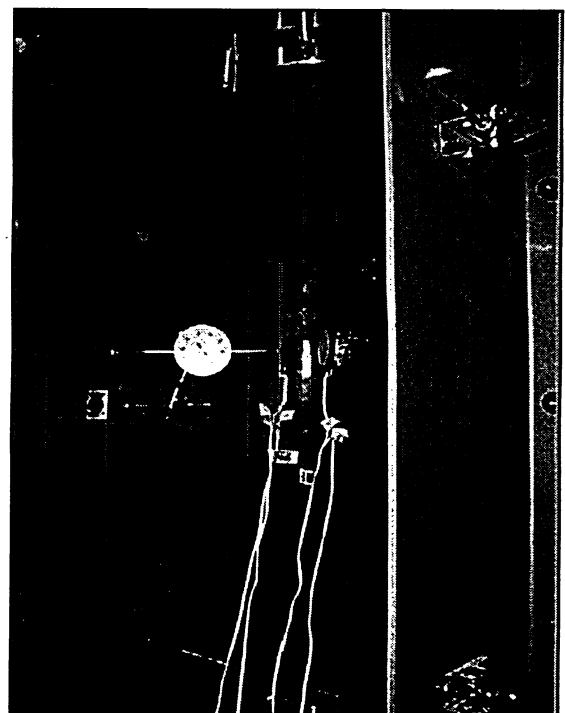
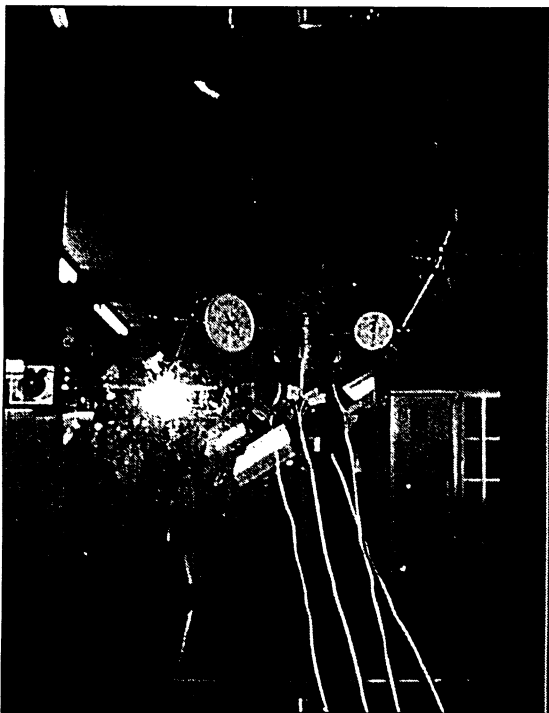


Figure 4.49 Views of specimen SR-8 before and after testing

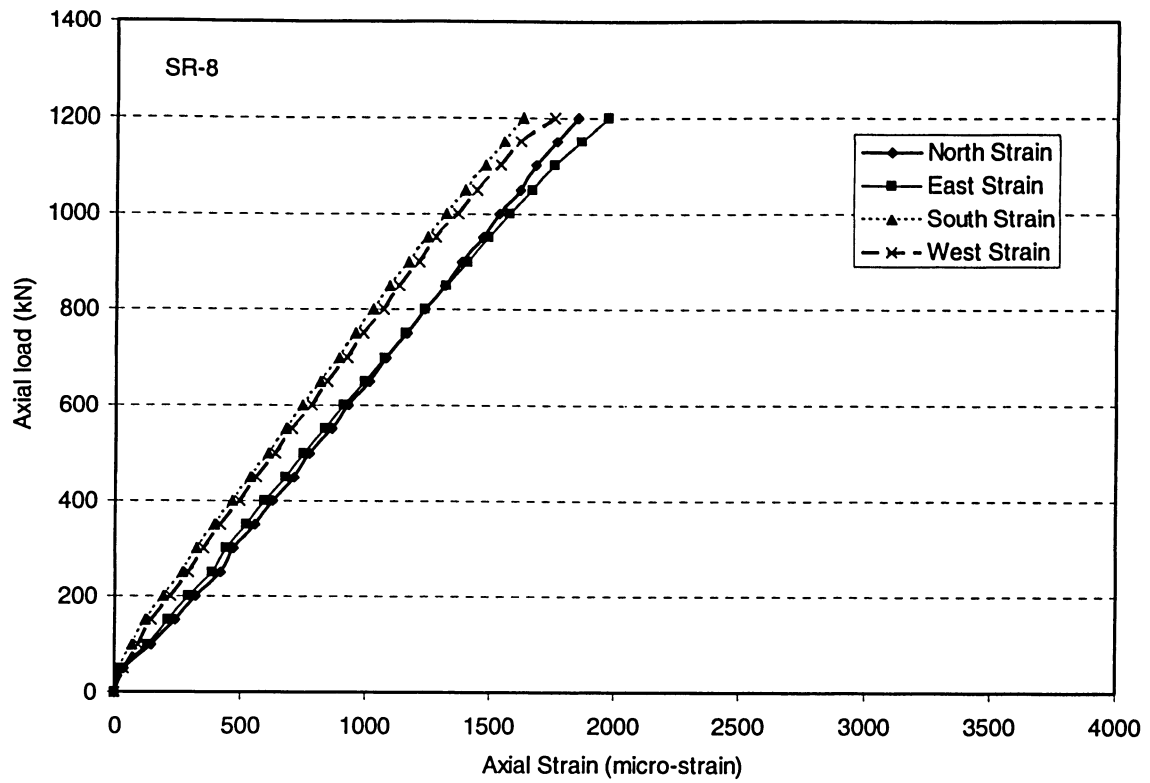


Figure 4.50 Axial load-strain relationships for specimen SR-8

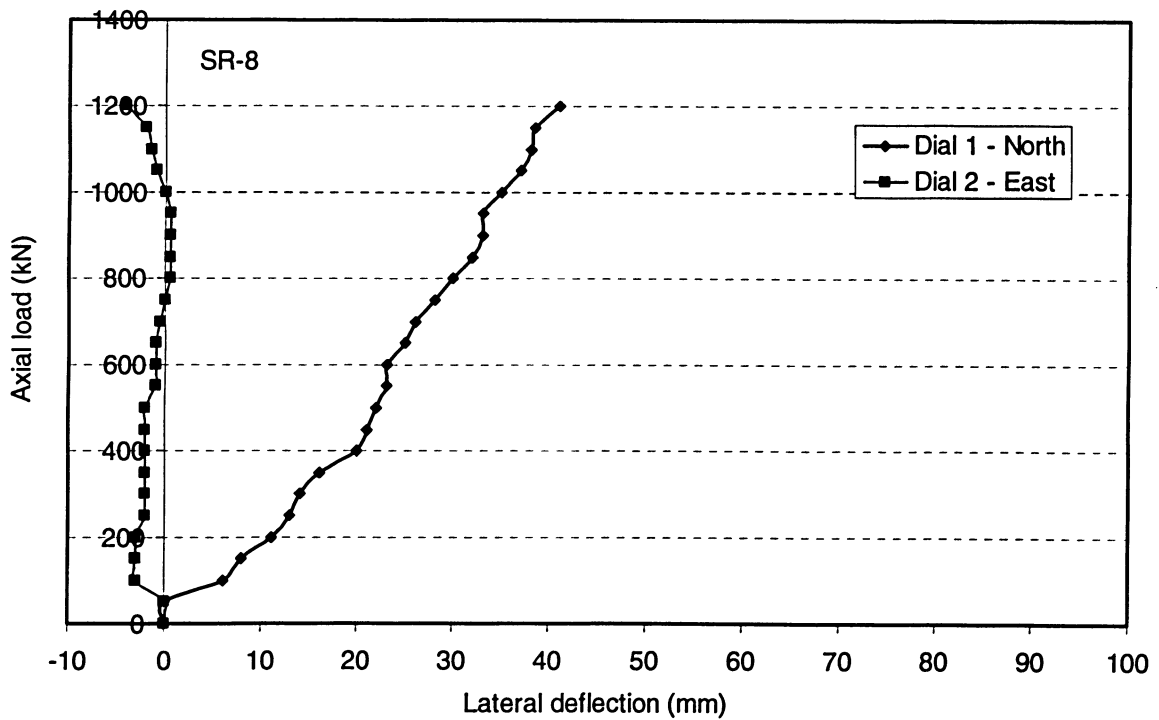


Figure 4.51 Load-lateral deflection curves for specimen SR-8

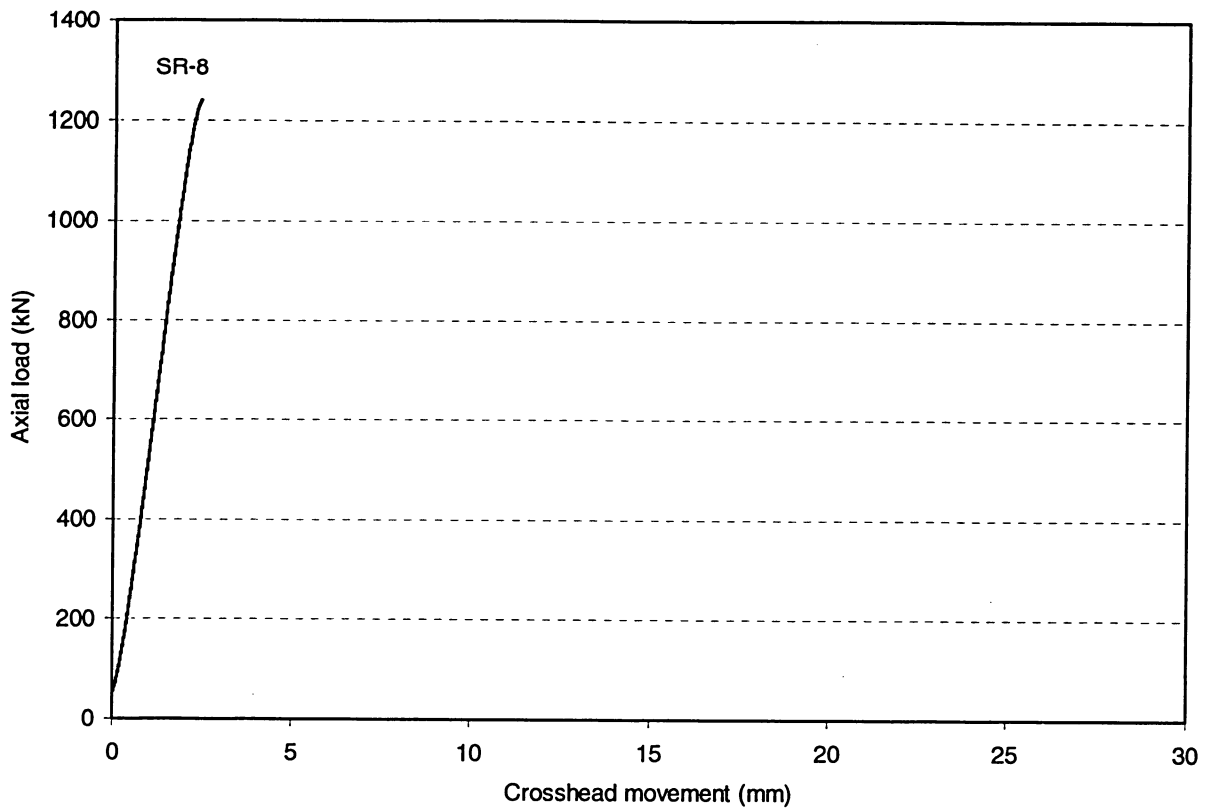


Figure 4.52 Load versus overall shortening curve for specimen SR-8

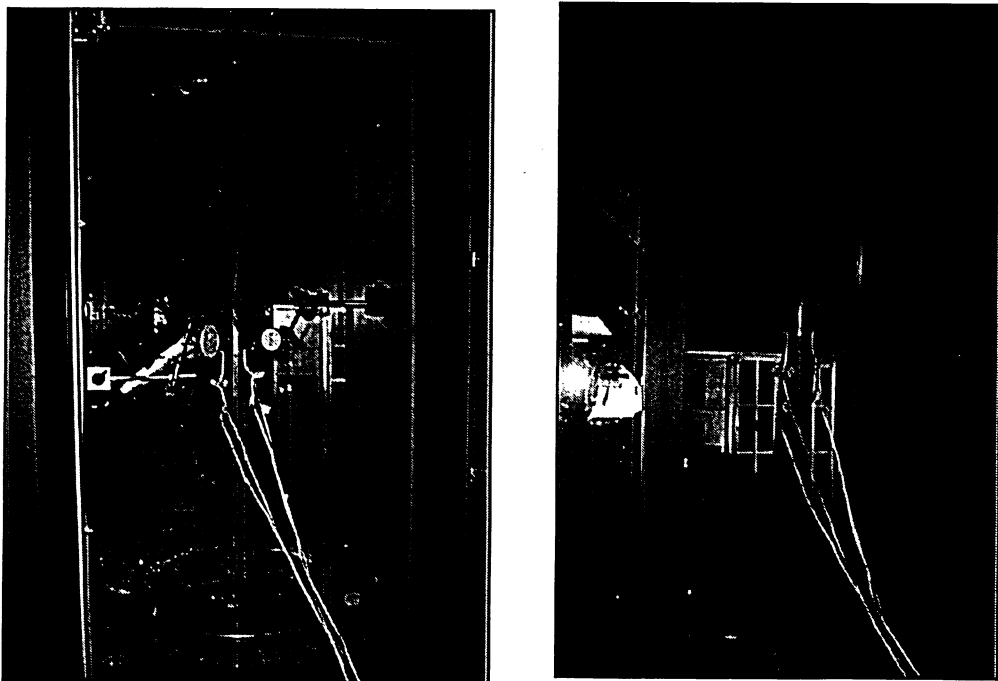


Figure 4.53 Views of specimen SR-9 before and after testing

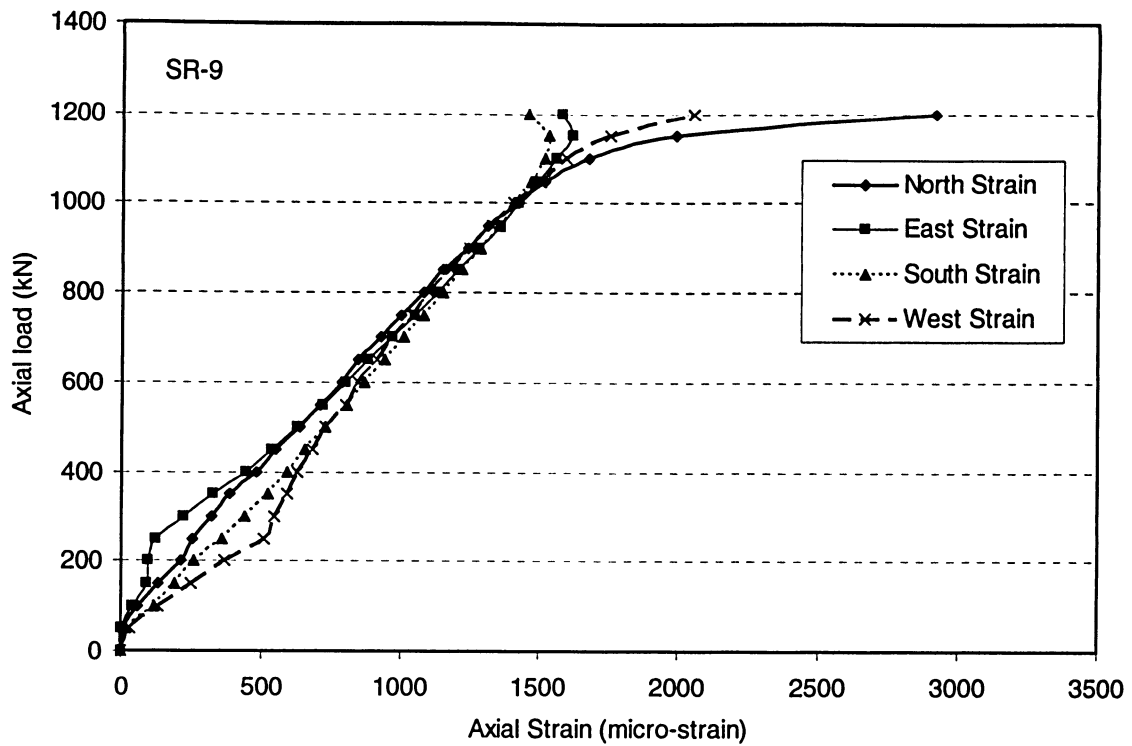


Figure 4.54 Axial load-strain relationships for specimen SR-9

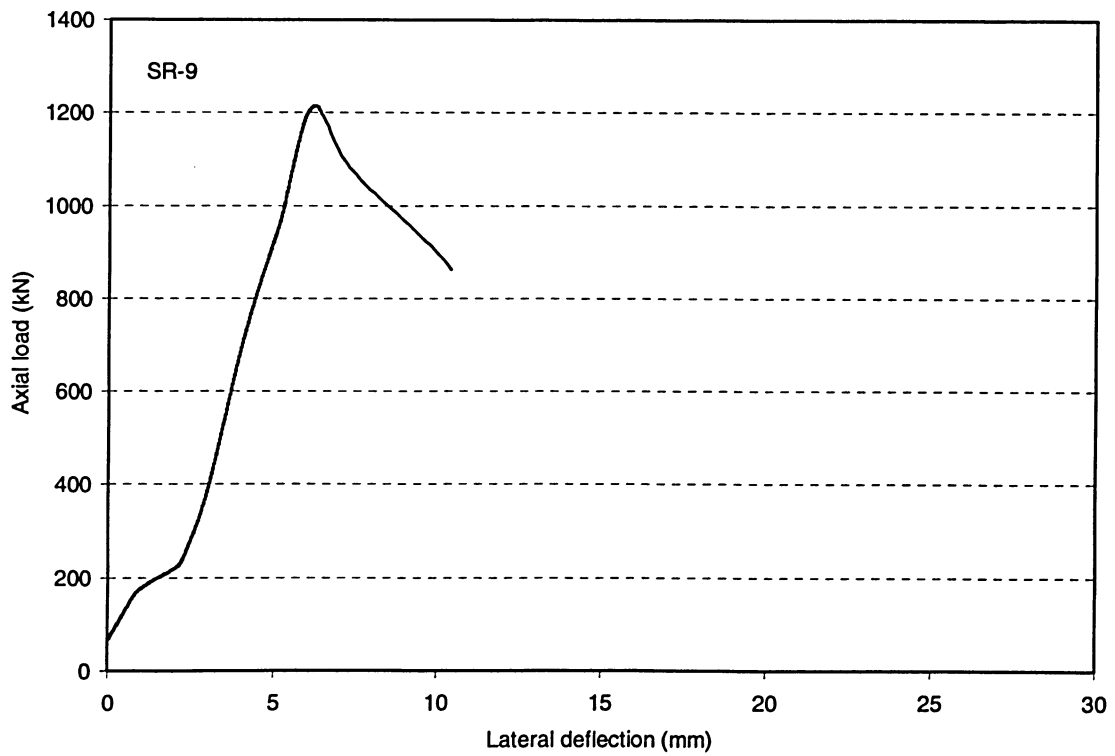


Figure 4.55 Load versus overall shortening curve for specimen SR-9

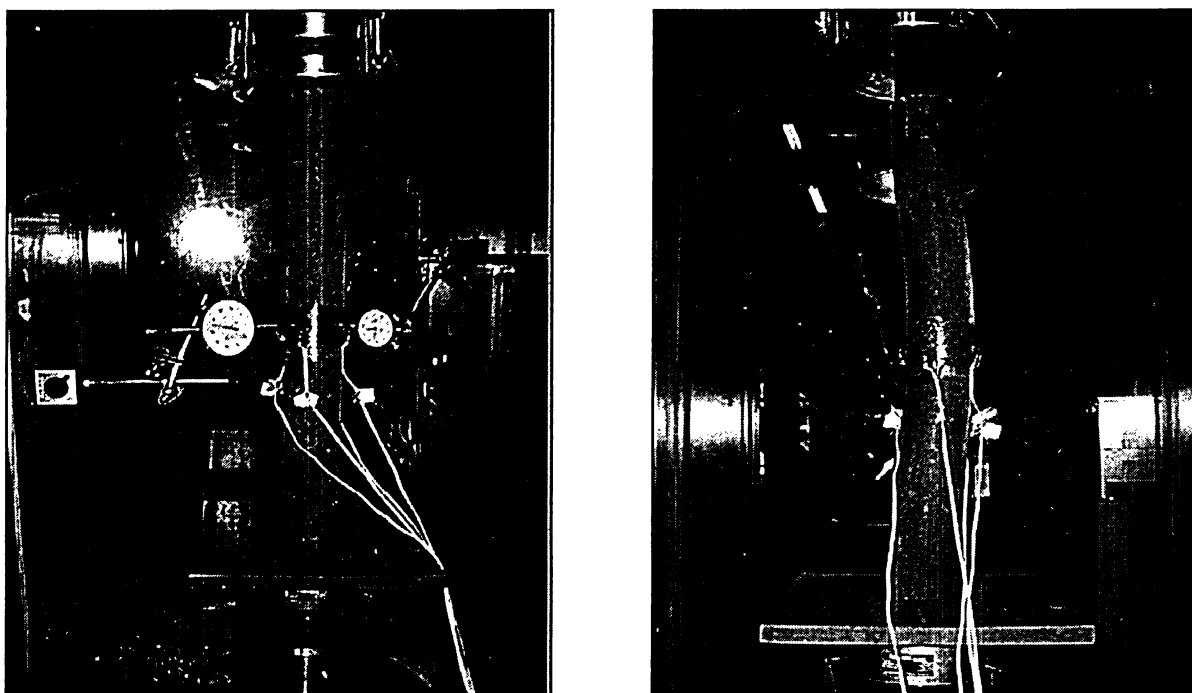


Figure 4.56 Views of specimen SR-10 before and after testing

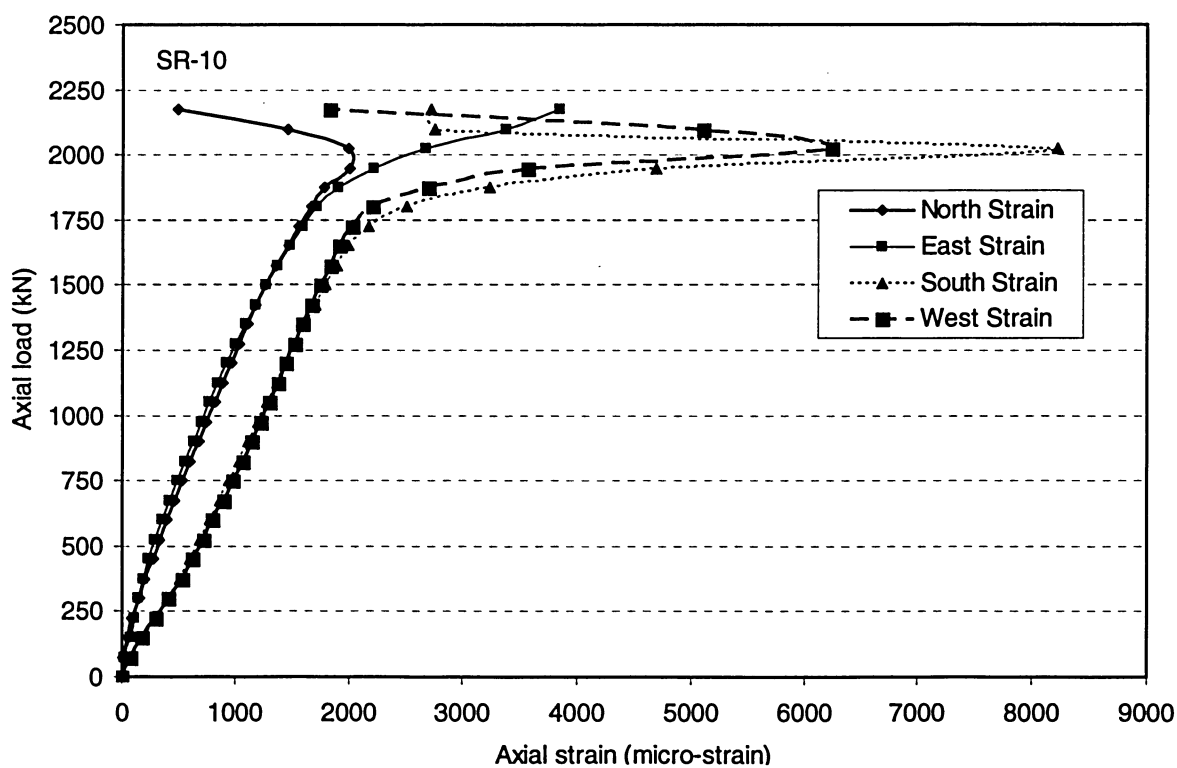


Figure 4.57 Axial load-strain relationships for specimen SR-10

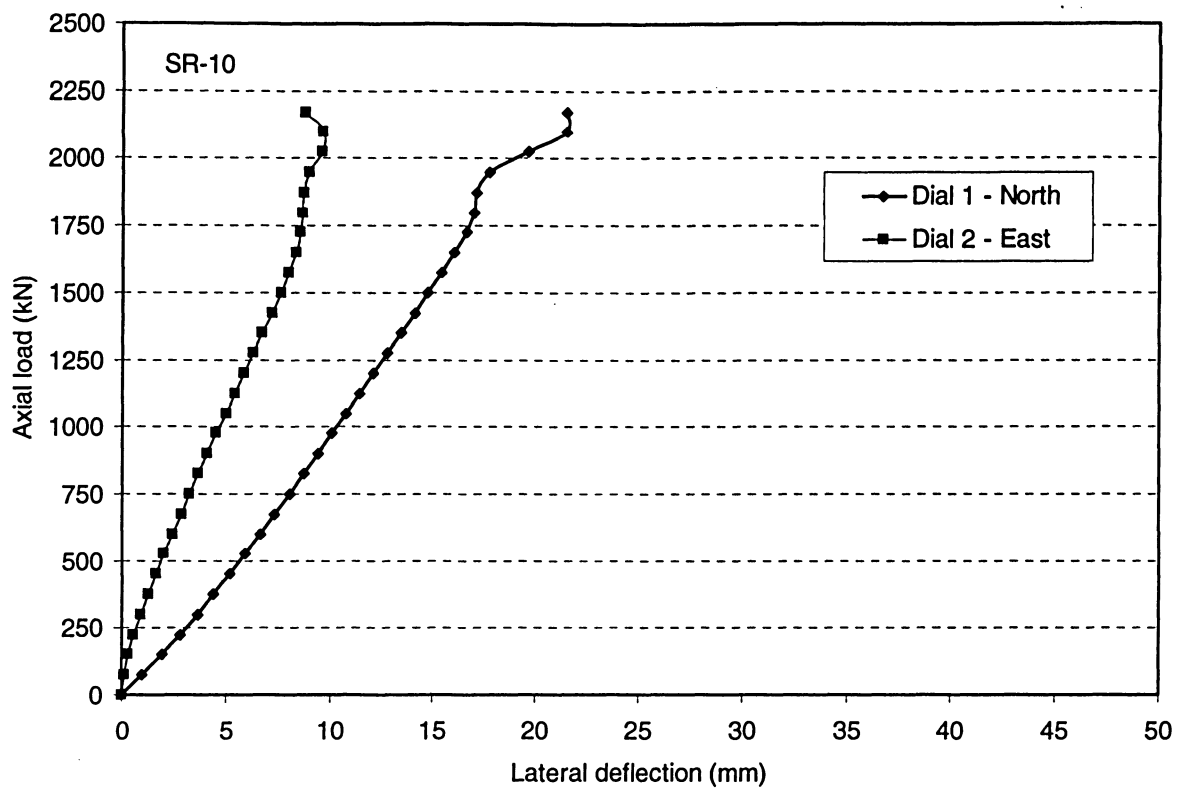


Figure 5.58 Load-lateral deflection curves for specimen SR-10

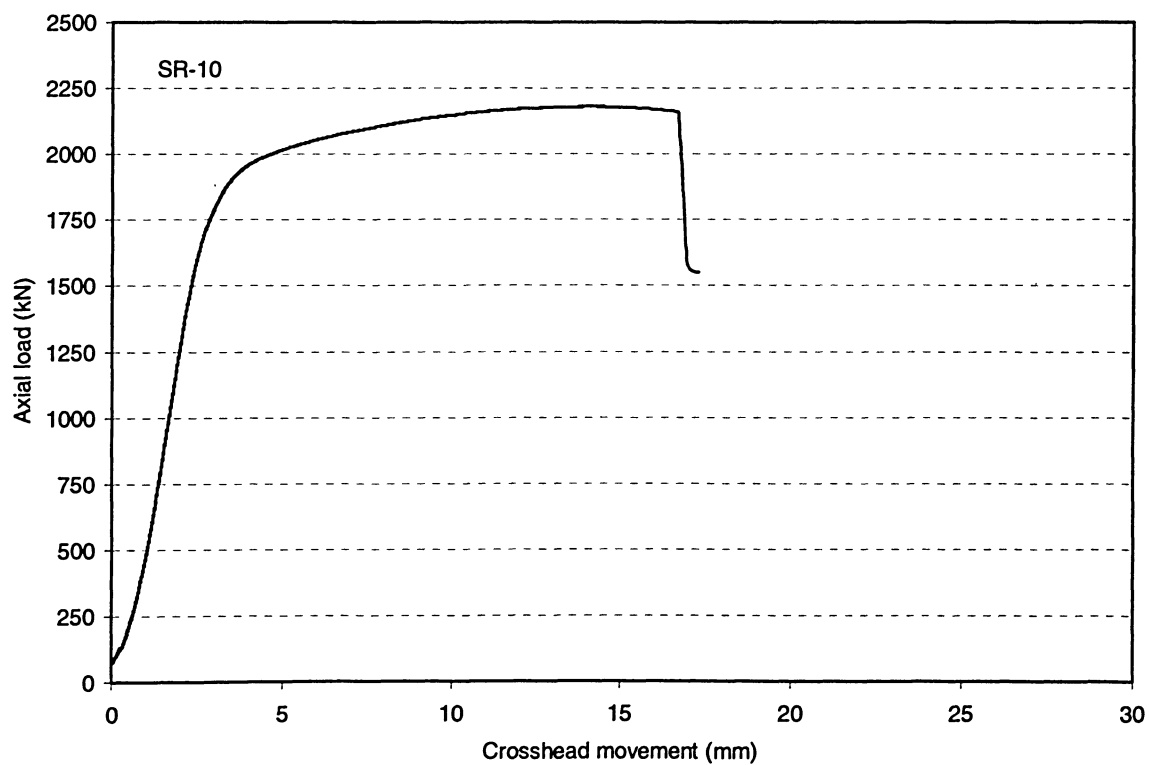


Figure 4.59 Load versus overall shortening curve for specimen SR-10

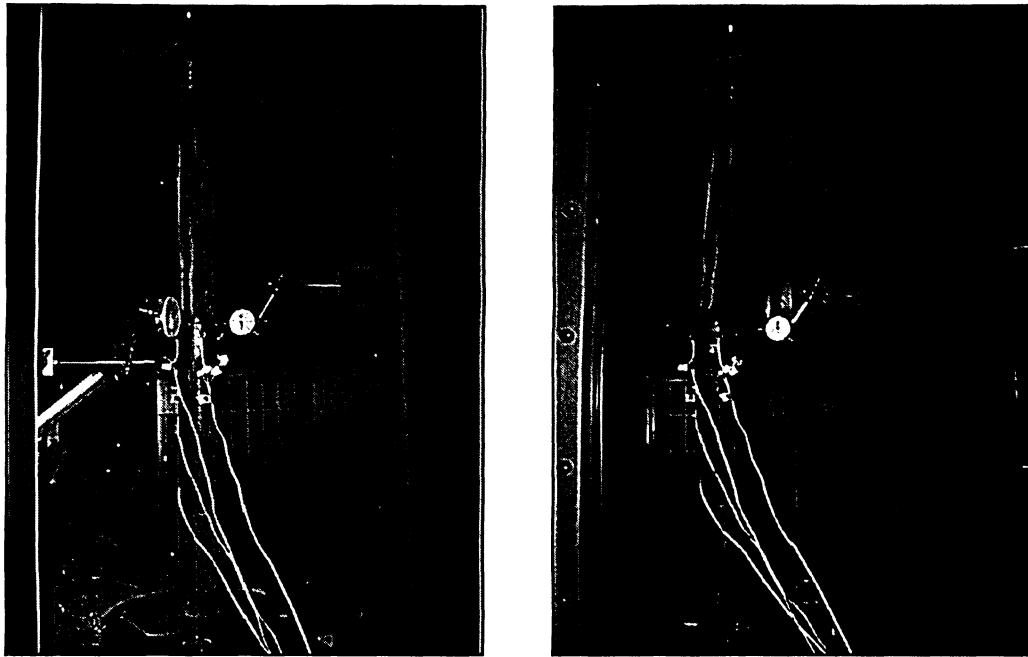


Figure 4.60 Views of specimen SR-11 before and after testing

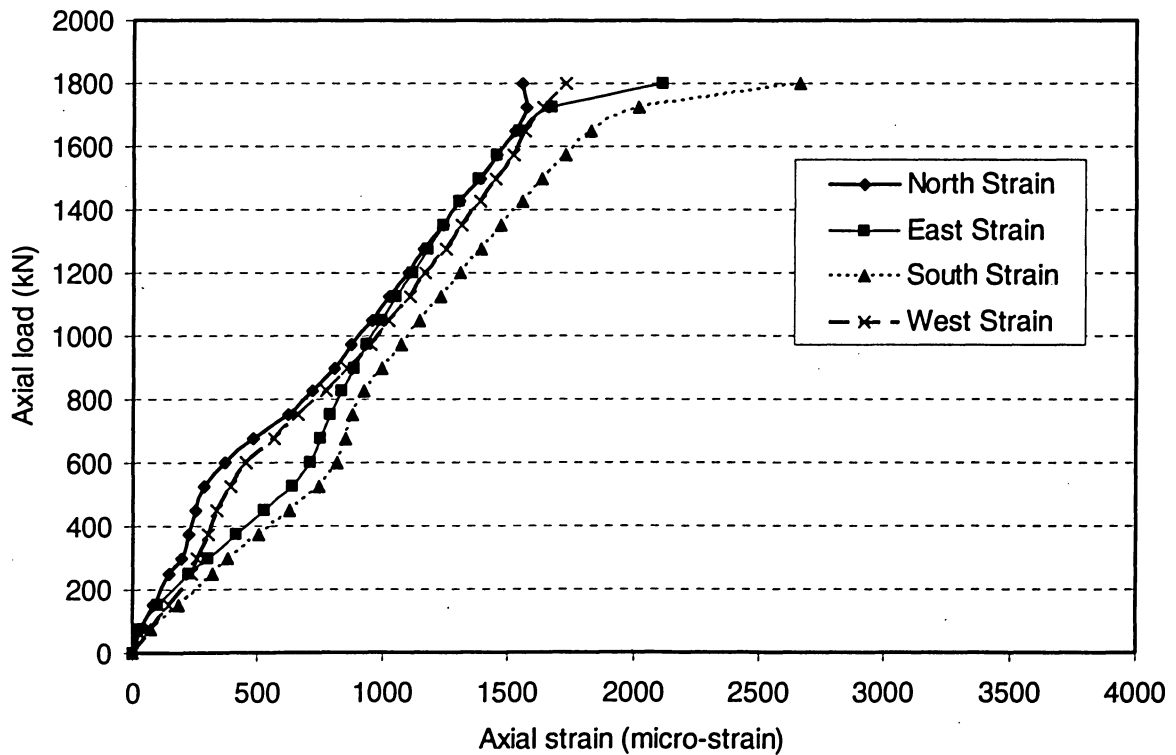


Figure 4.61 Axial load-strain relationships for specimen SR-11

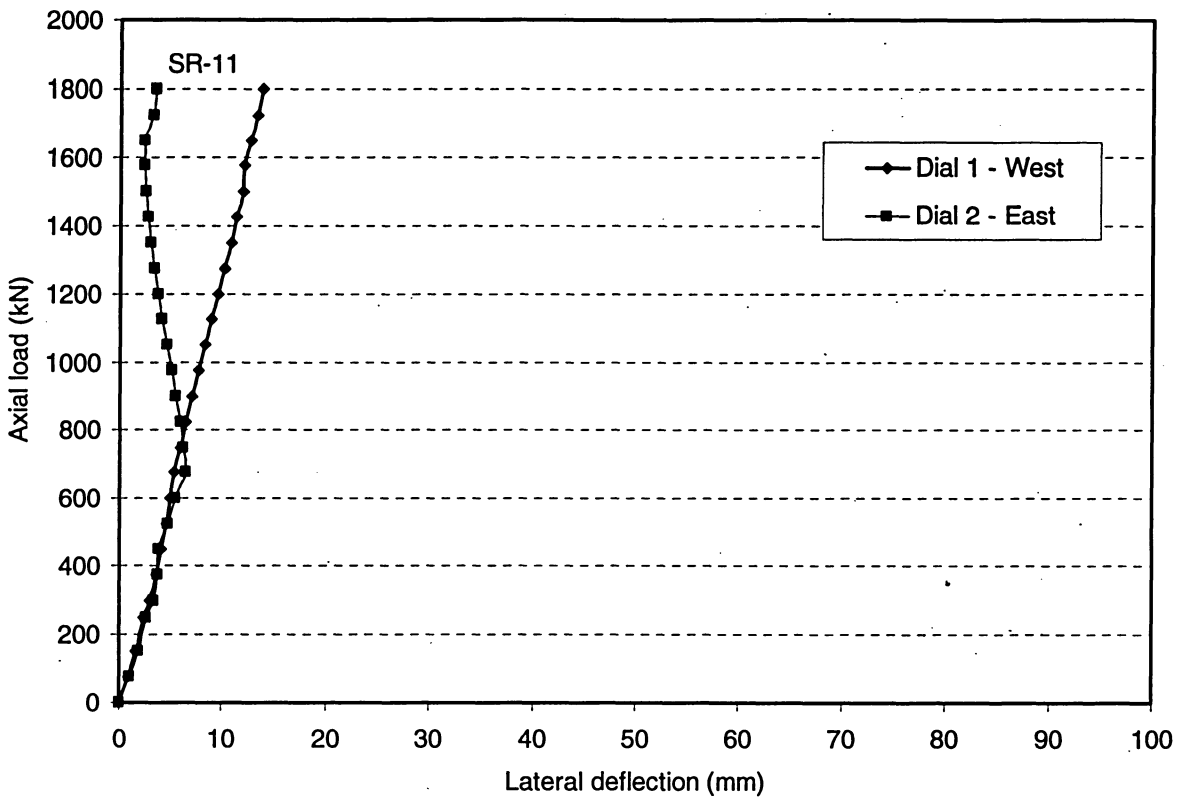


Figure 4.62 Load-lateral deflection curves for specimen SR-11

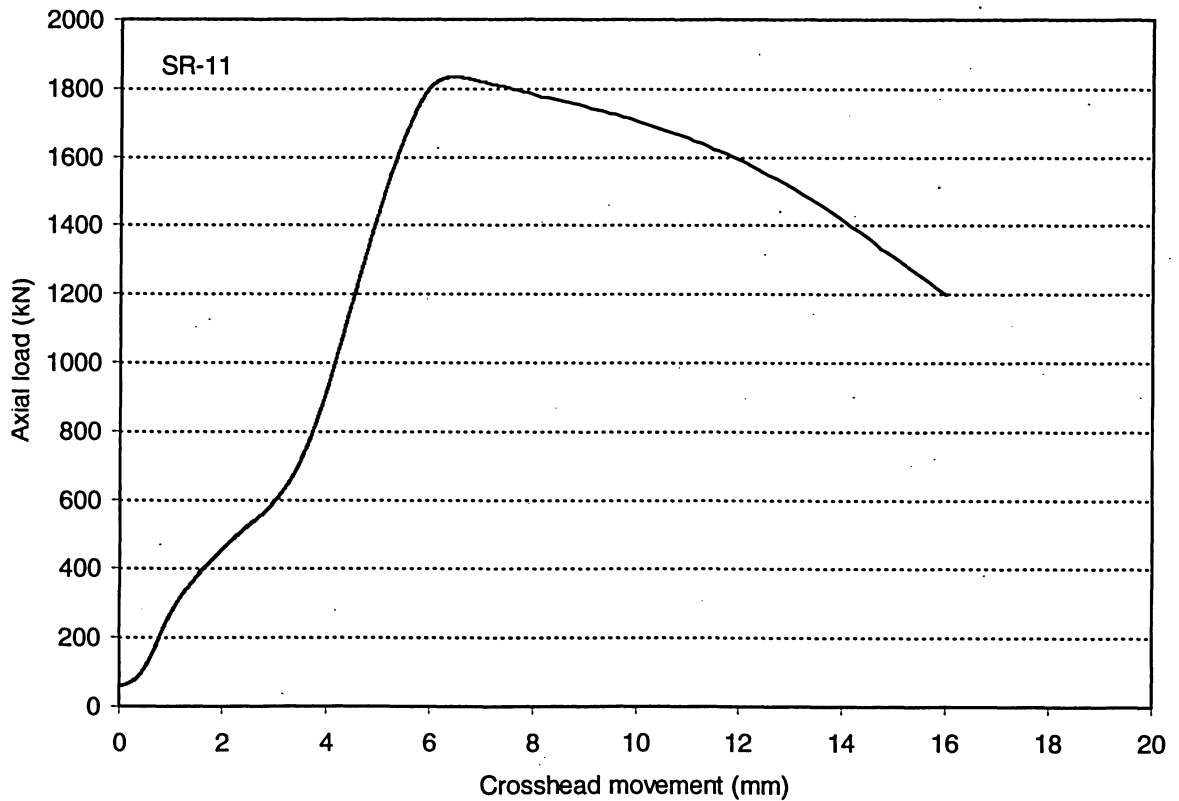


Figure 4.63 Load versus overall shortening curve for specimen SR-11

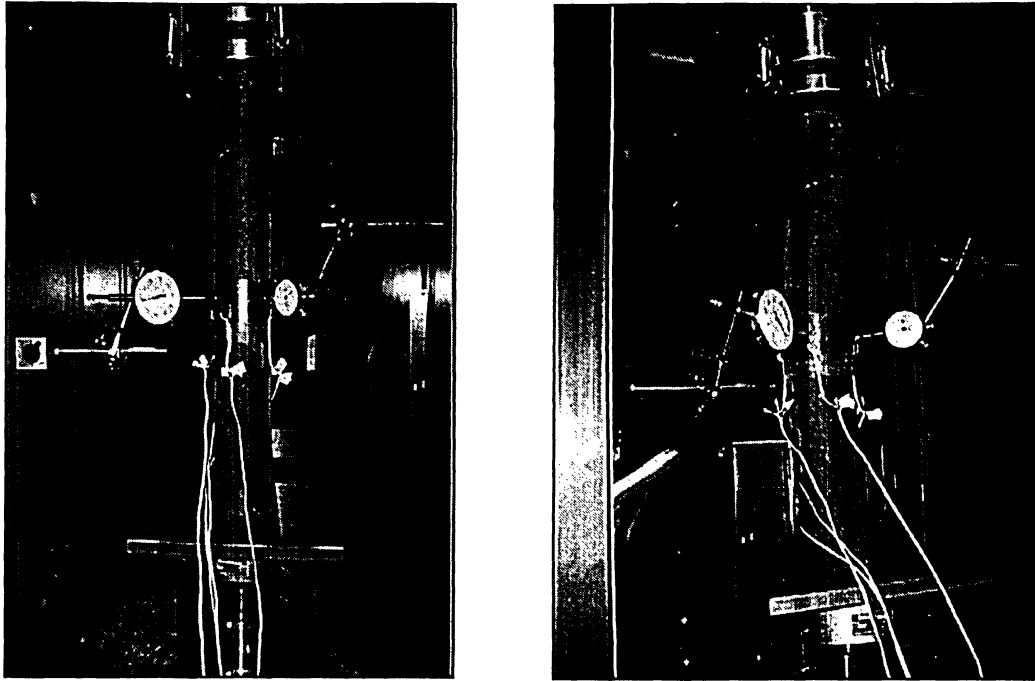


Figure 4.64 Views of specimen SR-12 before and after testing

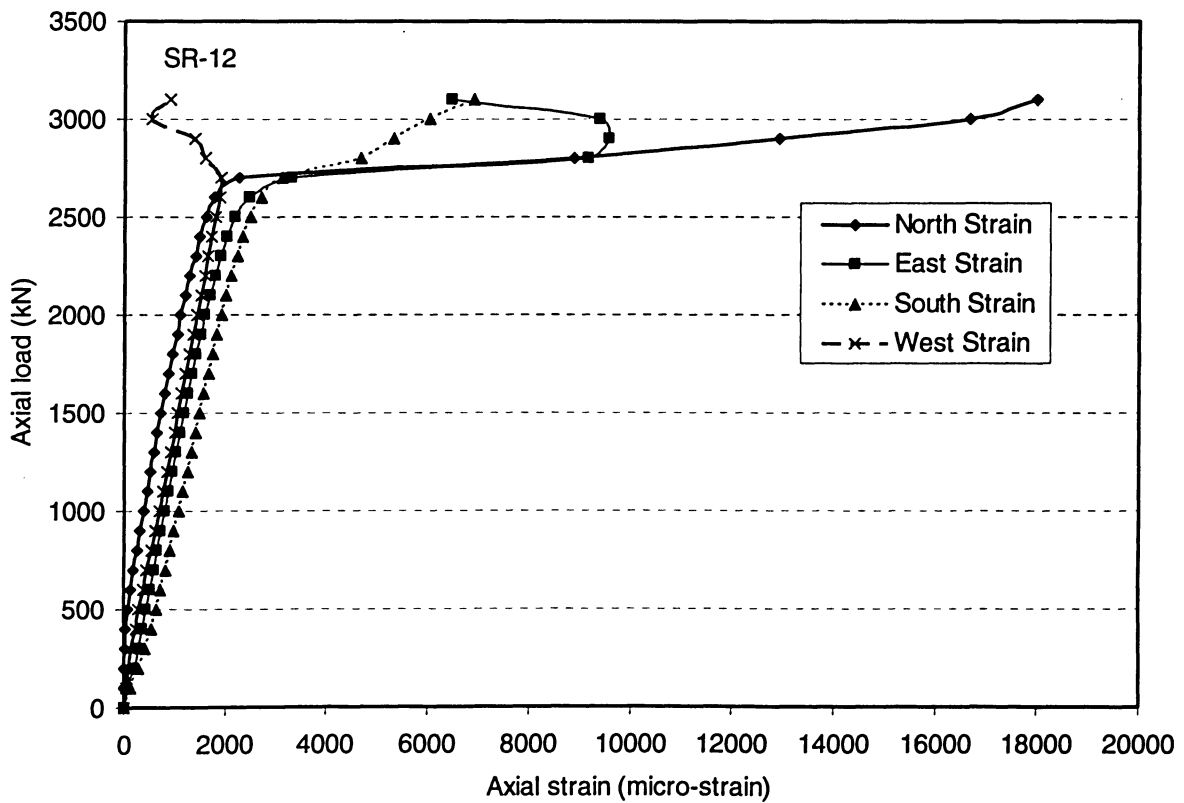


Figure 4.65 Axial load-strain relationships for specimen SR-12

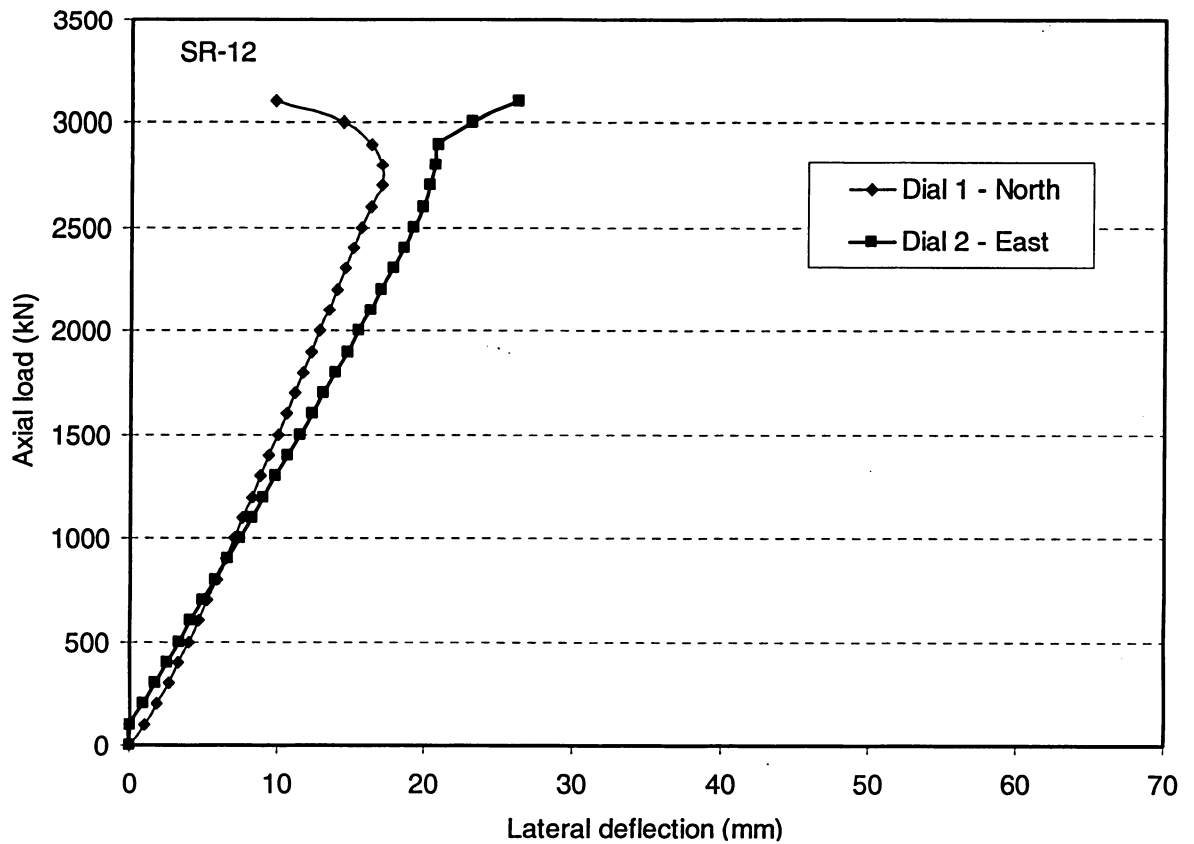


Figure 4.66 Load-lateral deflection curves for specimen SR-12

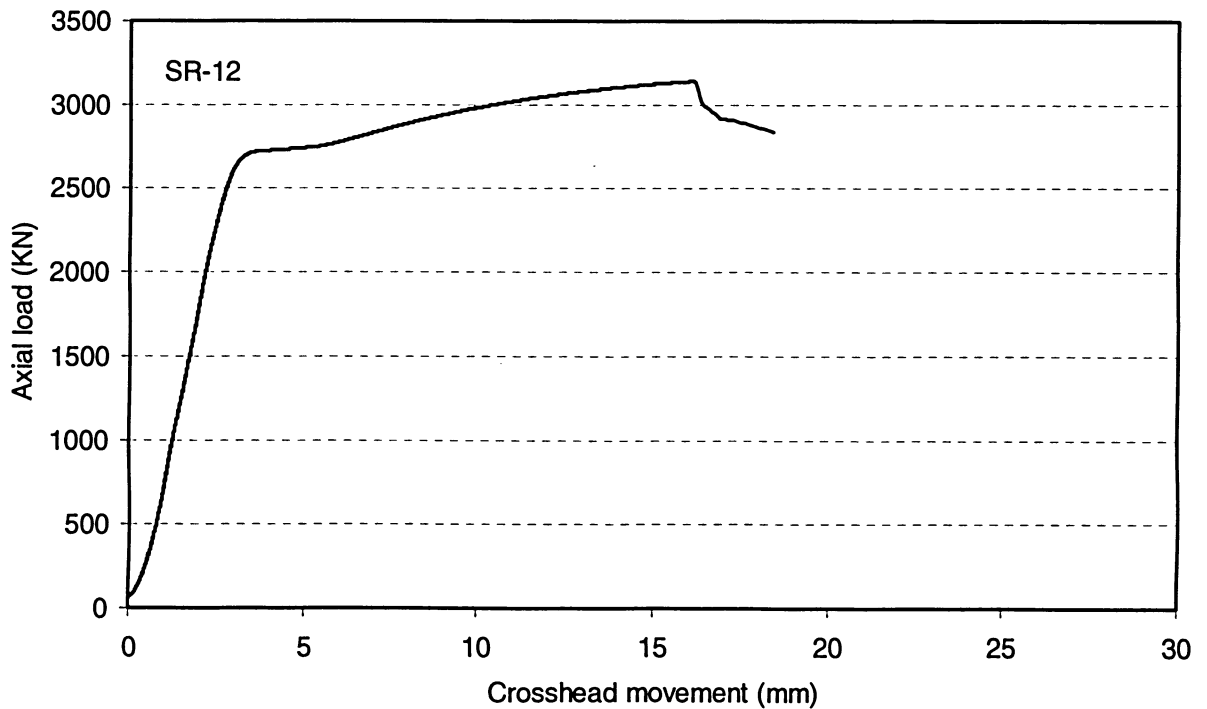


Figure 4.67 Load versus overall shortening curve for specimen SR-12

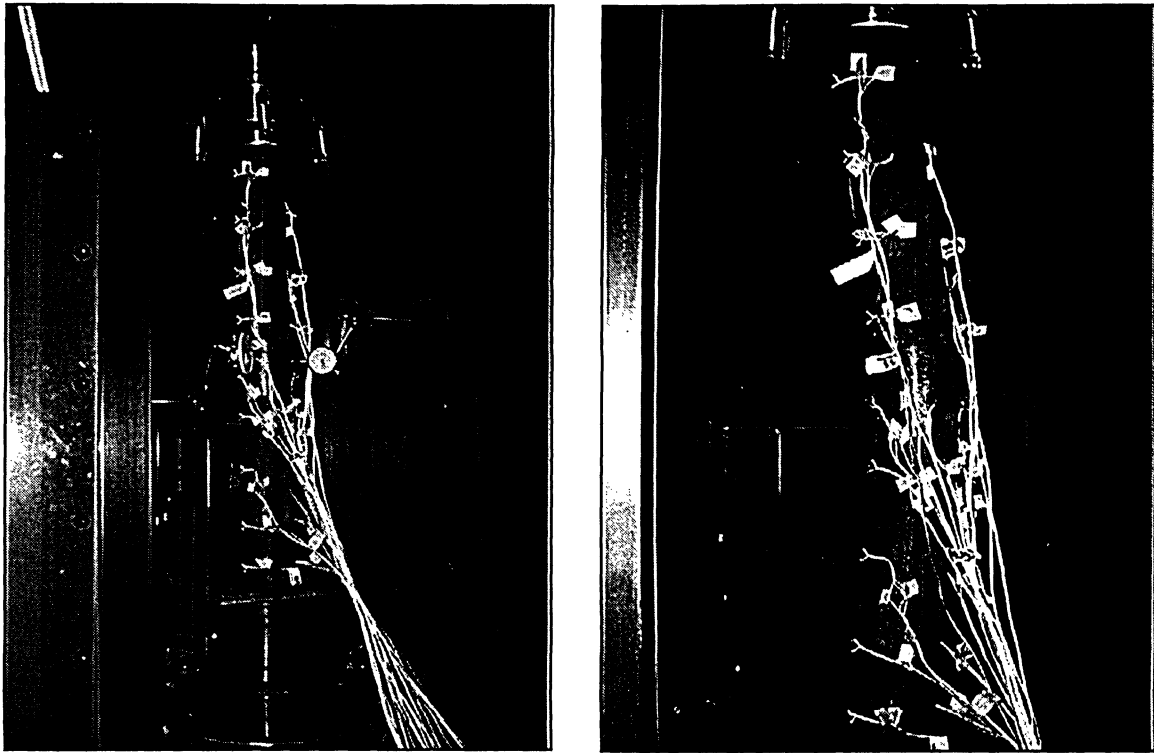


Figure 4.68 Views of specimen SR-13 before and after testing

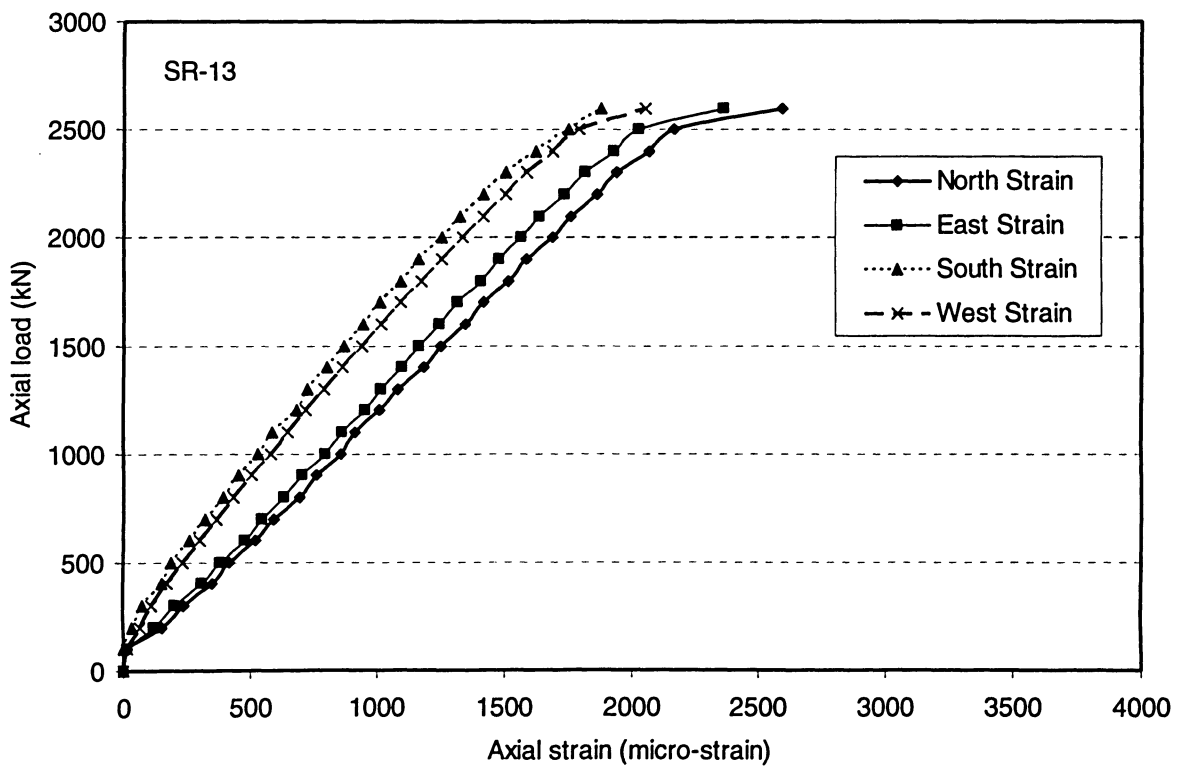


Figure 4.69 Axial load-strain relationships for specimen SR-13

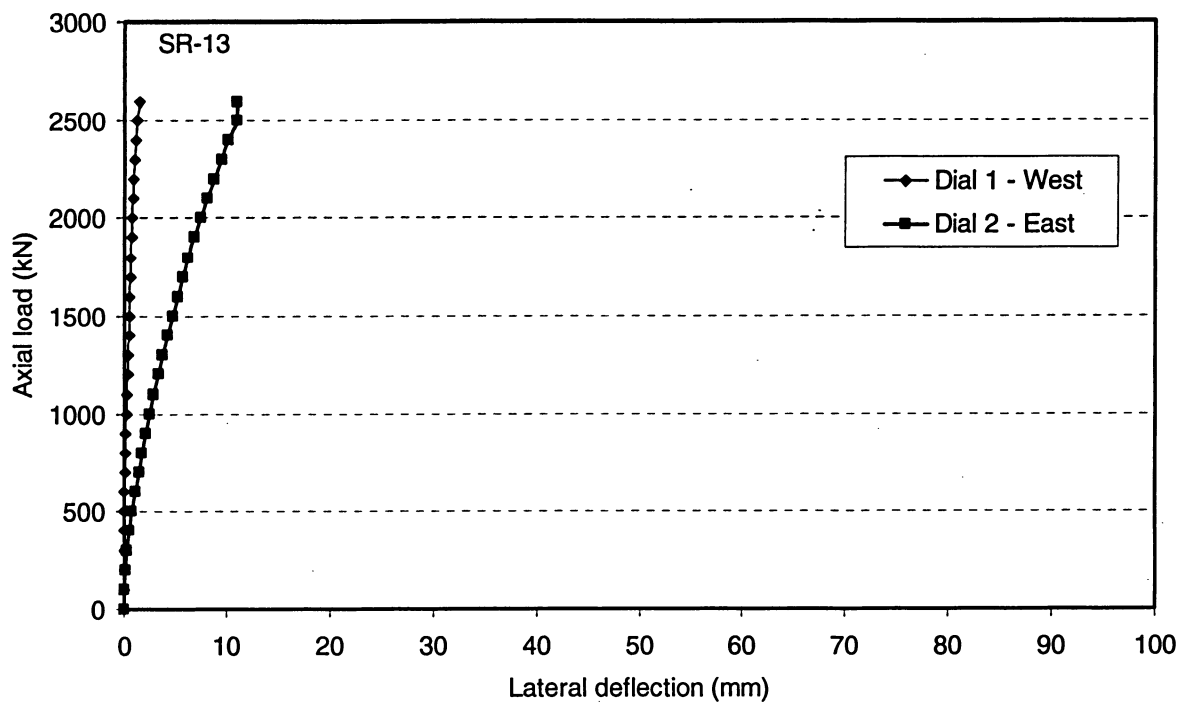


Figure 4.70 Load-lateral deflection curves for specimen SR-13

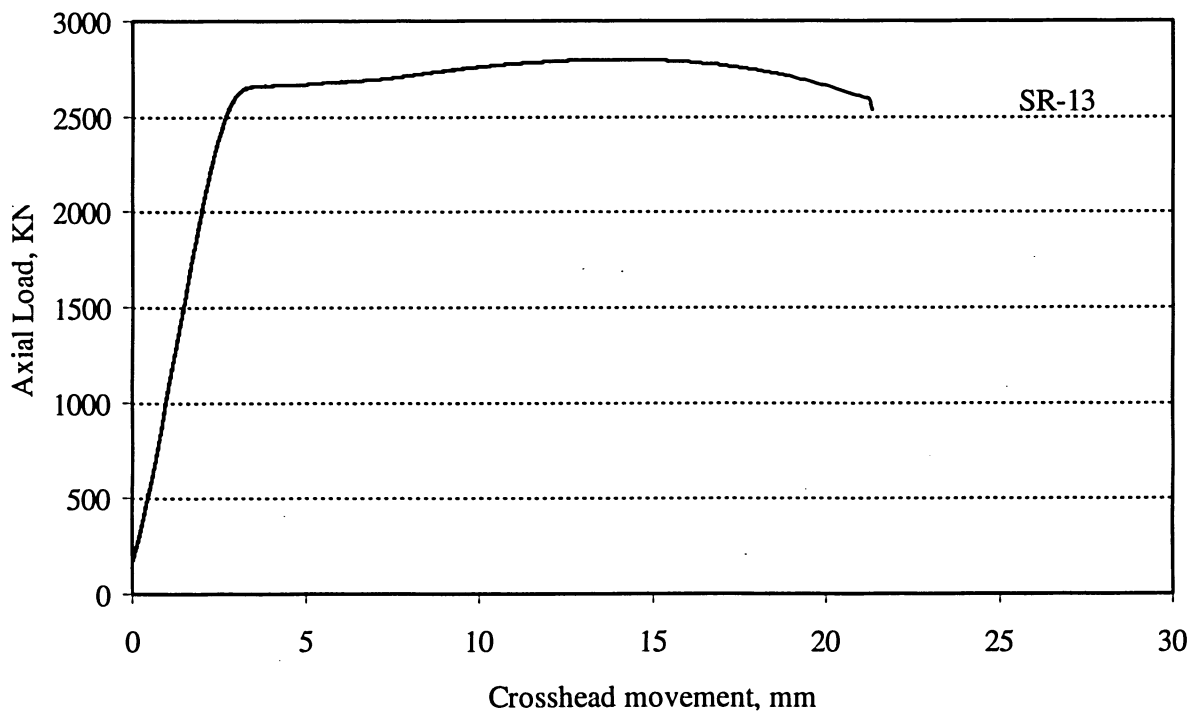


Figure 4.71 Load versus overall shortening curve for specimen SR-13

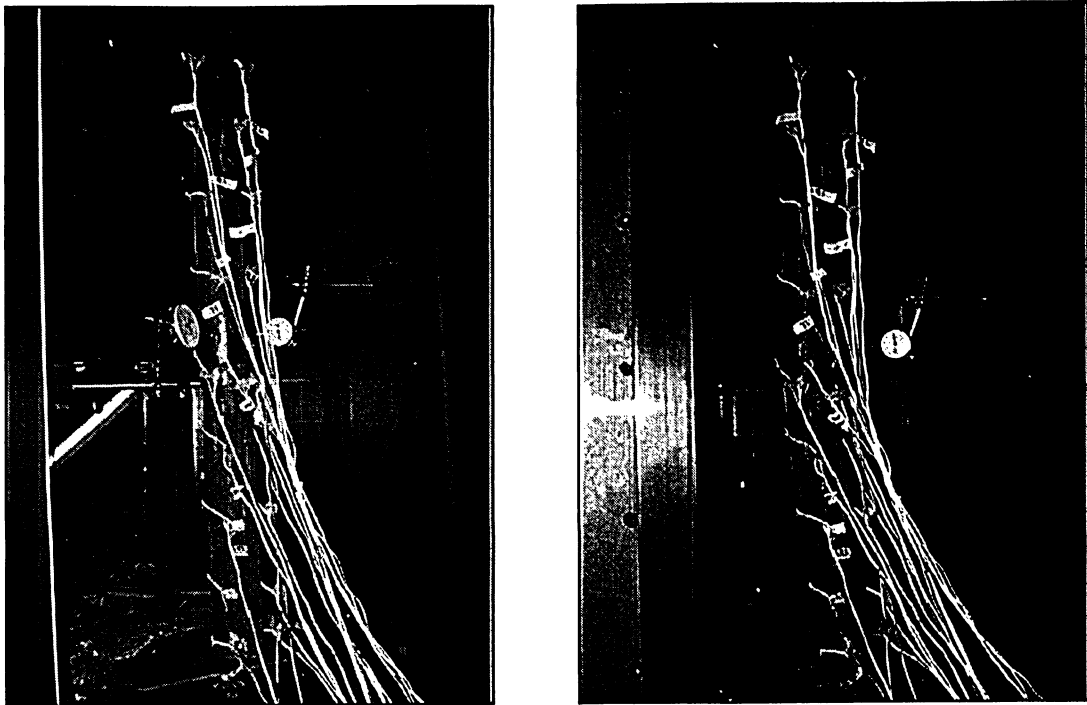


Figure 4.72 Views of specimen SR-14 before and after testing

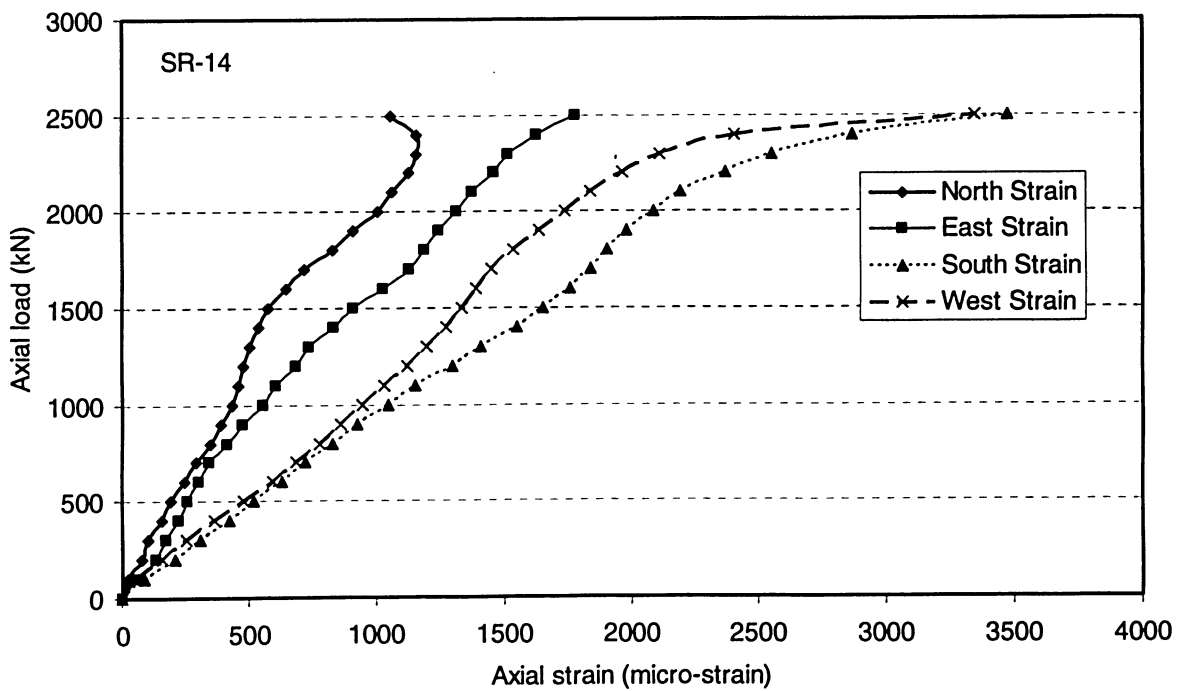


Figure 4.73 Axial load-strain relationships for specimen SR-14

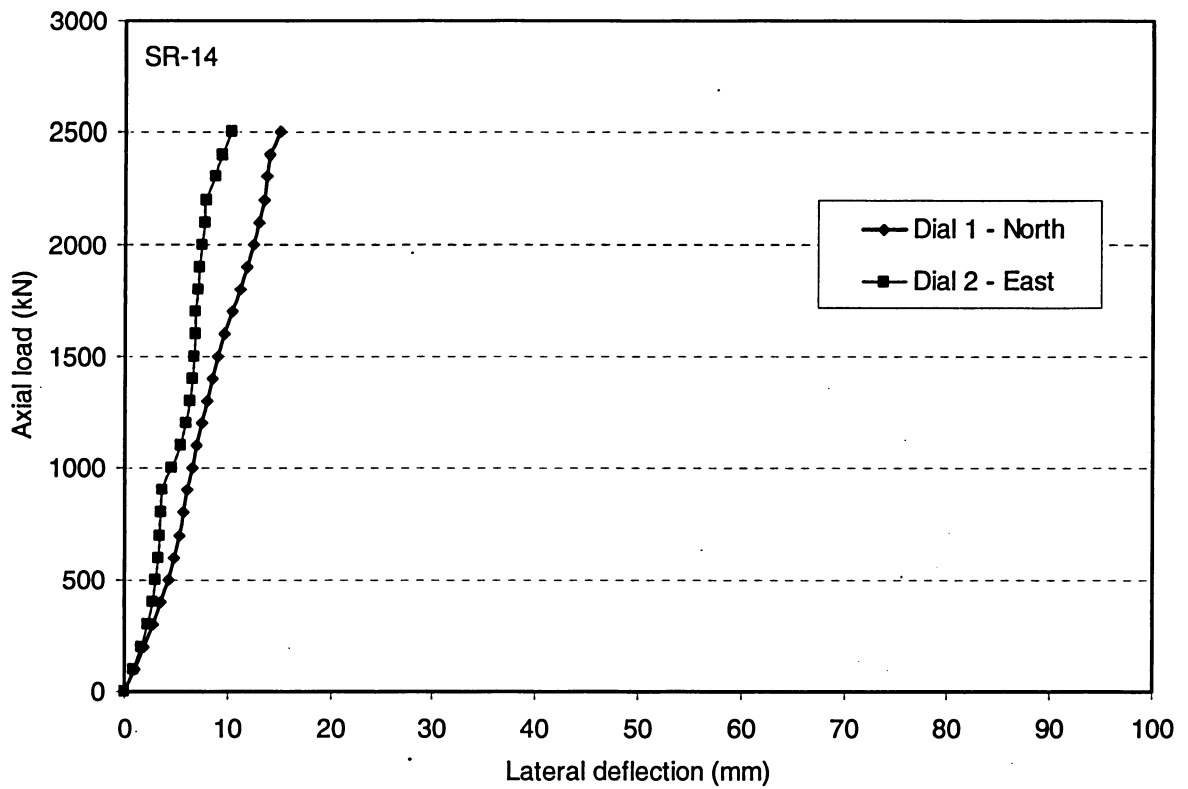


Figure 4.74 Load-lateral deflection curves for specimen SR-14

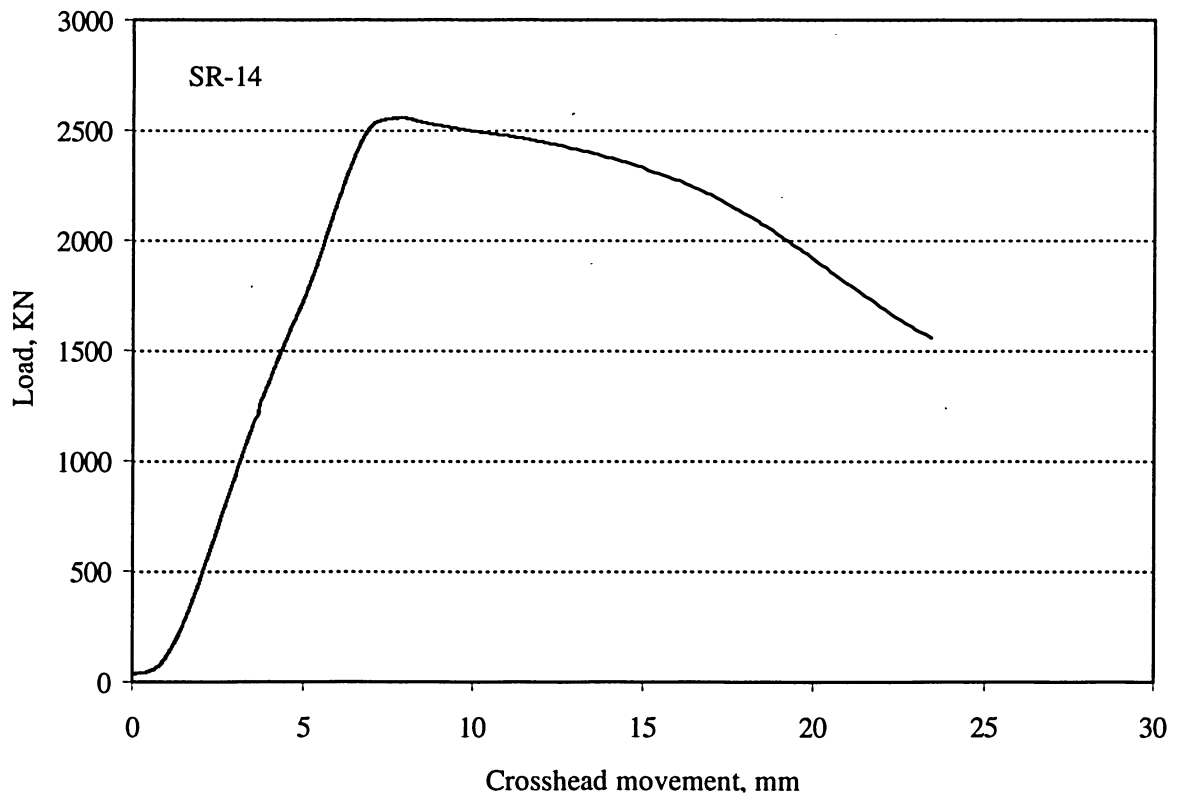


Figure 4.75 Load versus overall shortening curve for specimen SR-14

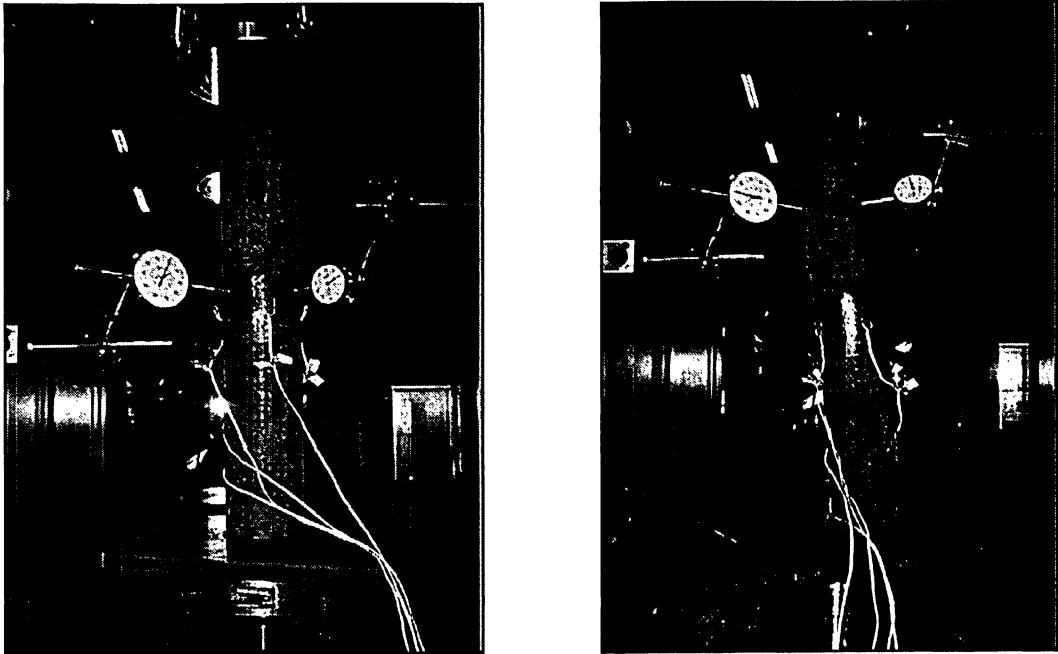


Figure 4.76 Views of specimen SR-15 before and after testing

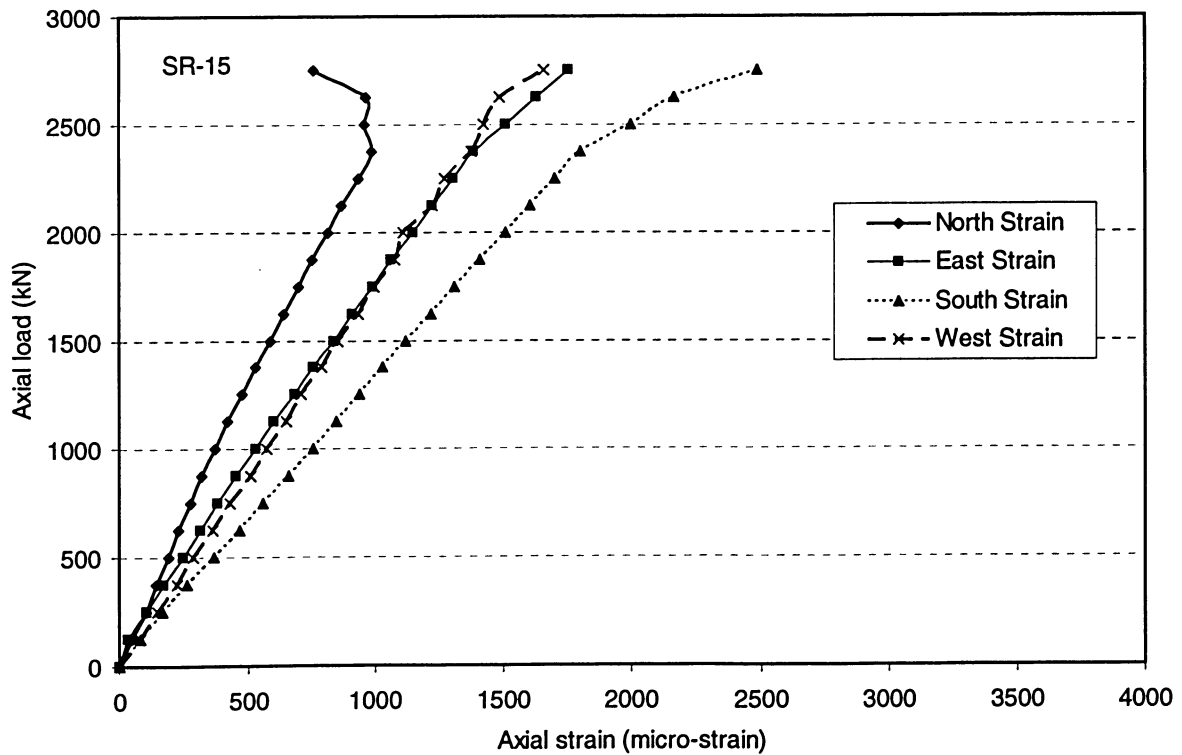


Figure 4.77 Axial load-strain relationships for specimen SR-15

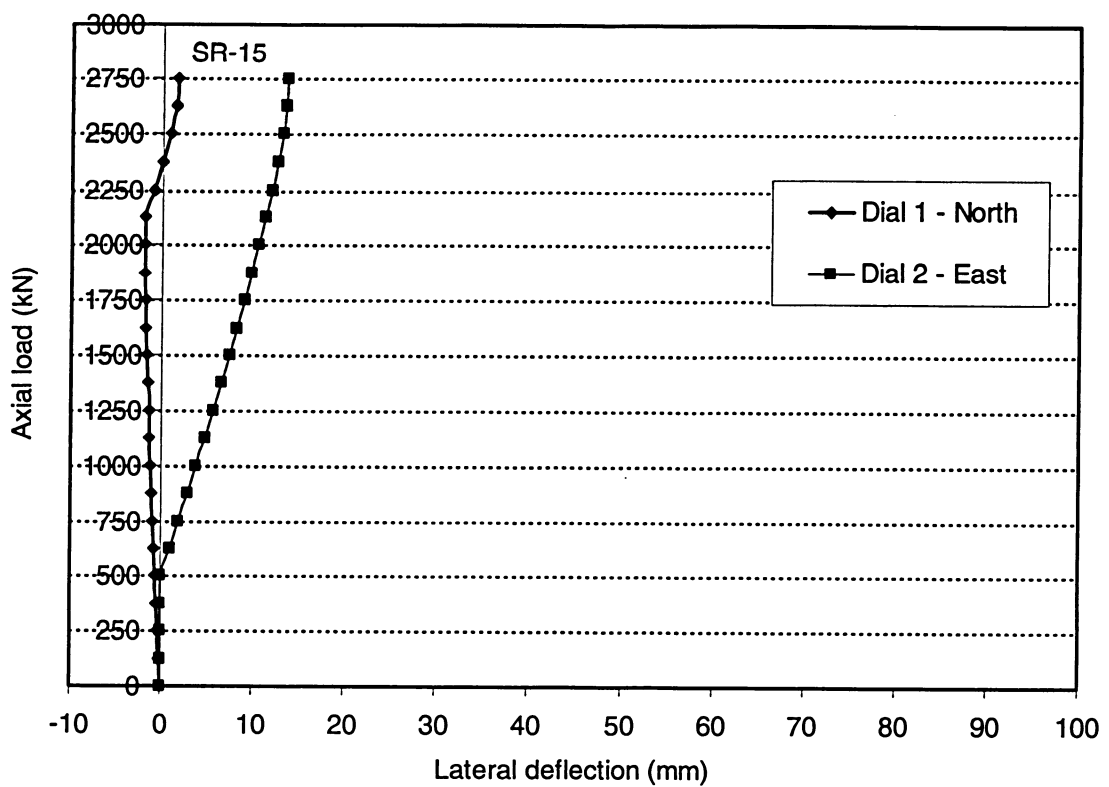


Figure 4.78 Load-lateral deflection curves for specimen SR-15

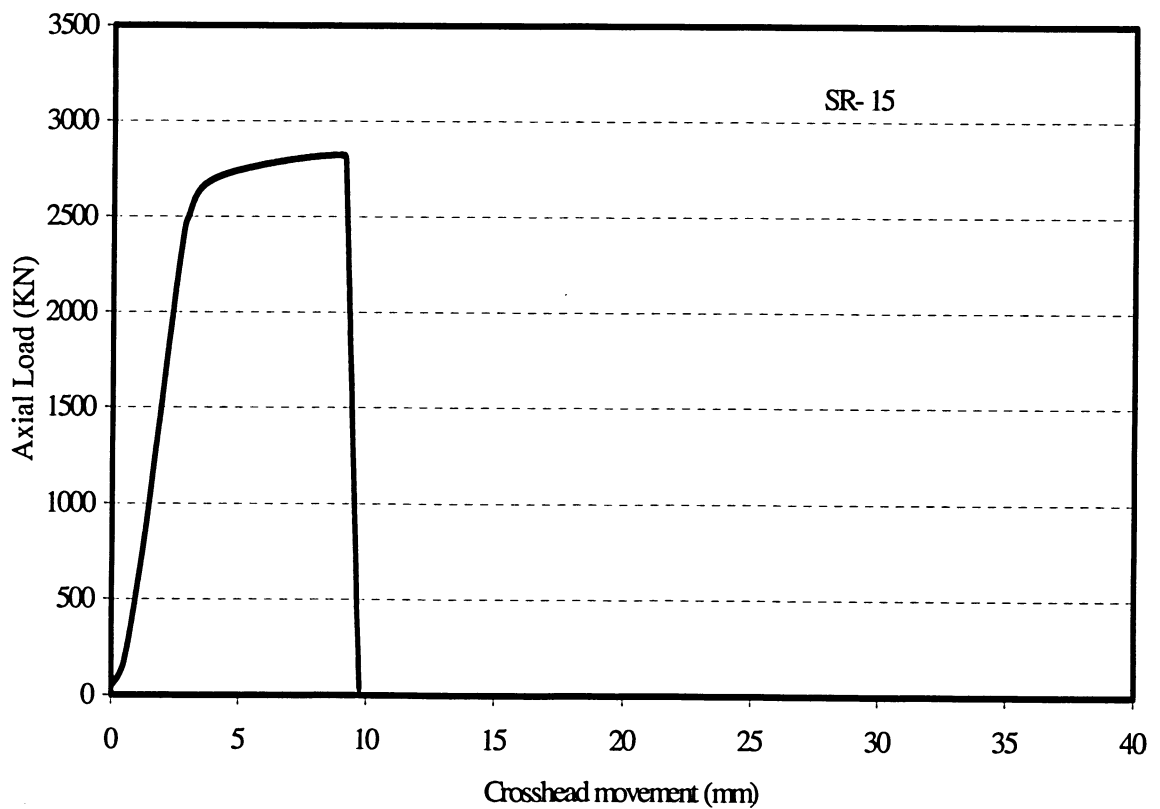


Figure 4.79 Load versus overall shortening curve for specimen NSR-15

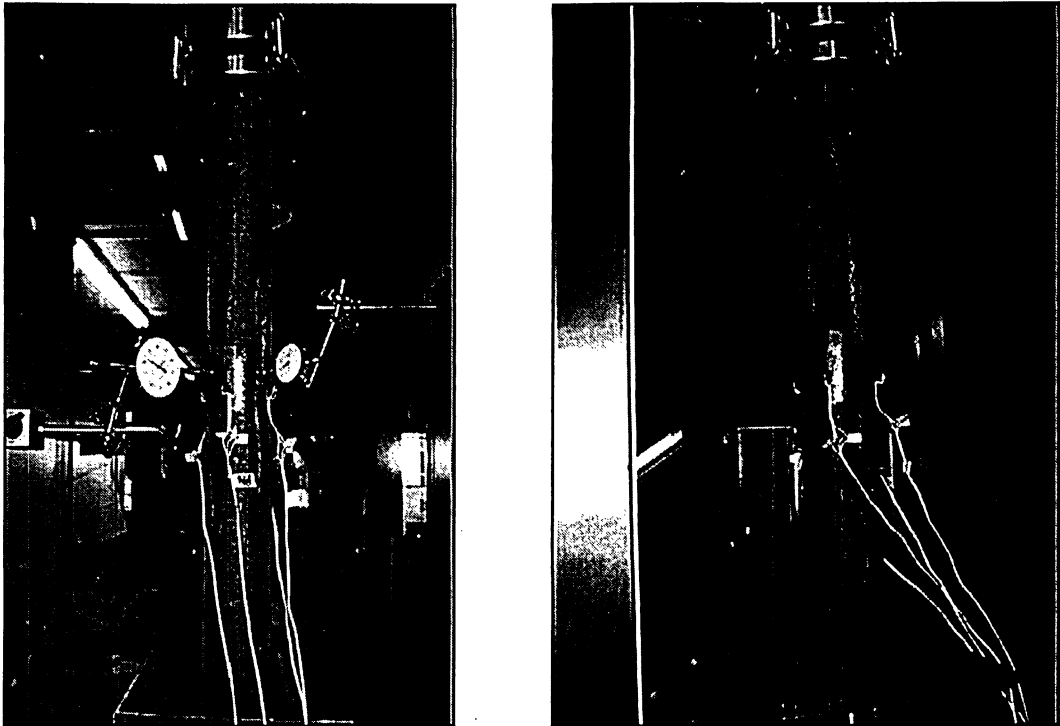


Figure 4.80 Views of specimen SR-16 before and after testing

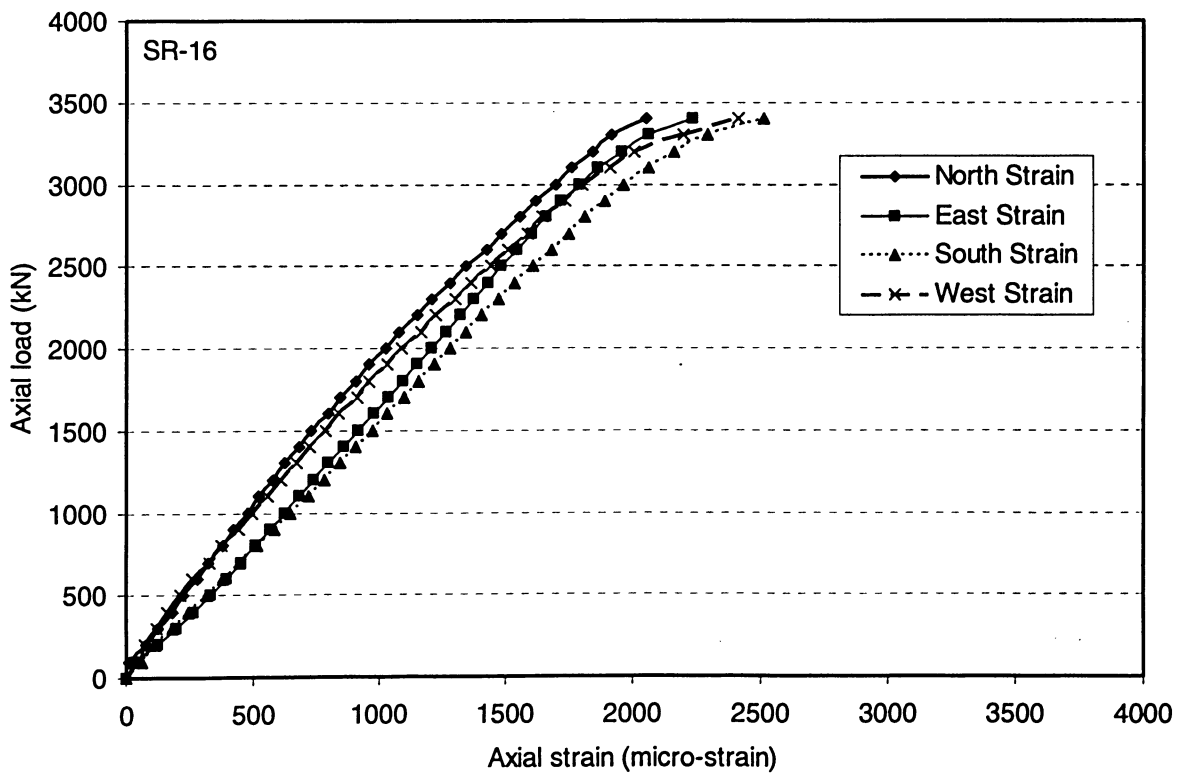


Figure 4.81 Axial load-strain relationships for specimen SR-16

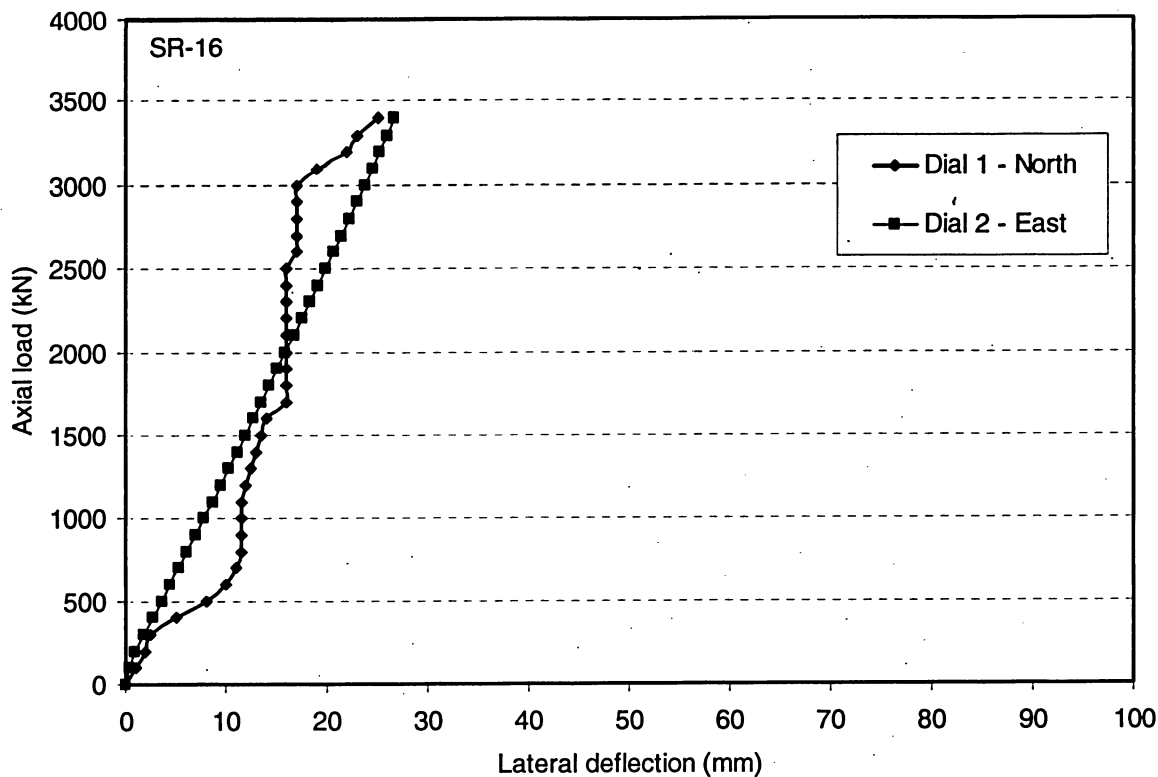


Figure 4.82 Load-lateral deflection curves for specimen SR-16

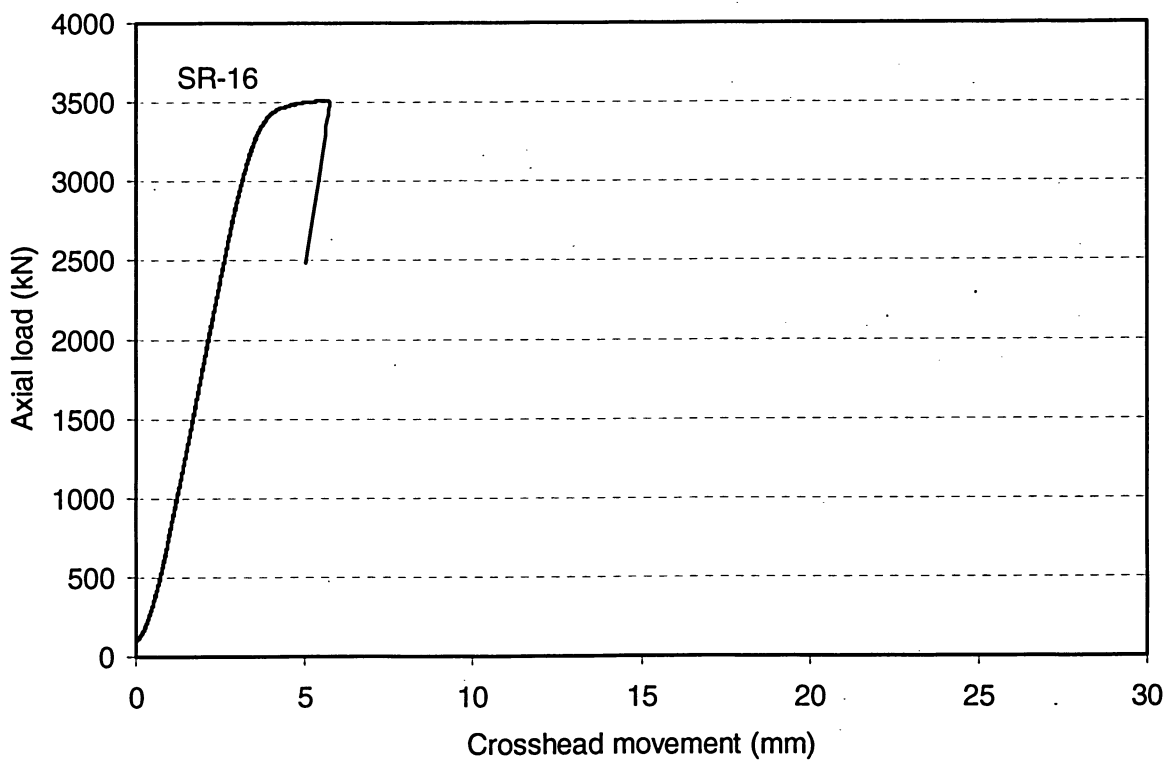


Figure 4.83 Load versus overall shortening curve for specimen SR-16

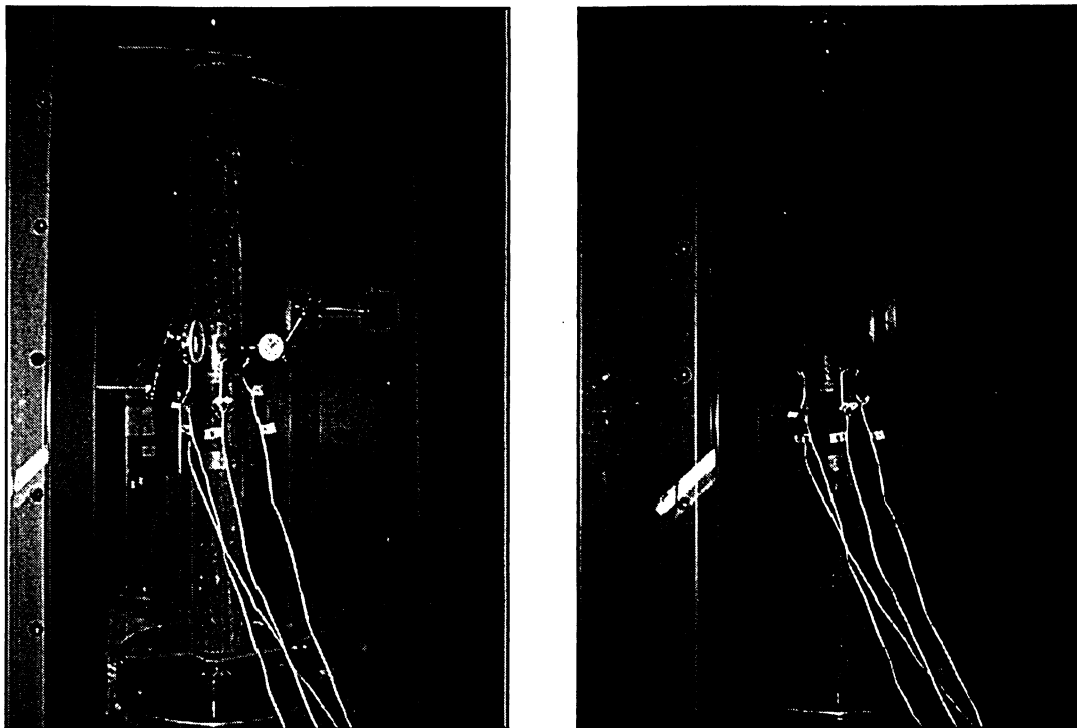


Figure 4.84 Views of specimen SR-17 before and after testing

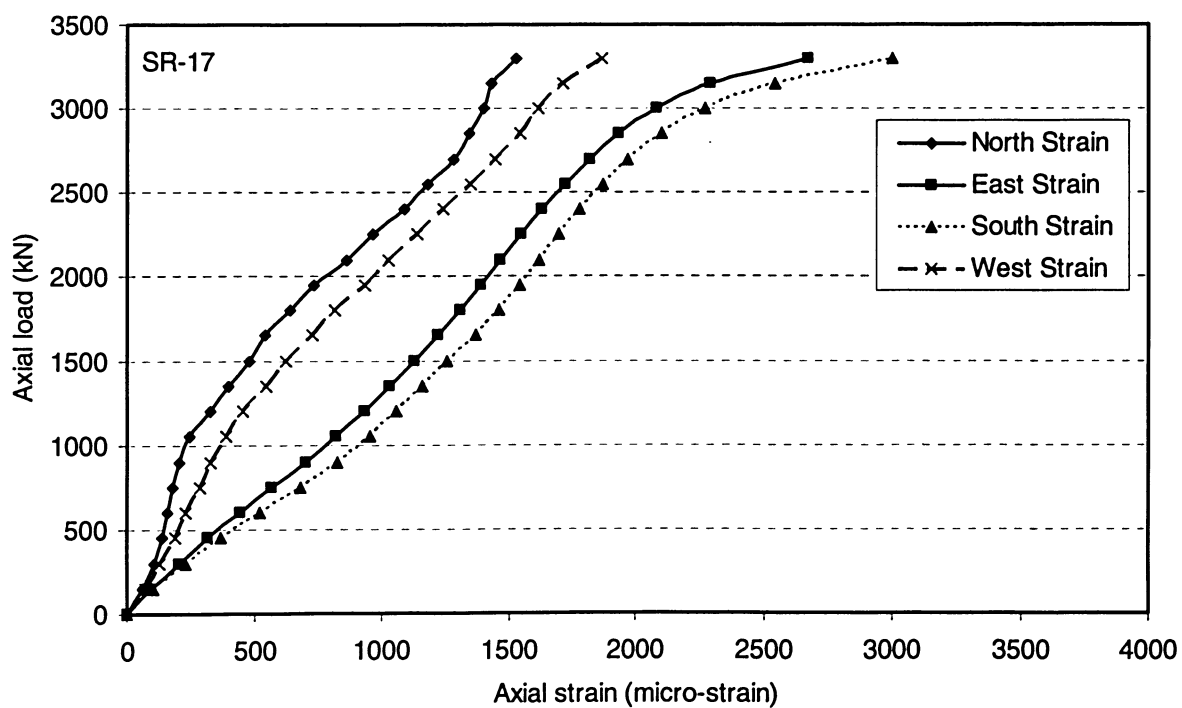


Figure 4.85 Axial load-strain relationships for specimen SR-17

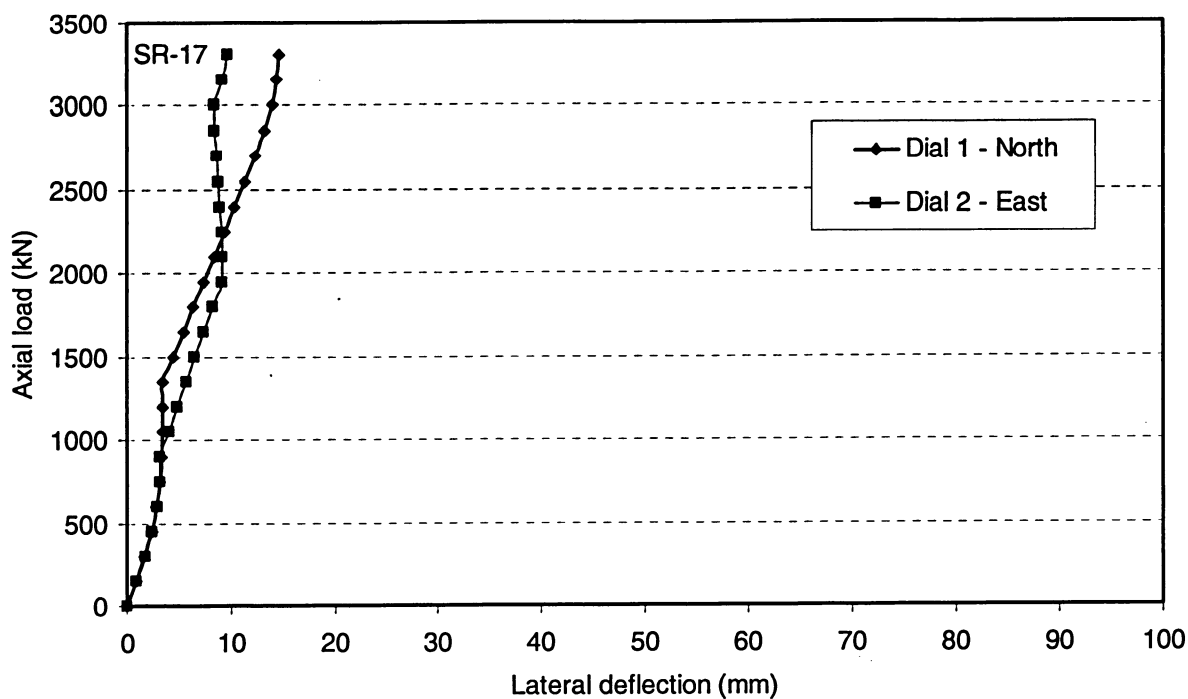


Figure 4.86 Load-lateral deflection curves for specimen SR-17

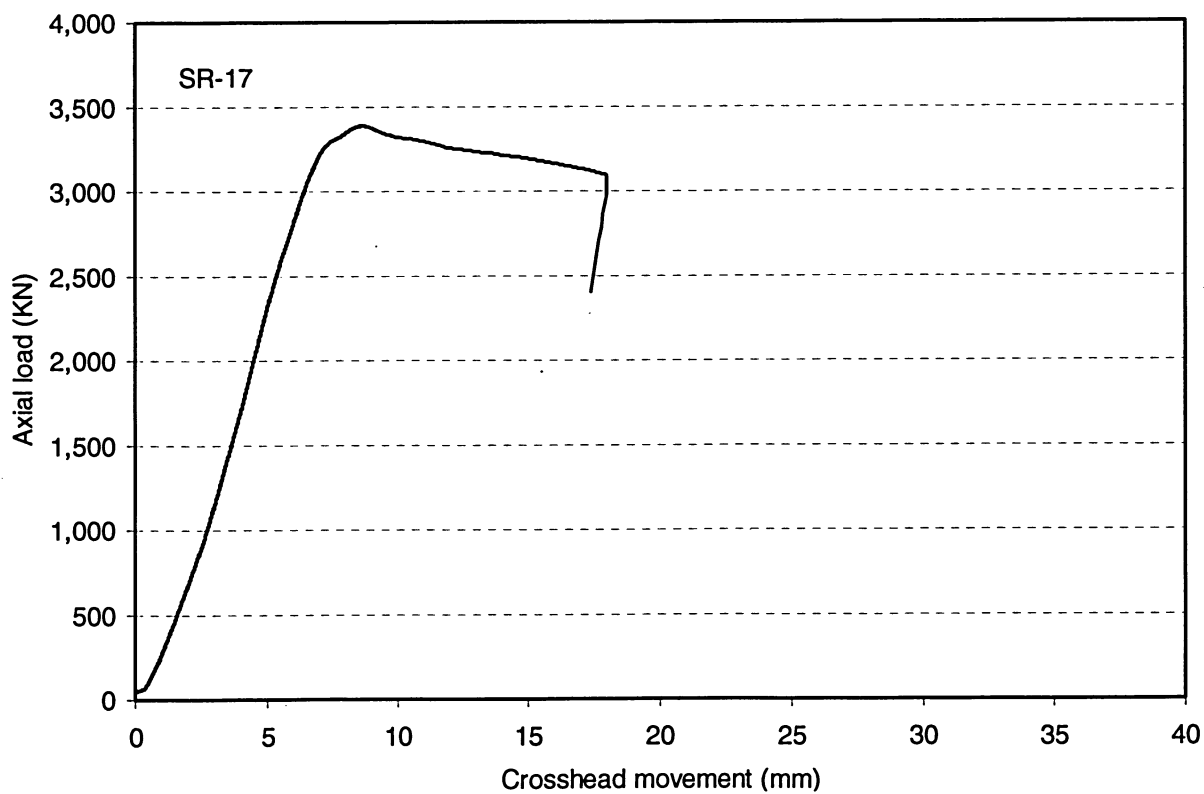


Figure 4.87 Load versus overall shortening curve for specimen SR-17

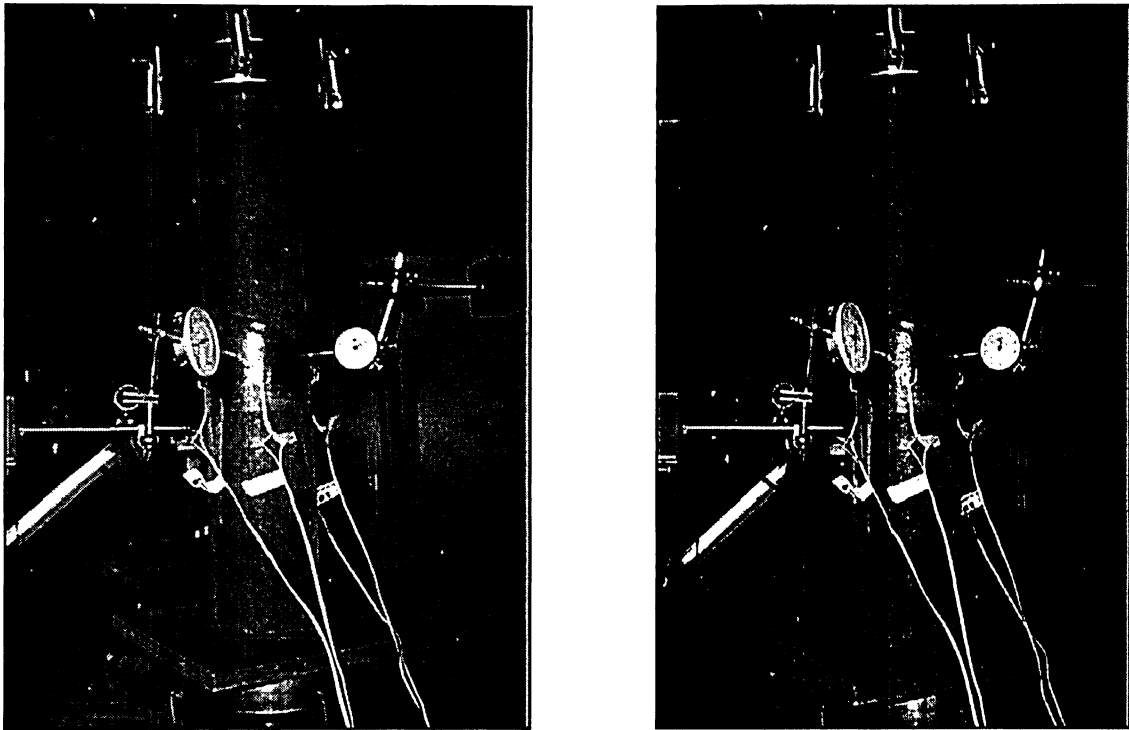


Figure 4.88 Views of specimen SR-18 before and after testing

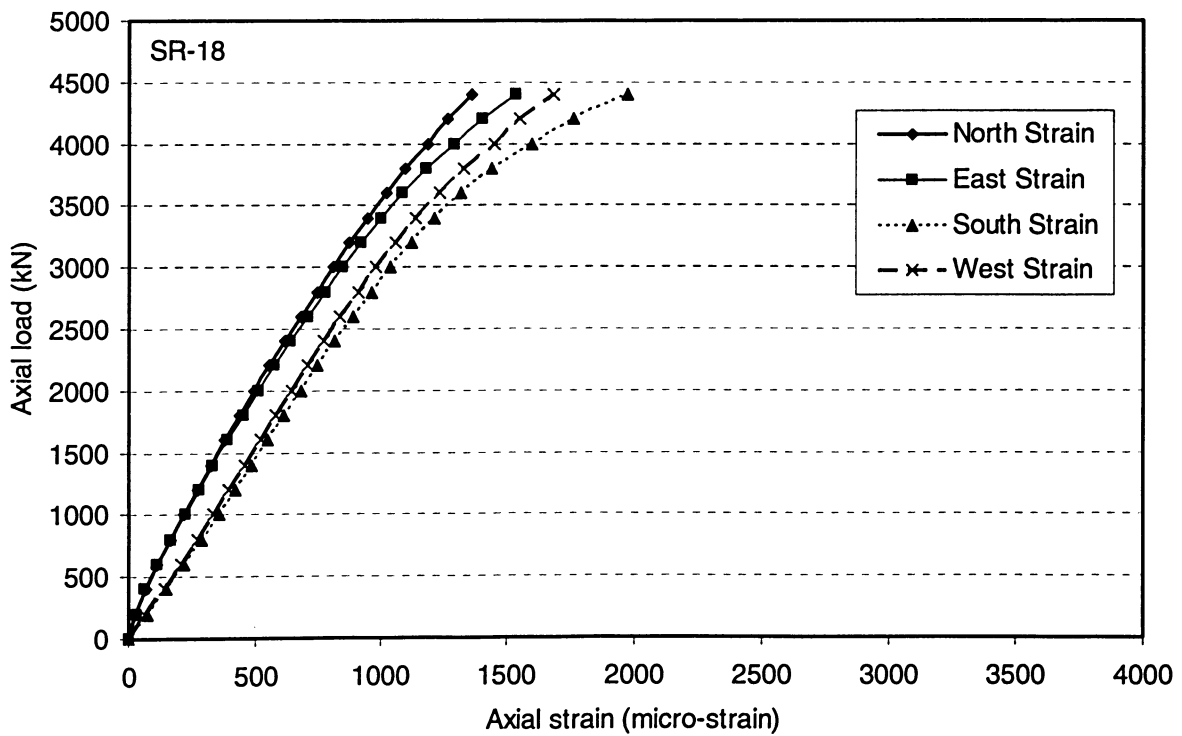


Figure 4.89 Axial load-strain relationships for specimen SR-18

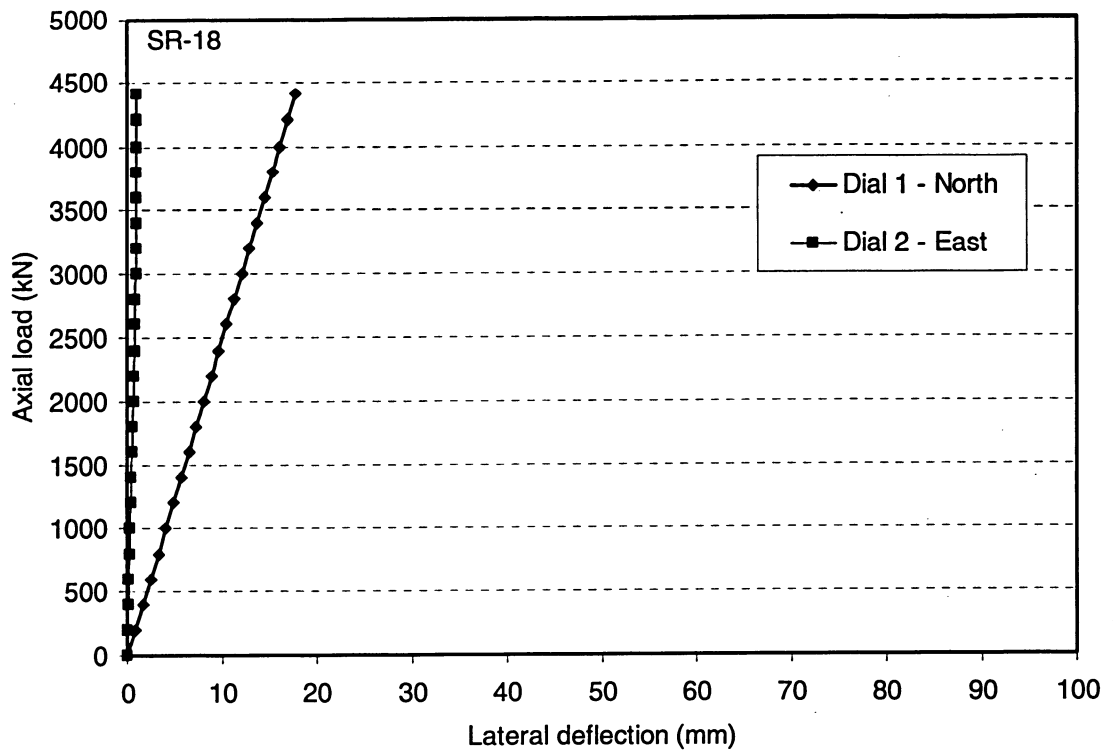


Figure 4.90 Load-lateral deflection curves for specimen SR-18

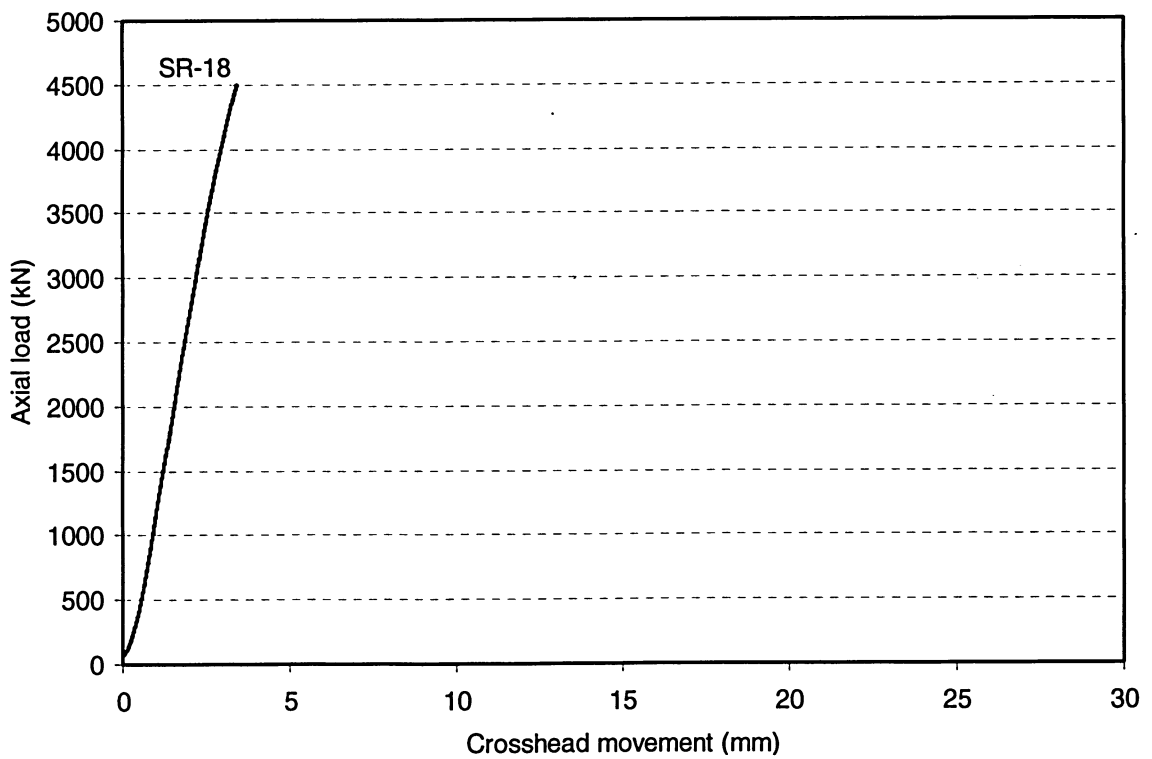


Figure 4.91 Load versus overall shortening curve for specimen SR-18

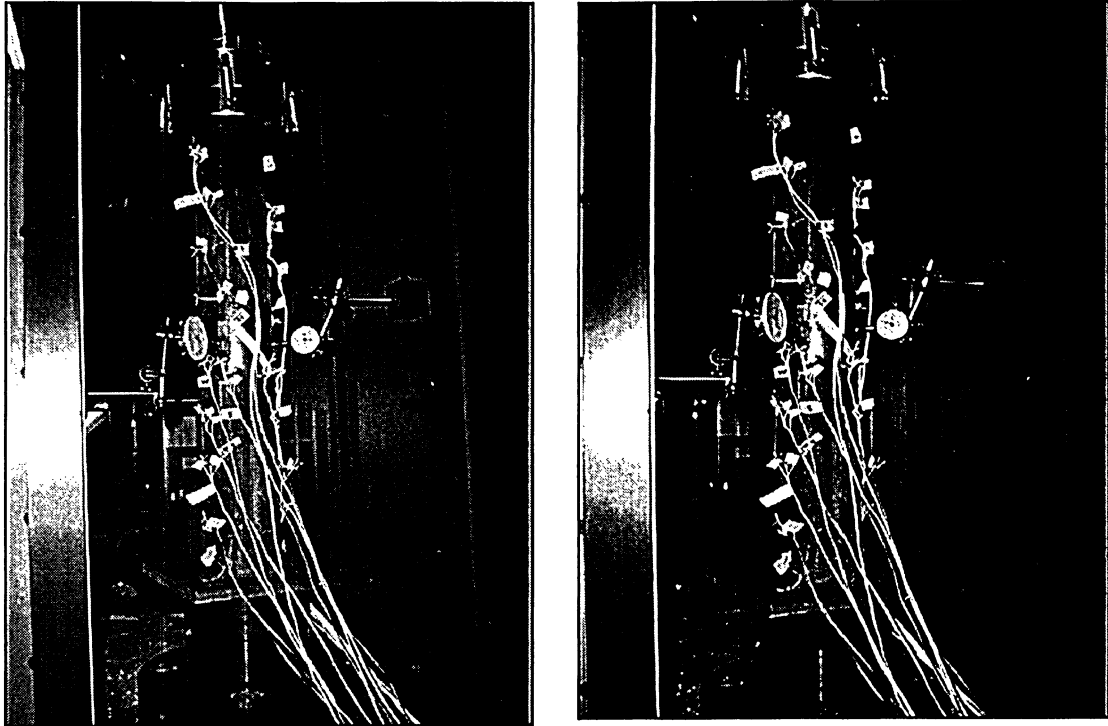


Figure 4.92 Views of specimen SR-19 before and after testing

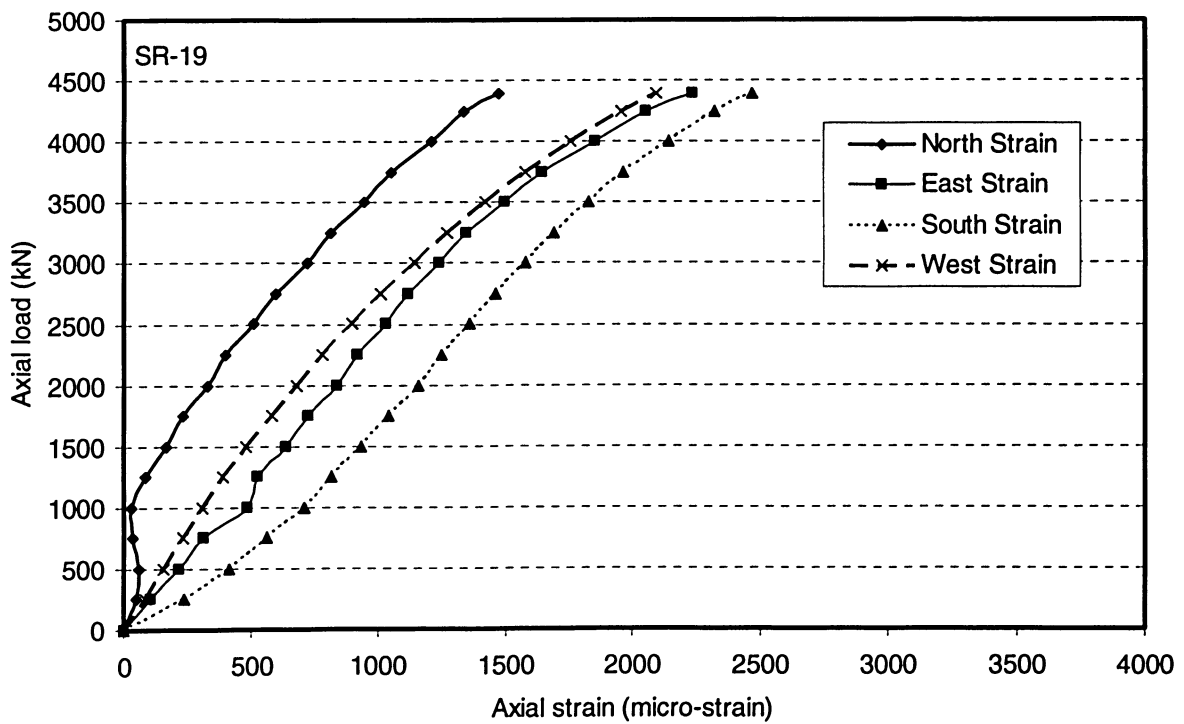


Figure 4.93 Axial load-strain relationships for specimen SR-19

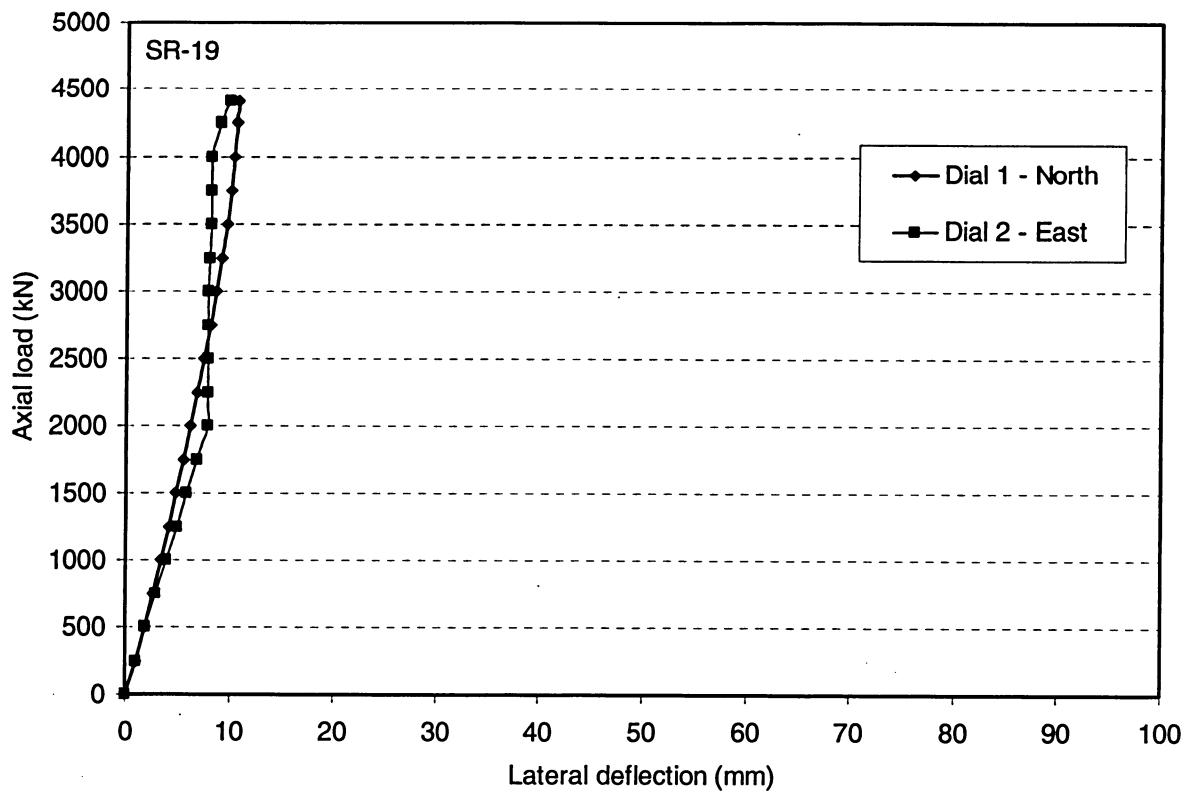


Figure 4.94 Load-lateral deflection curves for specimen SR-19

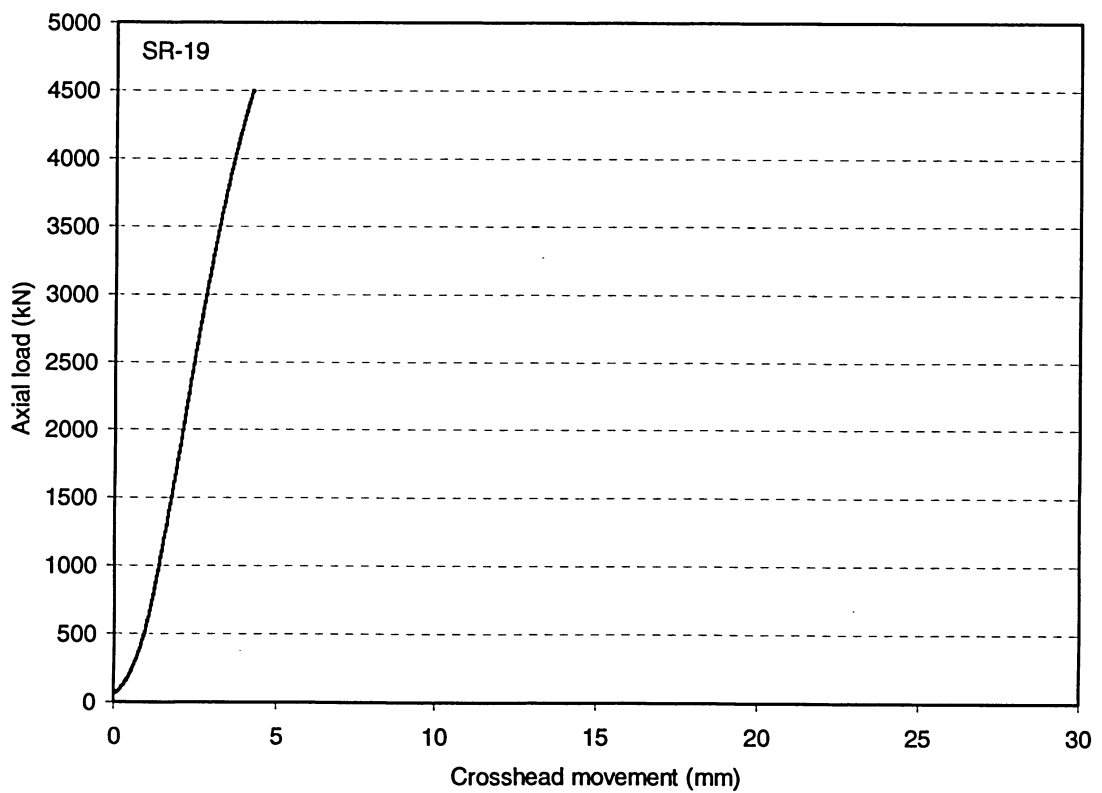


Figure 4.95 Load versus overall shortening curve for specimen SR-19

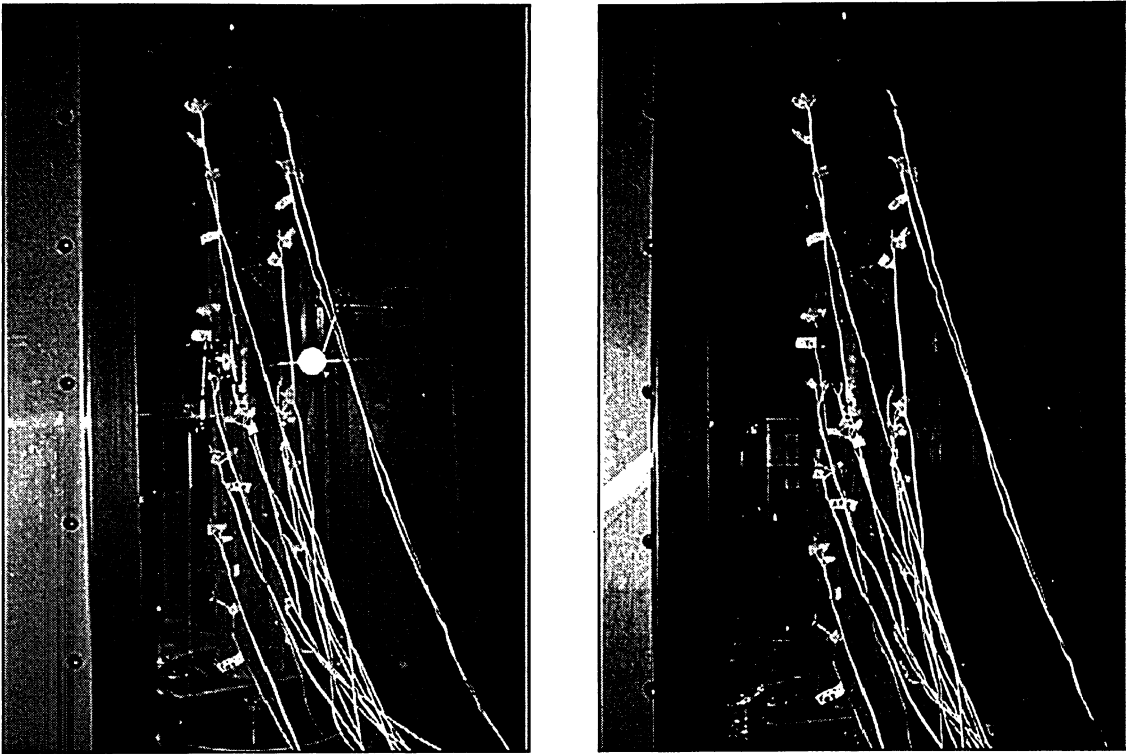


Figure 4.96 Views of specimen SR-20 before and after testing

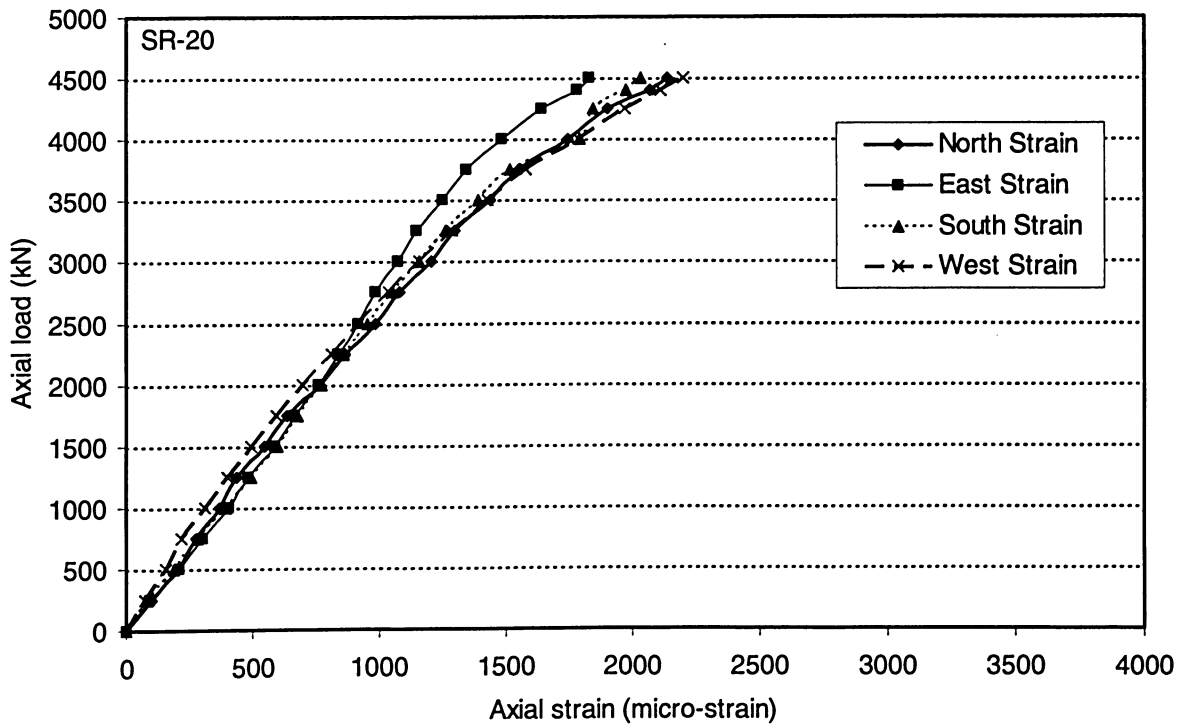


Figure4.97 Axial load-strain relationships for specimen SR-20

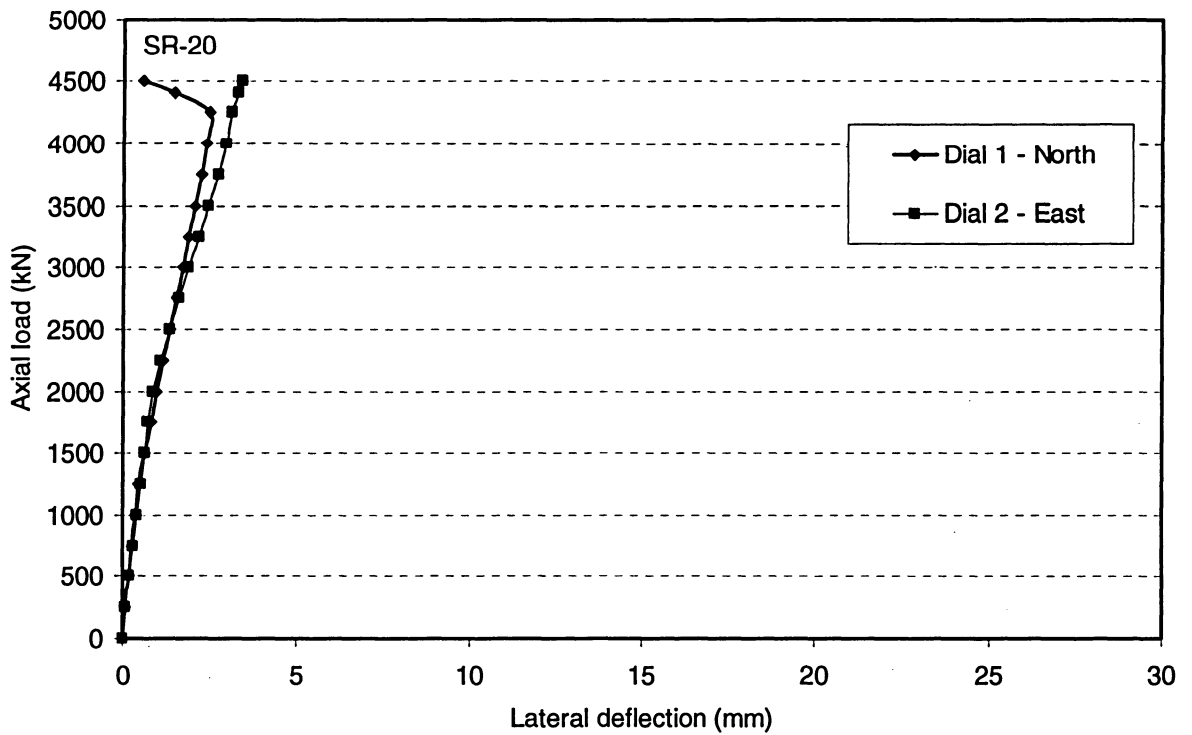


Figure 4.98 Load versus overall shortening curve for specimen SR-20

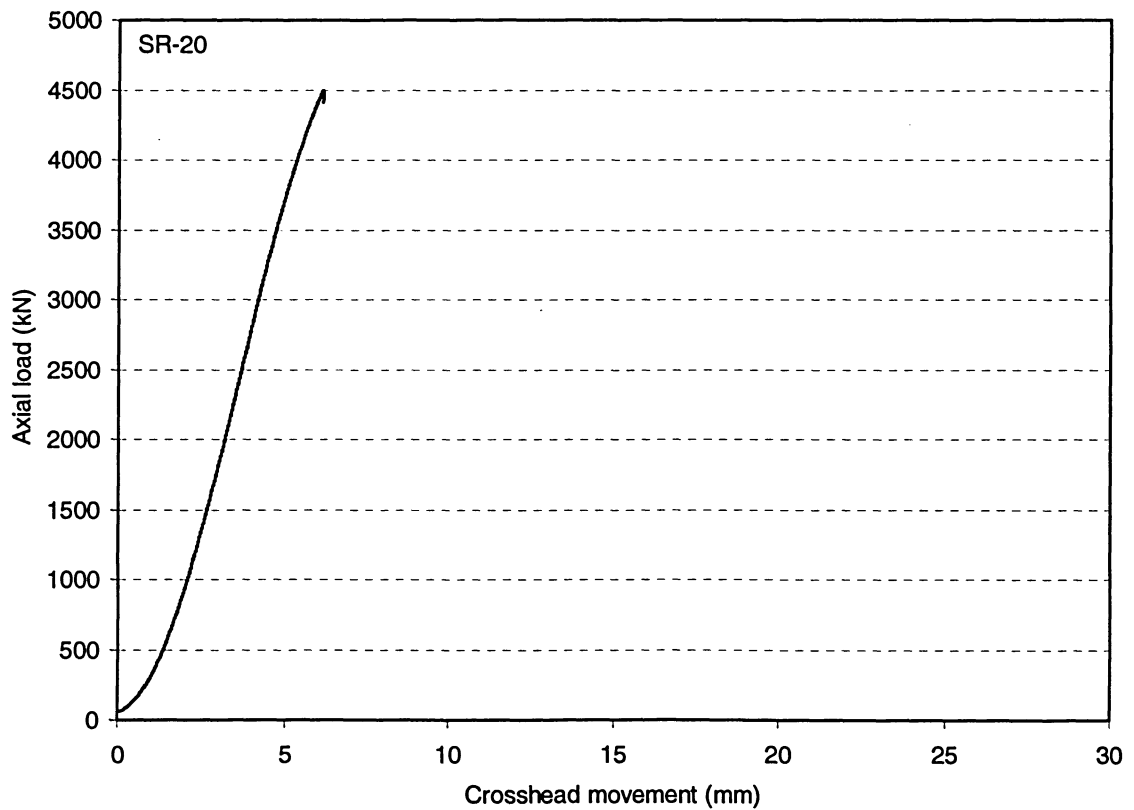


Figure 4.99 Load versus overall shortening curve for specimen SR-20

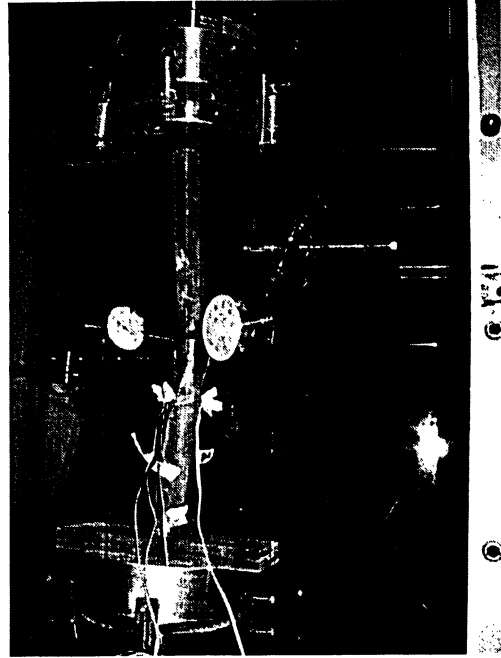
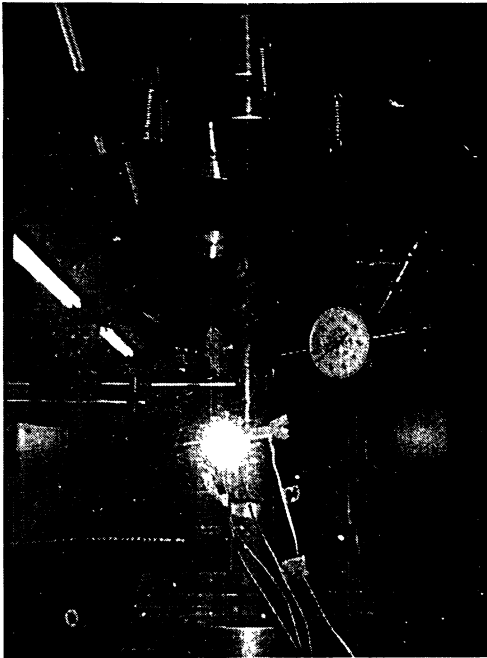


Figure 4.100 Views of specimen NSR-1 before and after testing

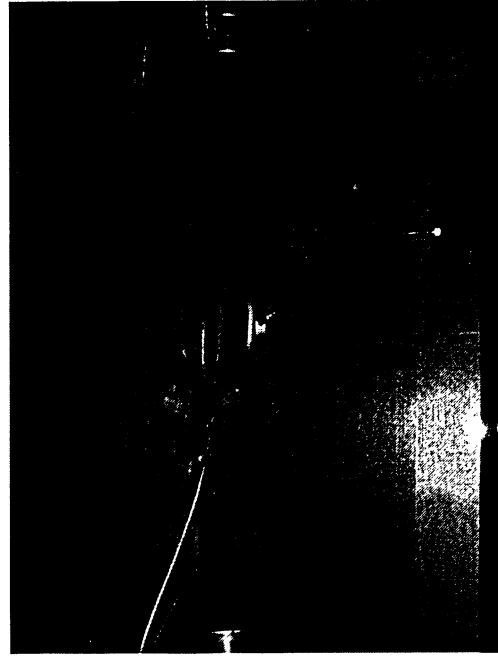
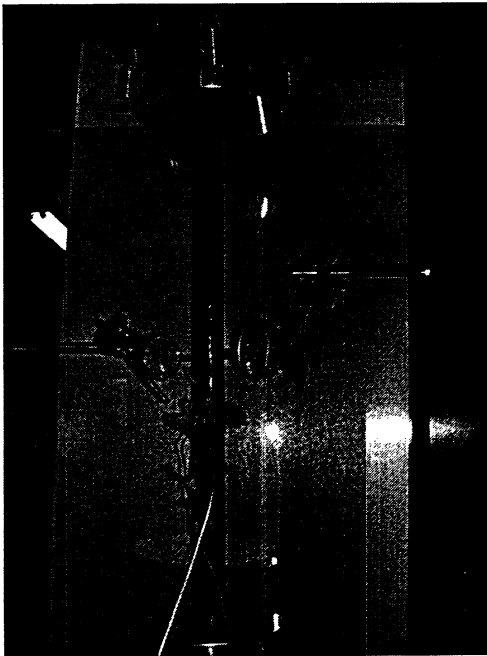


Figure 4.101 Views of specimen NSR-2 before and after testing

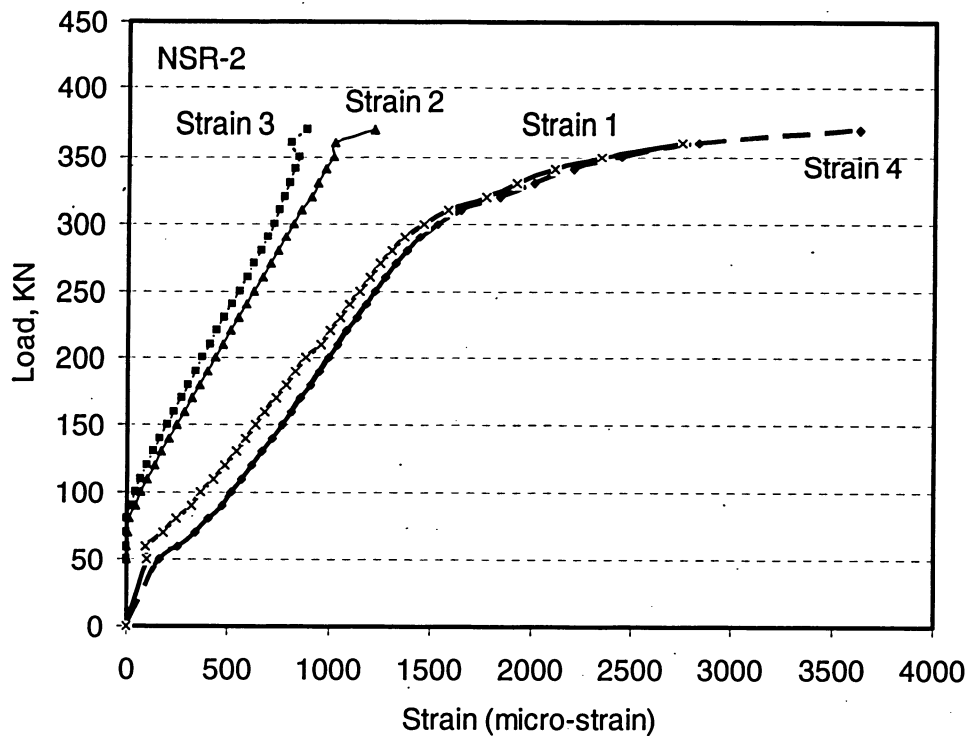


Figure 4.102 Axial load-strain relationships for specimen NSR-2

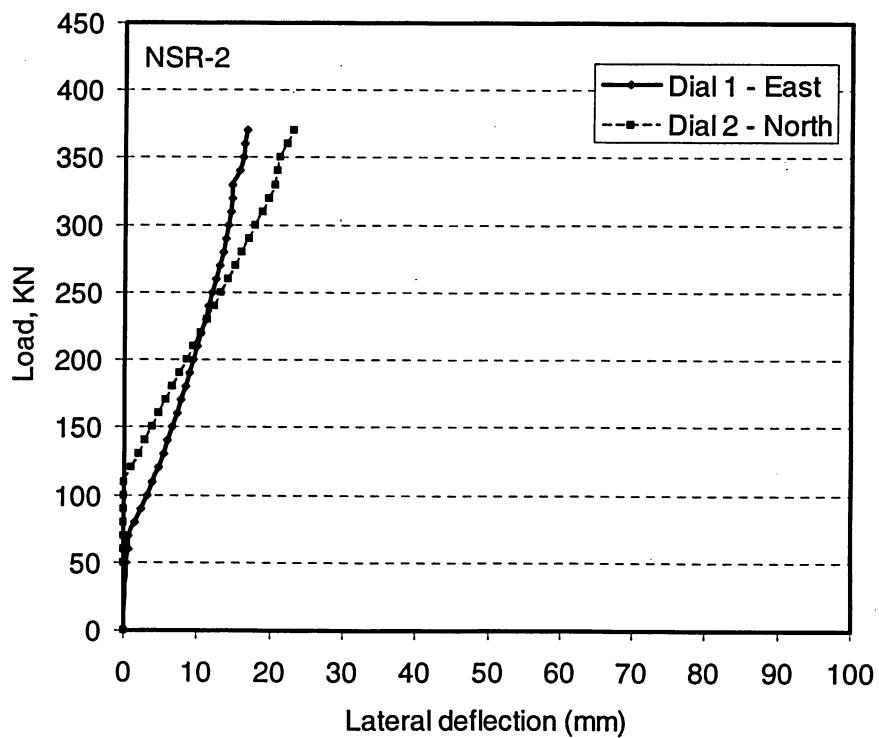


Figure 4.103 Load-lateral deflection curves for specimen NSR-2

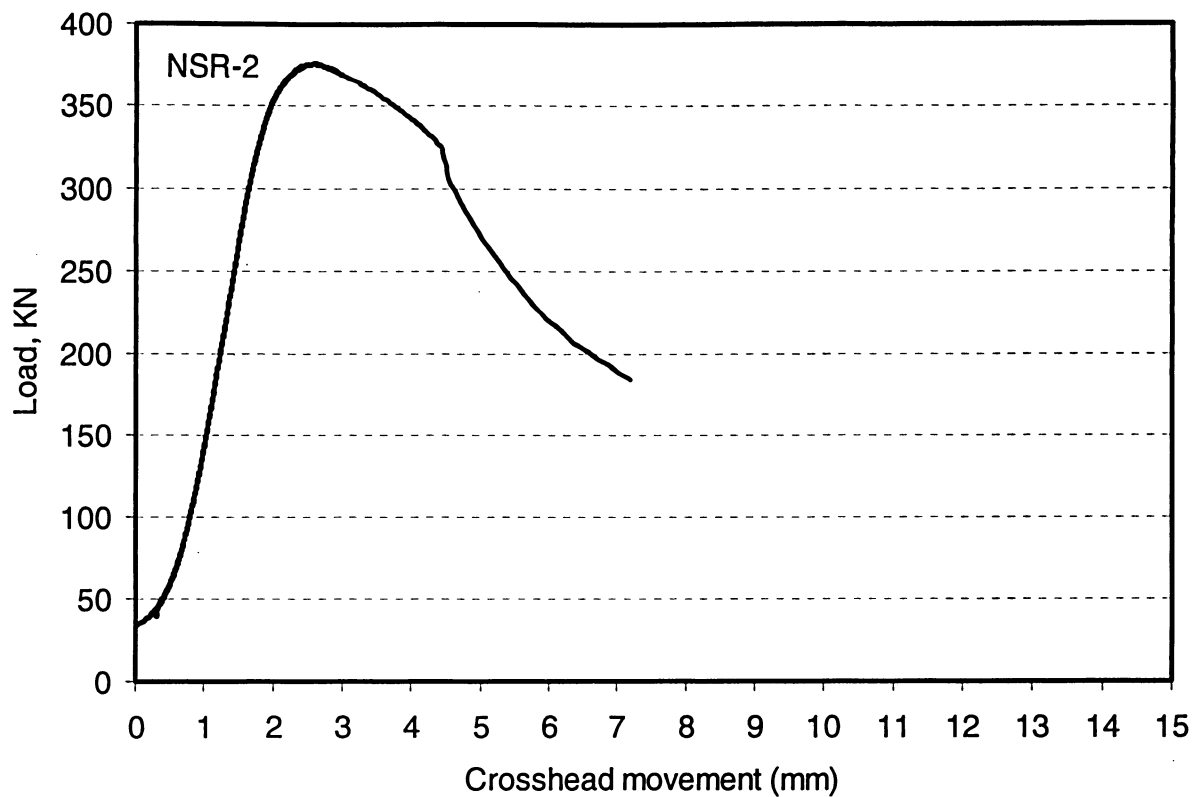


Figure 4.104 Load versus overall shortening curve for specimen NSR-2

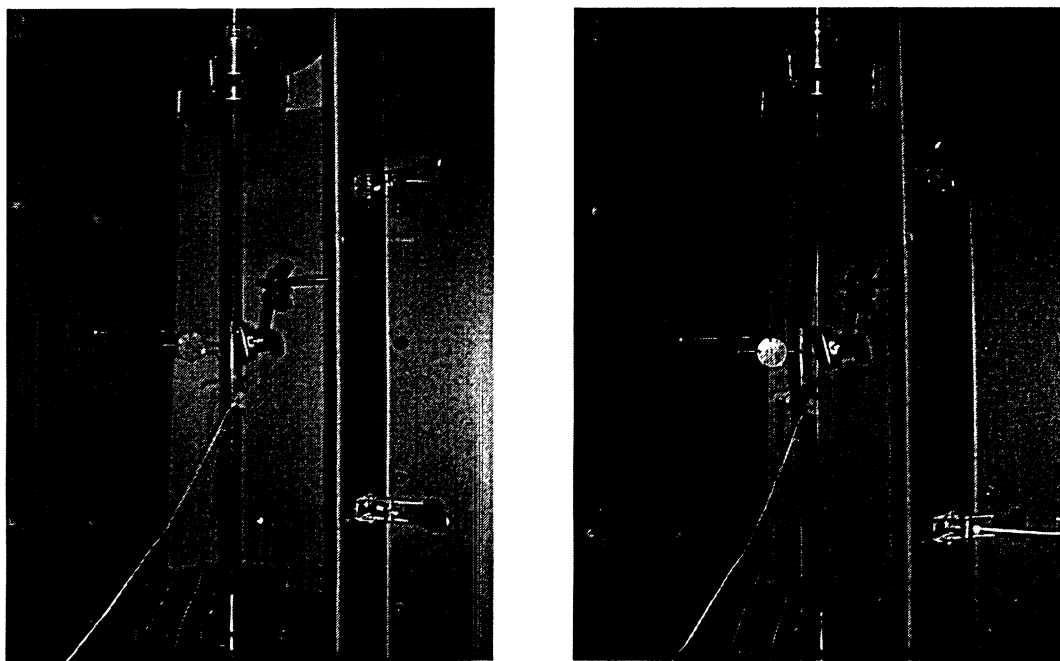


Figure 4.105 Views of specimen NSR-3 before and after testing

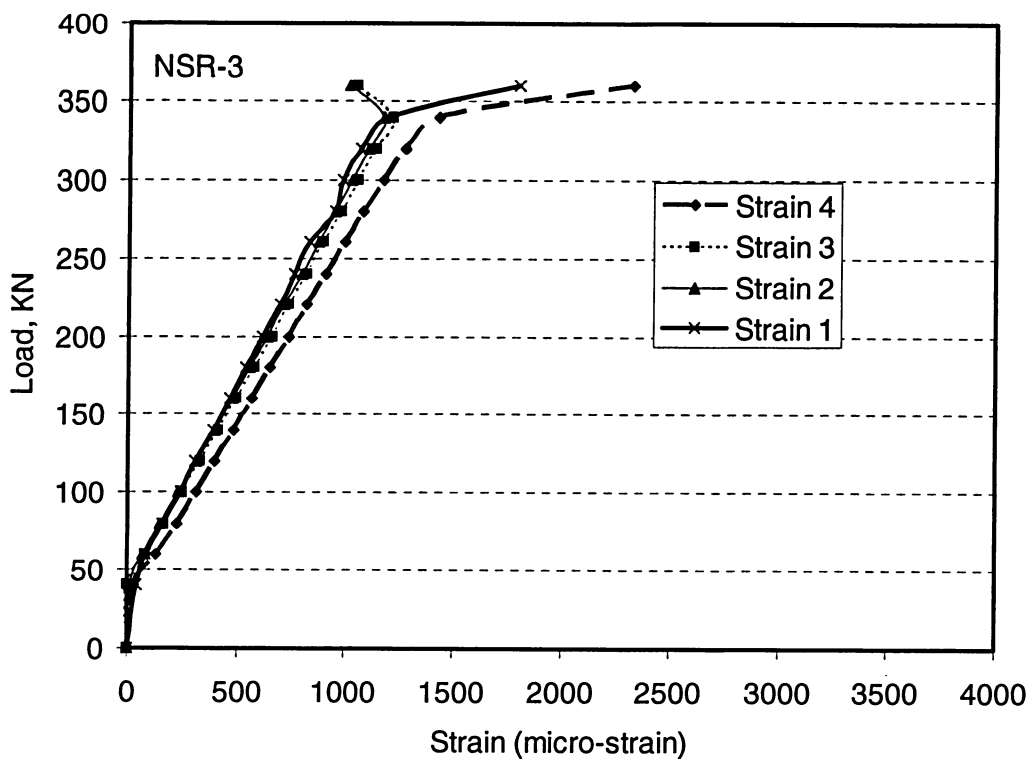


Figure 4.106 Axial load-strain relationships for specimen NSR-3

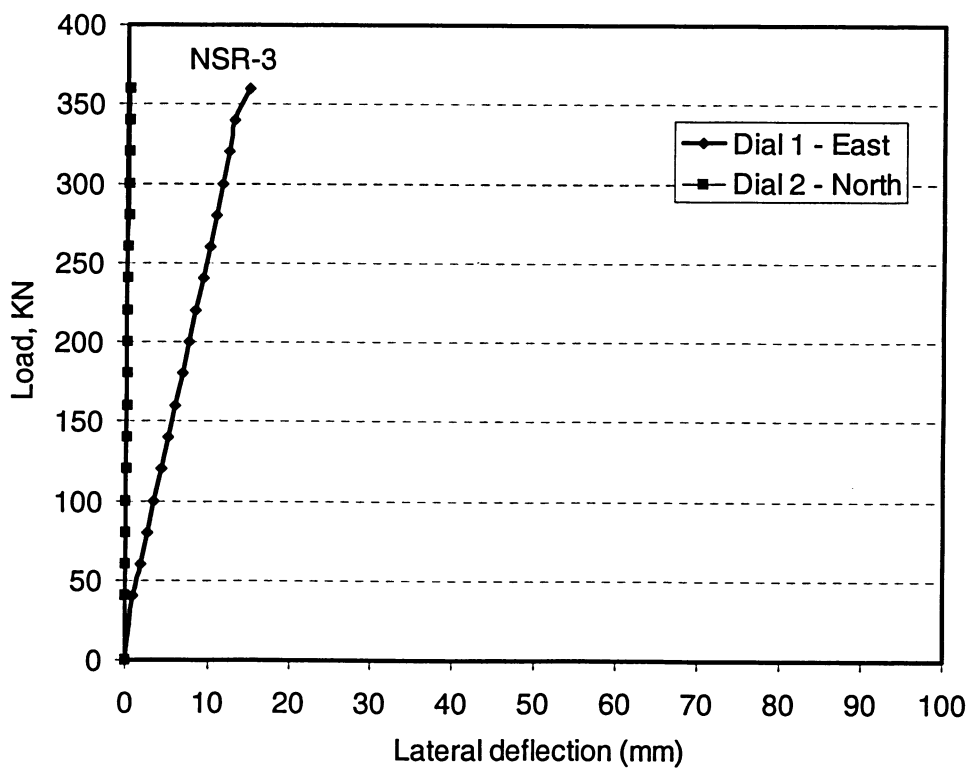


Figure 4.107 Load-lateral deflection curves for specimen NSR-3

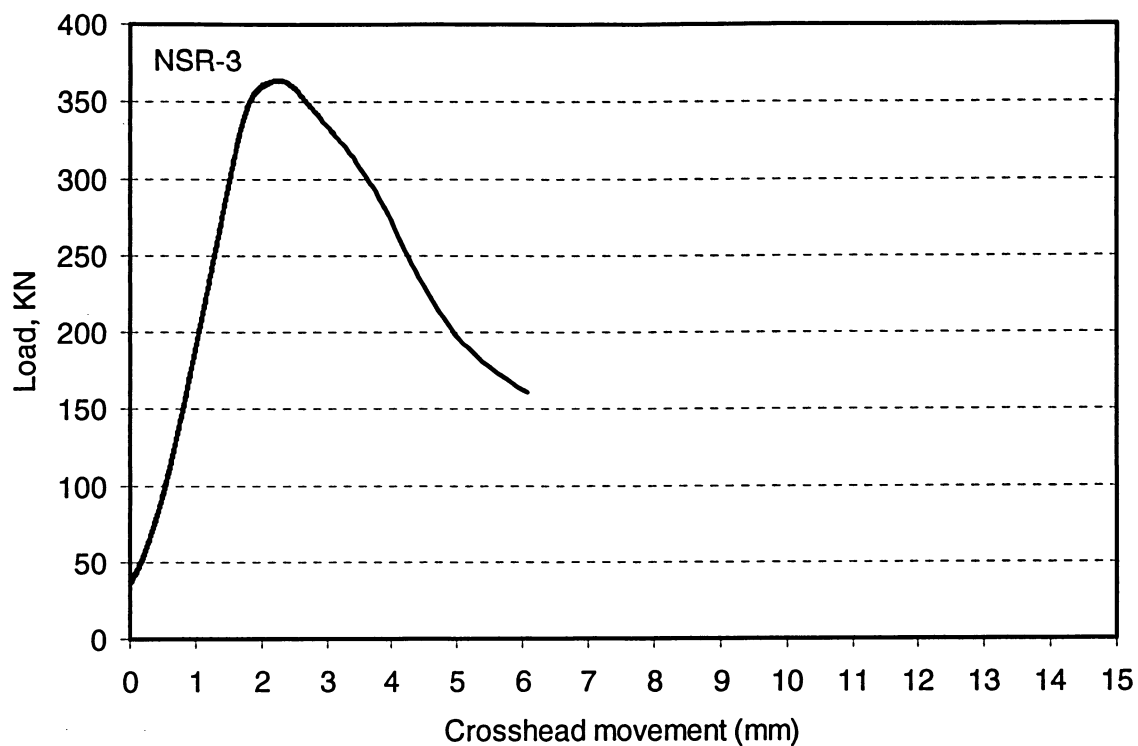


Figure 4.108 Load versus overall shortening curve for specimen NSR-3

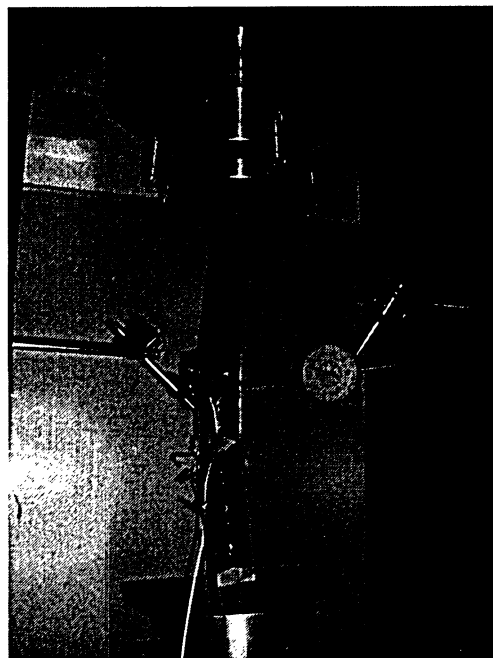
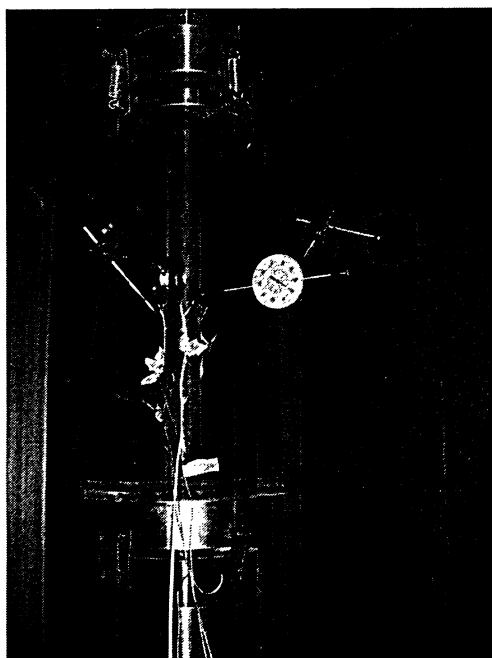


Figure 4.109 Views of specimen NSR-4 before and after testing

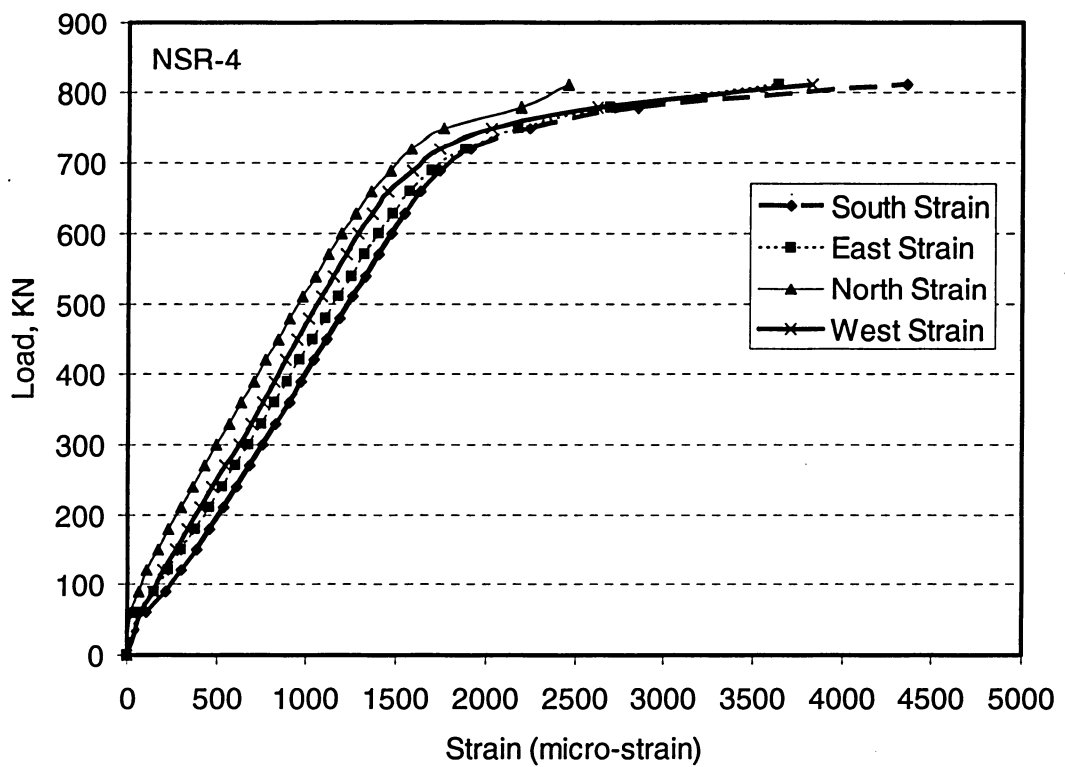


Figure 4.110 Axial load-strain relationships for specimen NSR-4

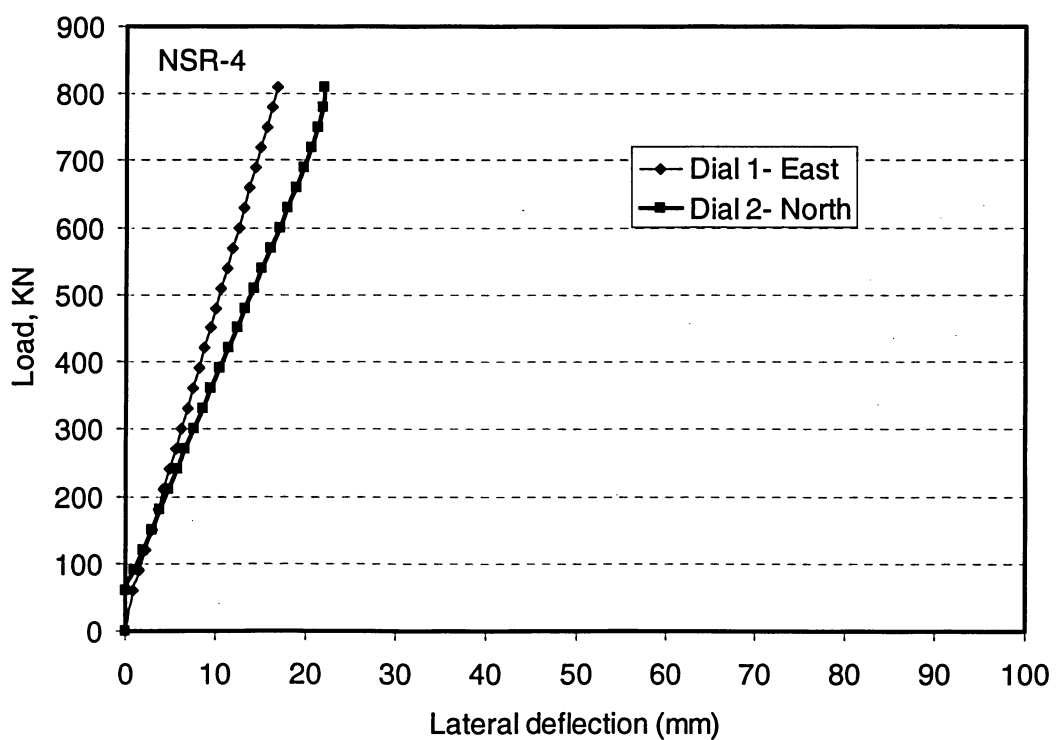


Figure 4.111 Load-lateral deflection curves for specimen NSR-4

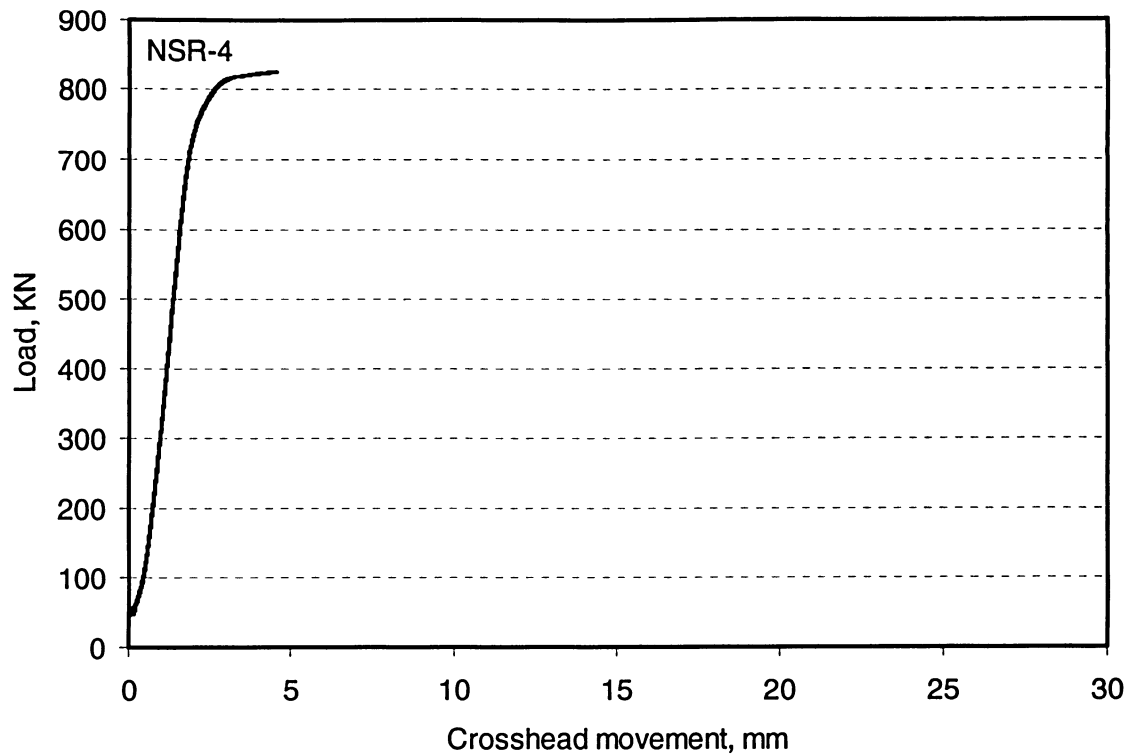


Figure 4.112 Load versus overall shortening curve for specimen NSR-4

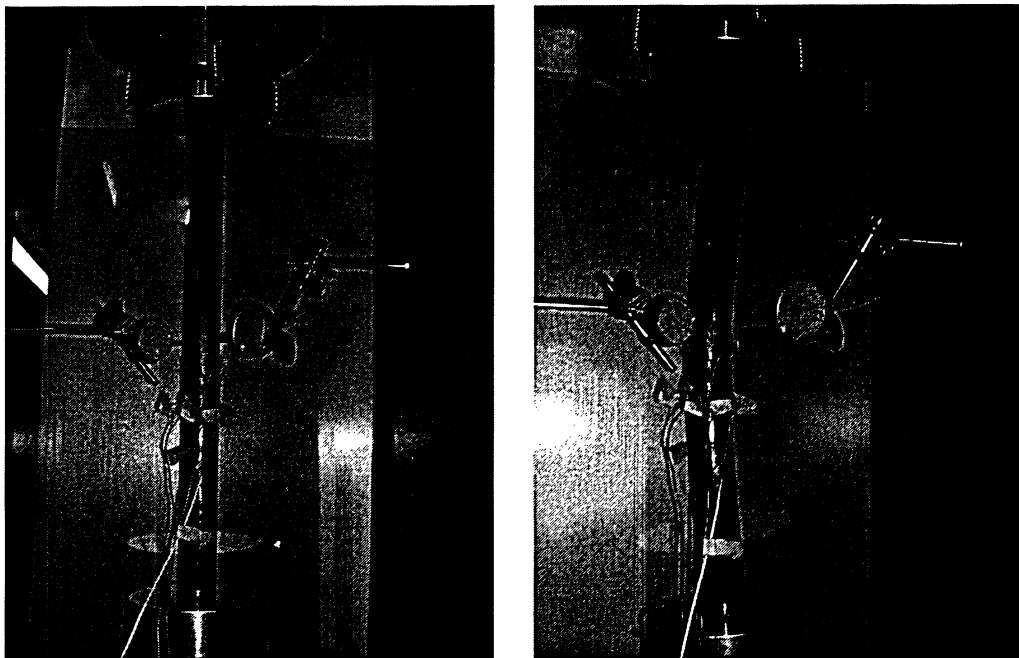


Figure 4.113 Views of specimen NSR-5 before and after testing

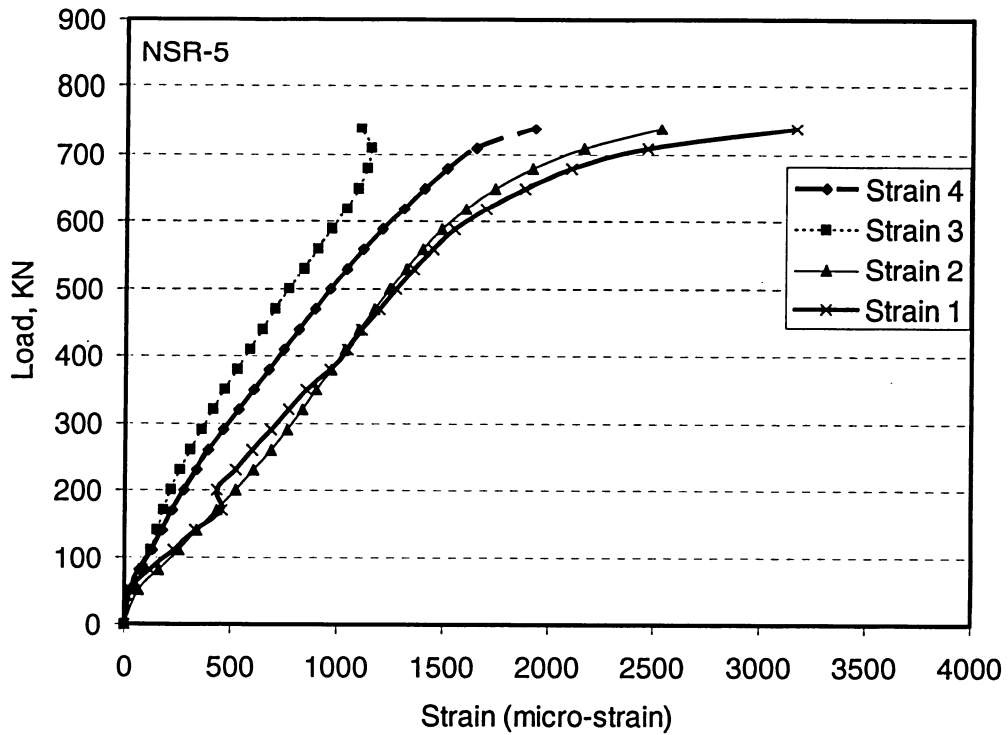


Figure 4.114 Axial load-strain relationships for specimen NSR-5

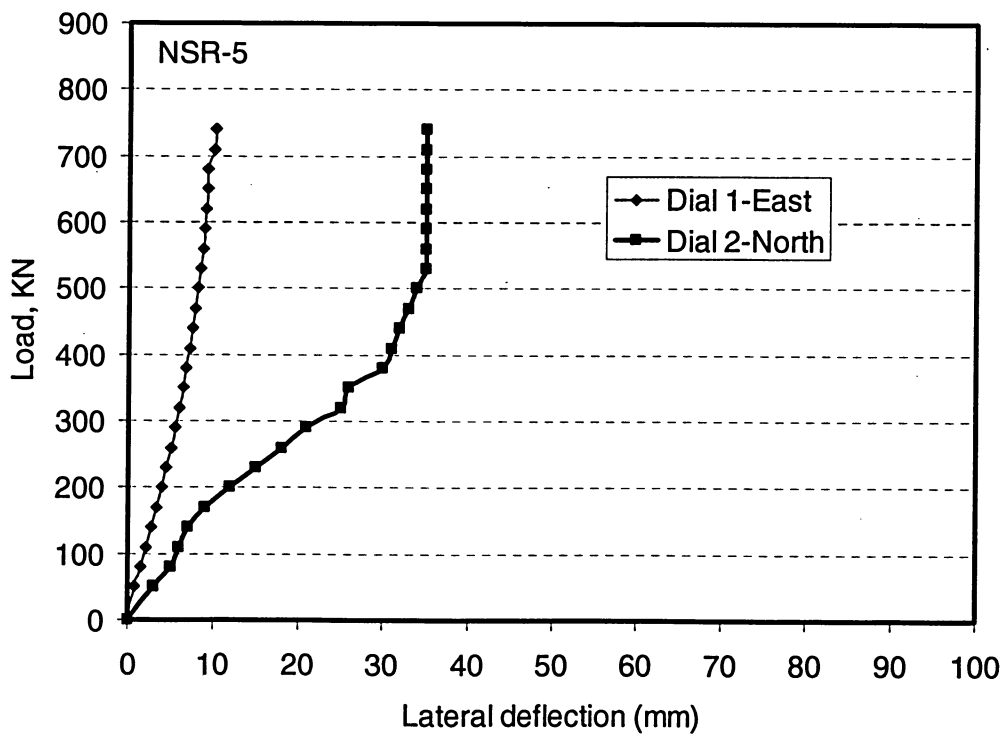


Figure 4.115 Load-lateral deflection curves for specimen NSR-5

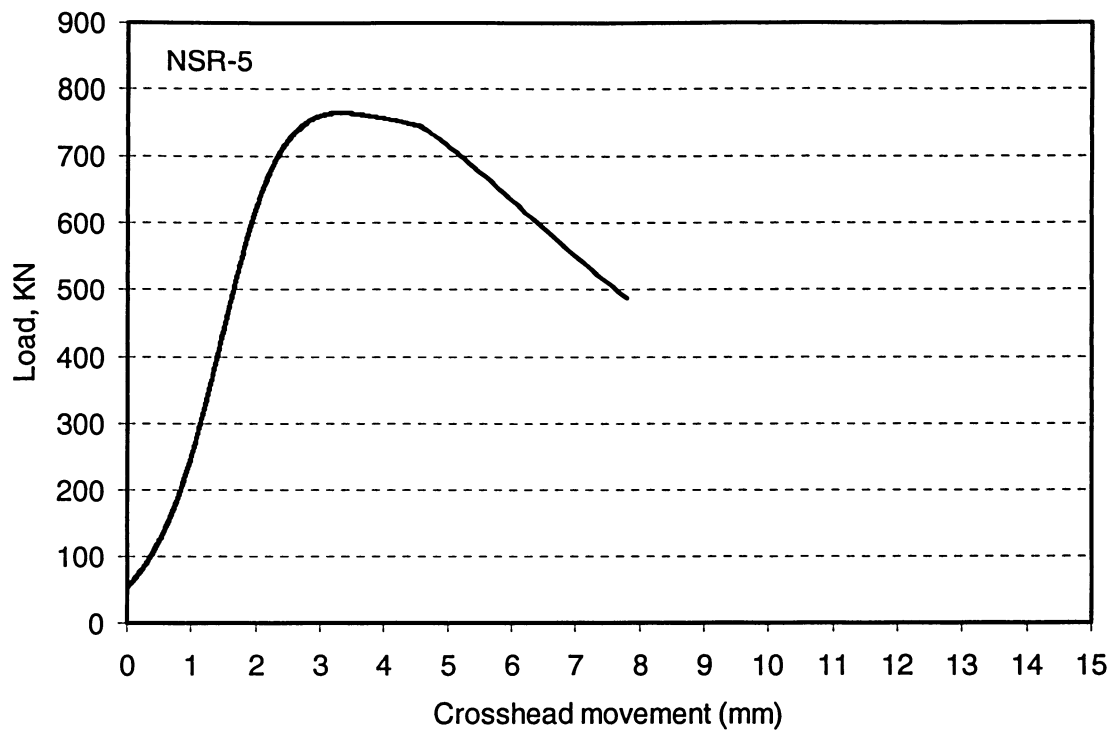


Figure 4.116 Load versus overall shortening curve for specimen NSR-5

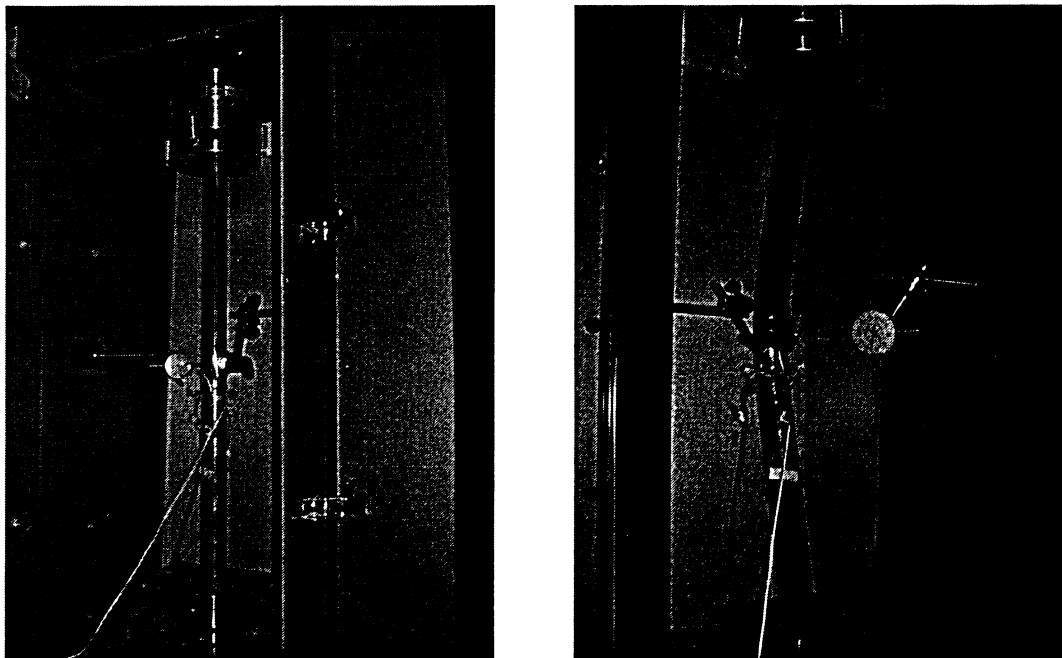


Figure 4.117 Views of specimen NSR-6 before and after testing

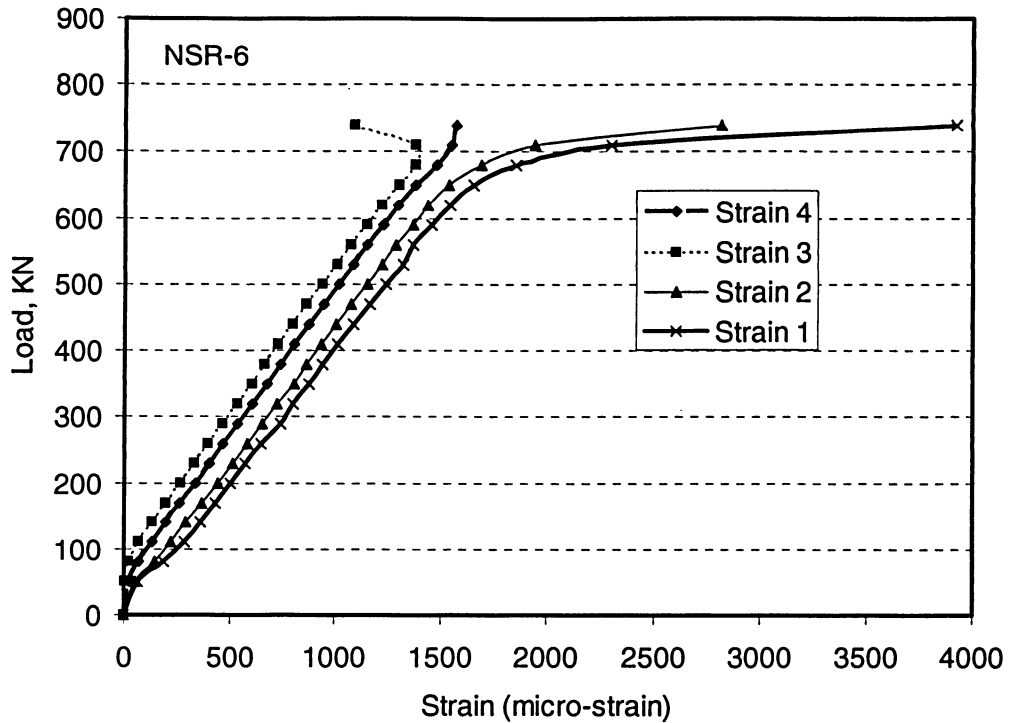


Figure 4.118 Axial load-strain relationships for specimen NSR-6

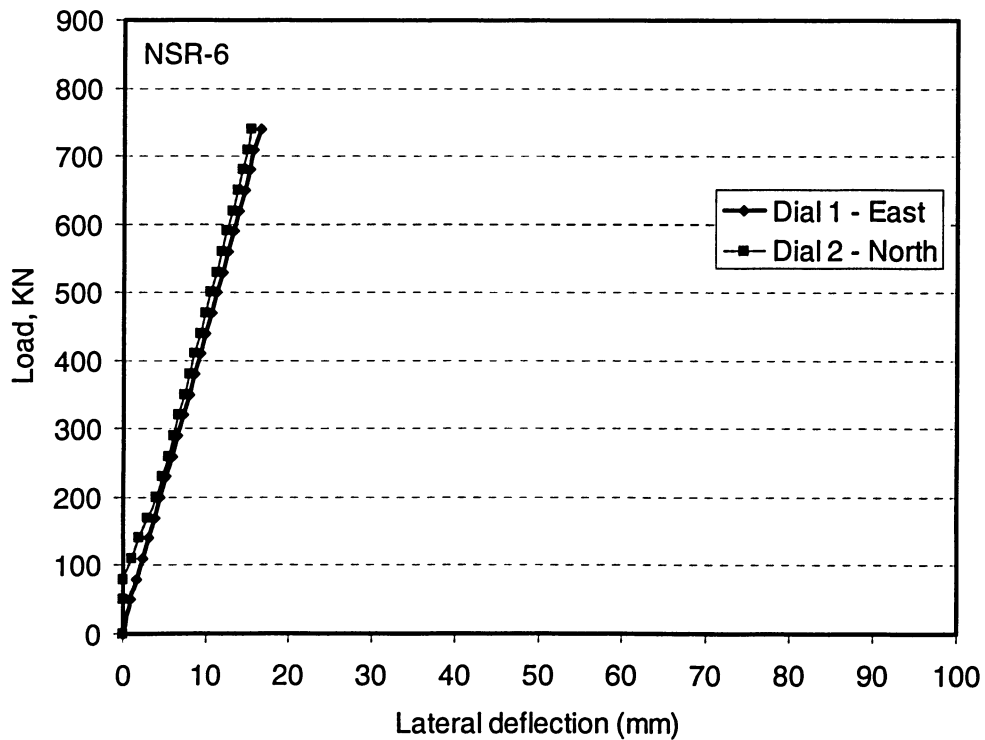


Figure 4.119 Load-lateral deflection curves for specimen NSR-6

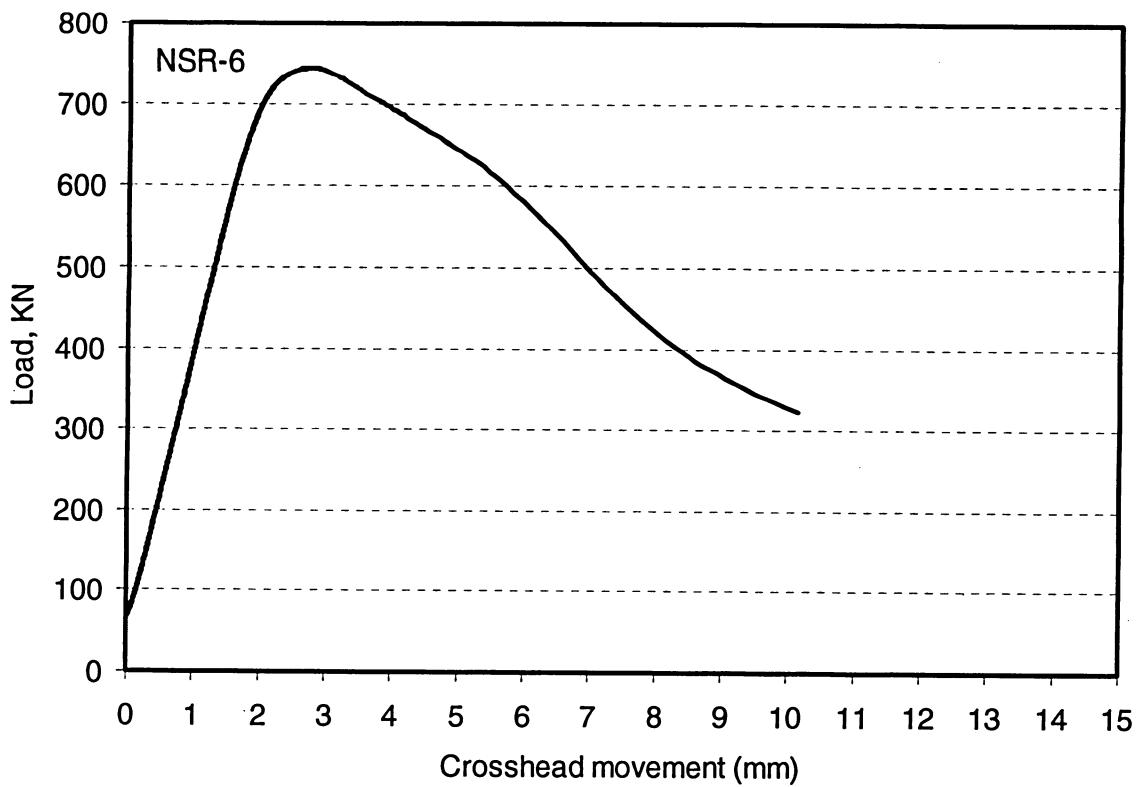


Figure 4.120 Load versus overall shortening curve for specimen NSR-6

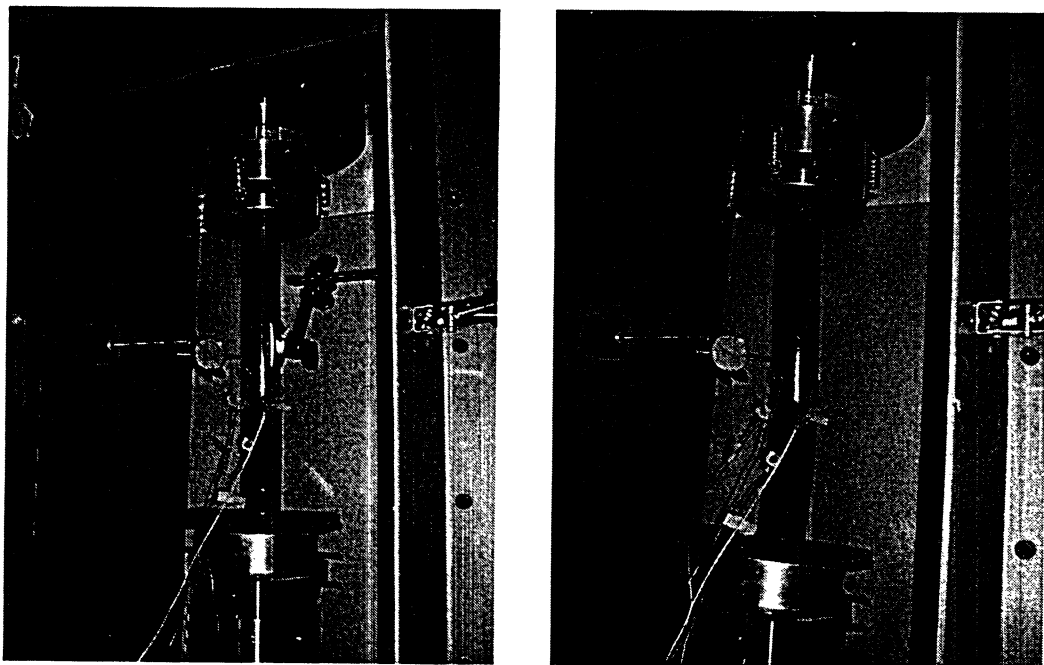


Figure 4.121 Views of specimen NSR-7 before and after testing

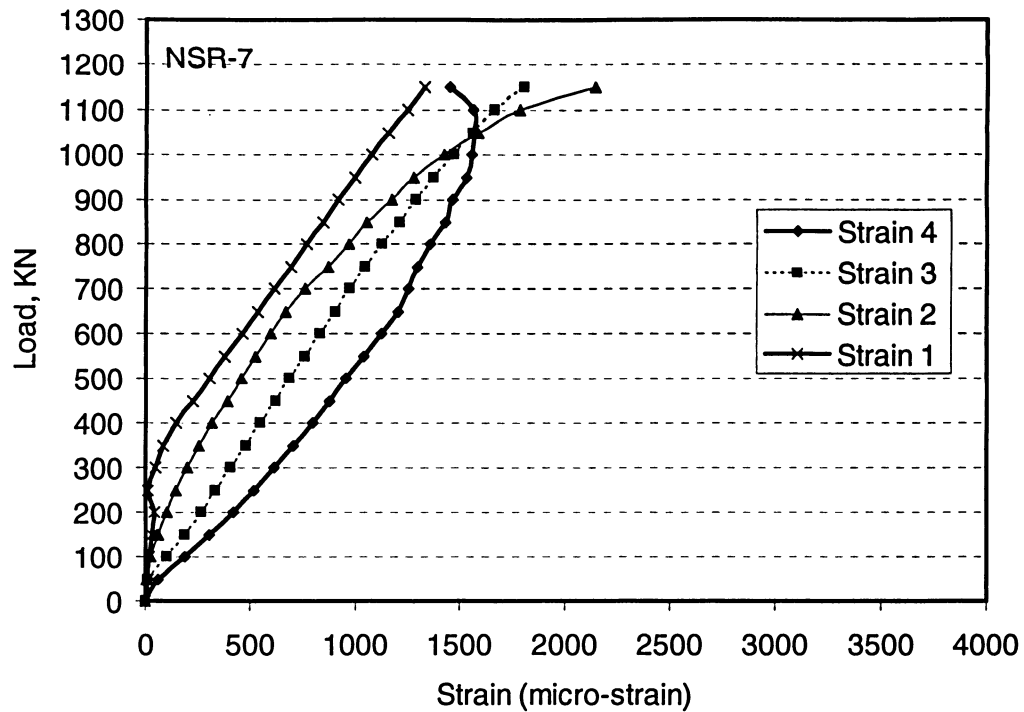


Figure 4.122 Axial load-strain relationships for specimen NSR-7

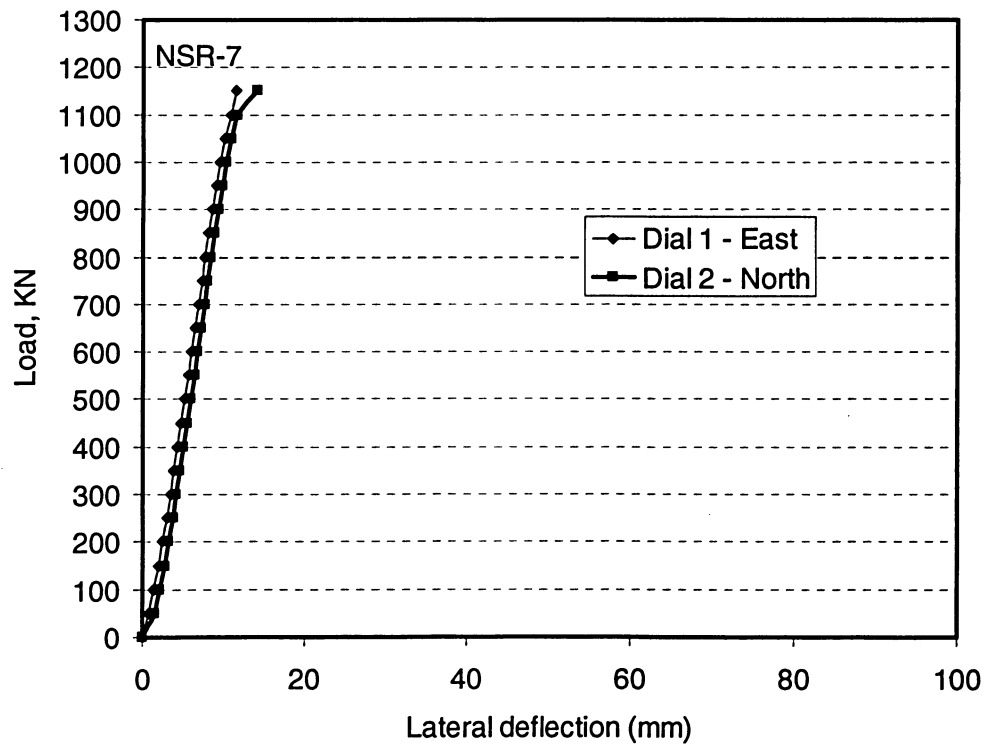


Figure 4.123 Load-lateral deflection curves for specimen NSR-7

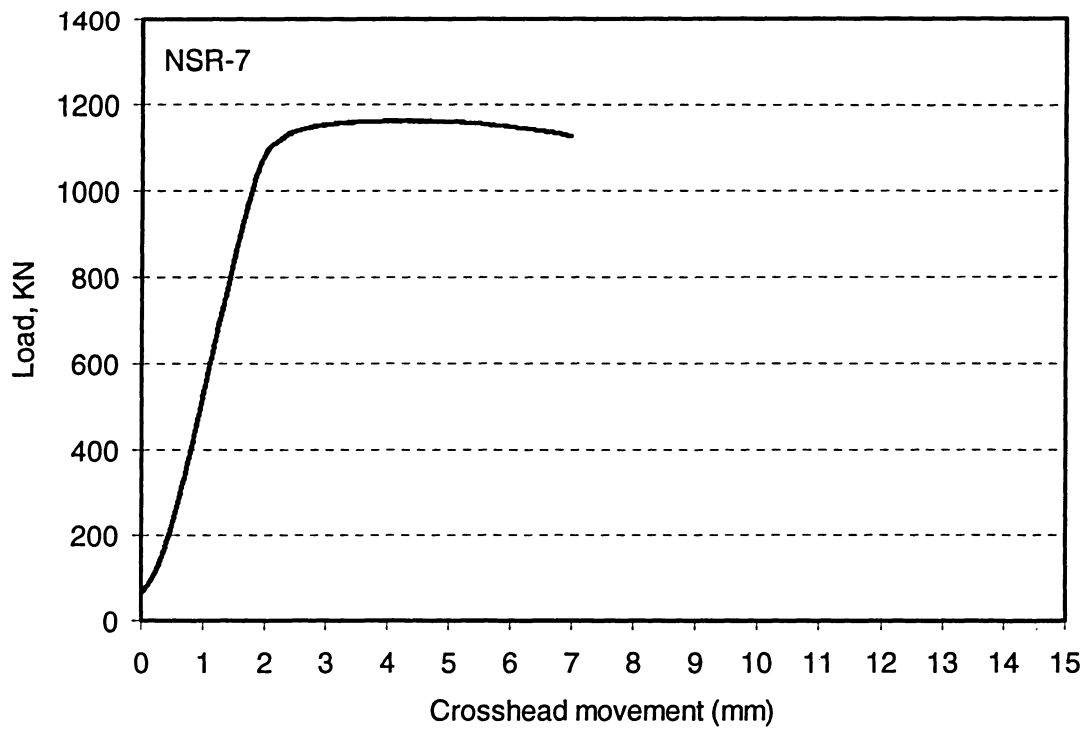


Figure 4.124 Load versus overall shortening curve for specimen NSR-7

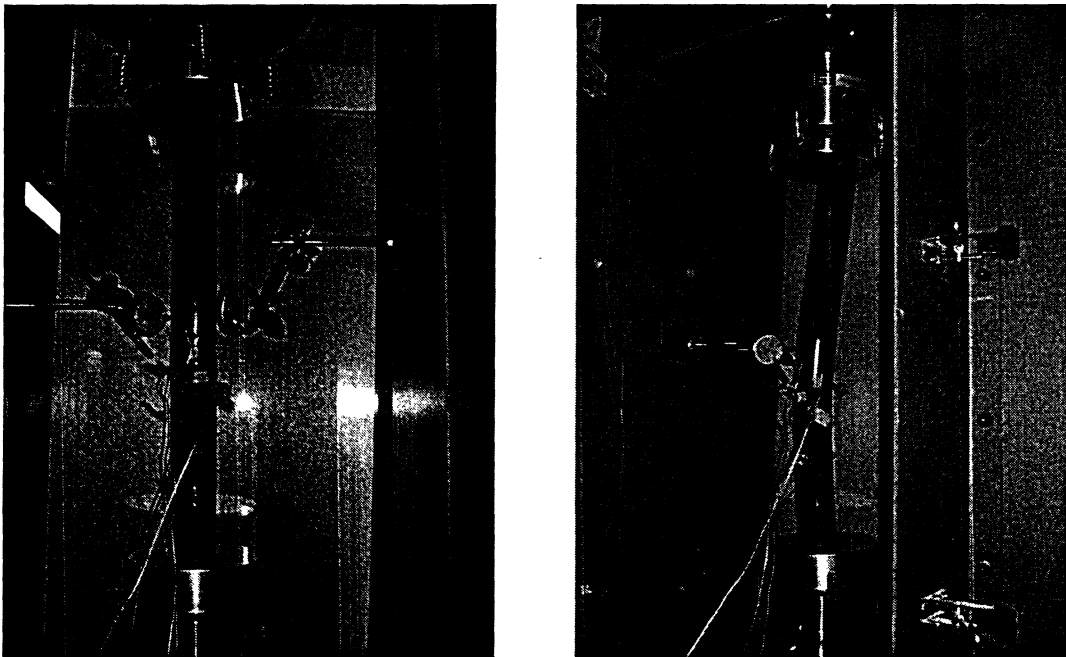


Figure 4.125 Views of specimen NSR-8 before and after testing

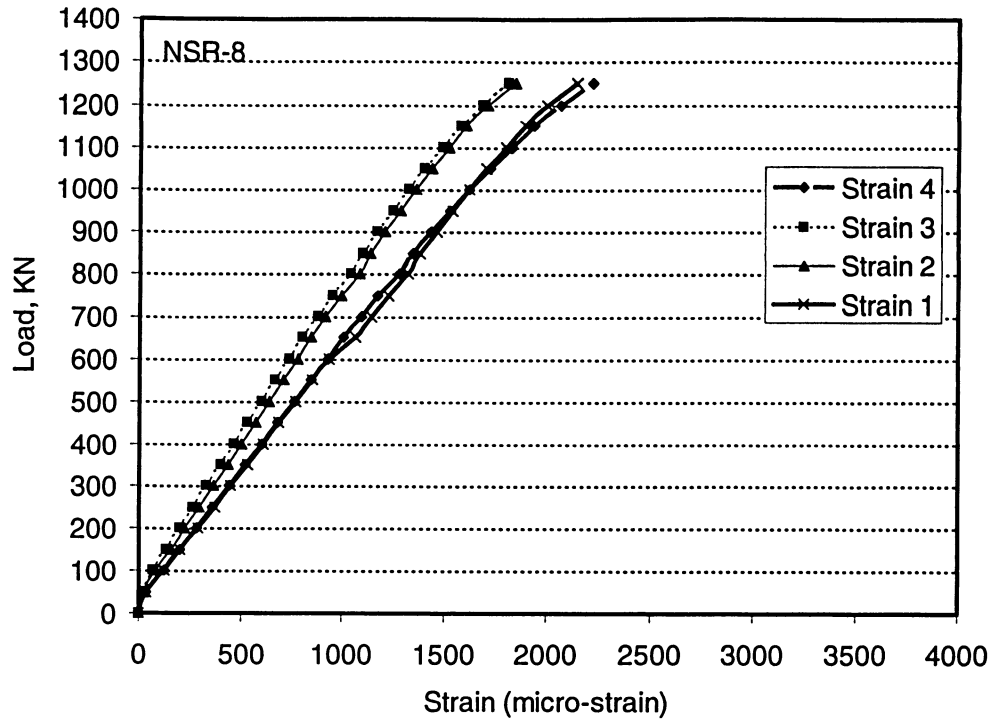


Figure 4.126 Axial load-strain relationships for specimen NSR-8

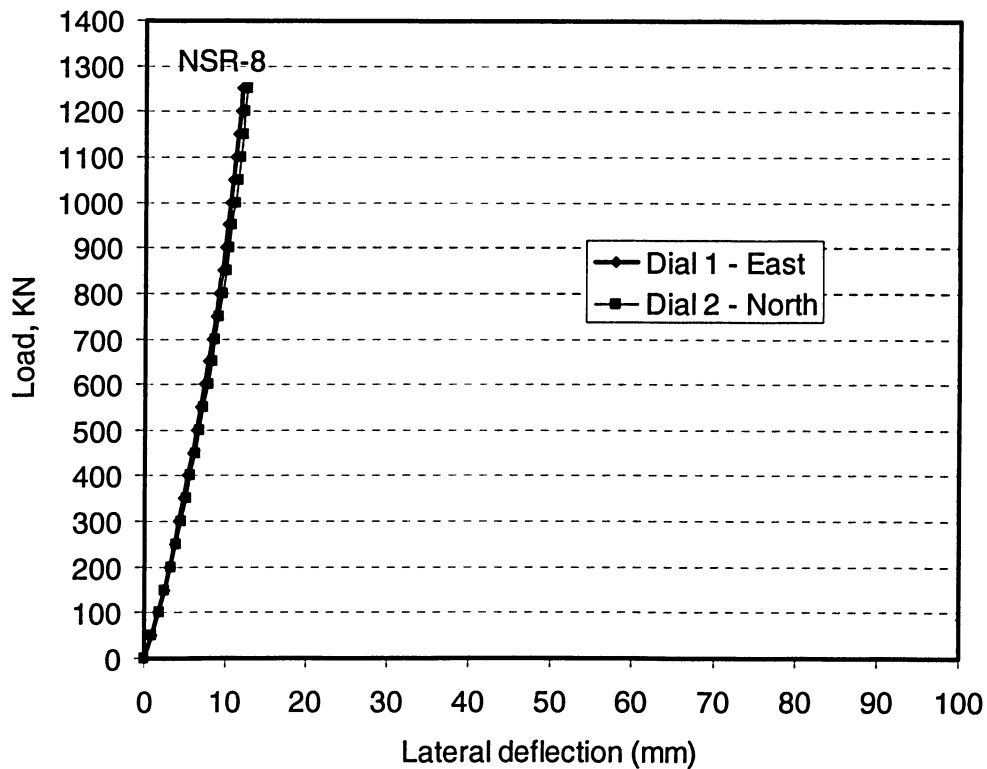


Figure 4.127 Load-lateral deflection curves for specimen NSR-8

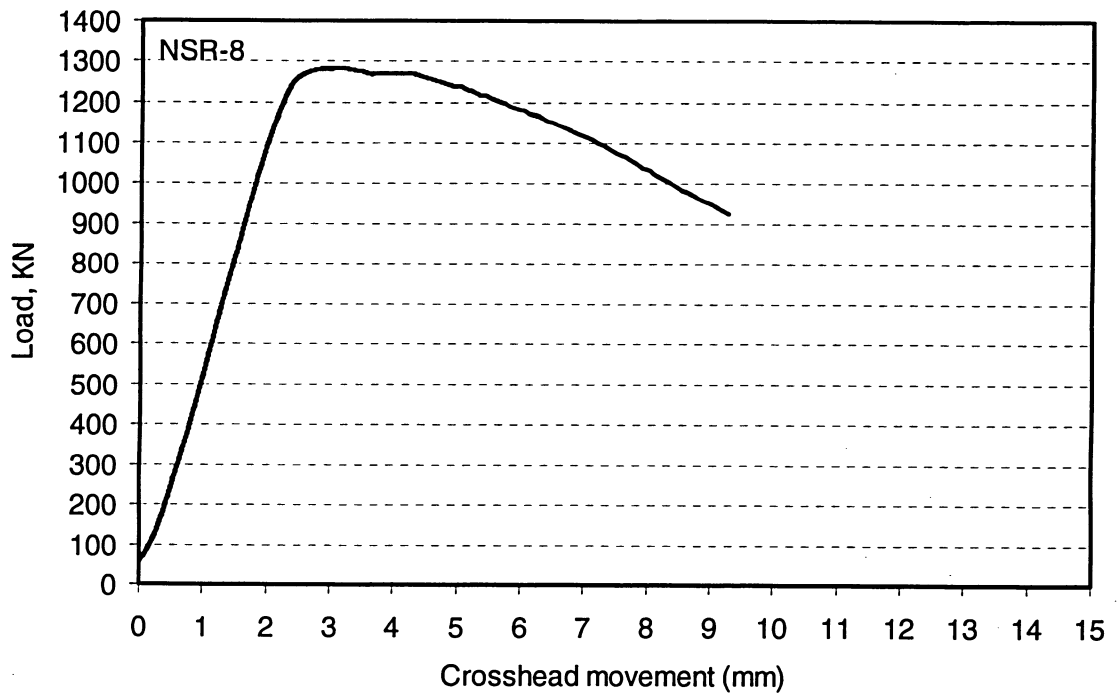


Figure 4.128 Load versus overall shortening curve for specimen NSR-8



Figure 4.129 Views of specimen NSR-9 before and after testing

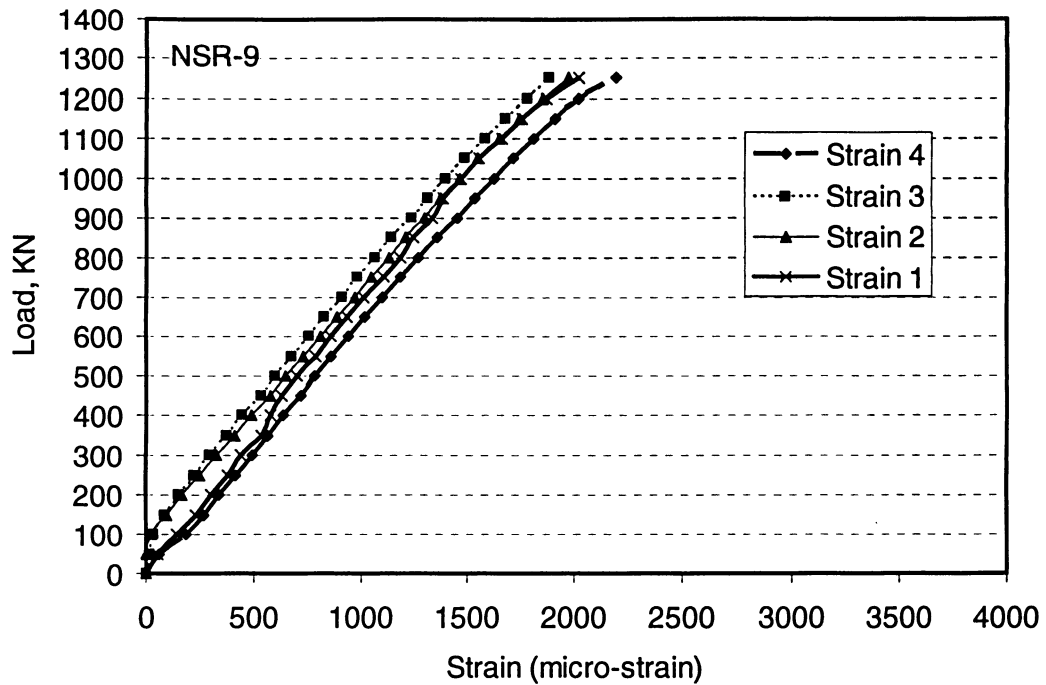


Figure 4.130 Axial load-strain relationships for specimen NSR-9

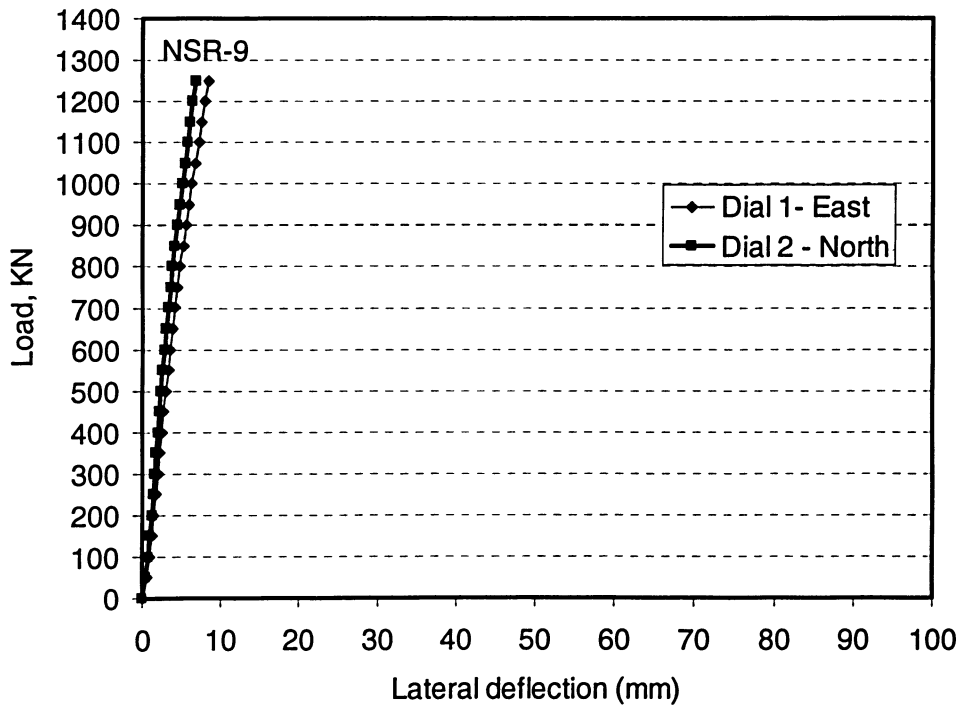


Figure 4.131 Load-lateral deflection curves for specimen NSR-9

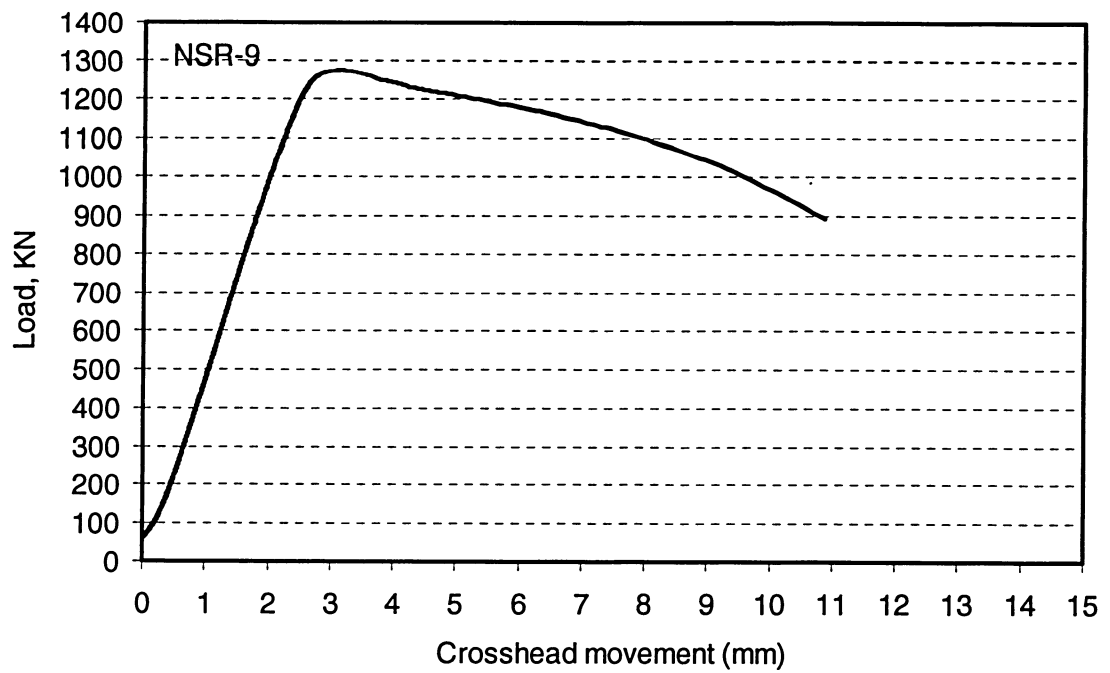


Figure 4.132 Load versus overall shortening curve for specimen NSR-9

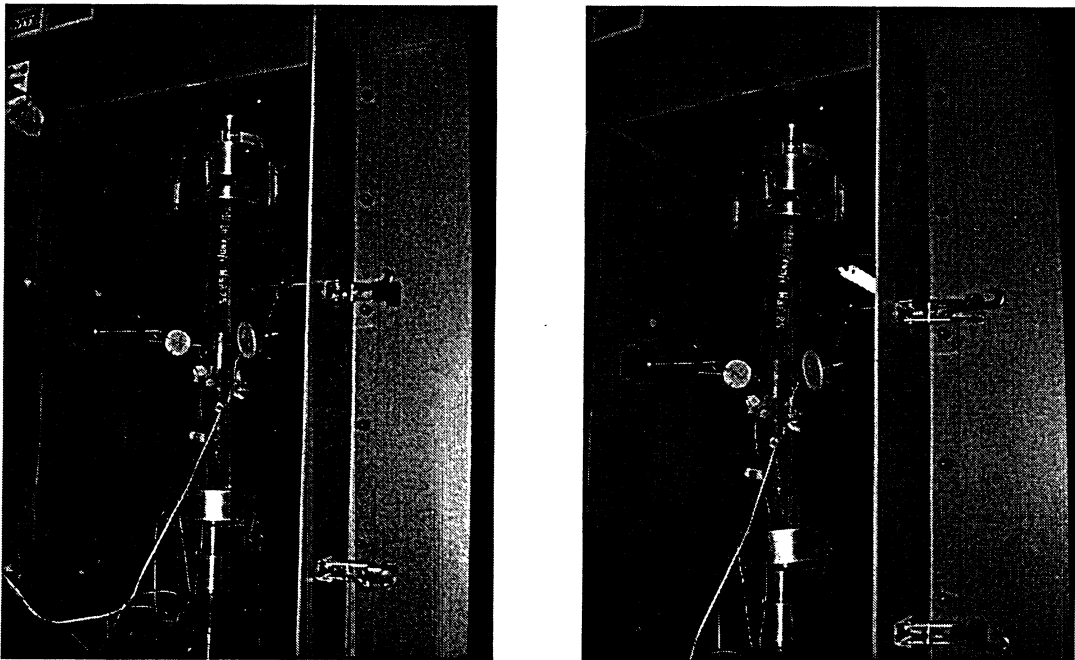


Figure 4.133 Views of specimen NSR-10 before and after testing

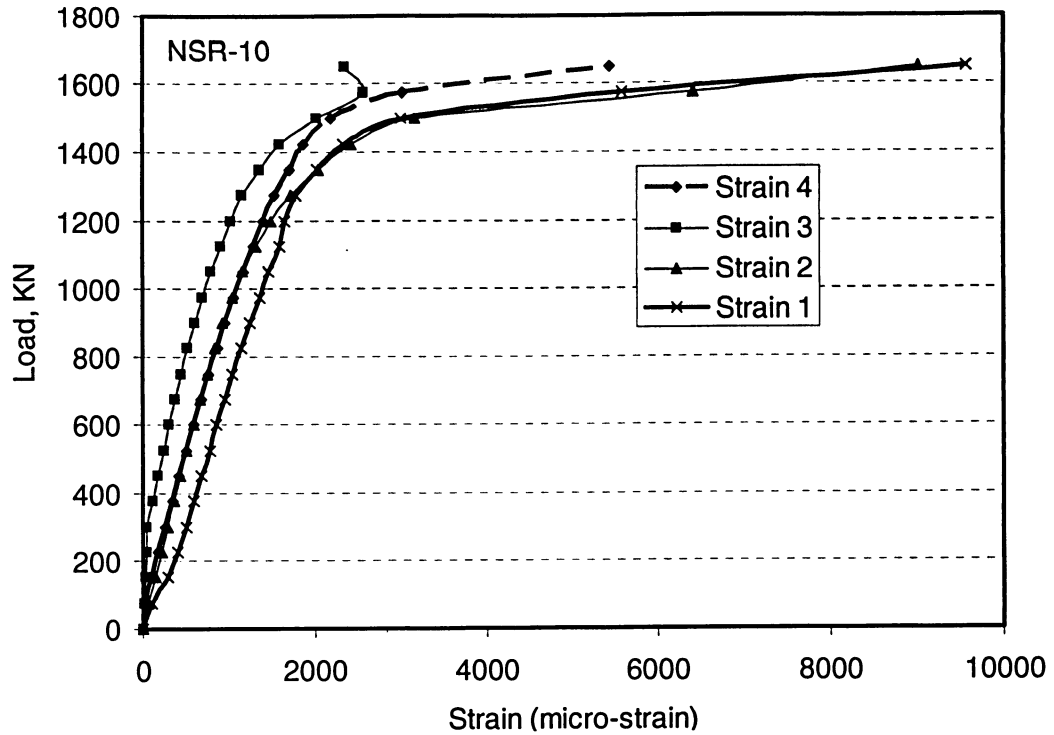


Figure 4.134 Axial load-strain relationships for specimen NSR-10

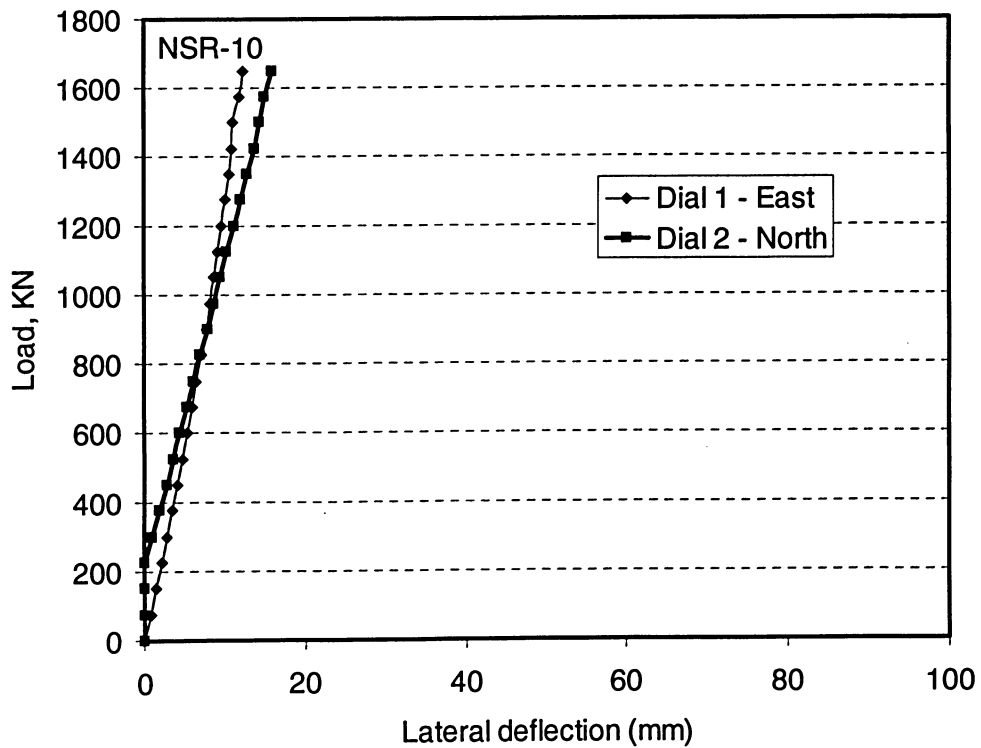


Figure 4.135 Load-lateral deflection curves for specimen NSR-10

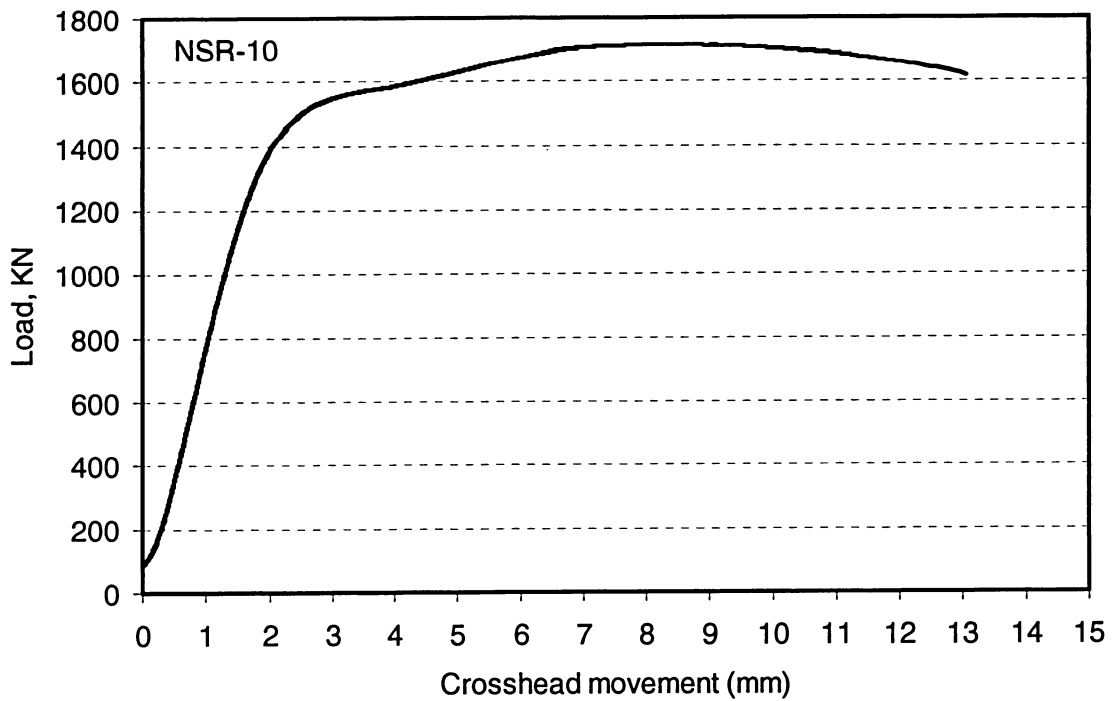


Figure 4.136 Load versus overall shortening curve for specimen NSR-10

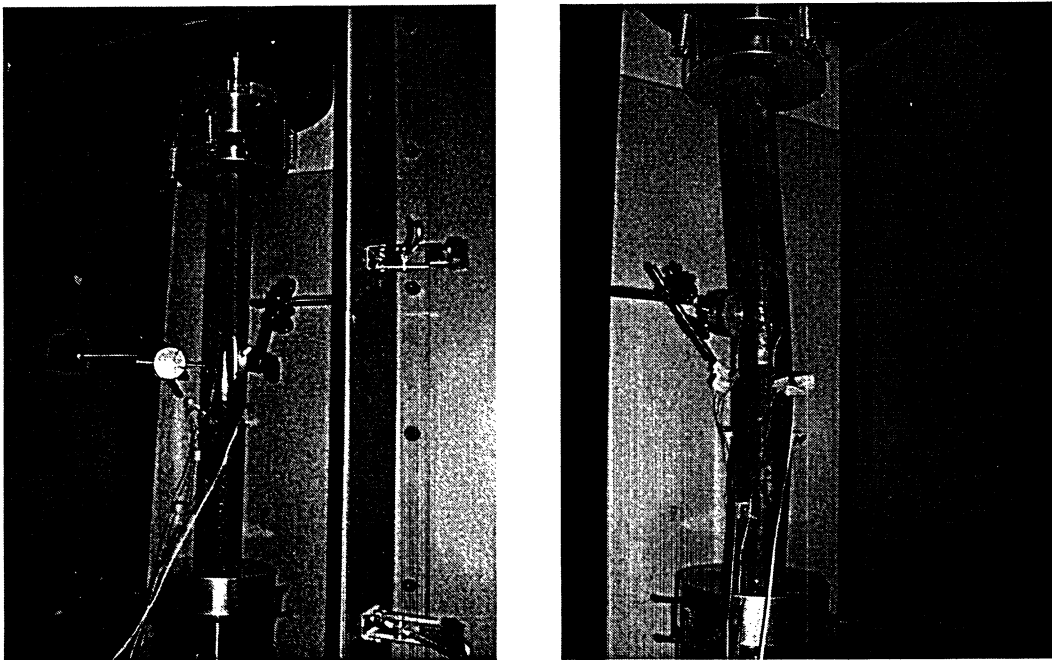


Figure 4.137 Views of specimen NSR-11 before and after testing

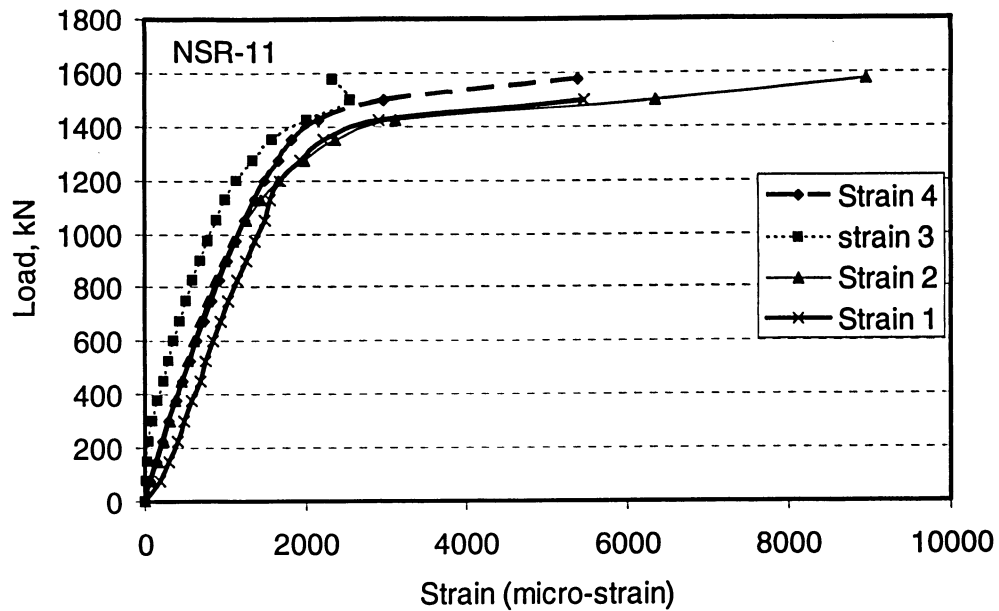


Figure 4.138 Axial load-strain relationships for specimen NSR-11

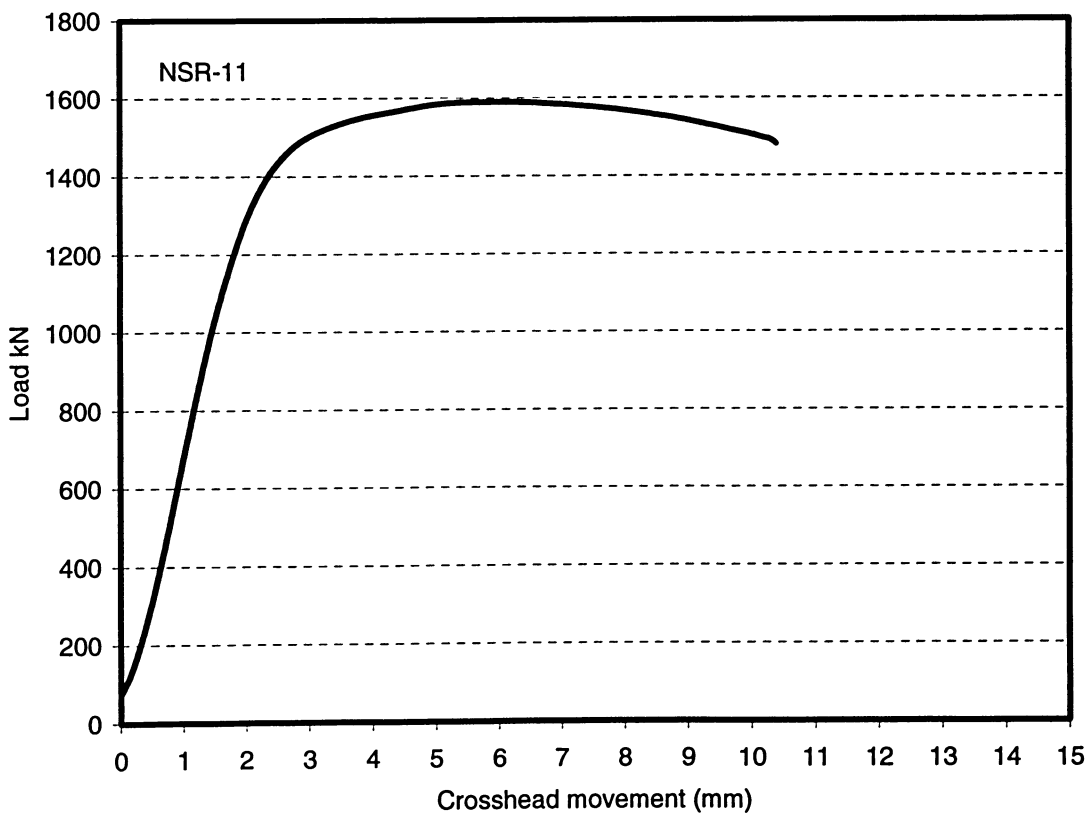


Figure 4.139 Load versus overall shortening curve for specimen NSR-11

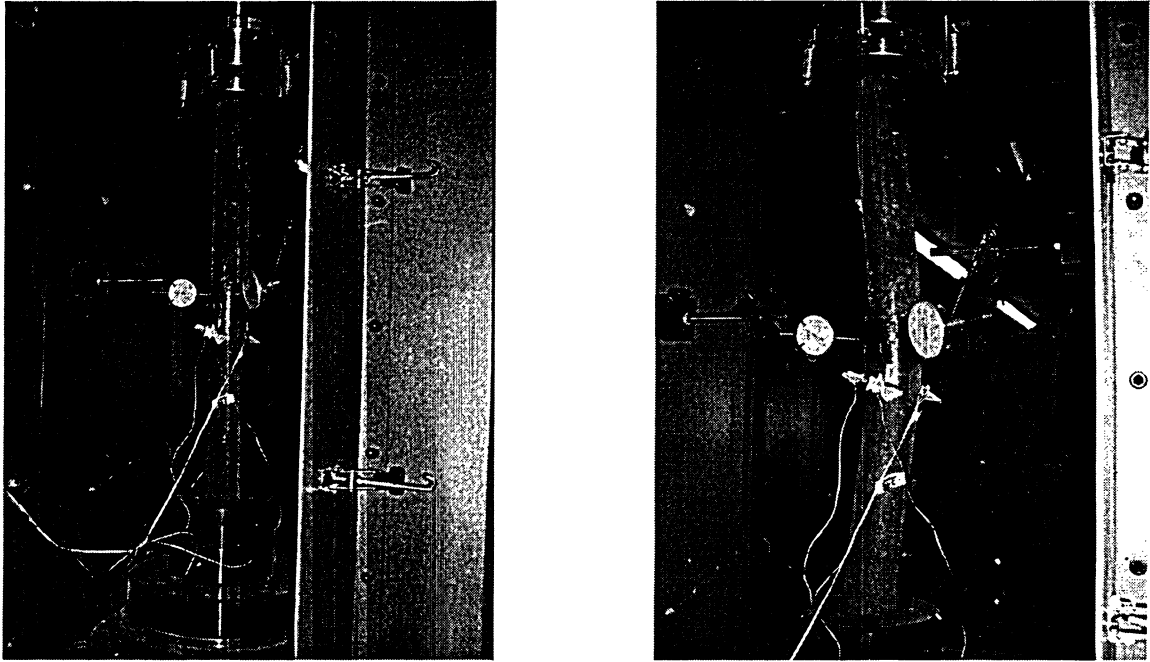


Figure 4.140 Views of specimen NSR-12 before and after testing

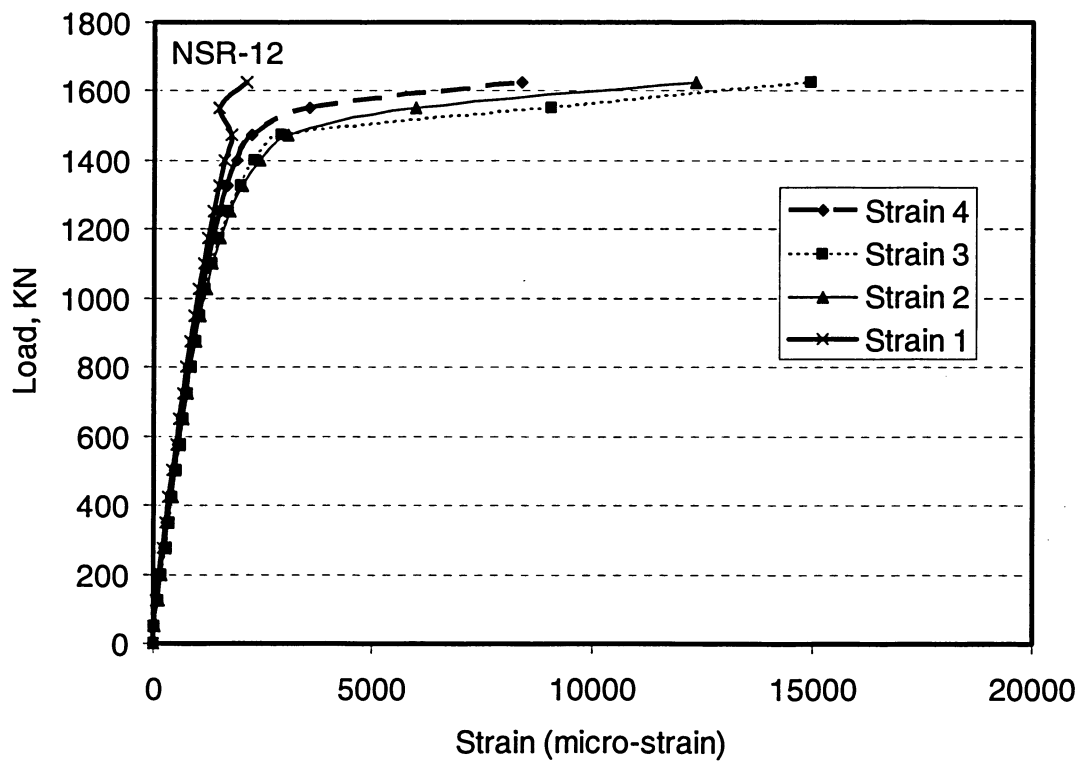


Figure 4.141 Axial load-strain relationships for specimen NSR-12

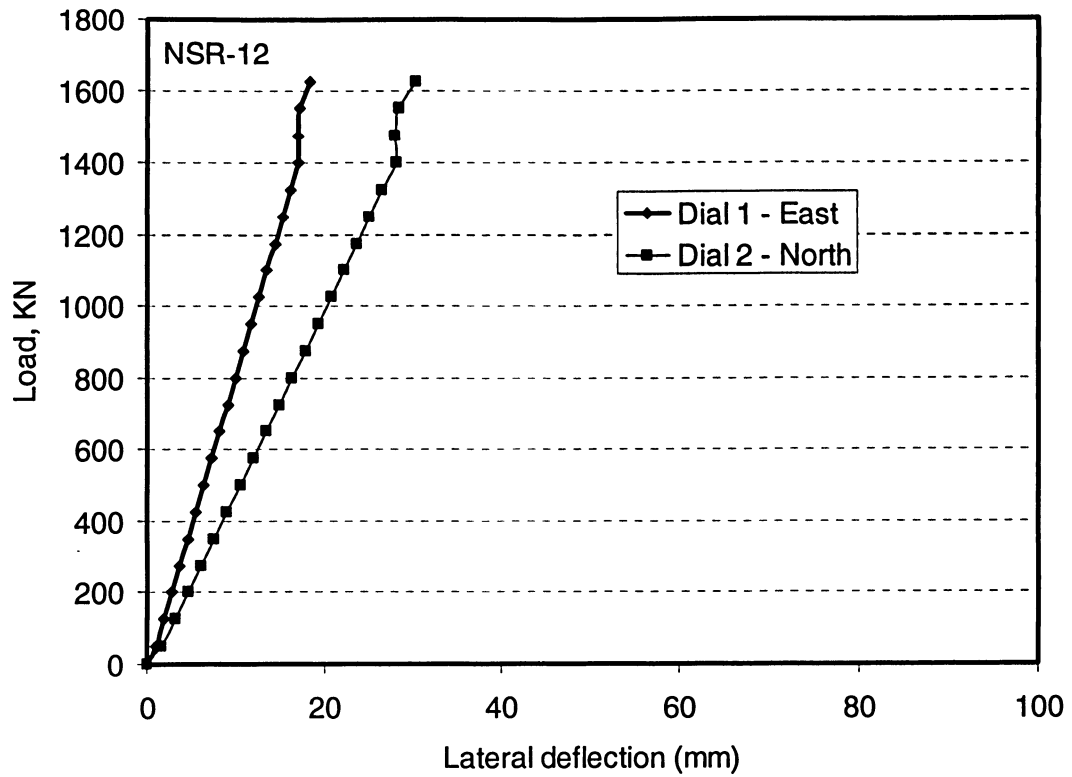


Figure 4.142 Load-lateral deflection curves for specimen NSR-12

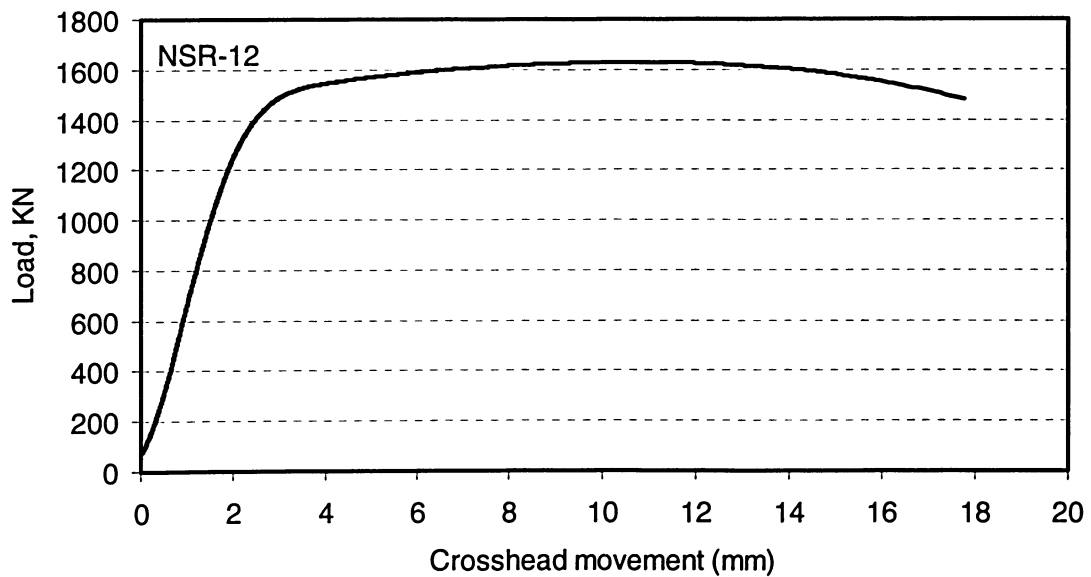


Figure 4.143 Load versus overall shortening curve for specimen NSR-12

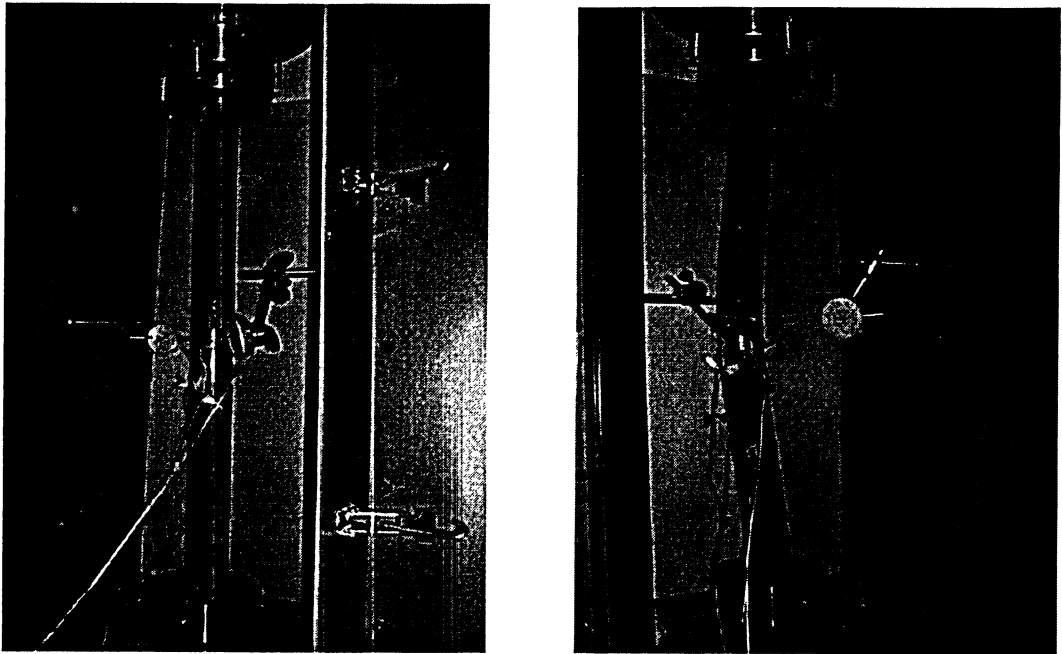


Figure 4.144 Views of specimen NSR-13 before and after testing

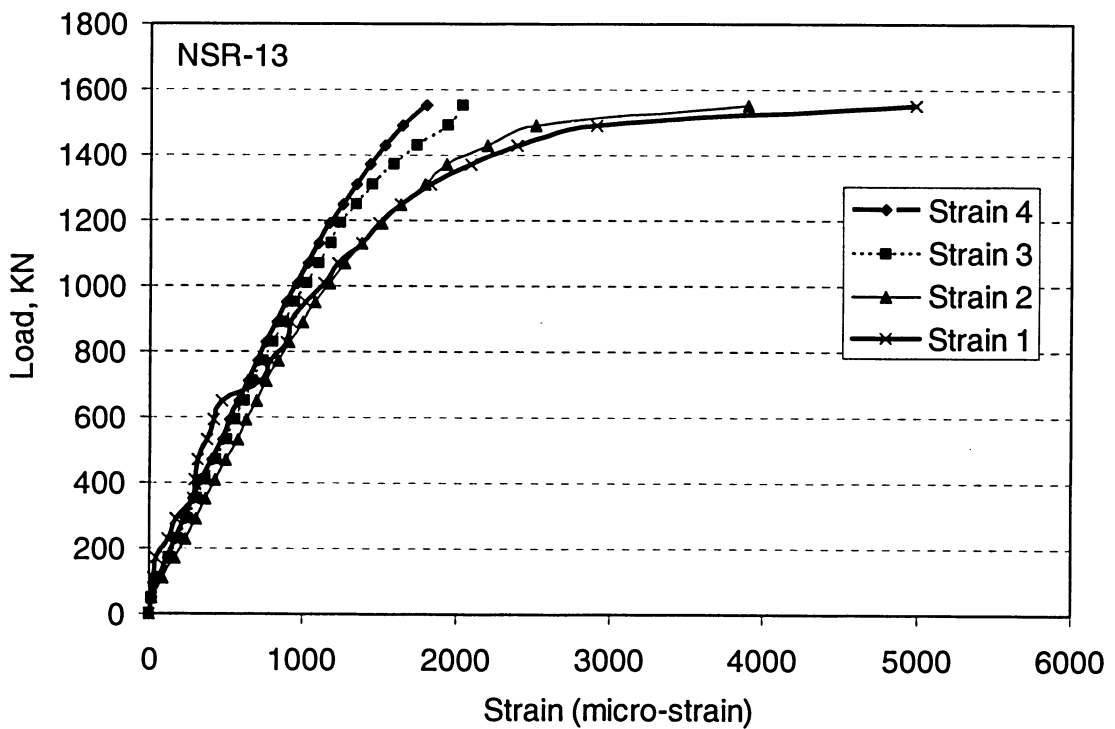


Figure 4.145 Axial load-strain relationships for specimen NSR-13

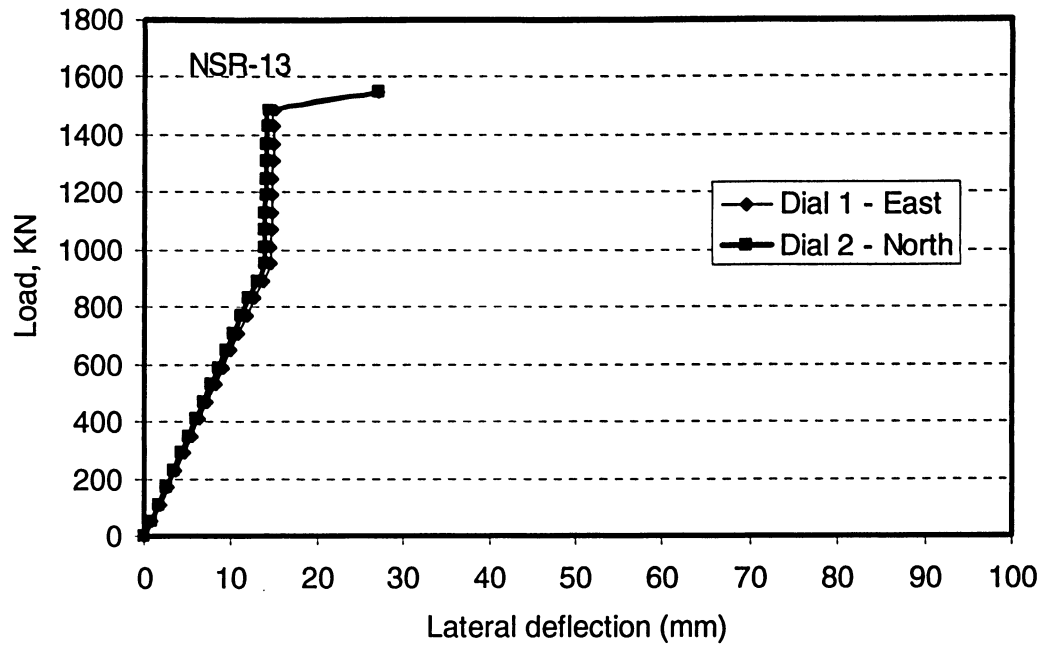


Figure 4.146 Load-lateral deflection curves for specimen NSR-13

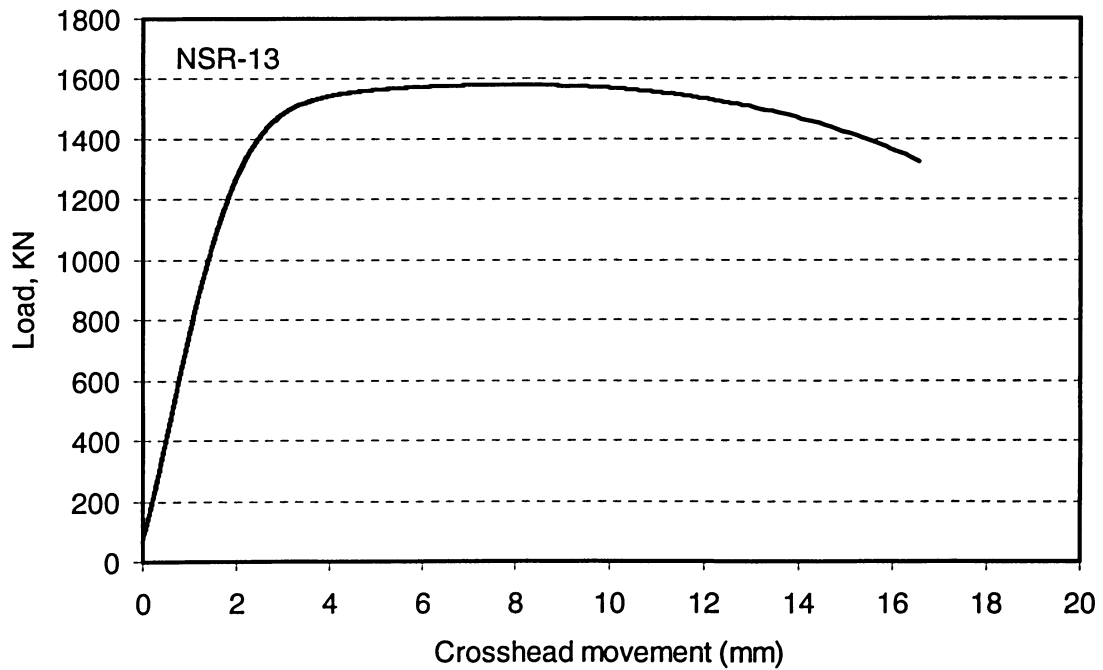


Figure 4.147 Load versus overall shortening curve for specimen NSR-13

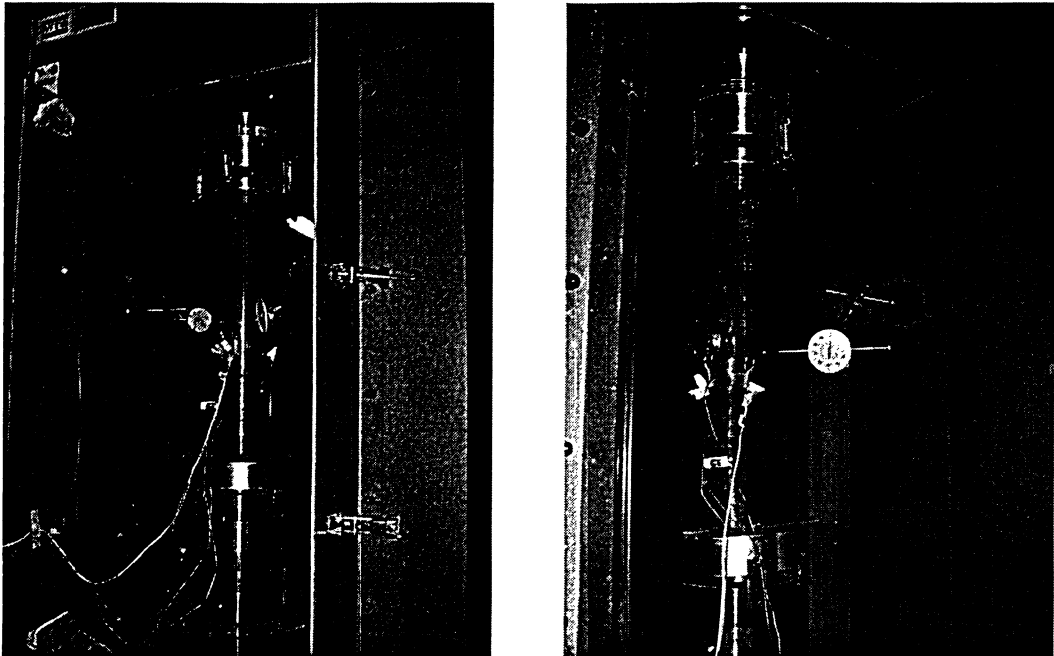


Figure 4.148 Views of specimen NSR-14 before and after testing

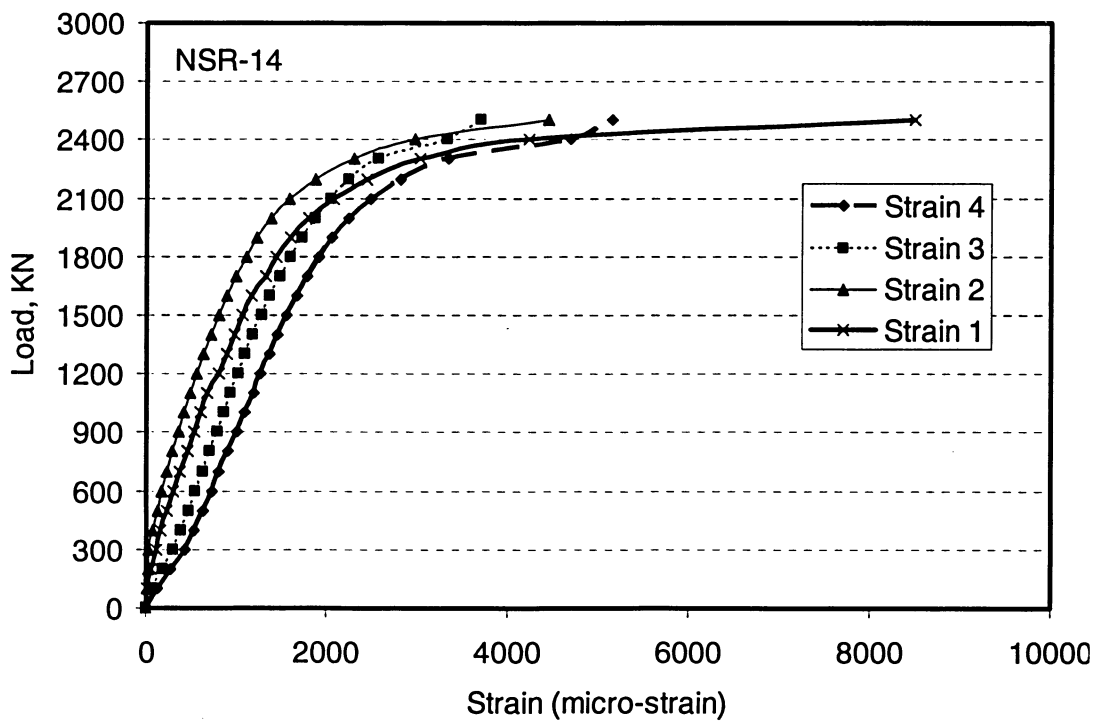


Figure 4.149 Axial load-strain relationships for specimen NSR-14

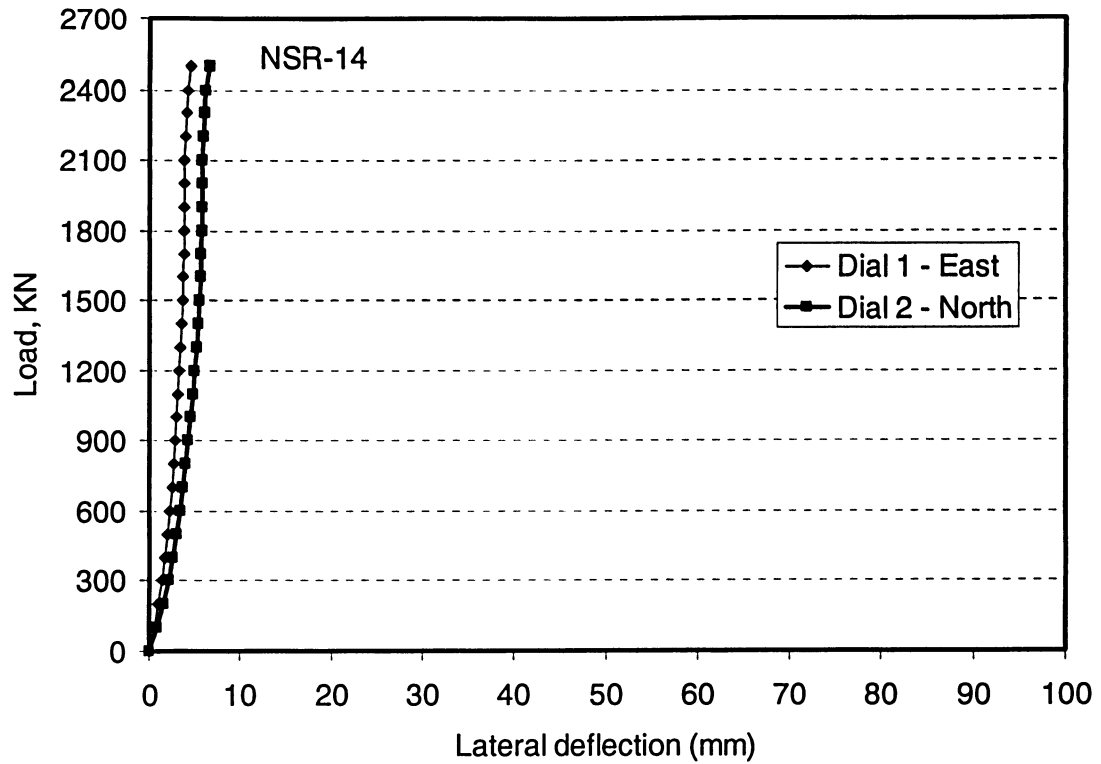


Figure 4.150 Load-lateral deflection curves for specimen NSR-14

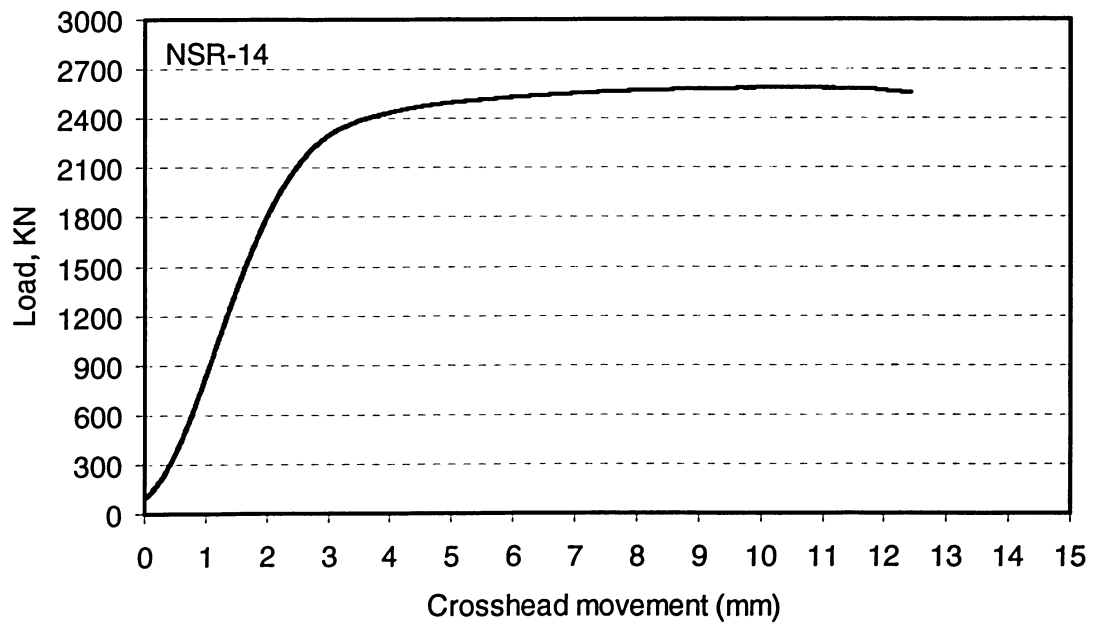


Figure 4.151 Load versus overall shortening curve for specimen NSR-14

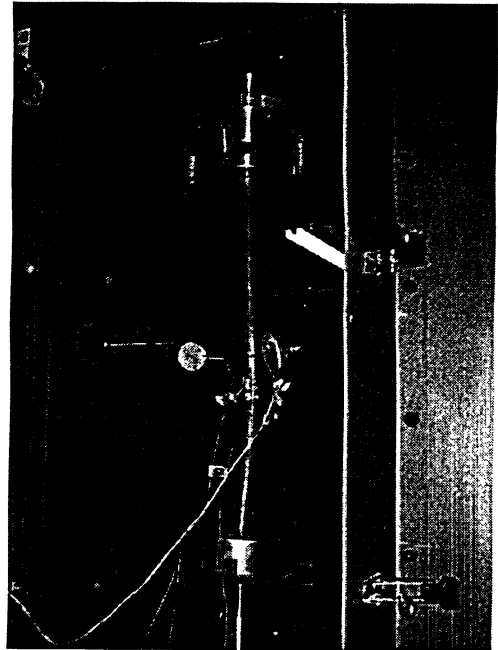
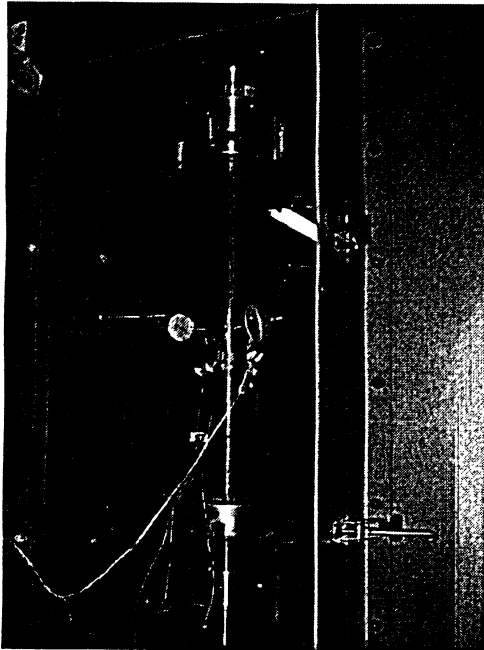


Figure 4.152 Views of specimen NSR-15 before and after testing

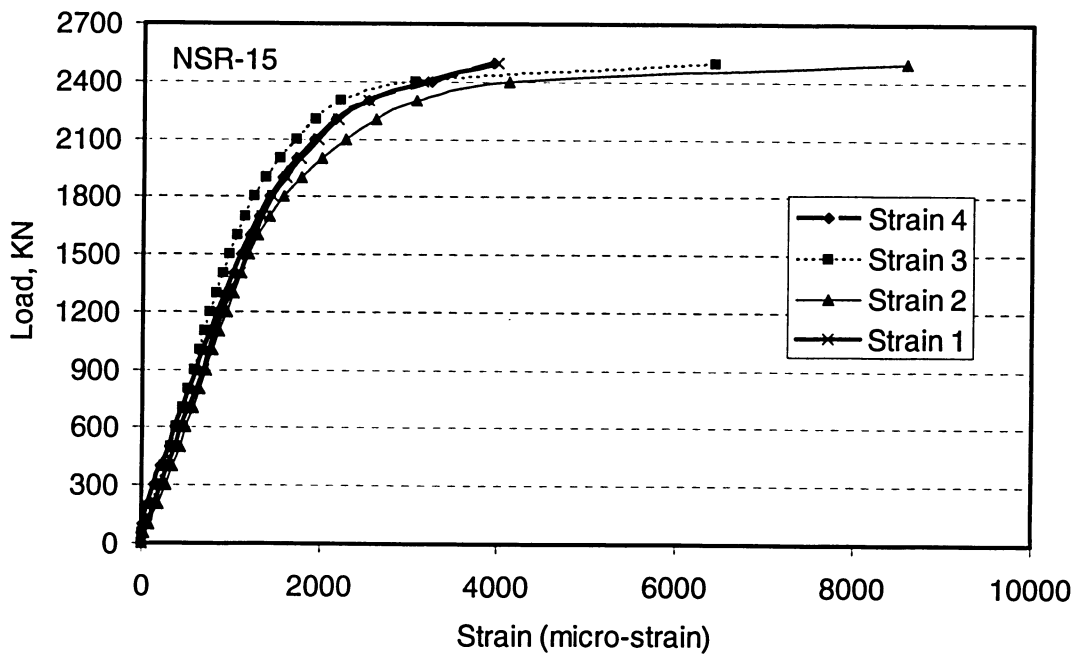


Figure 4.153 Axial load-strain relationships for specimen NSR-15

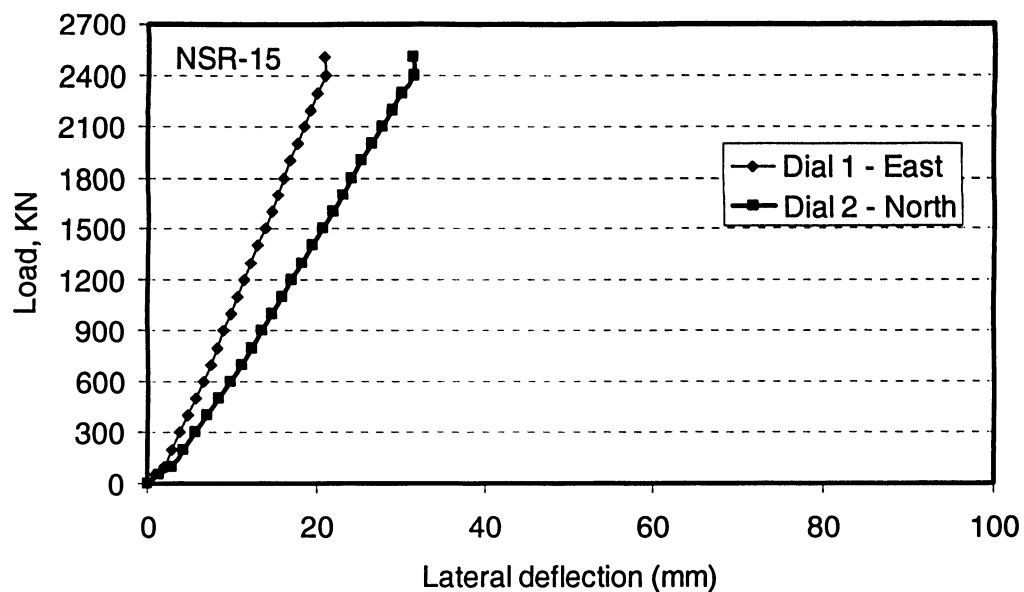


Figure 4.154 Load-lateral deflection curves for specimen NSR-15

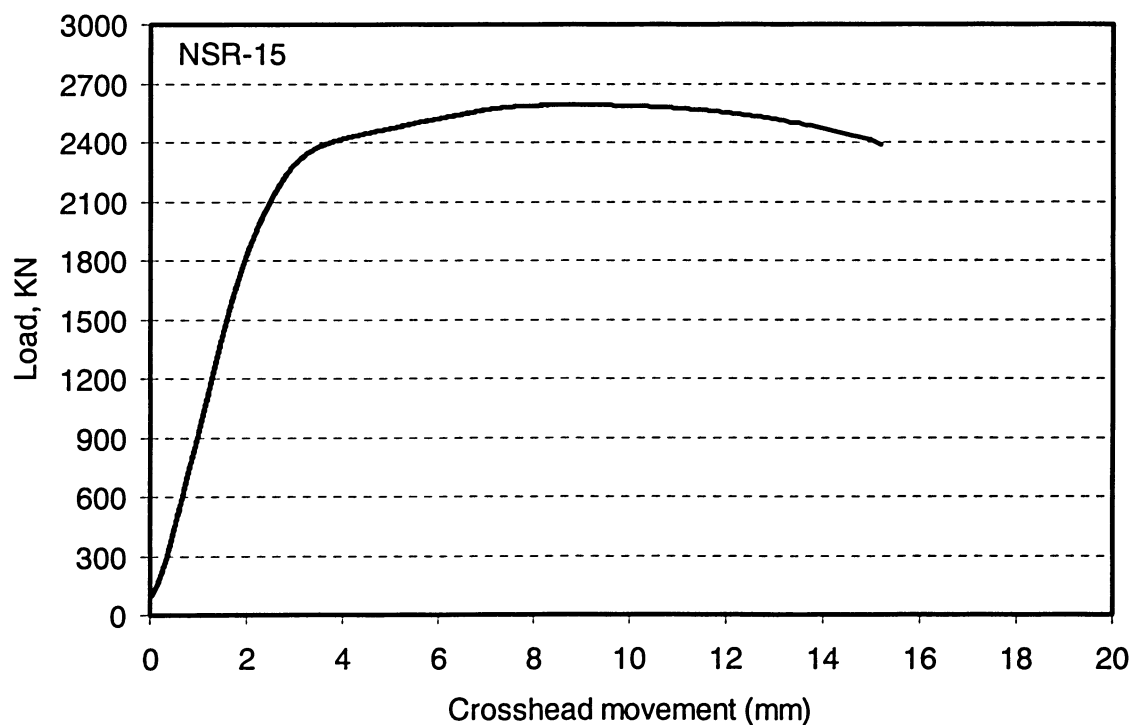


Figure 4.155 Load versus overall shortening curve for specimen NSR-15

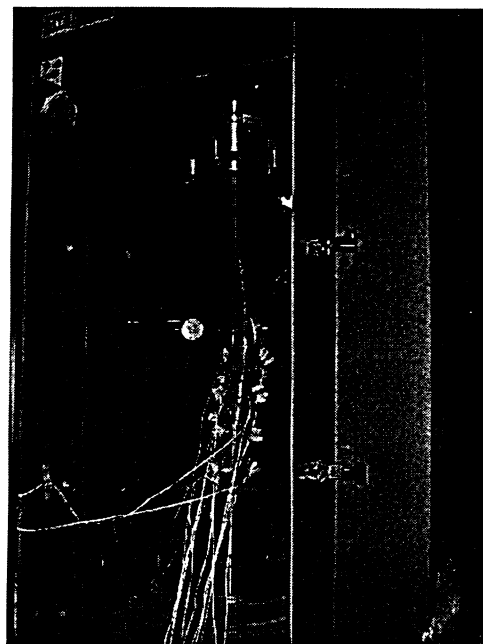
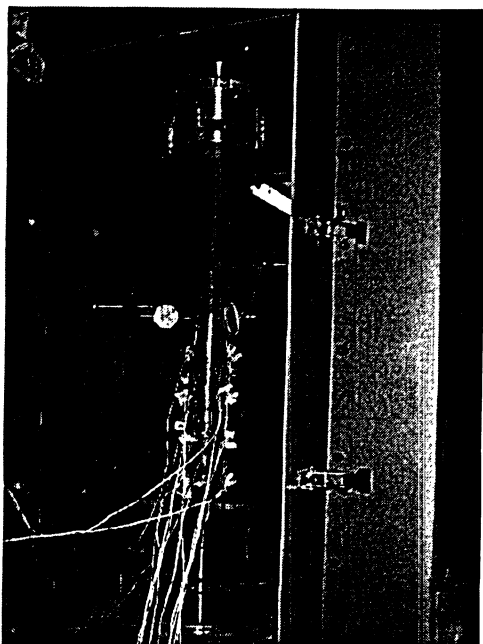


Figure 4.156 Views of specimen NSR-16 before and after testing

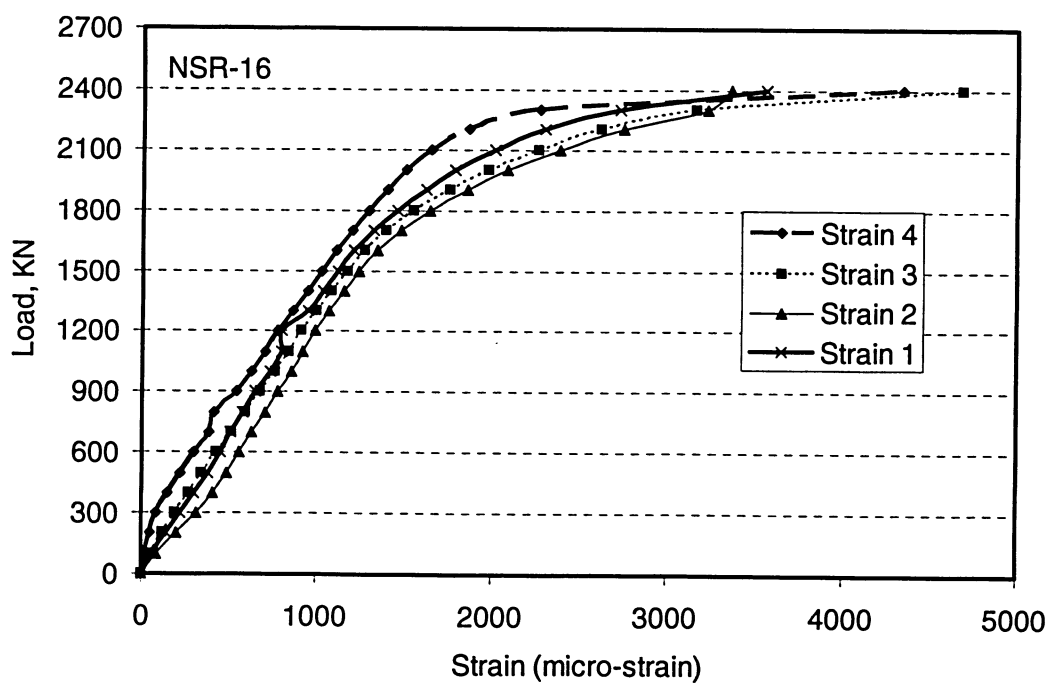


Figure 4.157 Axial load-strain relationships for specimen NSR-16

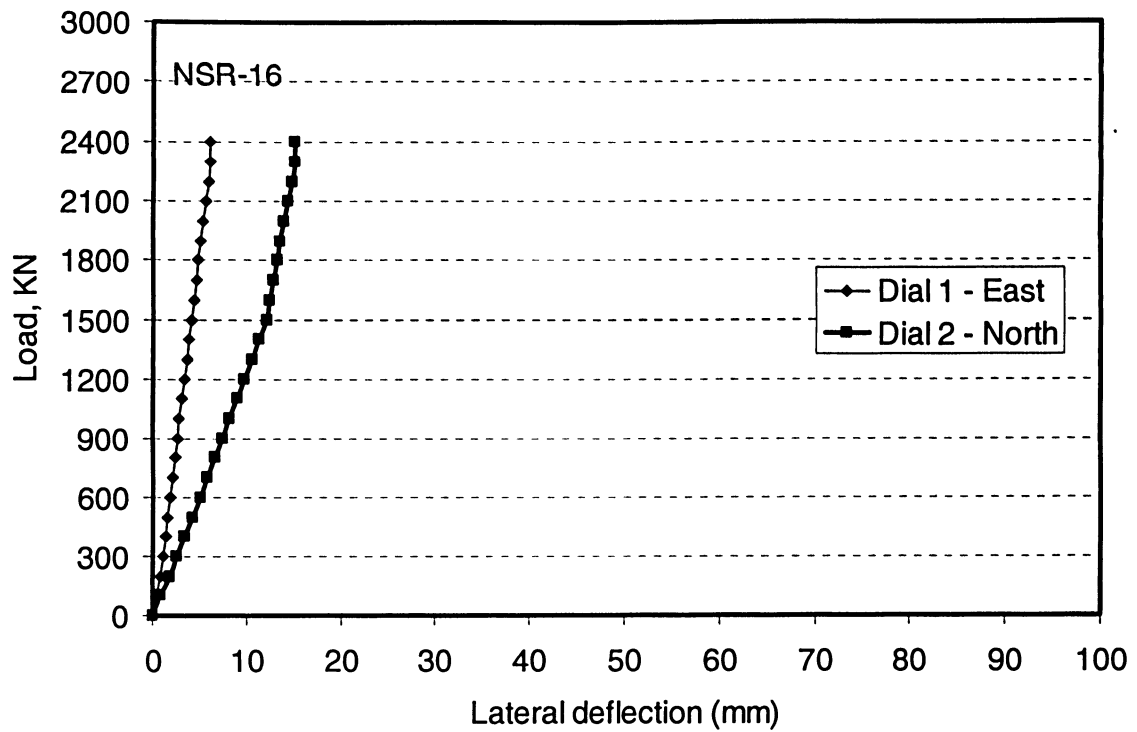


Figure 4.158 Load-lateral deflection curves for specimen NSR-16

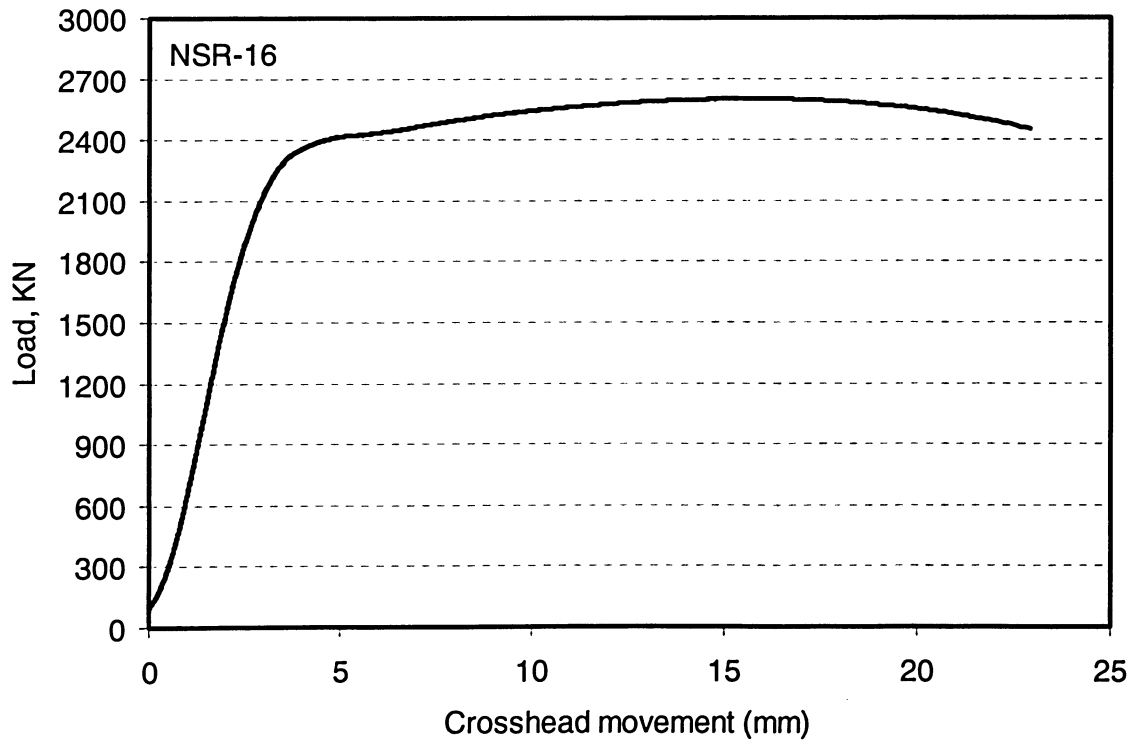


Figure 4.159 Load versus overall shortening curve for specimen NSR-16

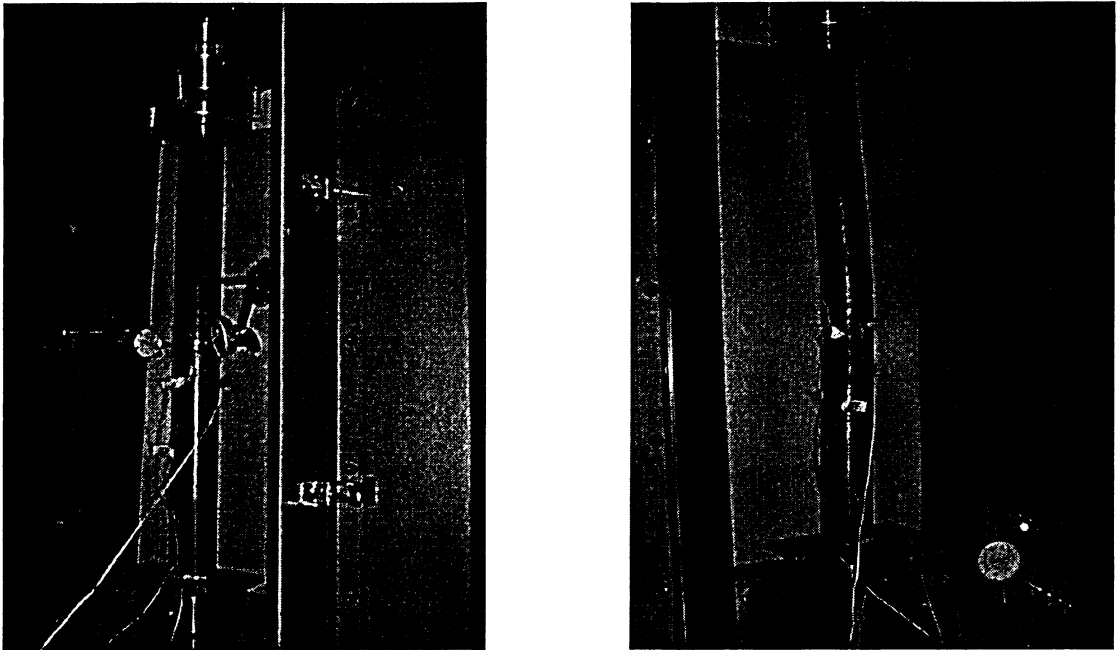


Figure 4.160 Views of specimen NSR-17 before and after testing

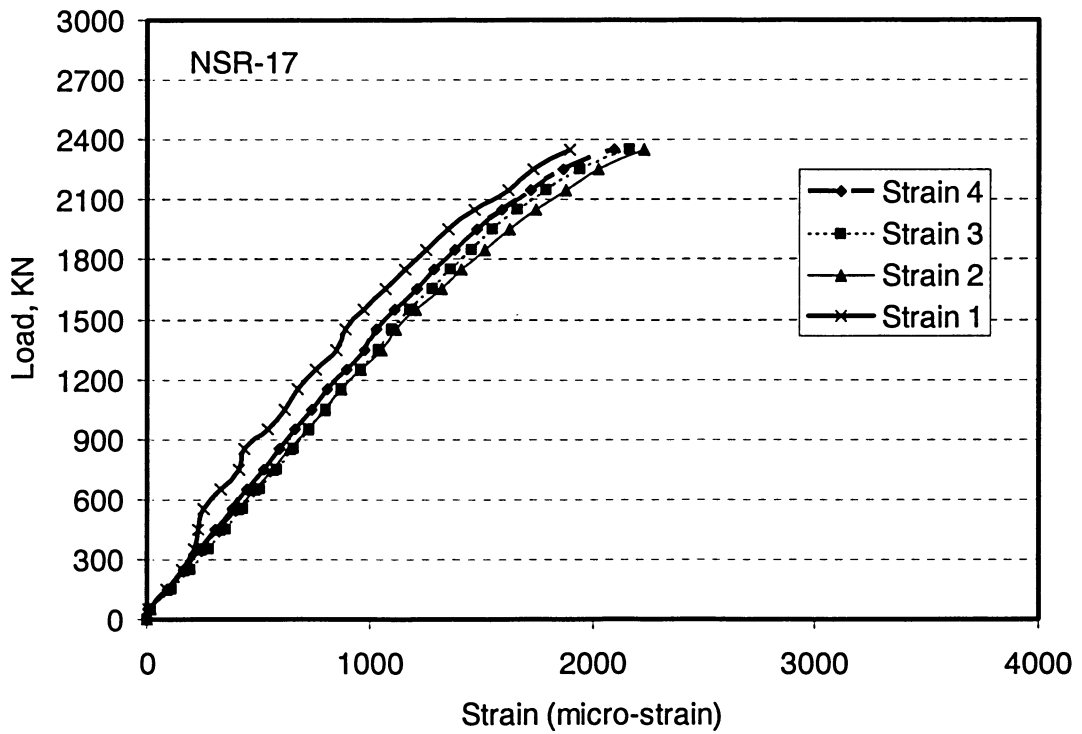


Figure 4.161 Axial load-strain relationships for specimen NSR-17

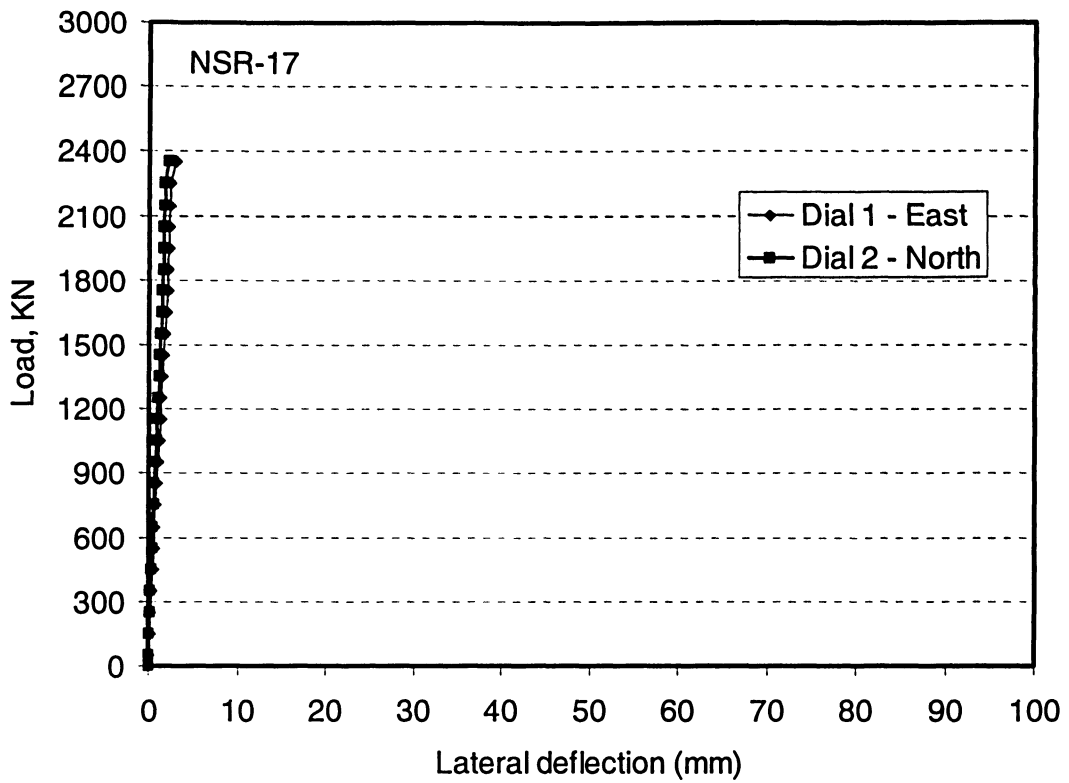


Figure 4.162 Load-lateral deflection curves for specimen NSR-17

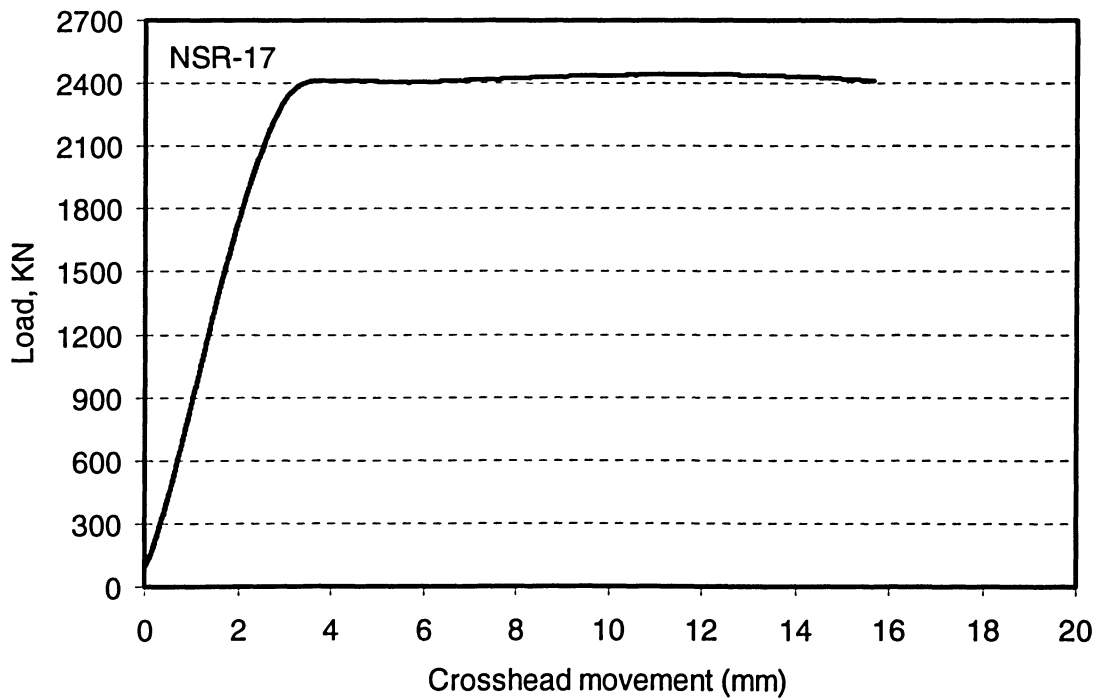


Figure 4.163 Load versus overall shortening curve for specimen NSR-17

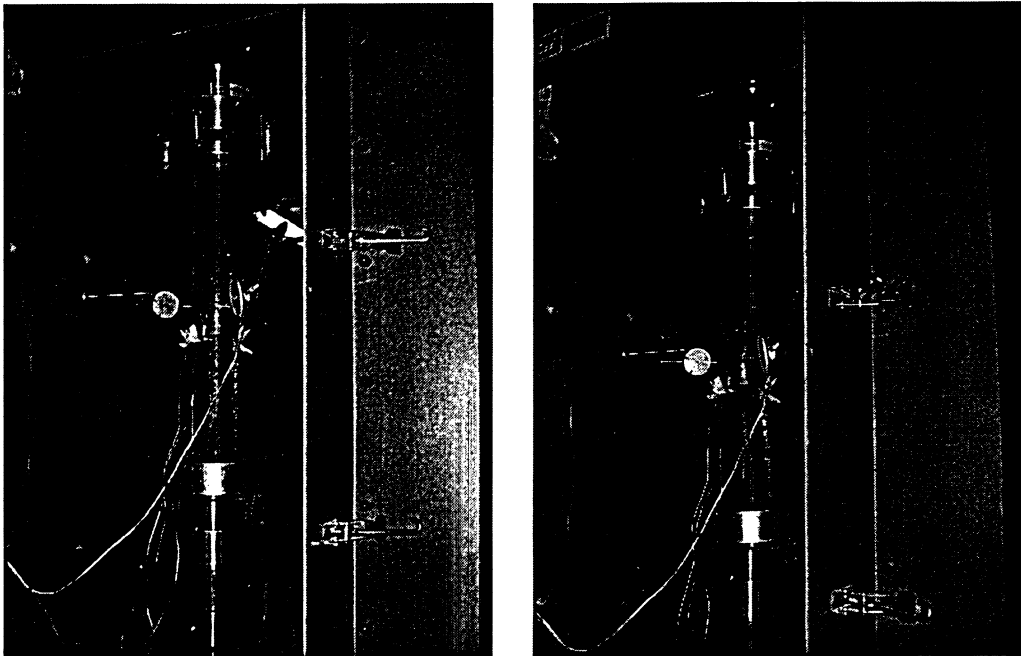


Figure 4.164 Views of specimen NSR-18 before and after testing

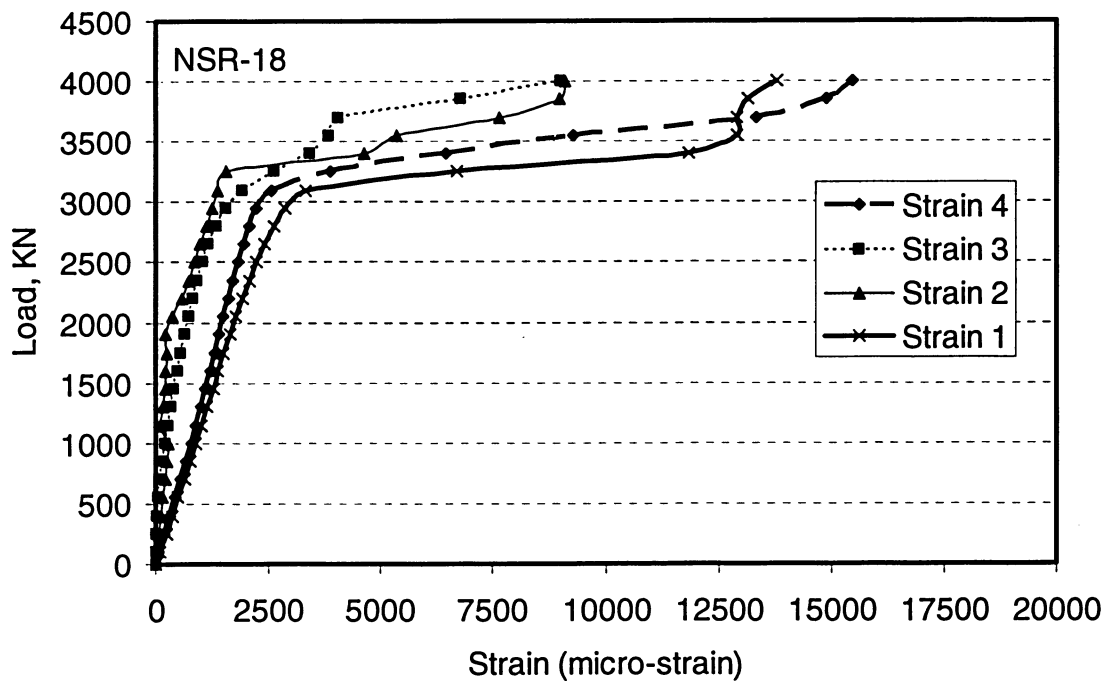


Figure 4.165 Axial load-strain relationships for specimen NSR-18

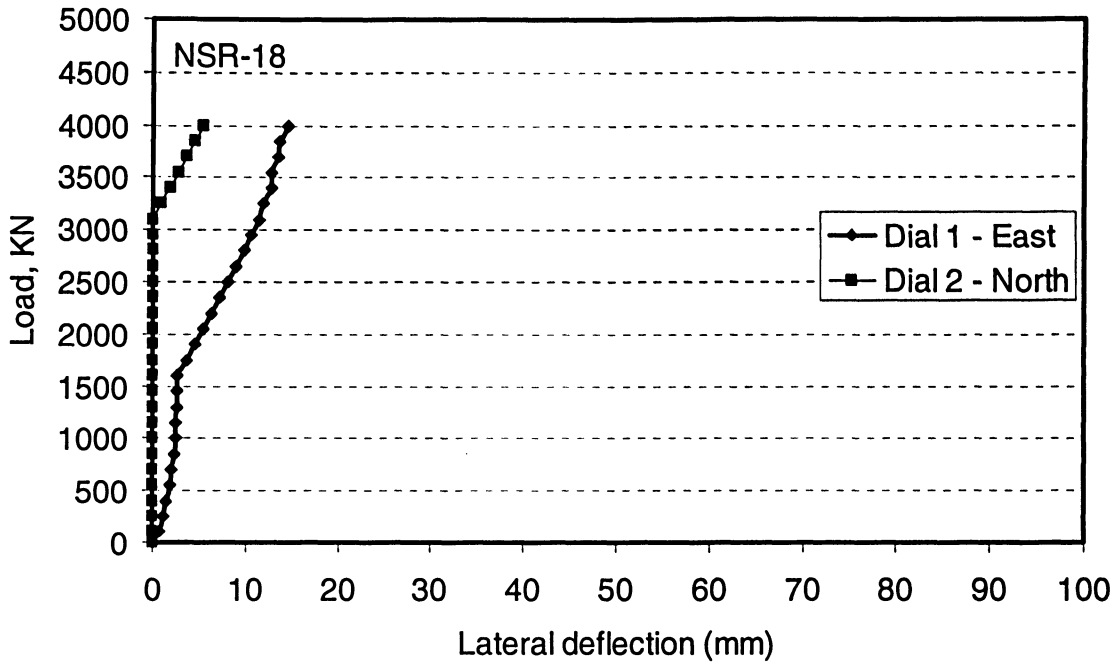


Figure 4.166 Load-lateral deflection curves for specimen NSR-18

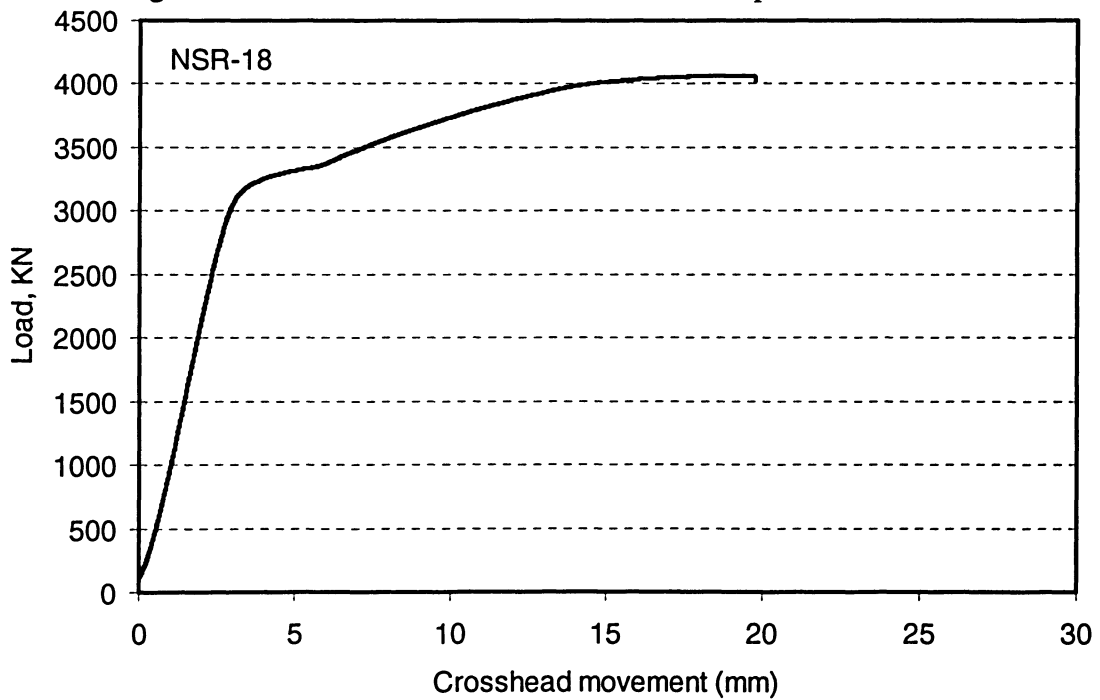


Figure 4.167 Load versus overall shortening curve for specimen NSR-18

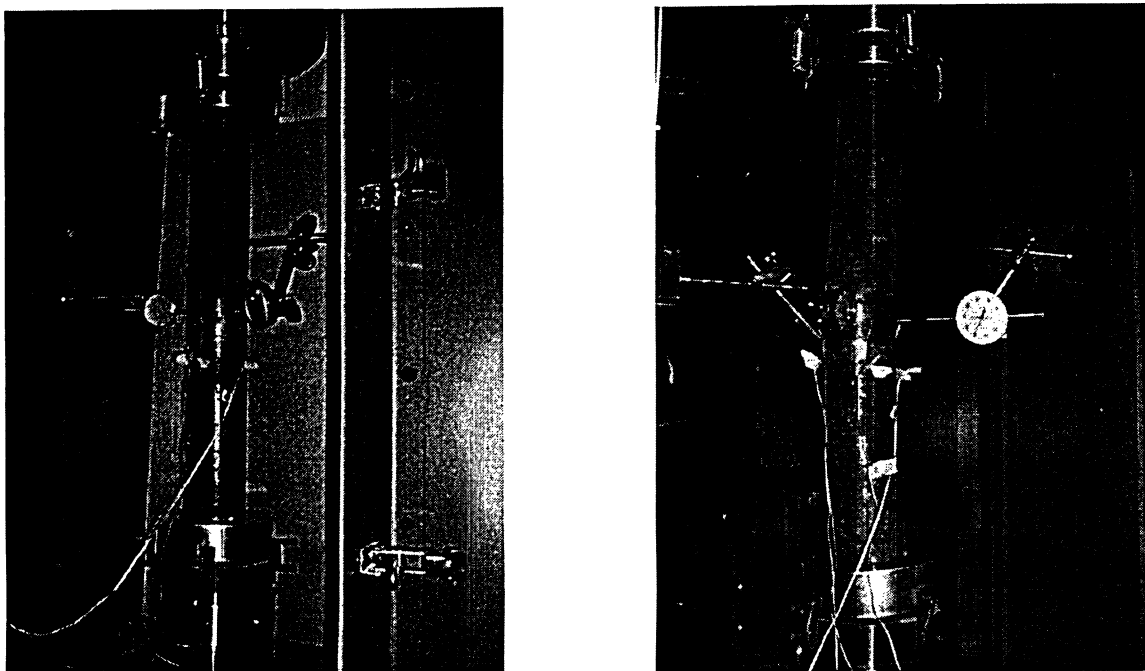


Figure 4.168 Views of specimen NSR-19 before and after testing

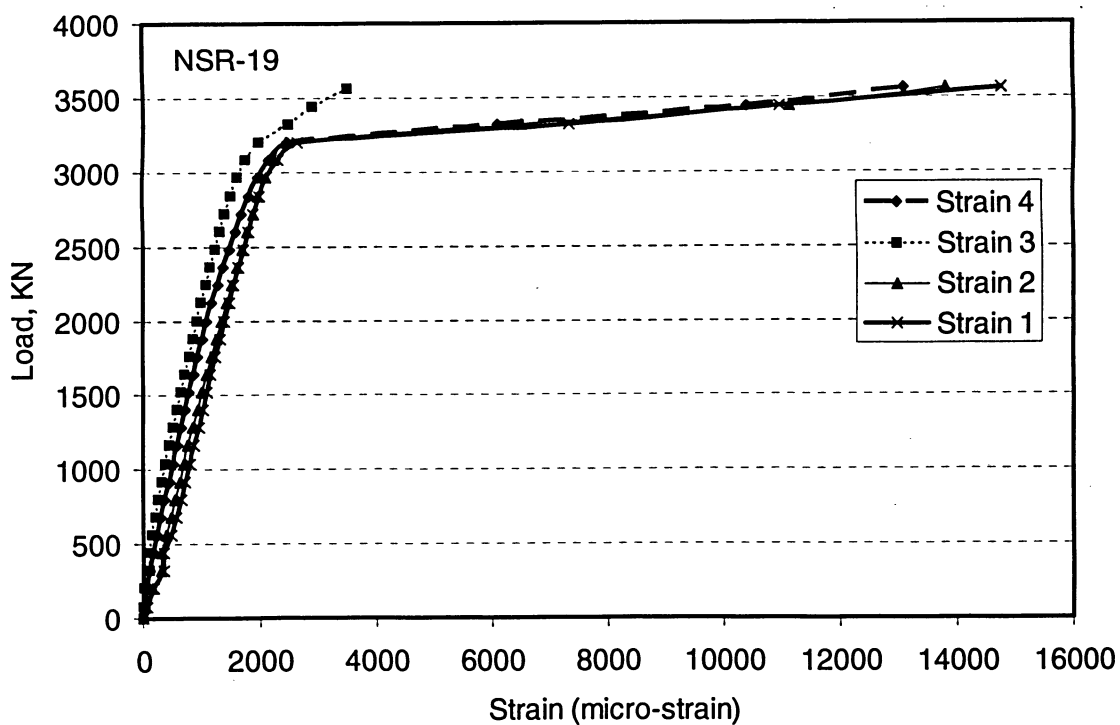


Figure 4.169 Axial load-strain relationships for specimen NSR-19

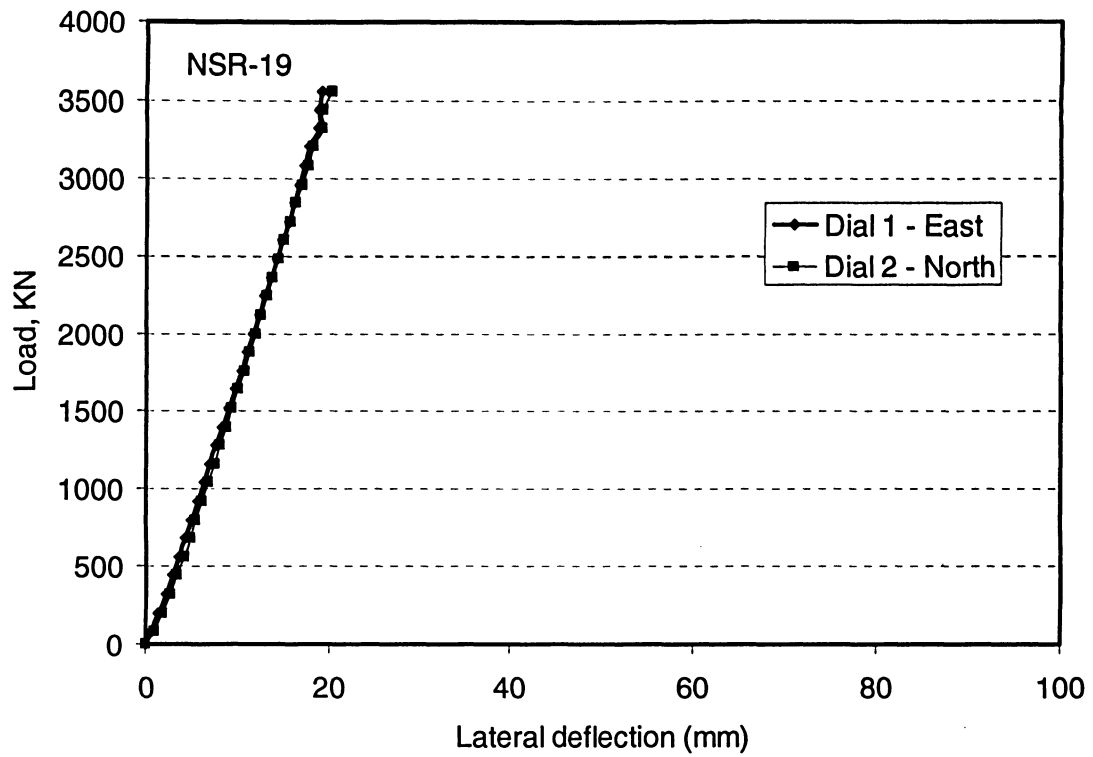


Figure 4.170 Load-lateral deflection curves for specimen NSR-19

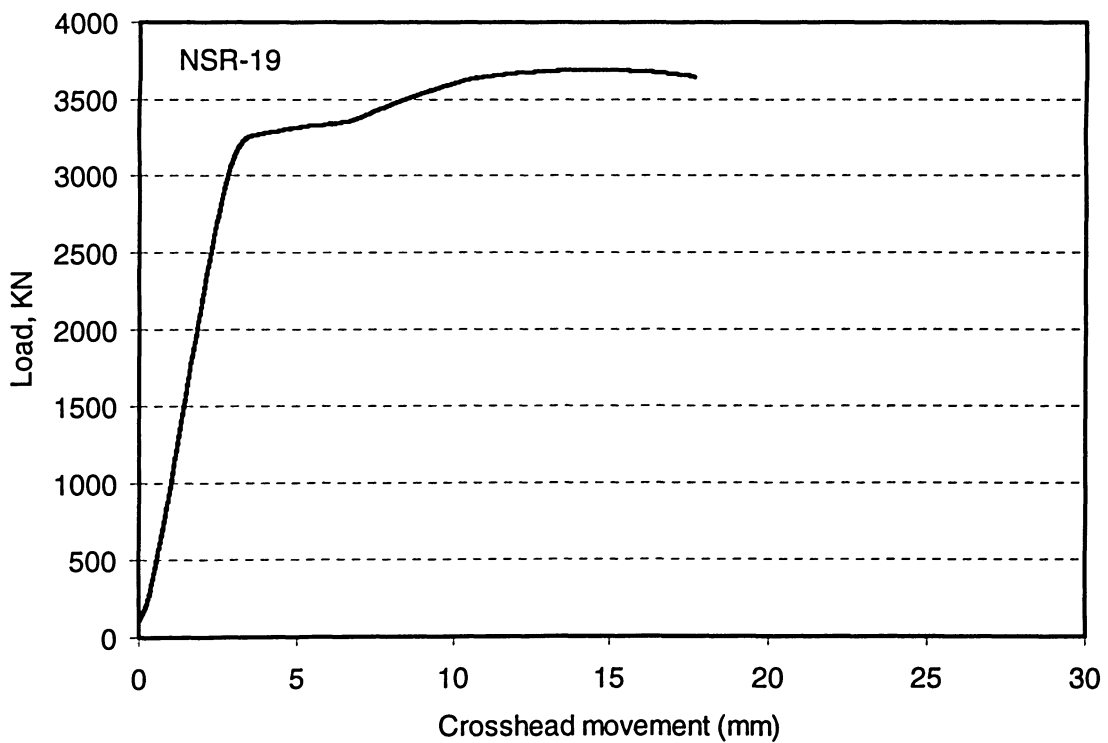


Figure 4.171 Load versus overall shortening curve for specimen NSR-19

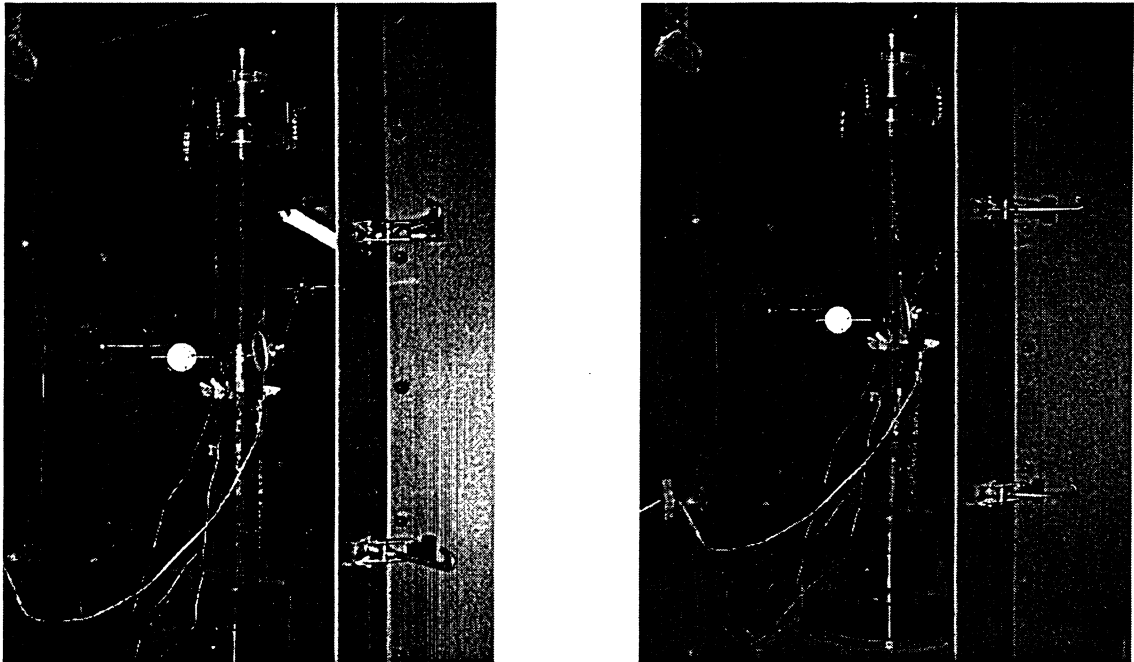


Figure 4.172 Views of specimen NSR-20 before and after testing

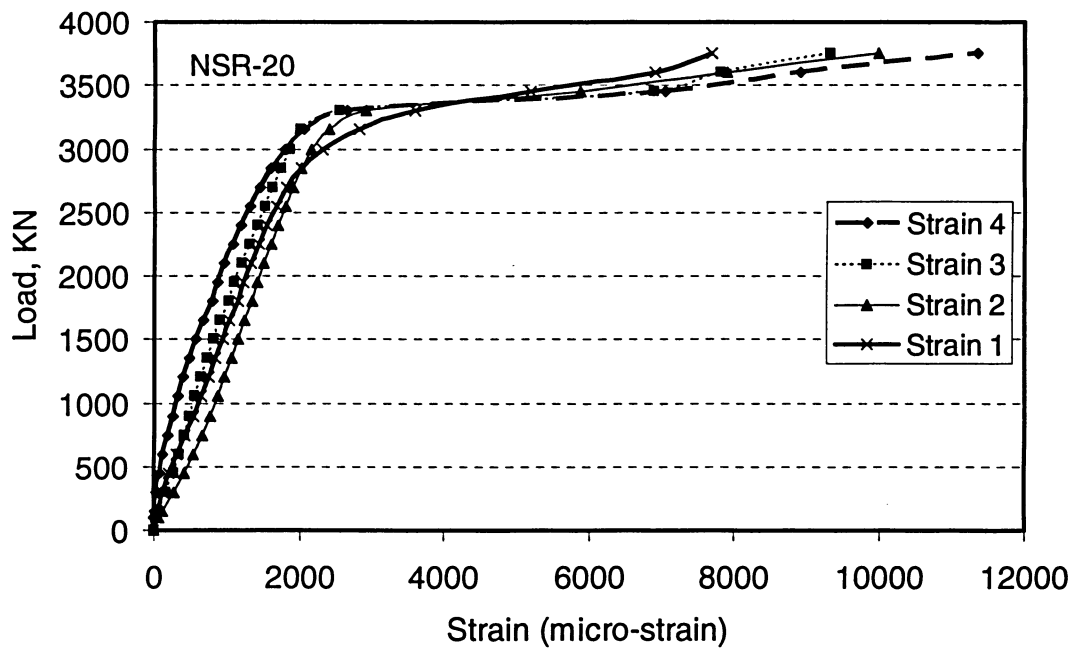


Figure 4.173 Axial load-strain relationships for specimen NSR-20

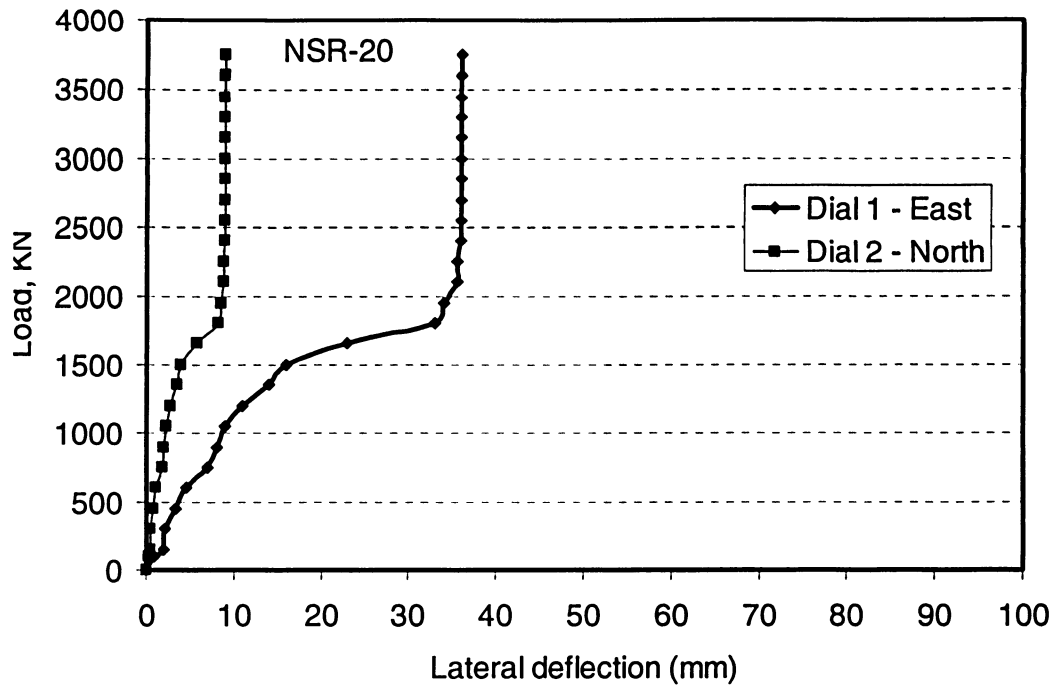


Figure 4.174 Load versus overall shortening curve for specimen NSR-20

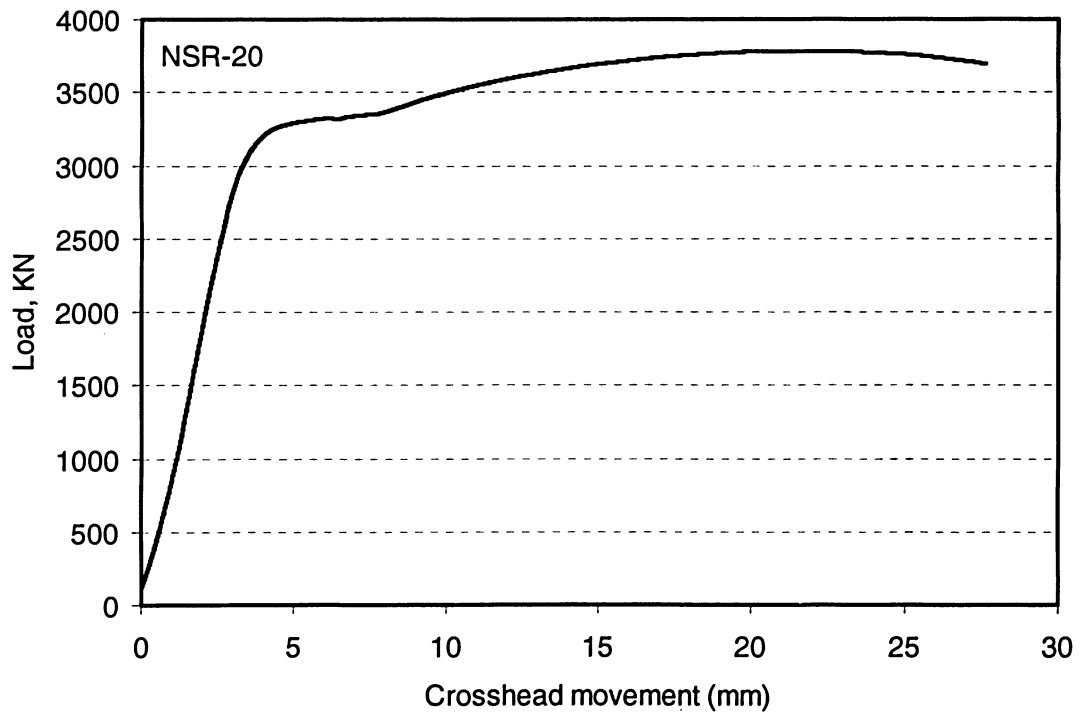


Figure 4.175 Load versus overall shortening curve for specimen NSR-20

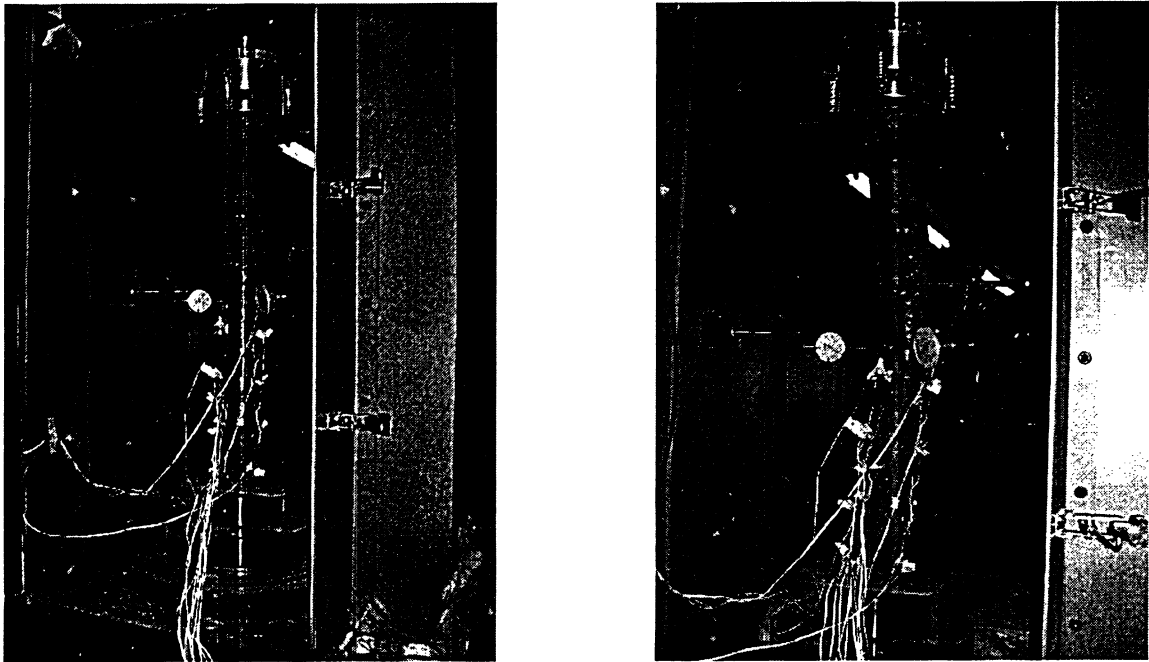


Figure 4.176 Views of specimen NSR-21 before and after testing

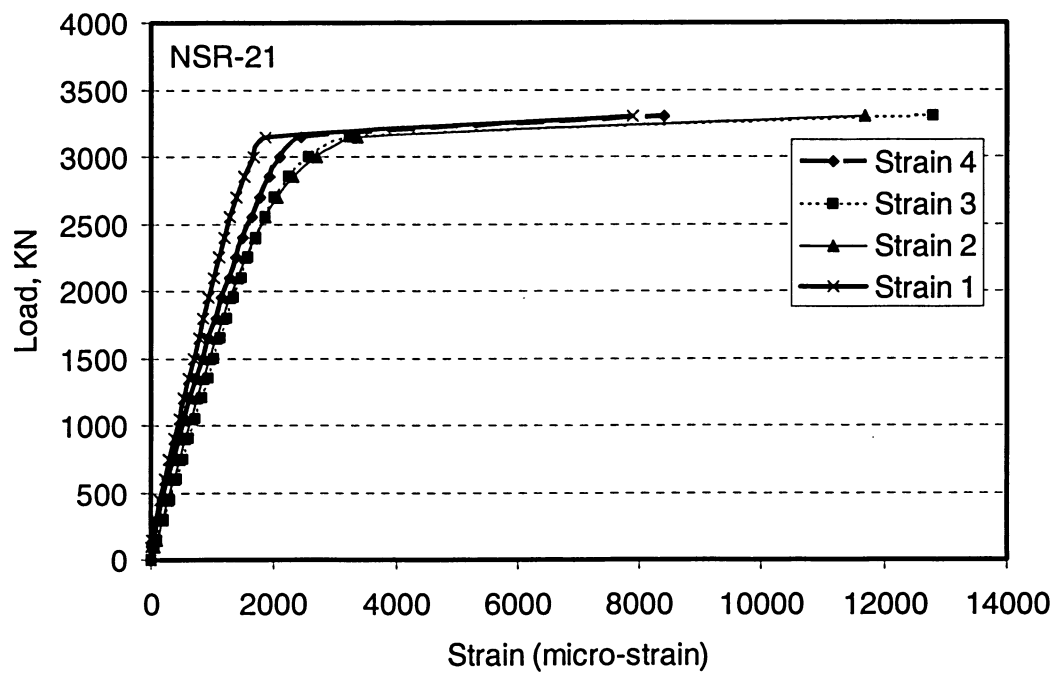


Figure 4.177 Axial load-strain relationships for specimen NSR-21

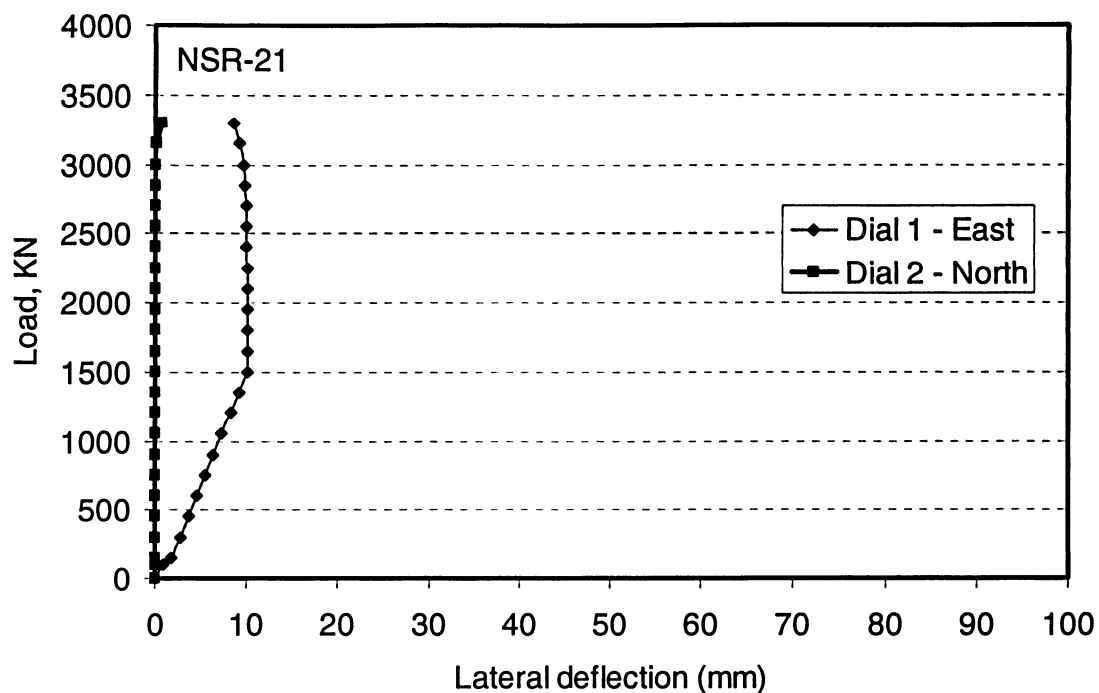


Figure 4.178 Load-lateral deflection curves for specimen NSR-21

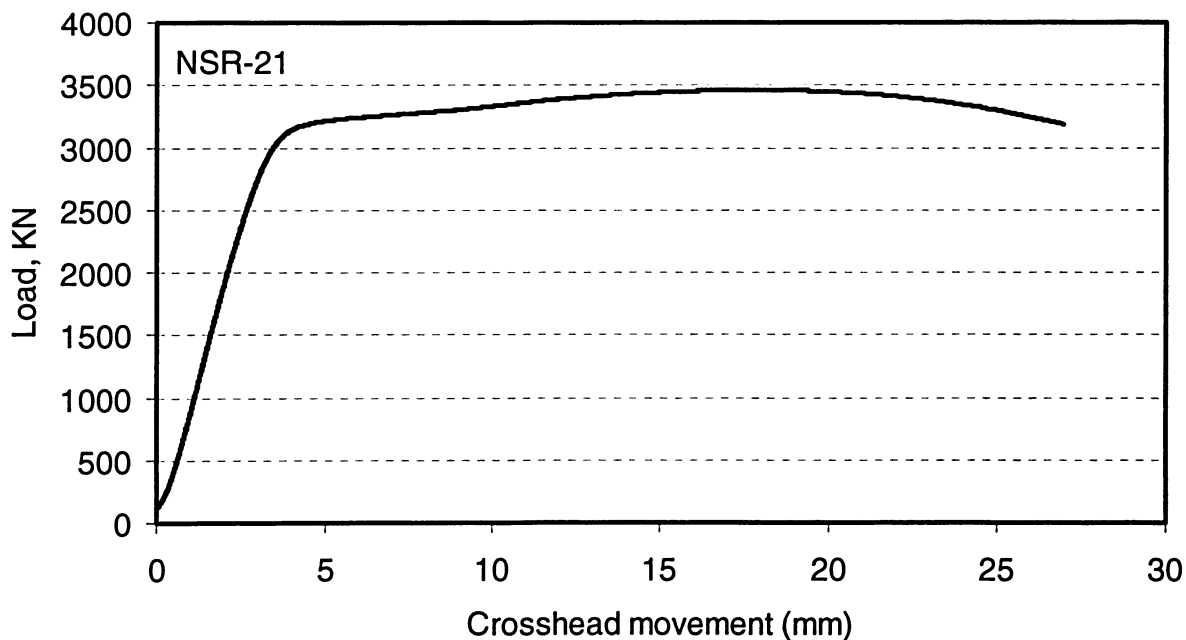


Figure 4.179 Load versus overall shortening curve for specimen NSR-21

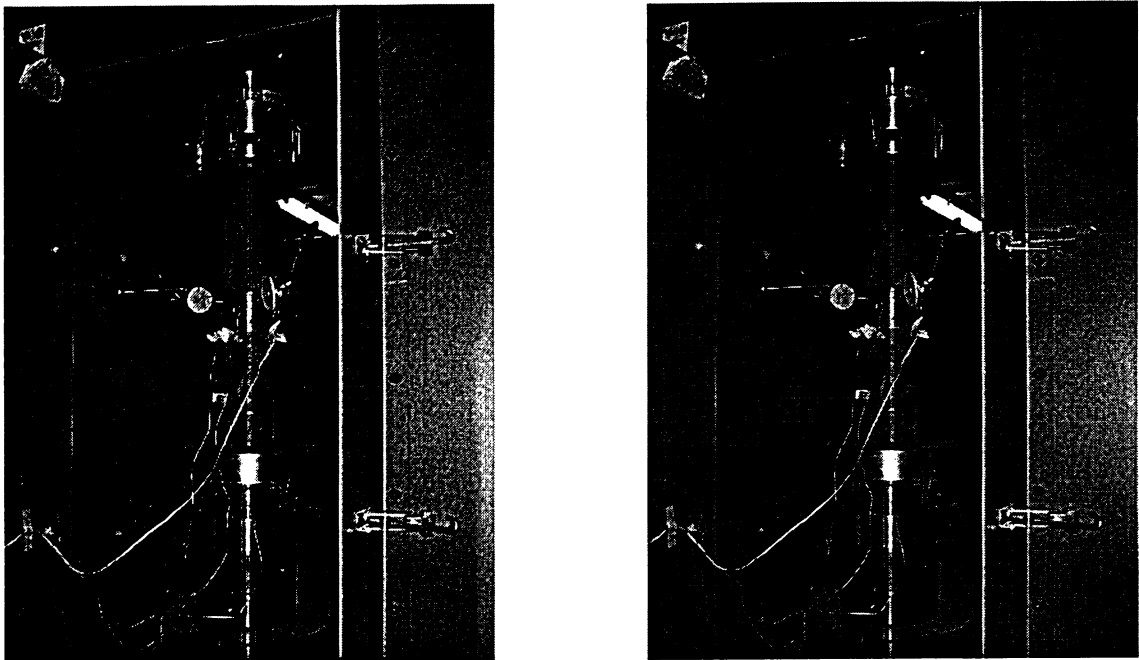


Figure 4.180 Views of specimen NSR-22 before and after testing

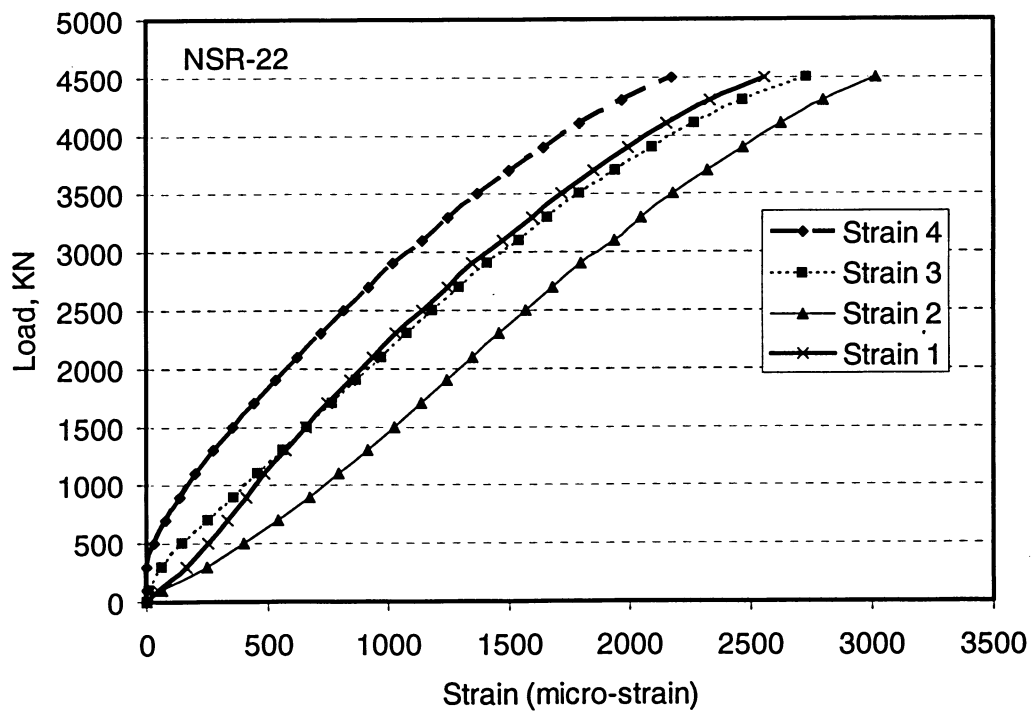


Figure 4.181 Axial load-strain relationships for specimen NSR-22

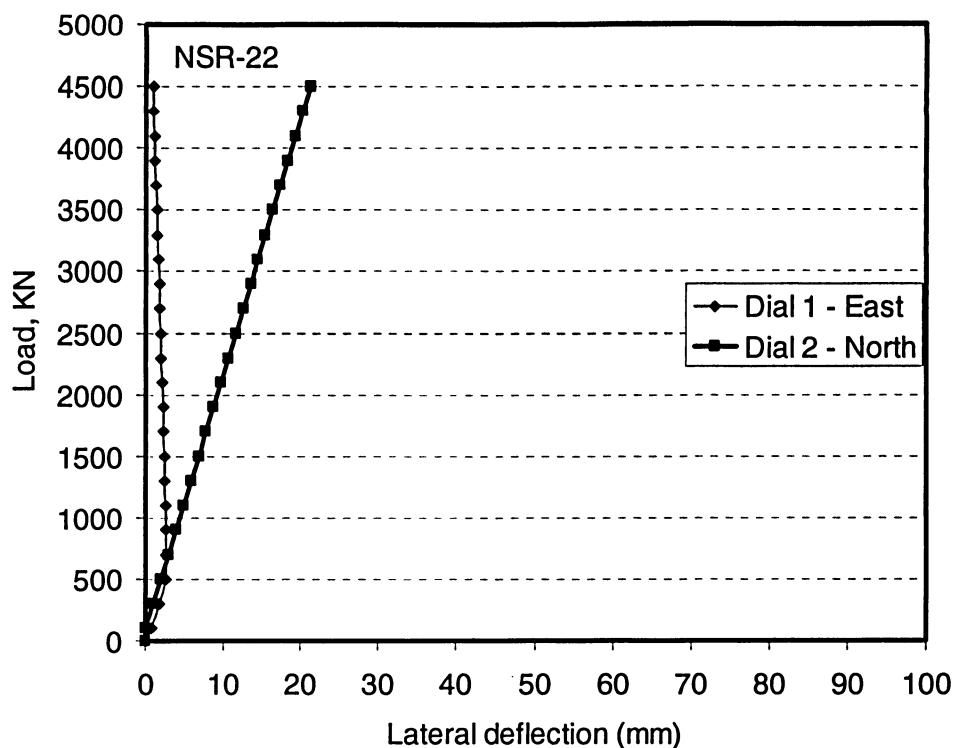


Figure 4.182 Load-lateral deflection curves for specimen NSR-22

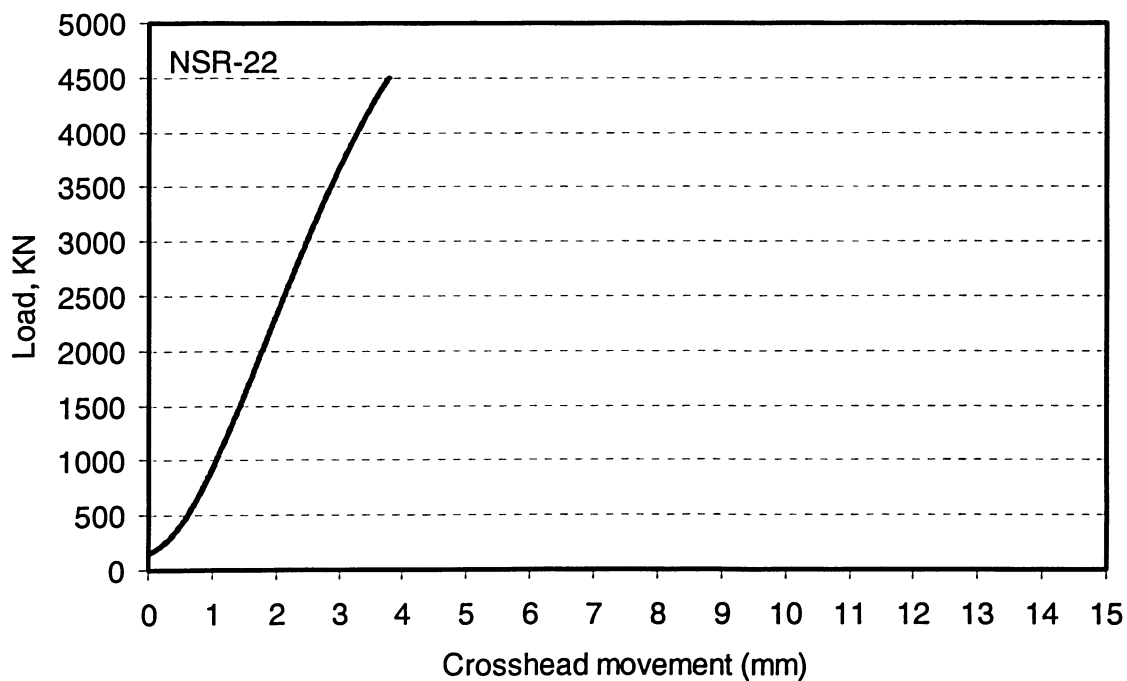


Figure 4.183 Load versus overall shortening curve for specimen NSR-22

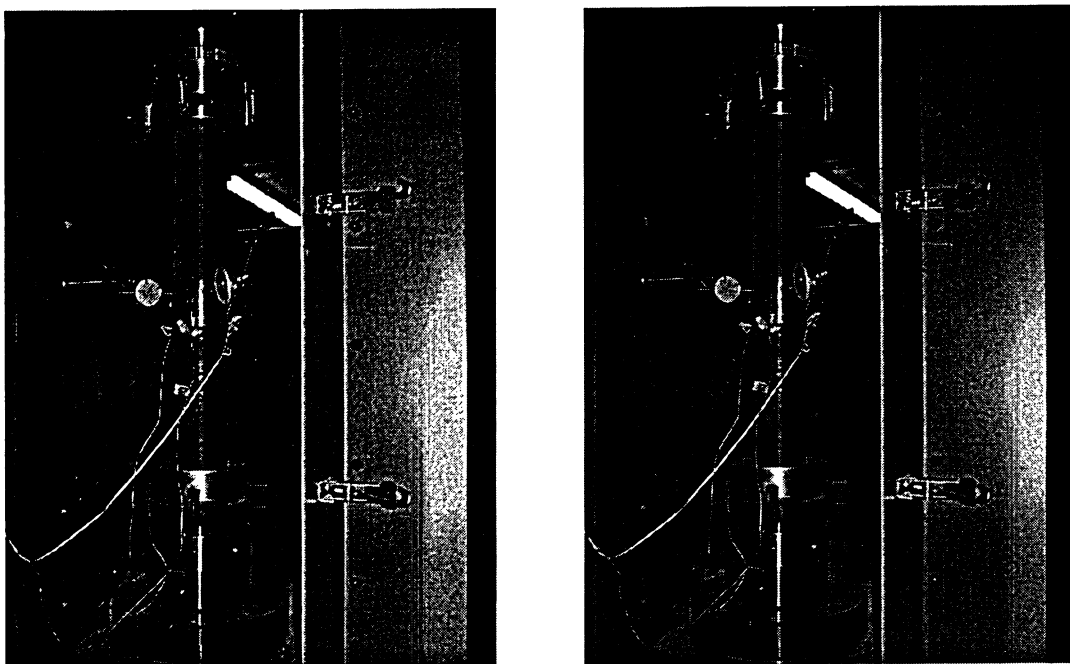


Figure 4.184 Views of specimen NSR-23 before and after testing

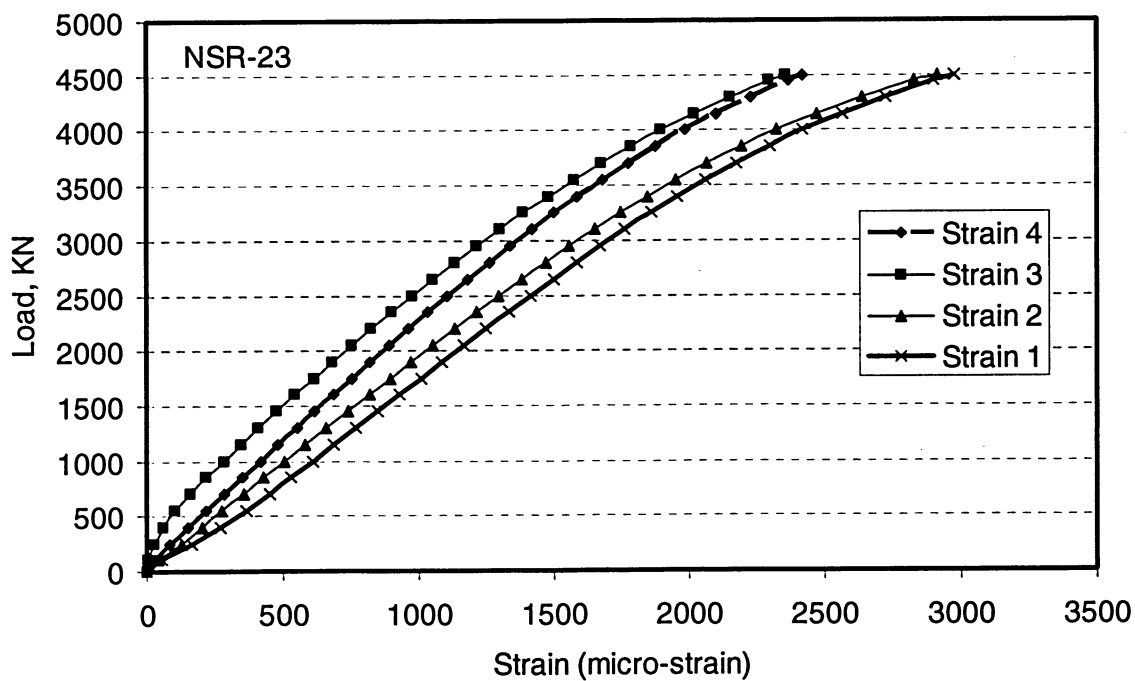


Figure 4.185 Axial load-strain relationships for specimen NSR-23

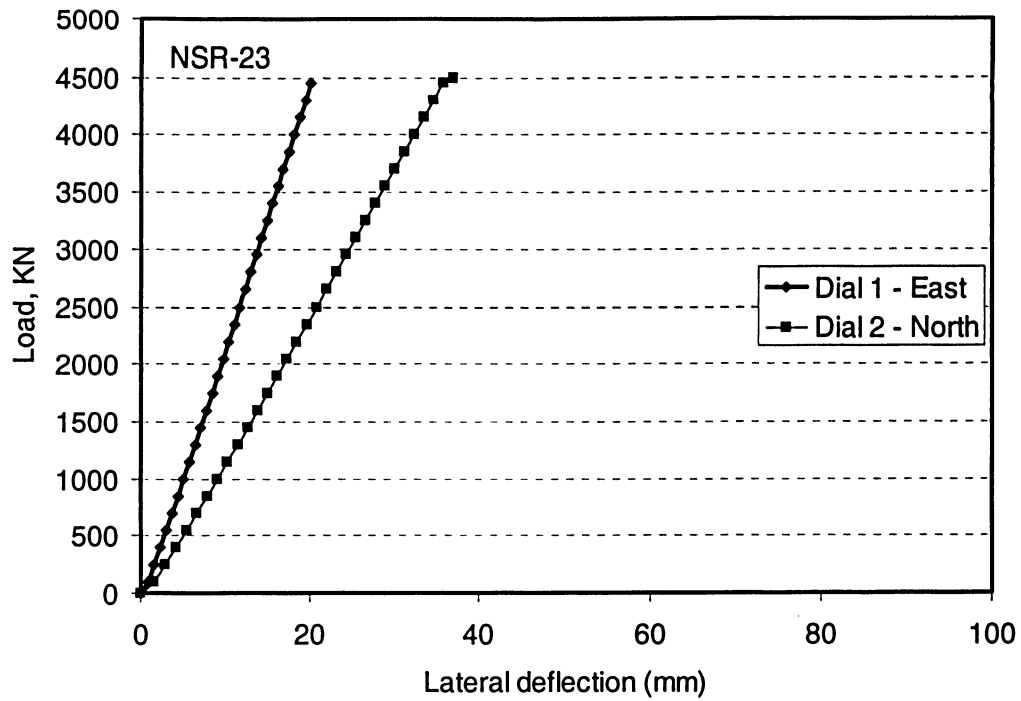


Figure 4.186 Load-lateral deflection curves for specimen NSR-23

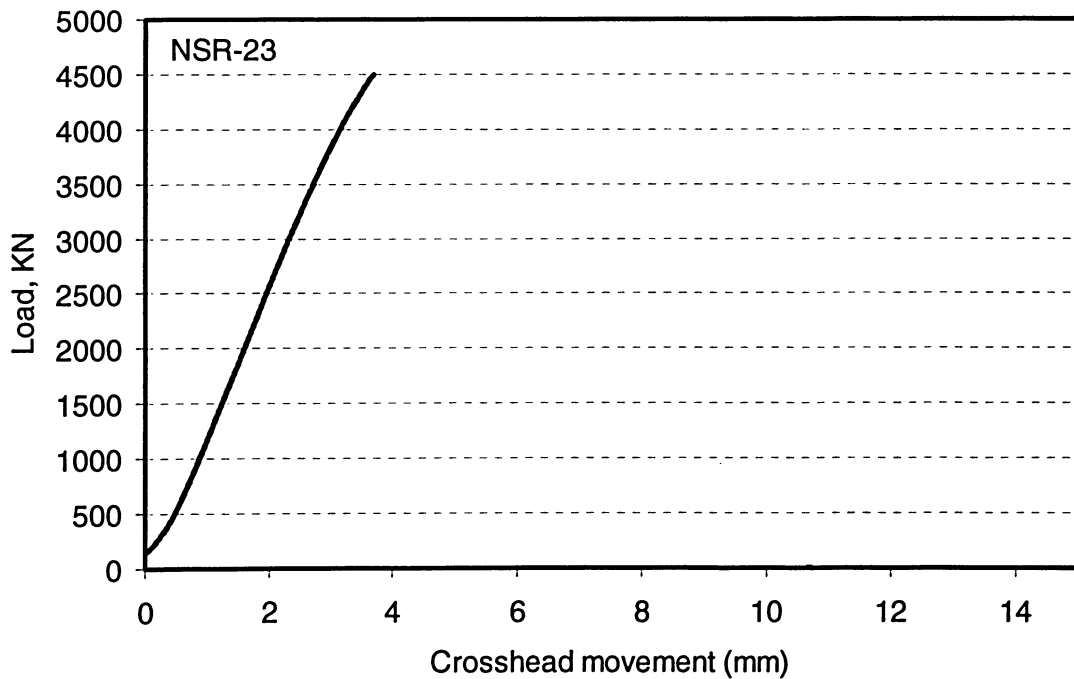


Figure 4.187 Load versus overall shortening curve for specimen NSR-23

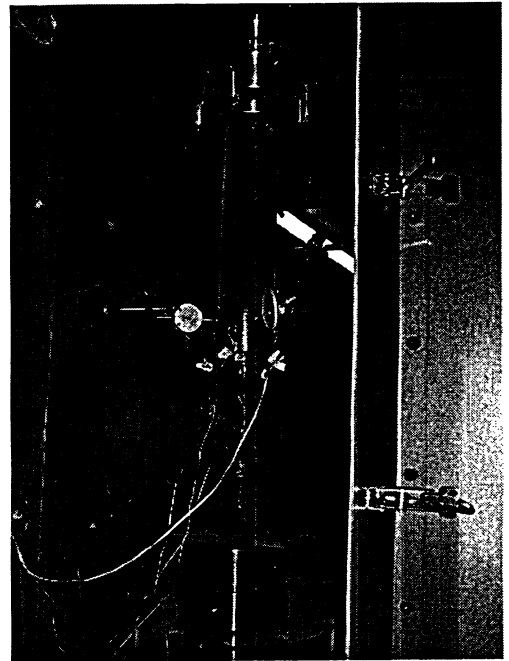
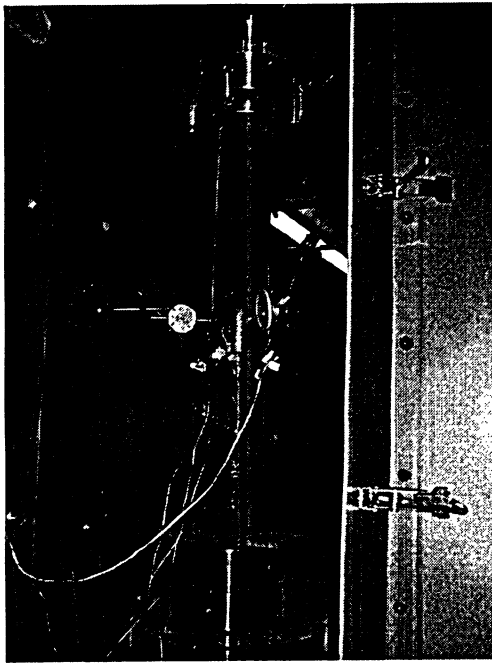


Figure 4.188 Views of specimen NSR-24 before and after testing

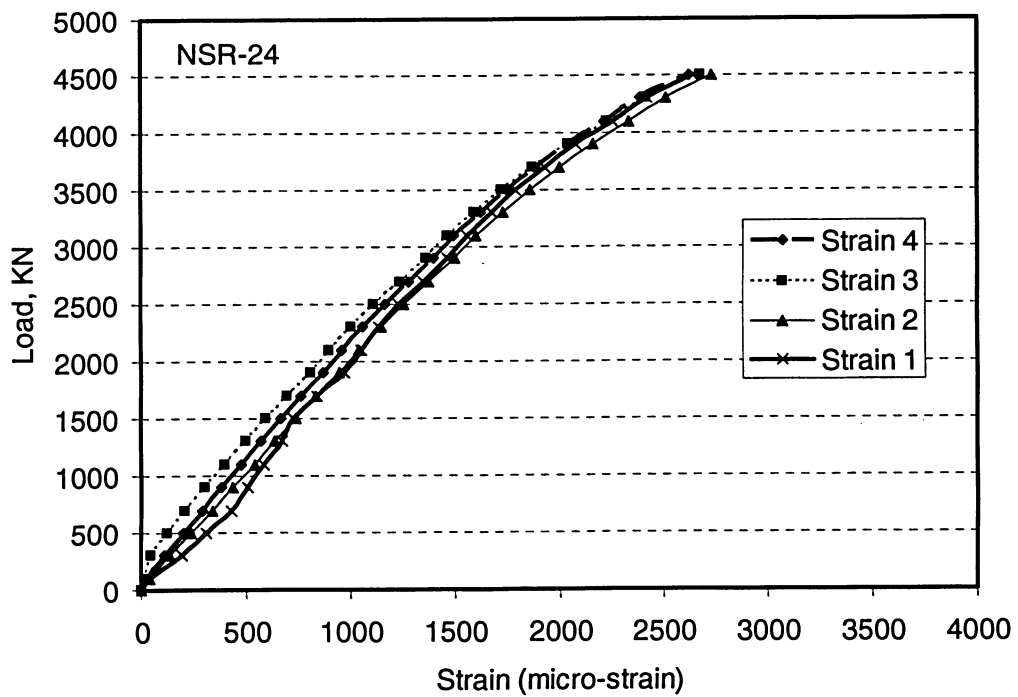


Figure 4.189 Axial load-strain relationships for specimen NSR-24

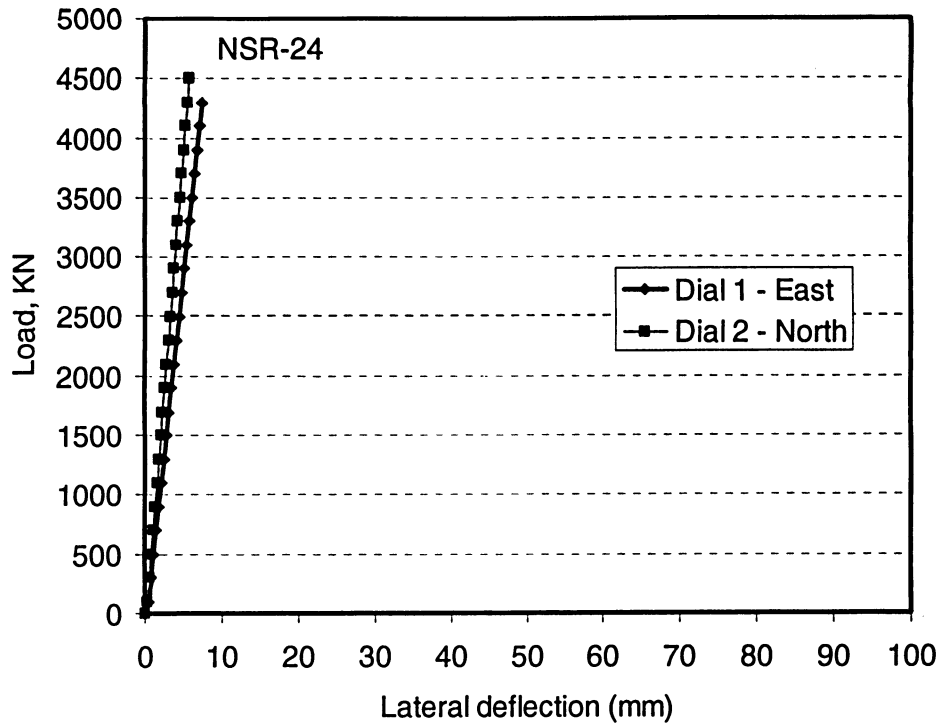


Figure 4.190 Load-lateral deflection curves for specimen NSR-24

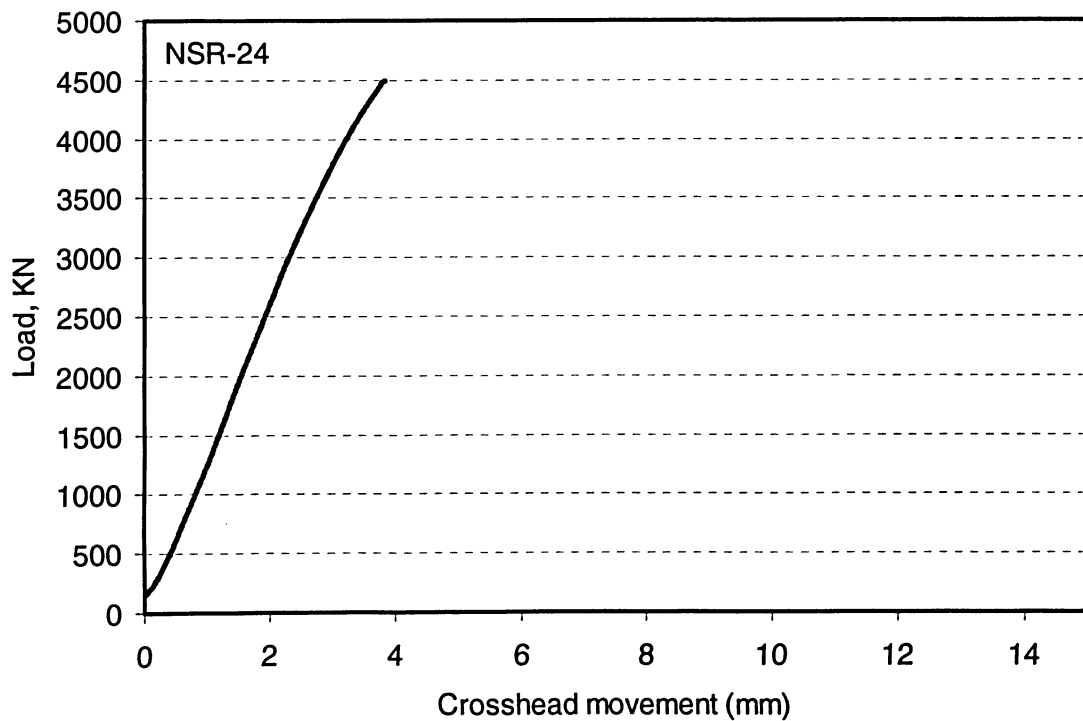


Figure 4.191 Load versus overall shortening curve for specimen NSR-24

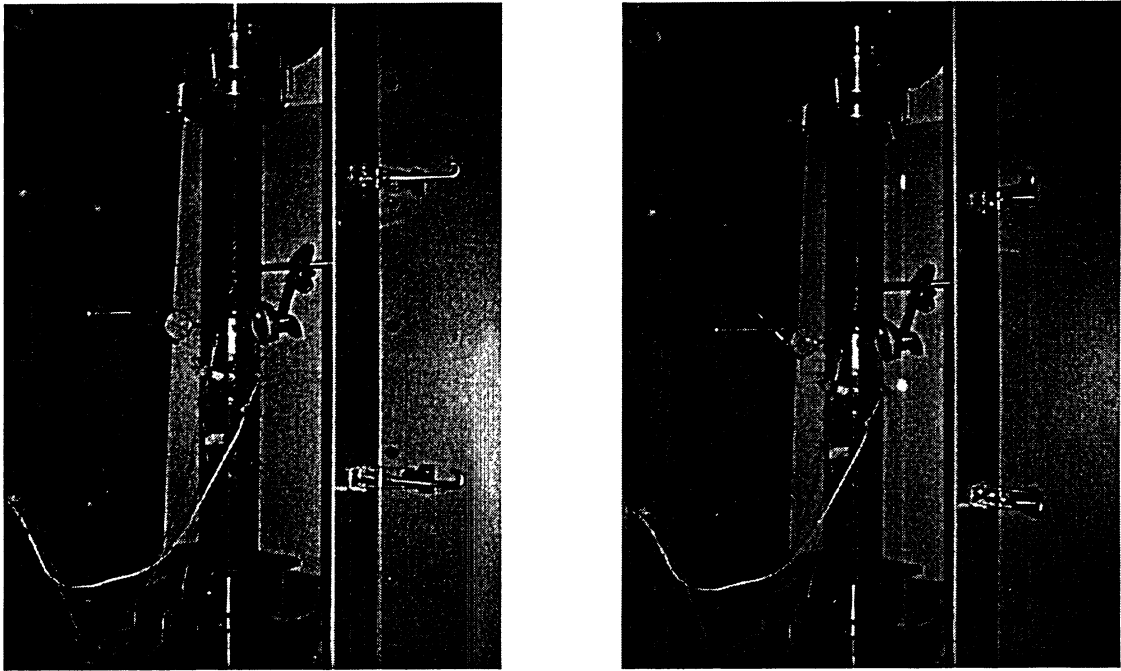


Figure 4.192 Views of specimen NSR-25 before and after testing

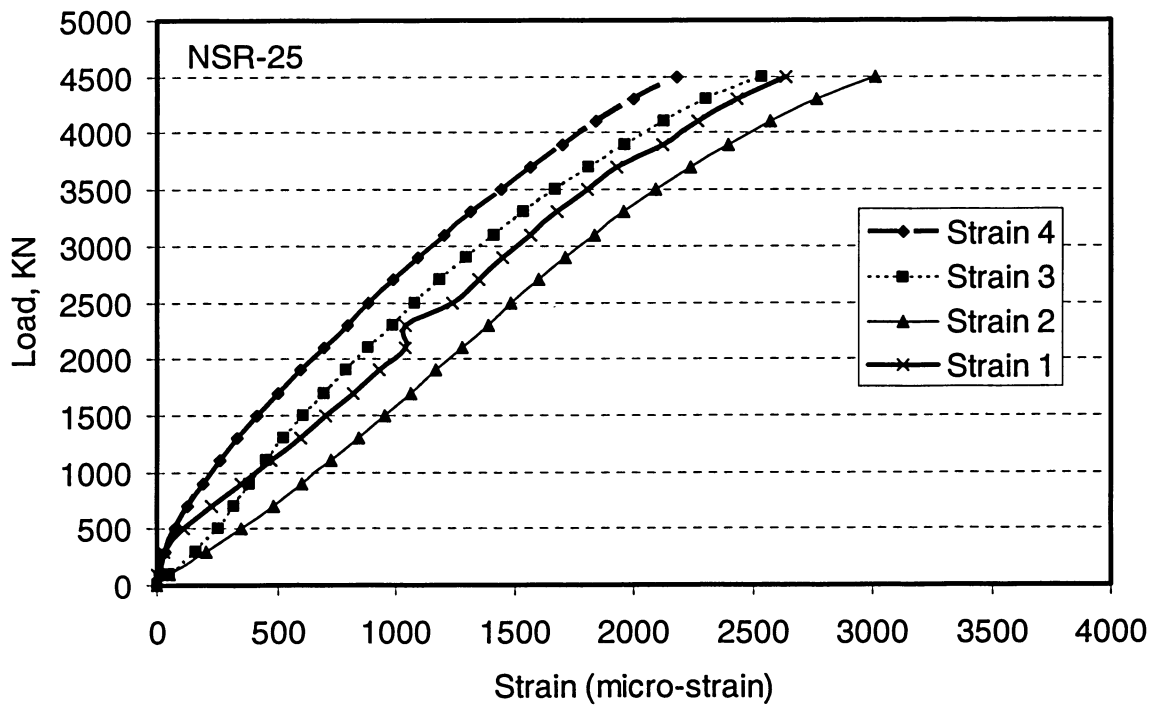


Figure 4.193 Axial load-strain relationships for specimen NSR-25

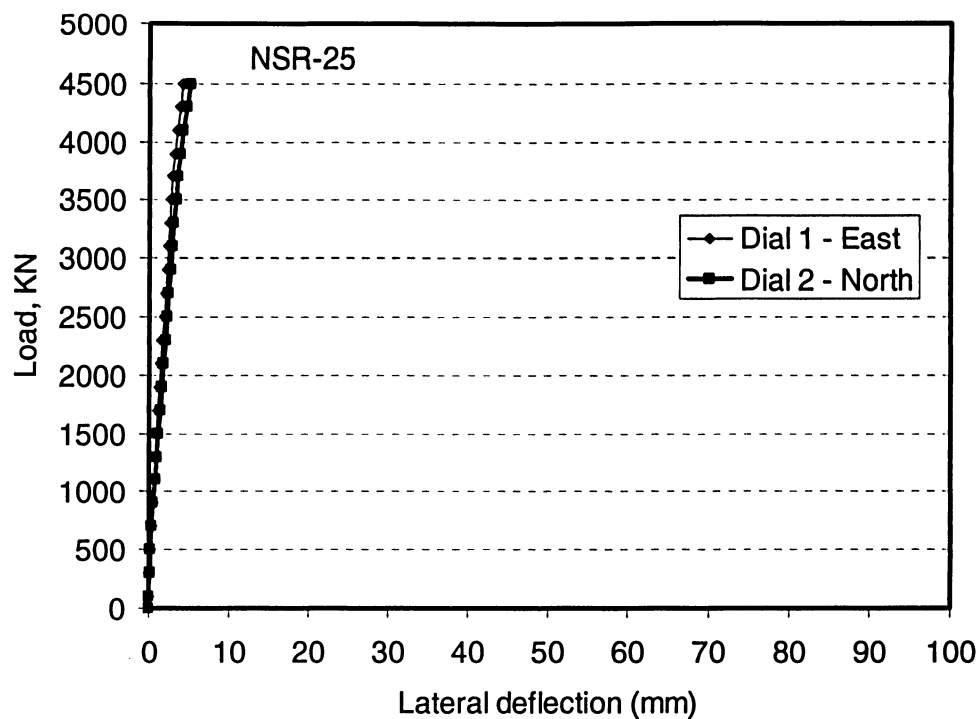


Figure 4.194 Load-lateral deflection curves for specimen NSR-25

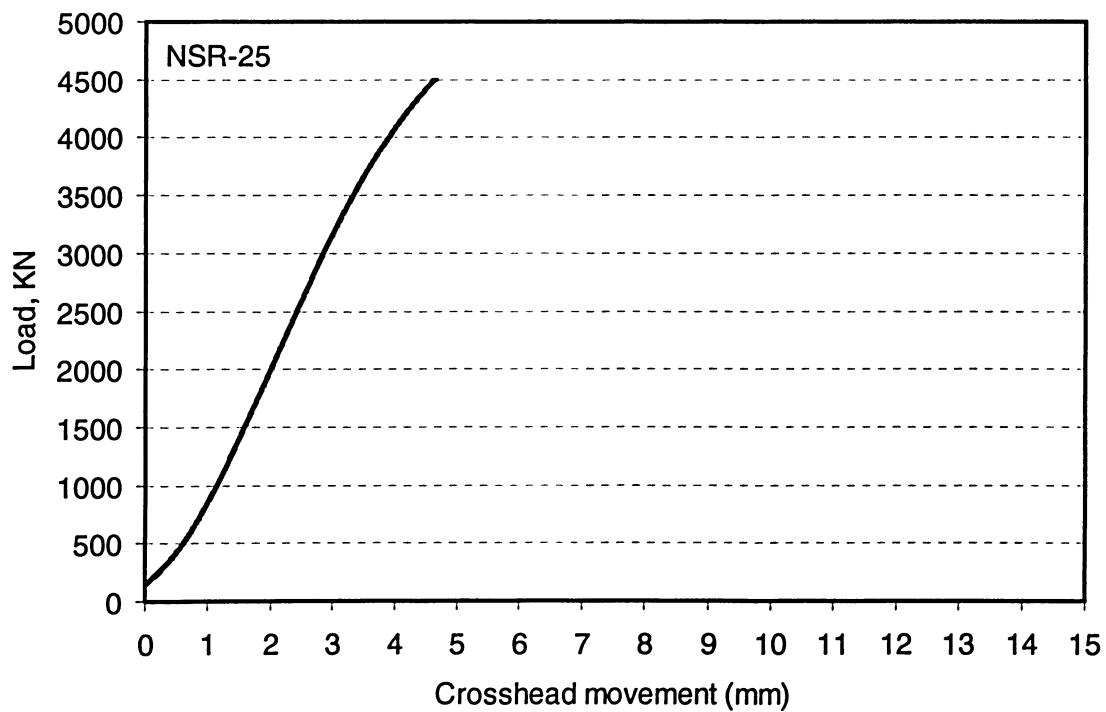


Figure 4.195 Load versus overall shortening curve for specimen NSR-25

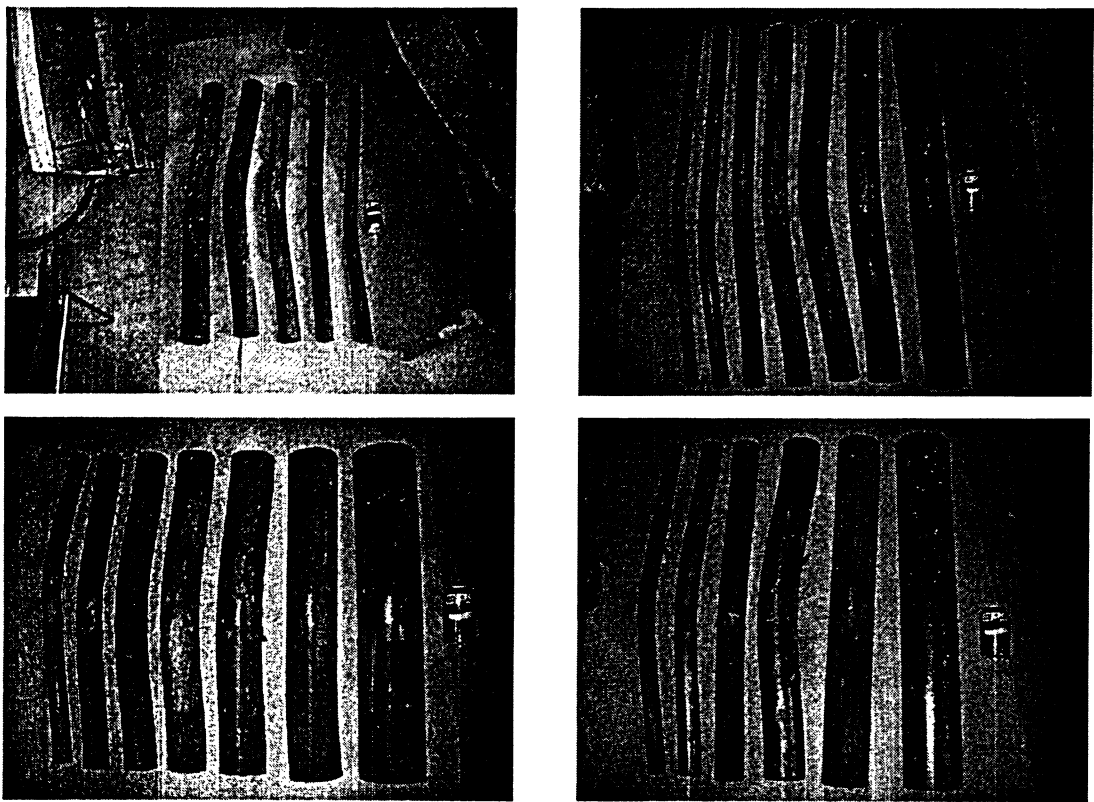


Figure 4.196 Views of the NSR tested specimens

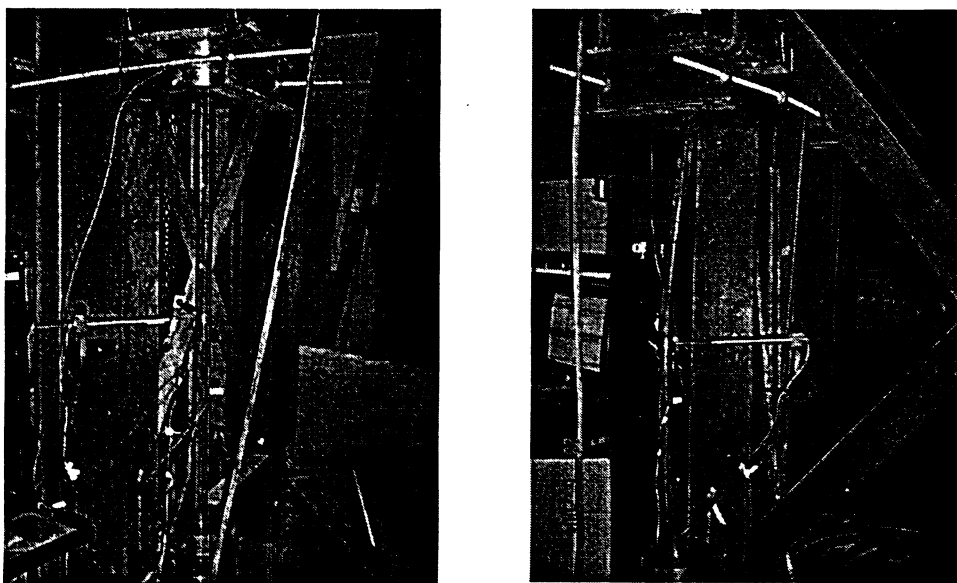


Figure 4.197 Views of specimen NSR-26 before and after testing

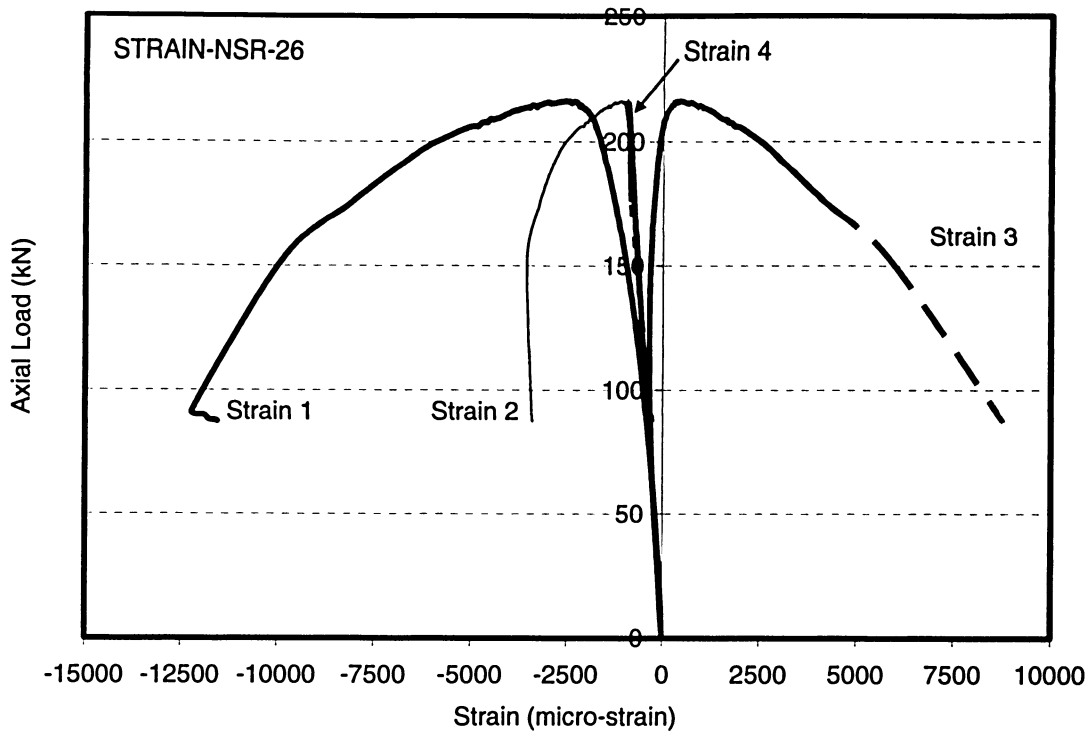


Figure 4.198 Axial load-strain relationships for specimen NSR-26

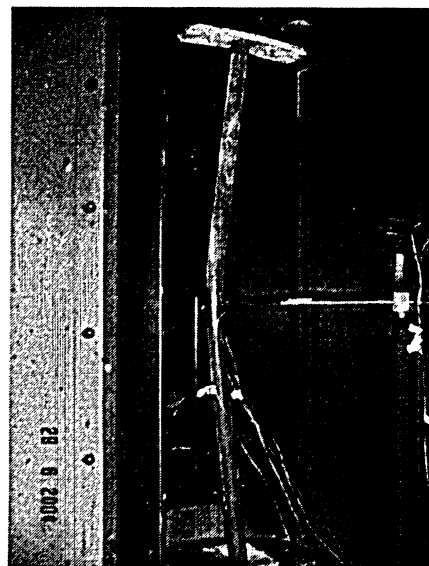
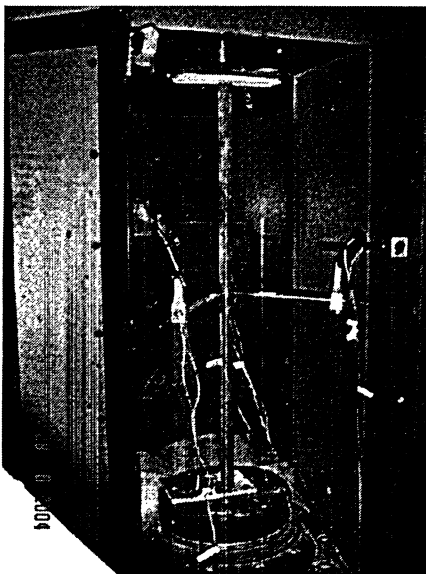


Figure 4.199 Views of specimen NSR-27 before and after testing

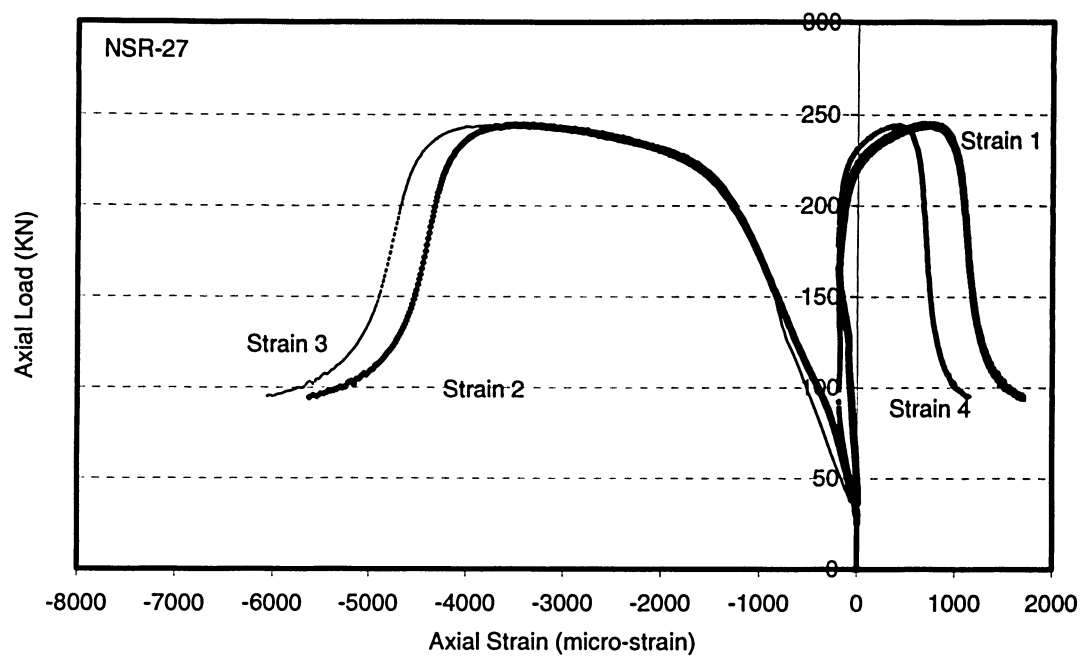


Figure 4.200 Axial load-strain relationships for specimen NSR-27

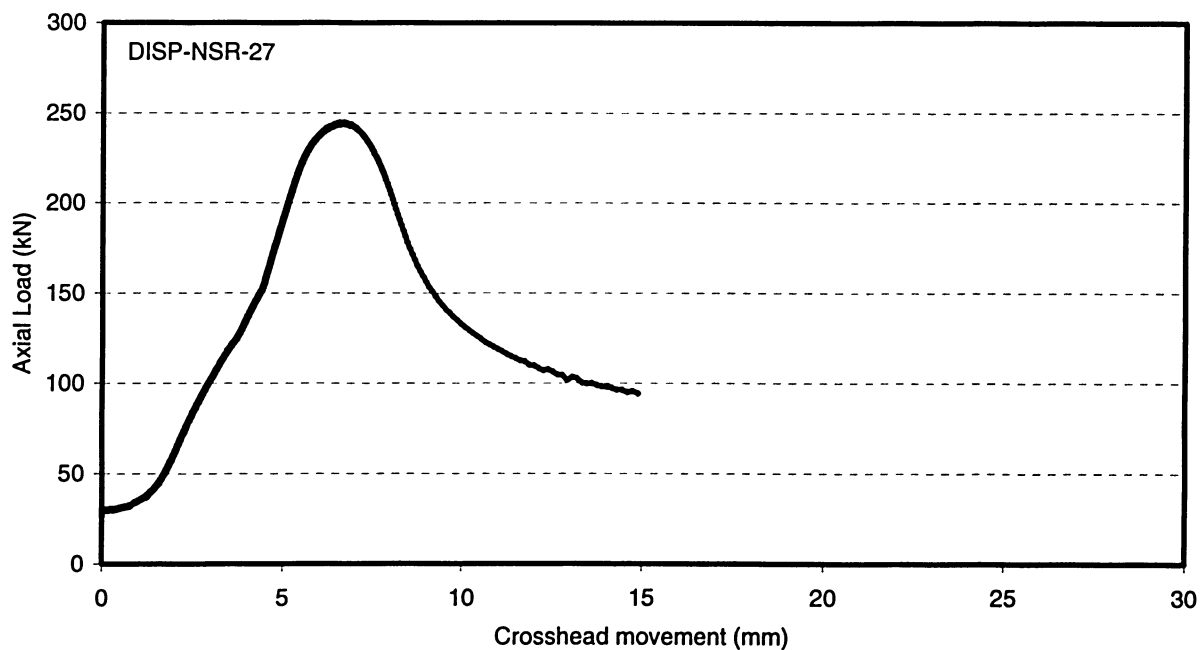


Figure 4.201 Load versus overall shortening curve for specimen NSR-27

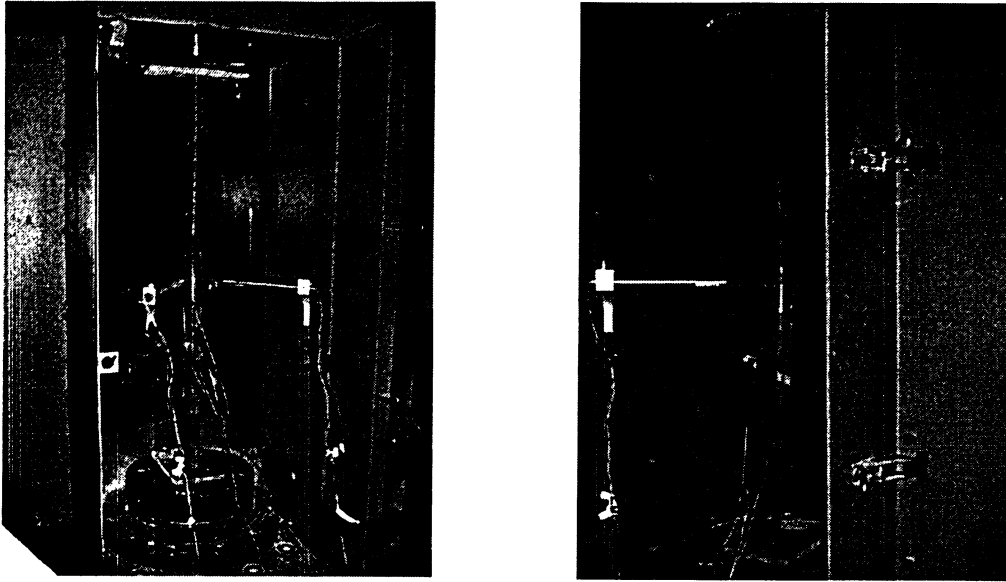


Figure 4.202 Views of specimen NSR-28 before and after testing

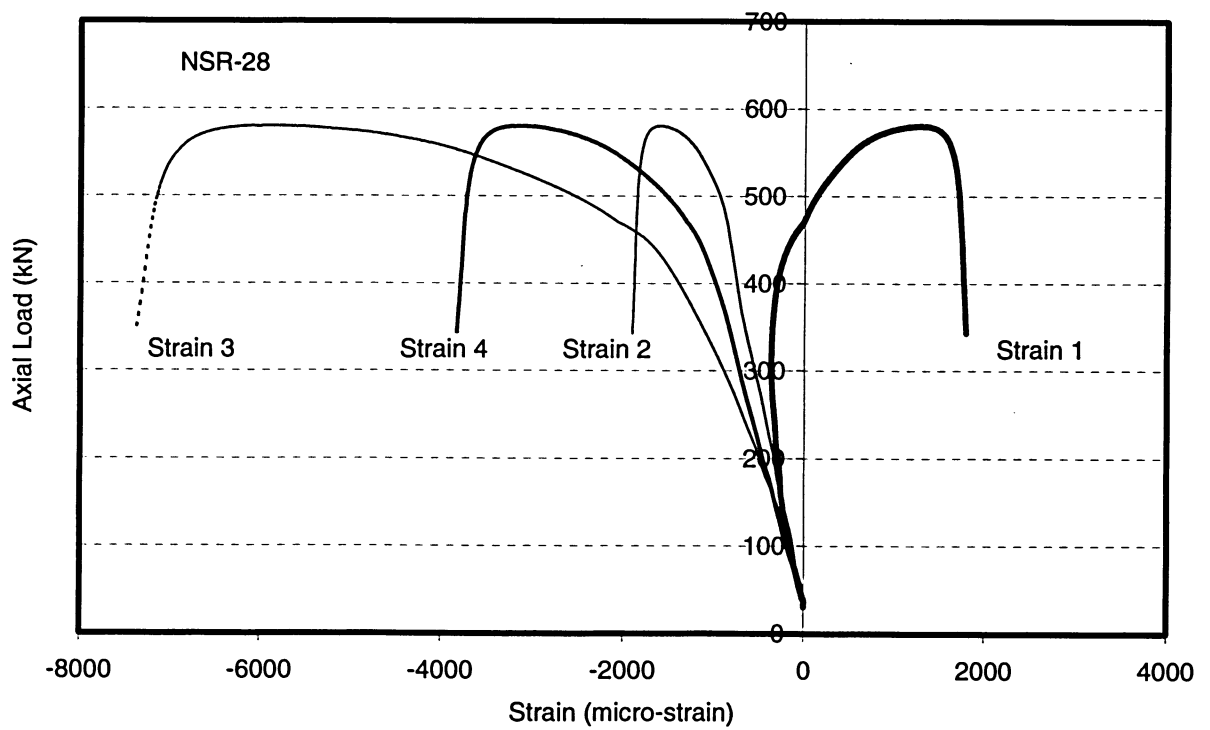


Figure 4.203 Axial load-strain relationships for specimen NSR-28

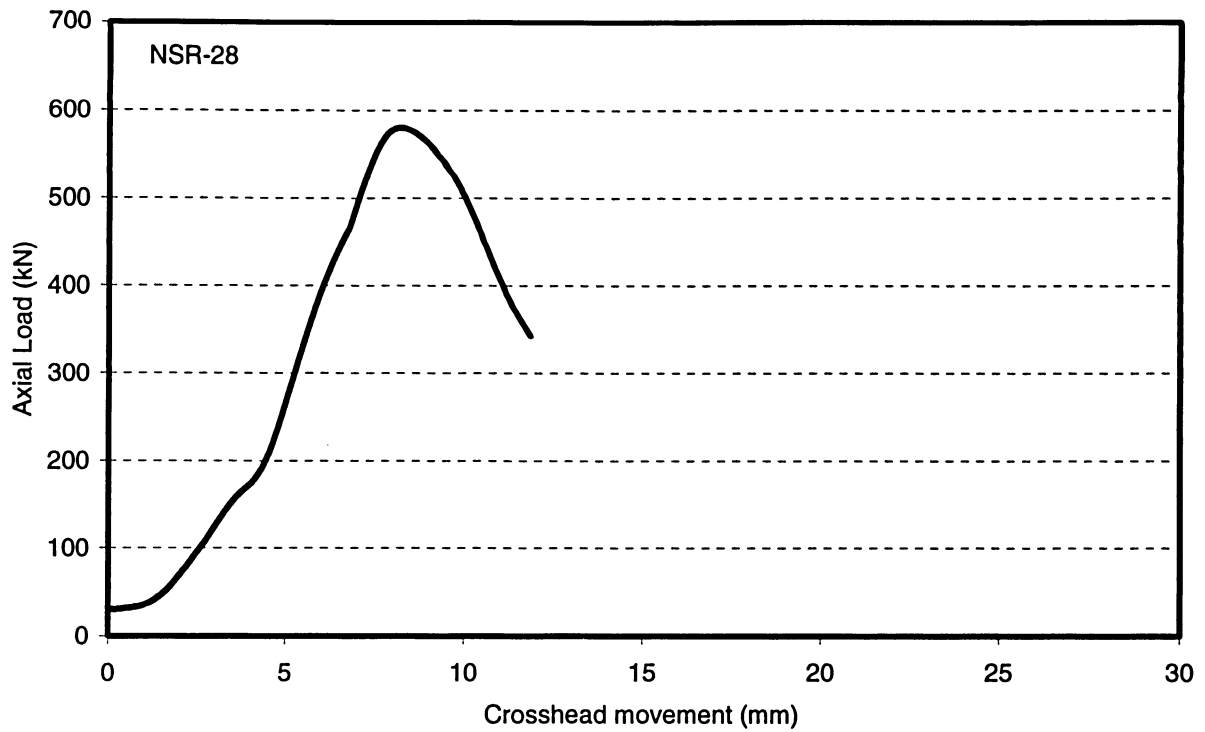


Figure 4.204 Load versus overall shortening curve for specimen NSR-28

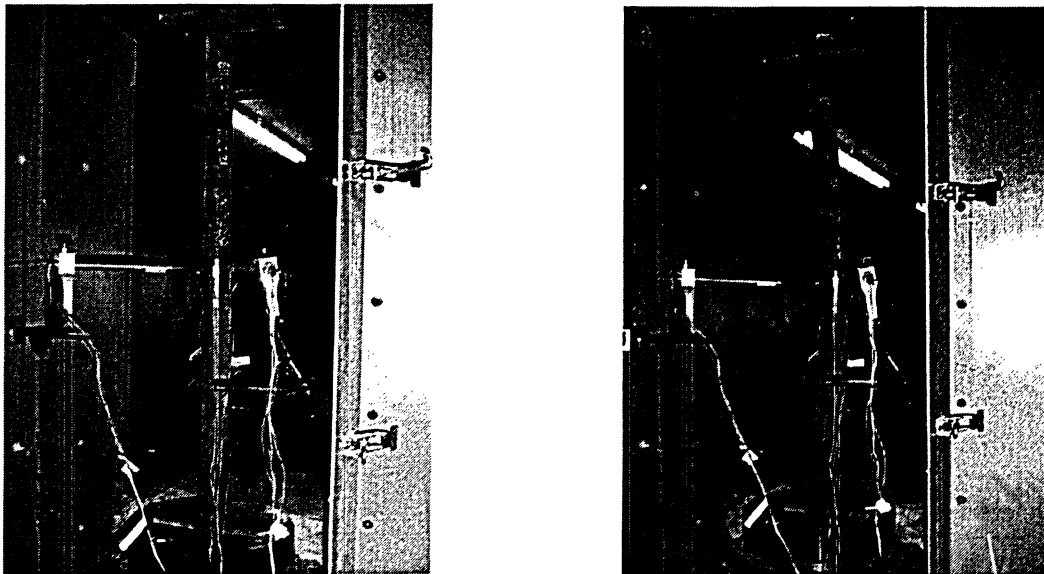


Figure 4.205 Views of specimen NSR-29 before and after testing

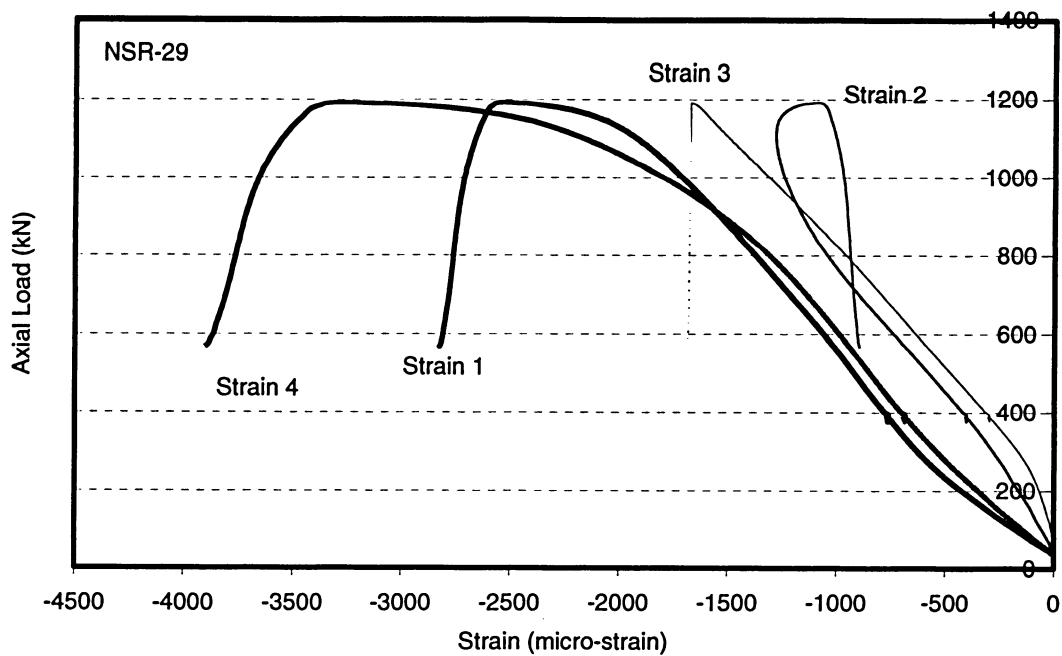


Figure 4.206 Axial load-strain relationships for specimen NSR-29

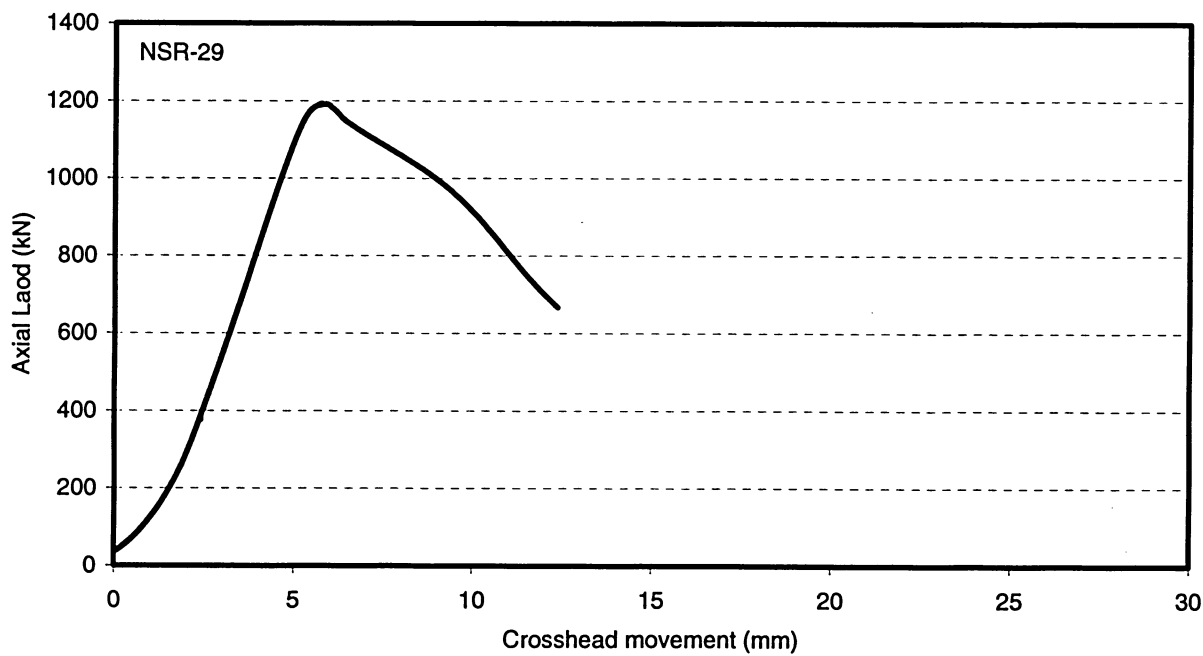


Figure 4.207 Load versus overall shortening curve for specimen NSR-29

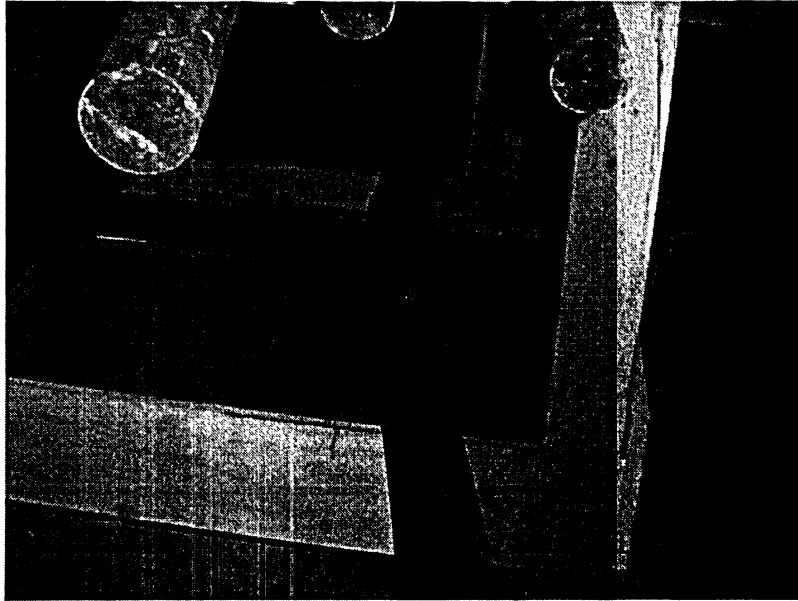


Figure 4.208 Views of specimen NSR-30 before and after testing

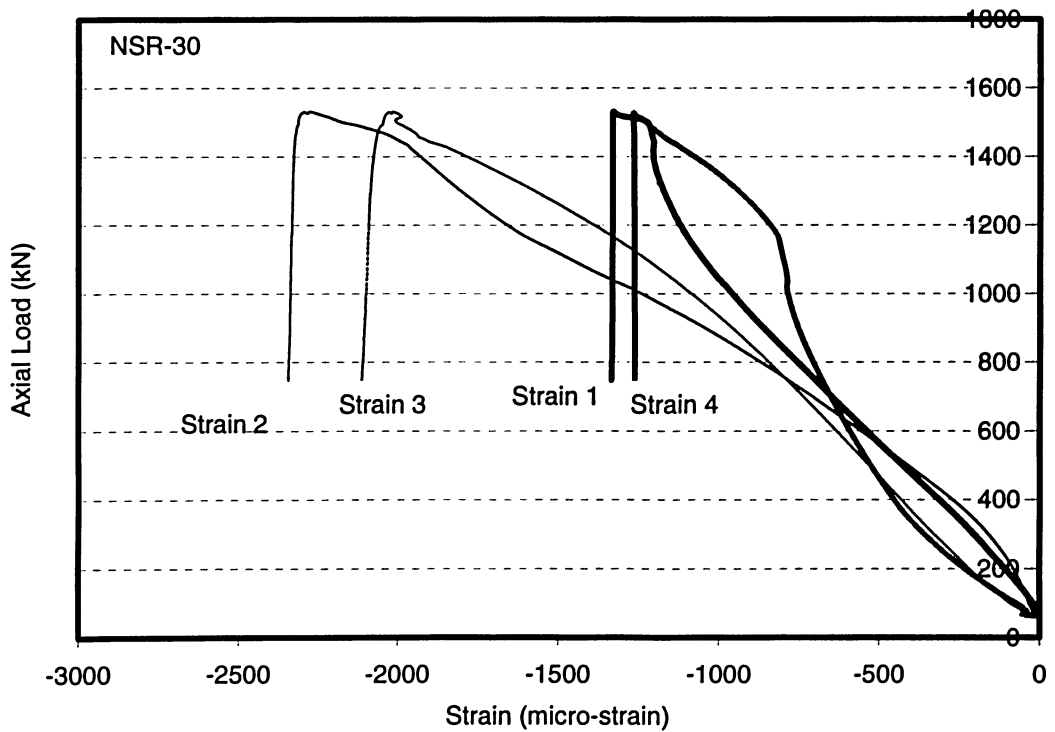


Figure 4.209 Axial load-strain relationships for specimen NSR-30

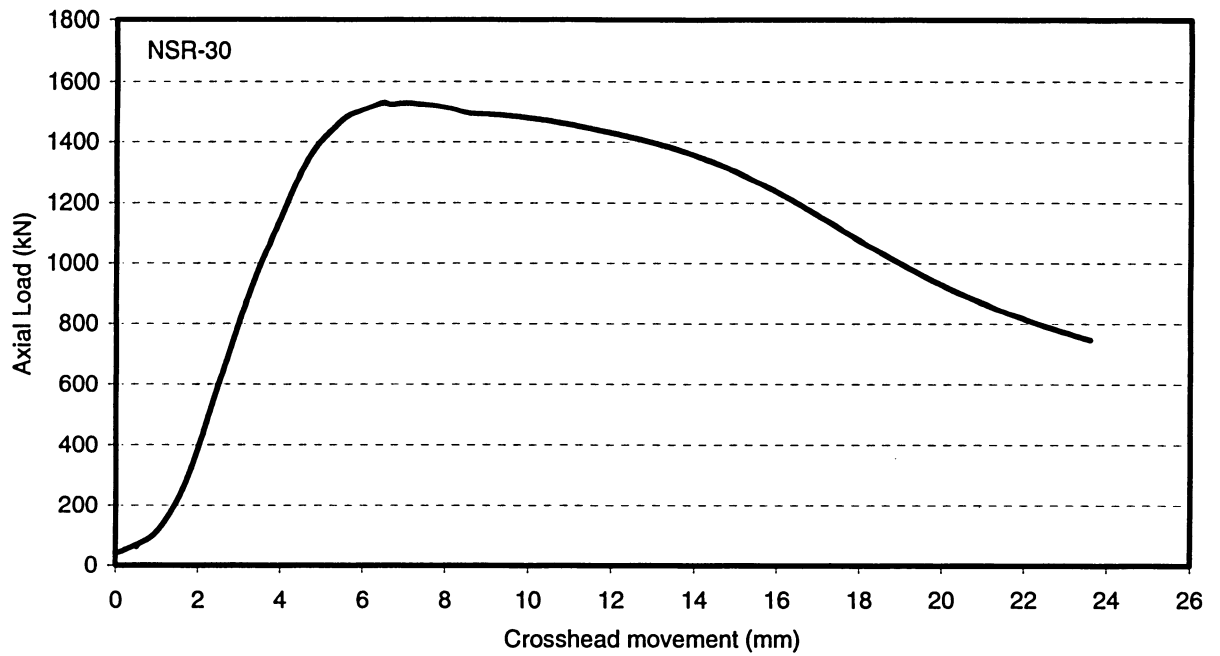


Figure 4.210 Load versus overall shortening curve for specimen NSR-30

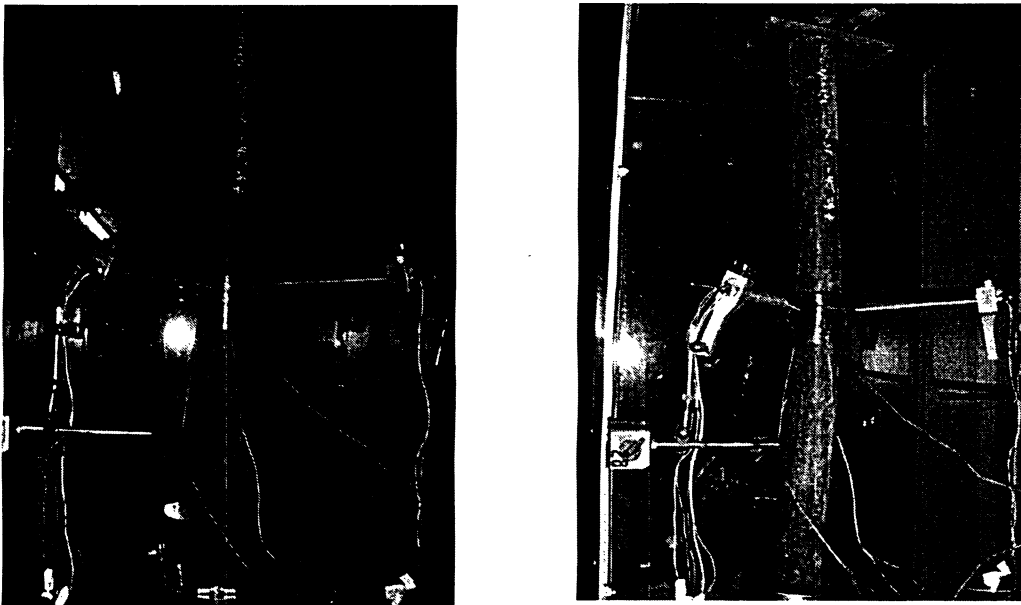


Figure 4.211 Views of specimen NSR-31 before and after testing

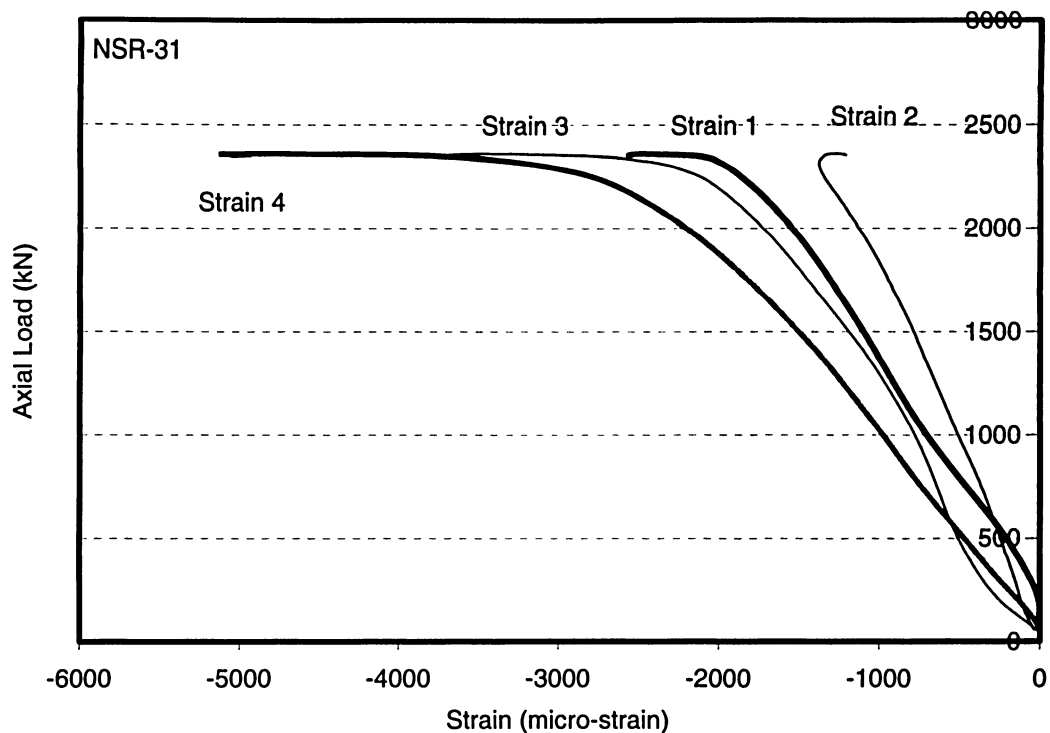


Figure 4.212 Axial load-strain relationships for specimen NSR-31

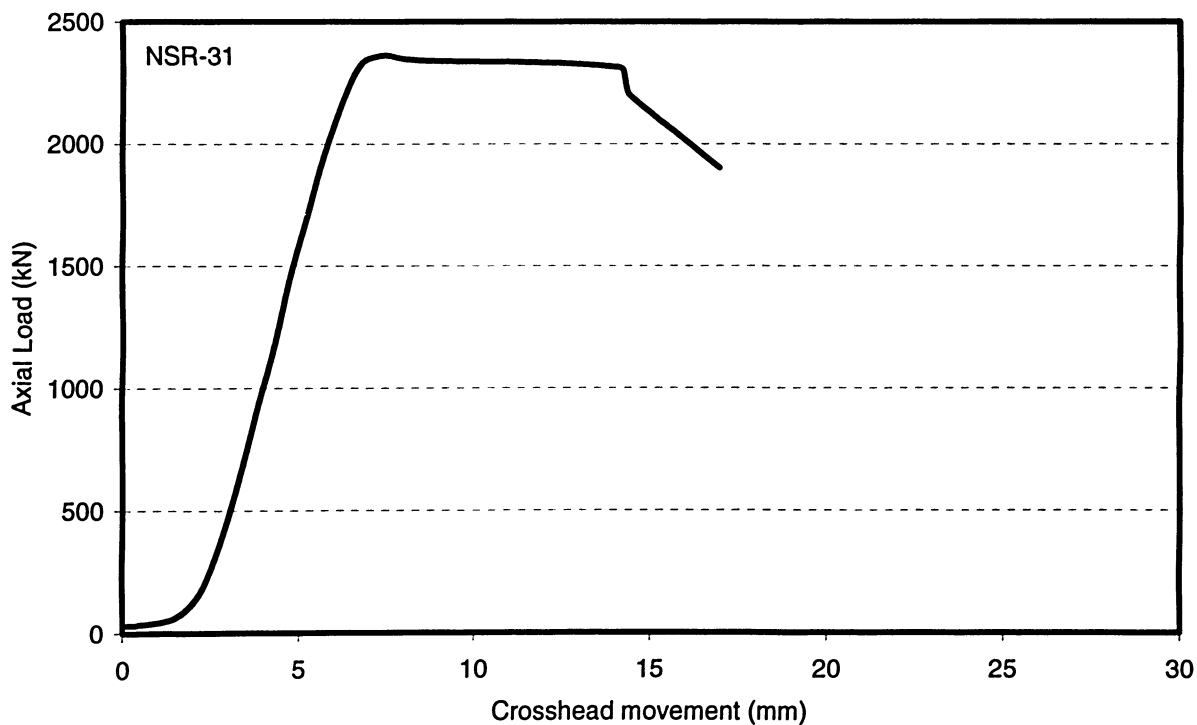


Figure 4.213 Load versus overall shortening curve for specimen NSR-31

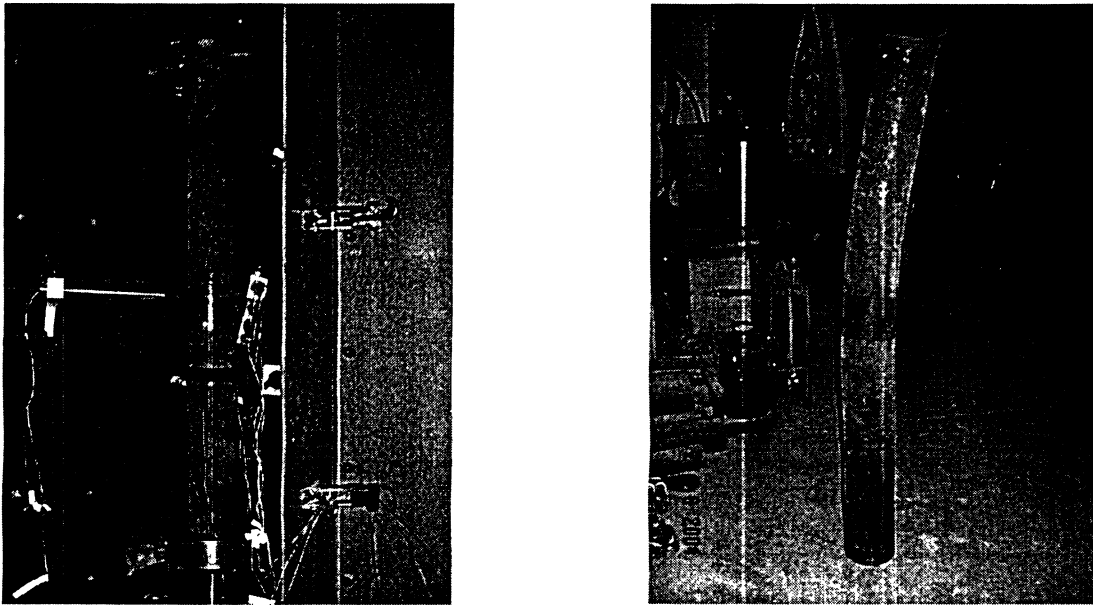


Figure 4.214 Views of specimen NSR-32 before and after testing

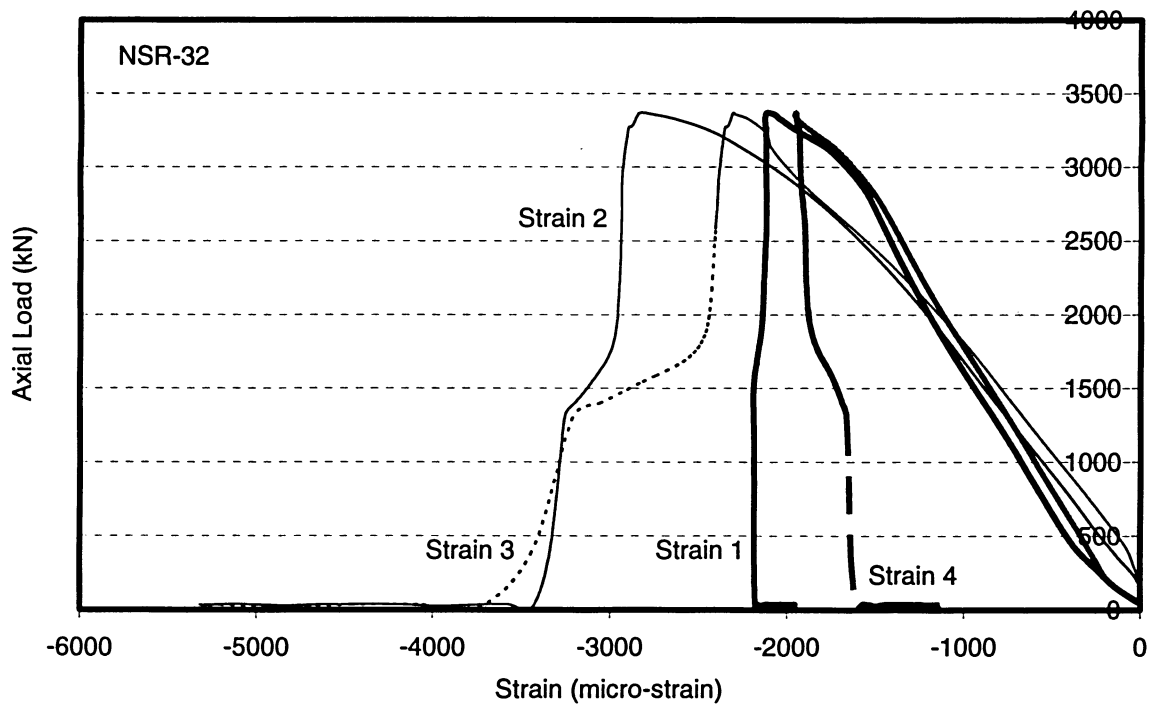


Figure 4.215 Axial load-strain relationships for specimen NSR-32

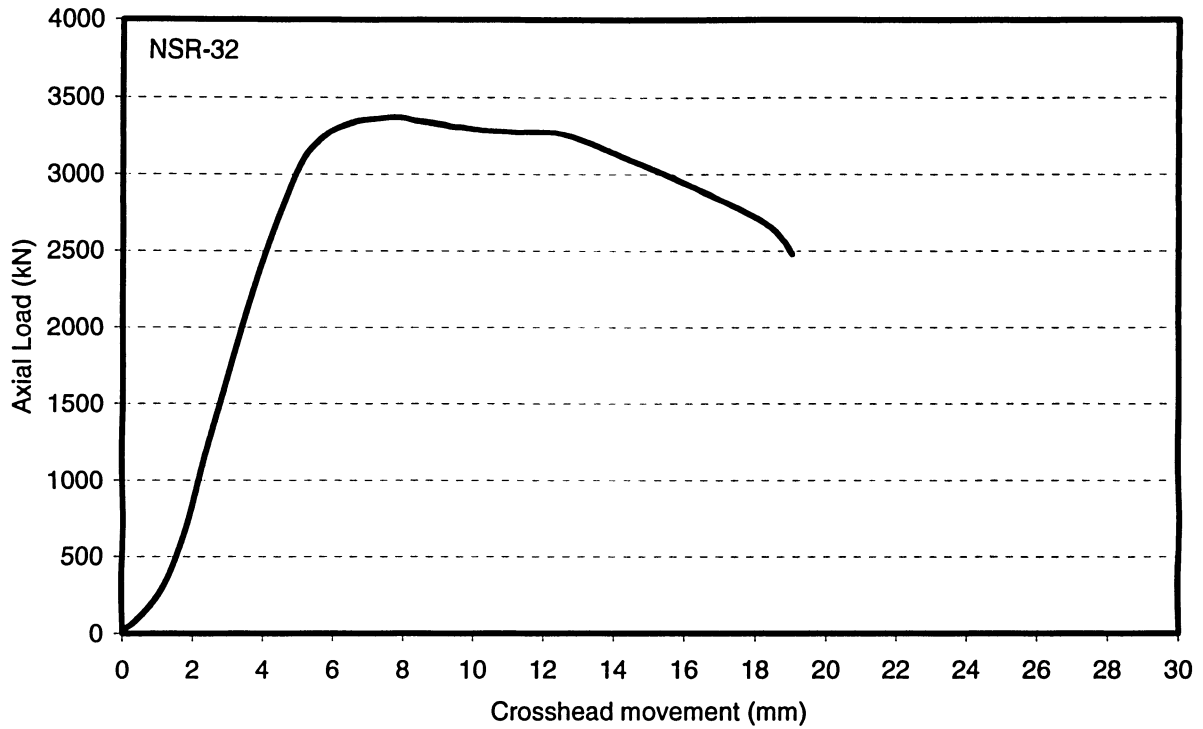


Figure 4.216 Load versus overall shortening curve for NSR-32

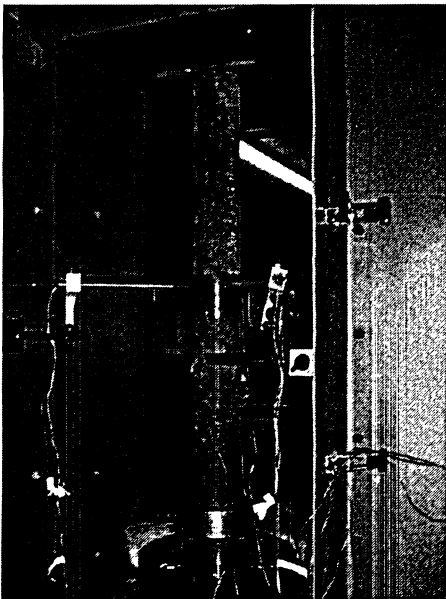


Figure 4.217 Views of specimen NSR-33 before and after testing

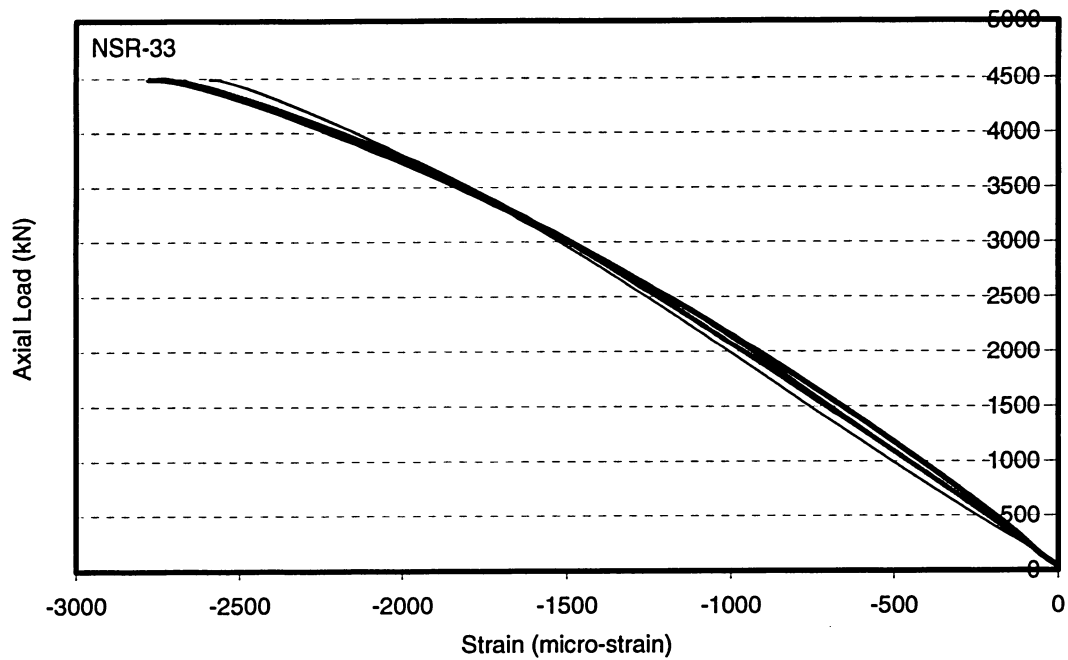


Figure 4.218 Axial load-strain relationships for specimen NSR-33

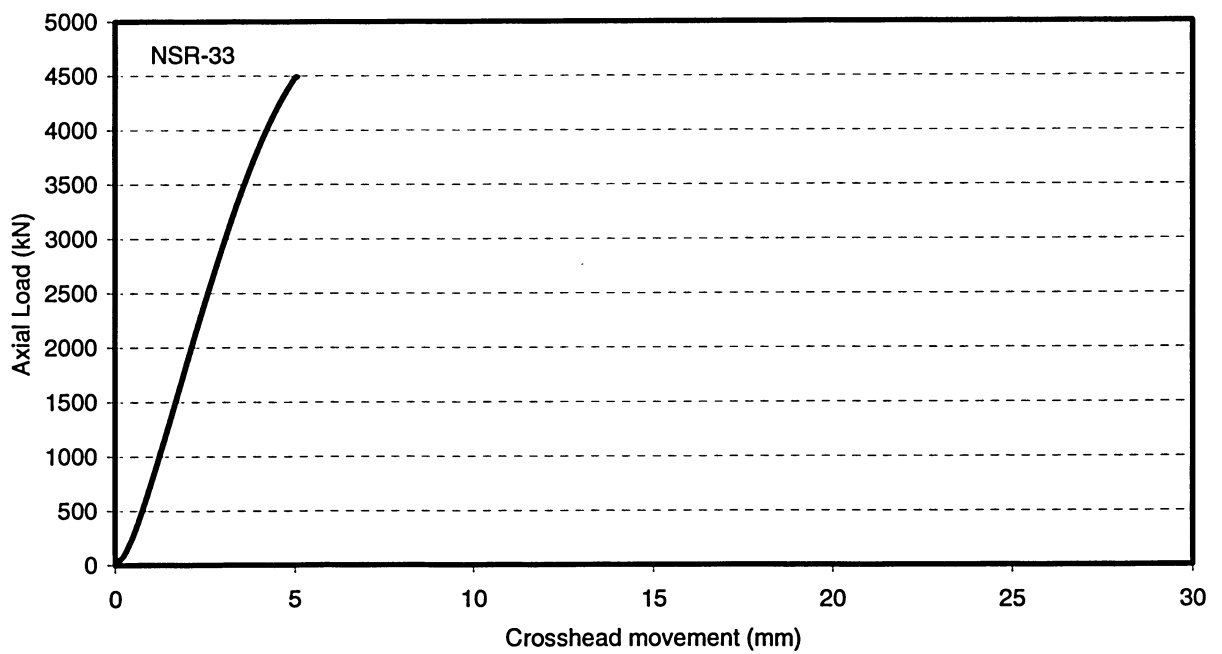


Figure 4.219 Load versus overall shortening for specimen NSR-33

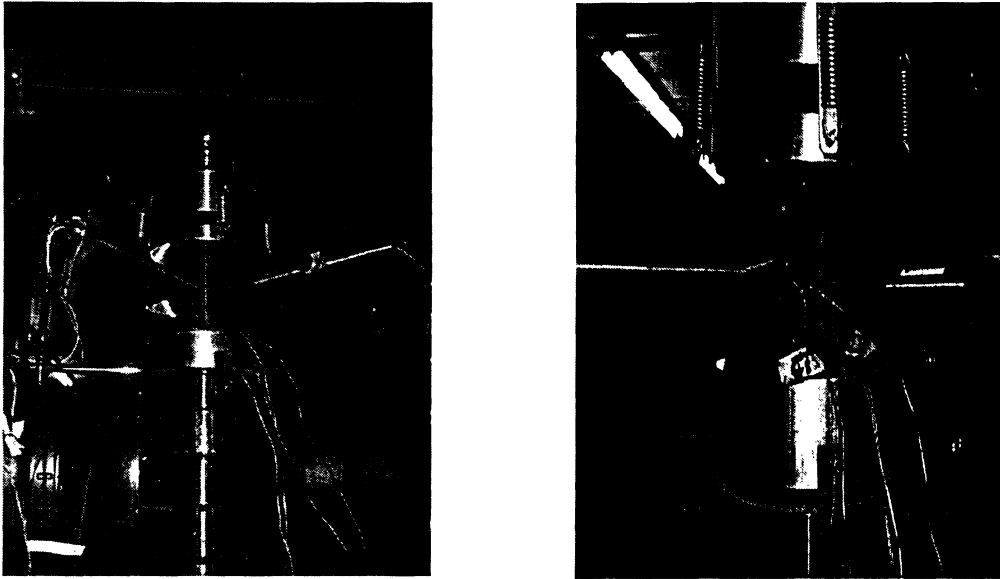


Figure 4.220 Views of specimen SC-1 before and after testing

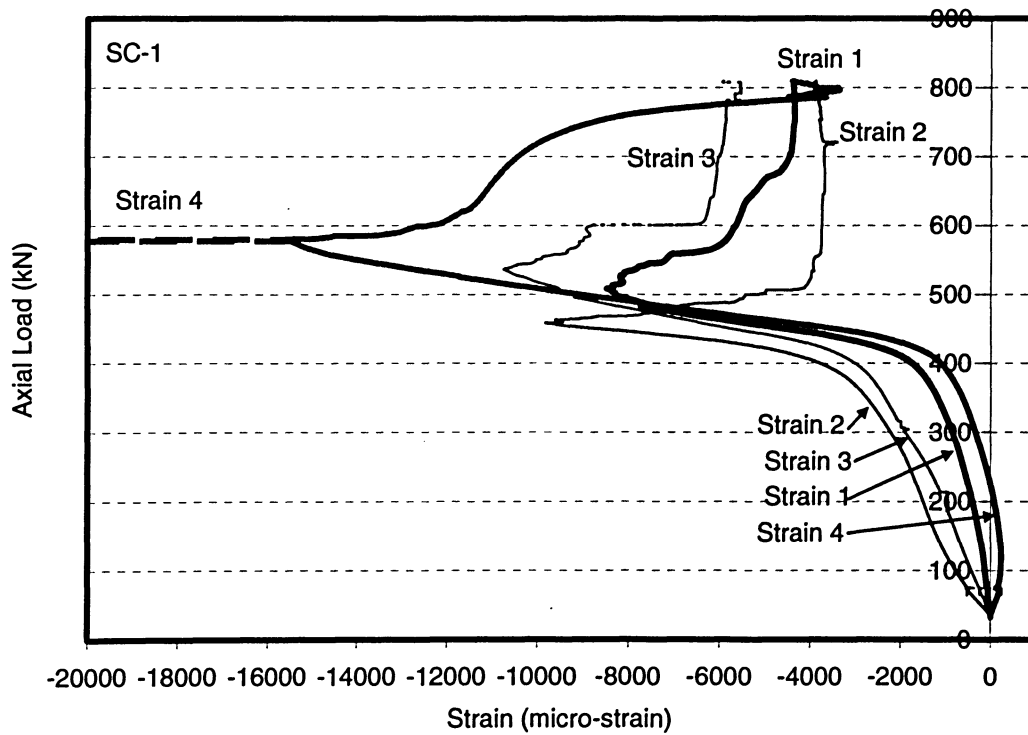


Figure 4.221 Axial load-strain relationships for specimen SC-1

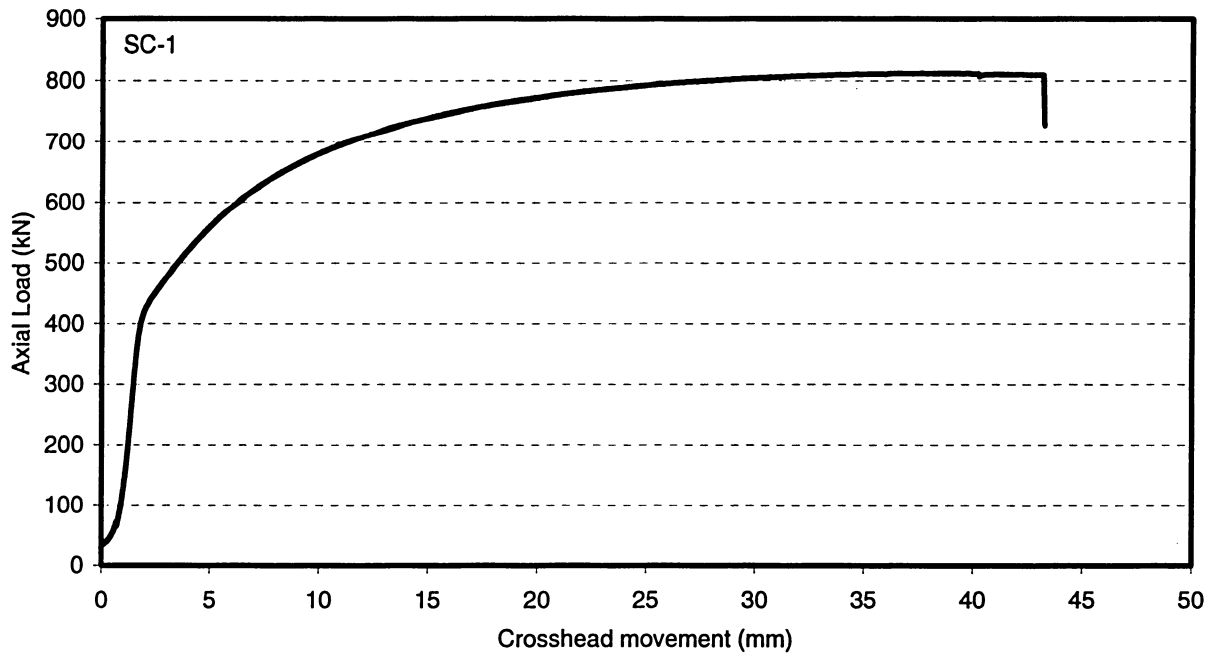


Figure 4.222 Load versus overall shortening curve for specimen SC-1

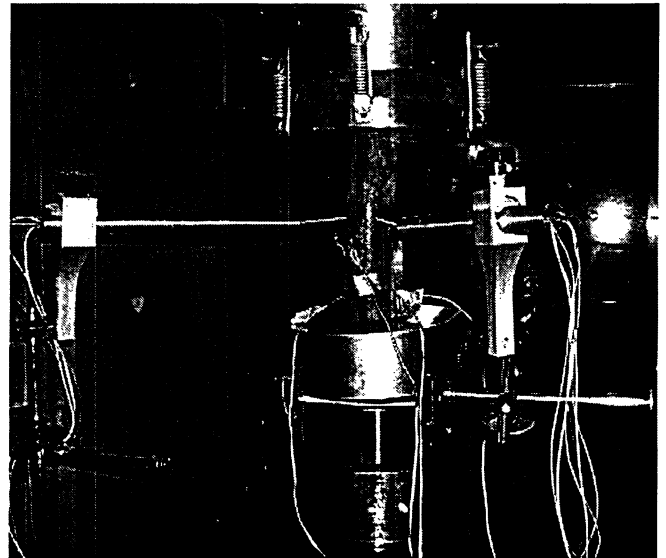
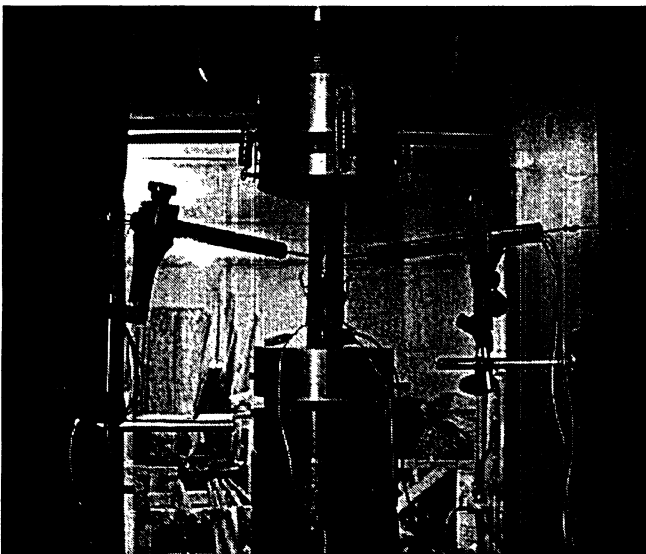


Figure 4.223 Views of specimen SC-2 before and after testing

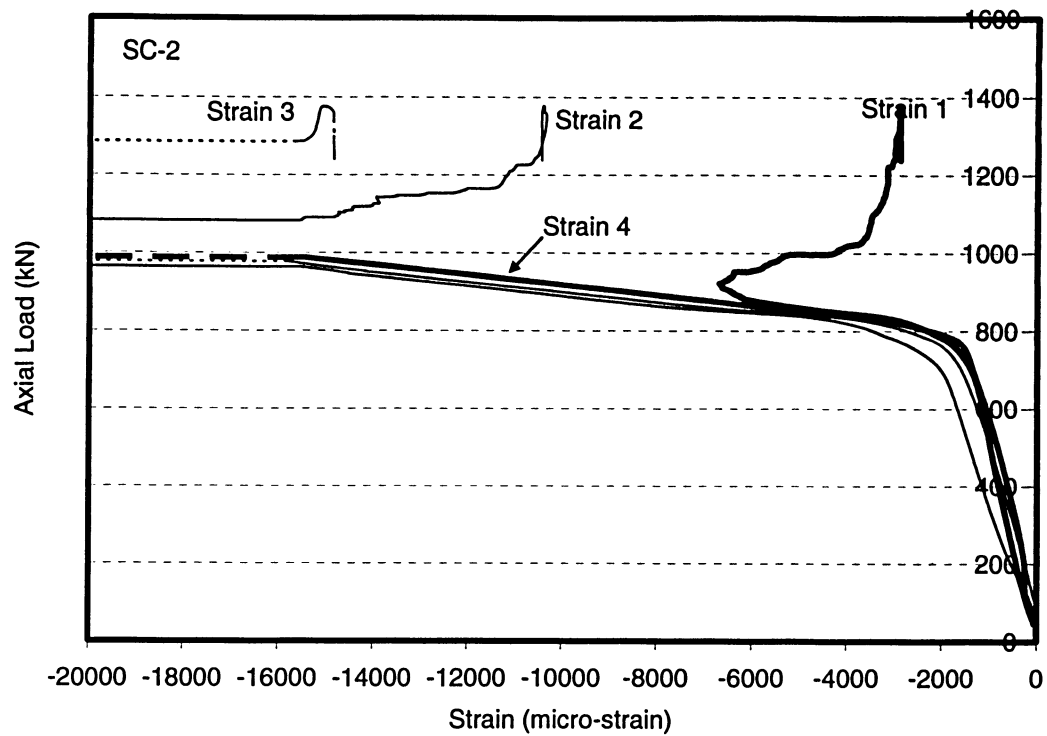


Figure 4.224 Axial load-strain relationships for specimen SC-2

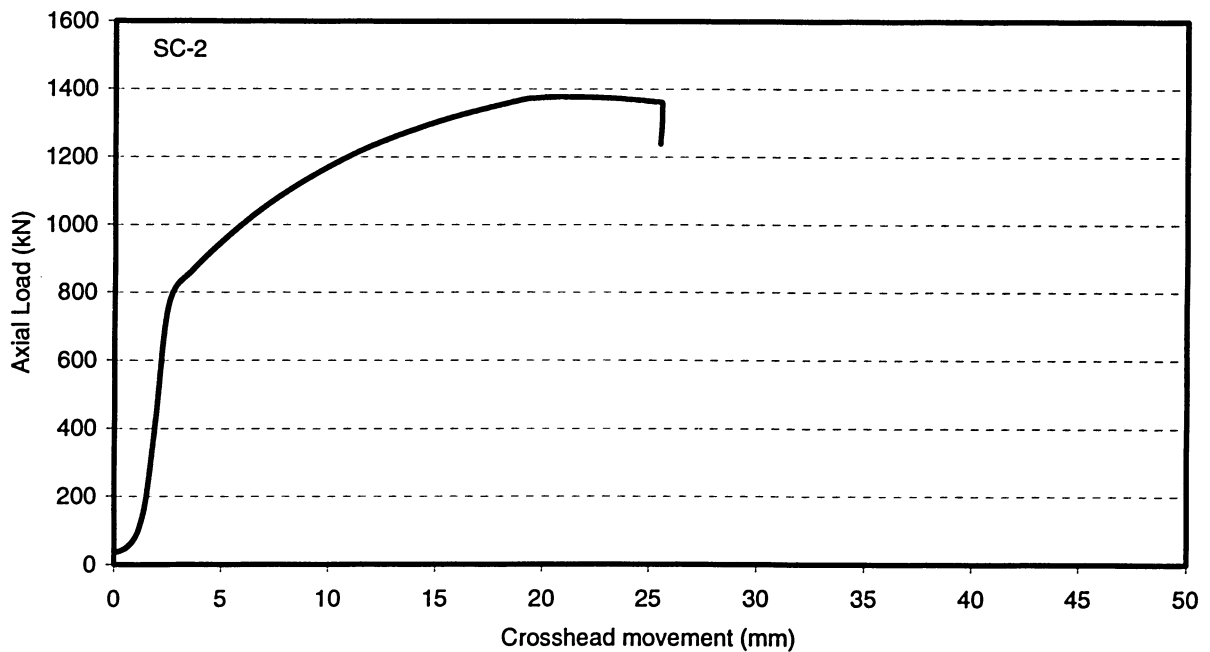


Figure 4.225 Load versus overall shortening curve for specimen SC-2

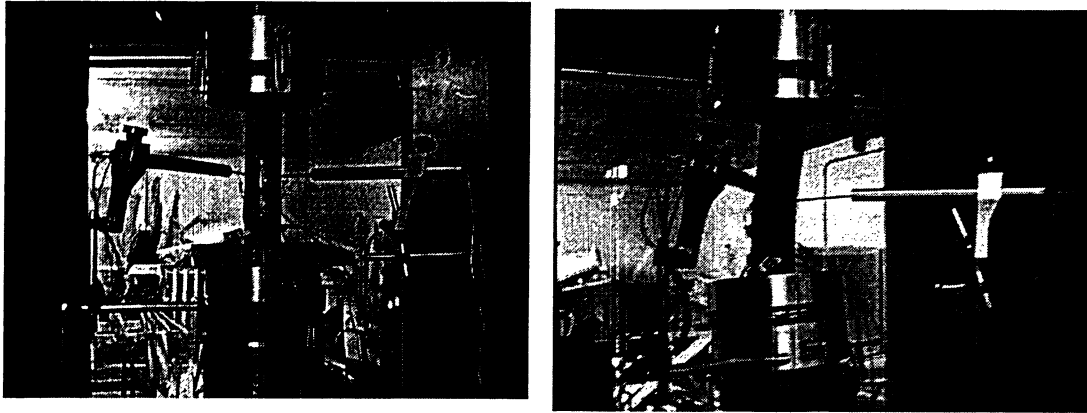


Figure 4.226 Views of specimen SC-3 before and after testing

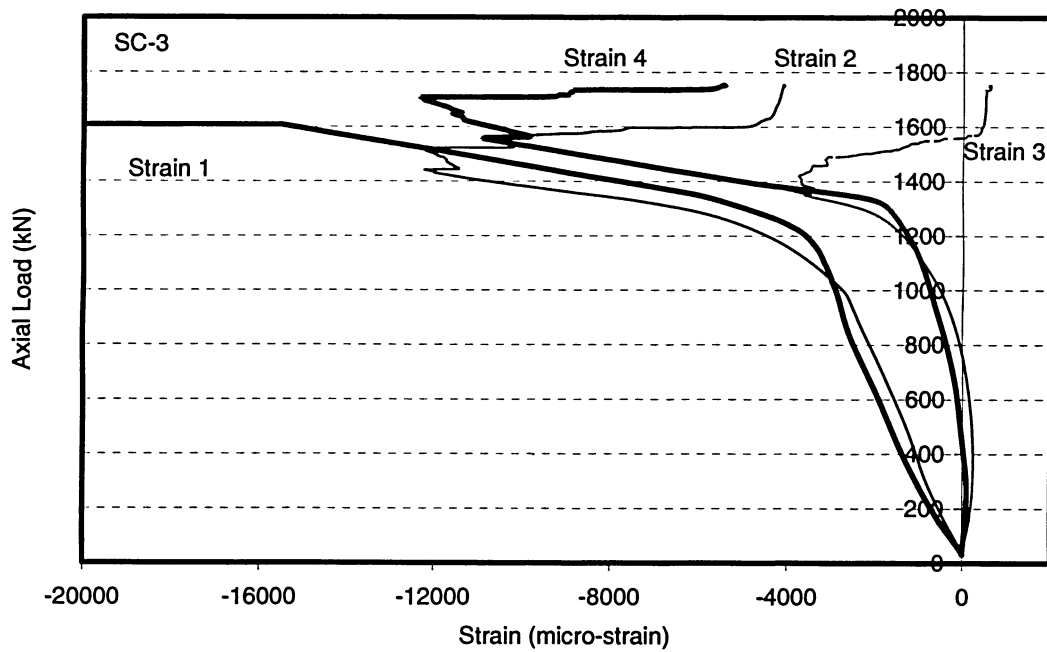


Figure 4.227 Axial load-strain relationships for specimen SC-3

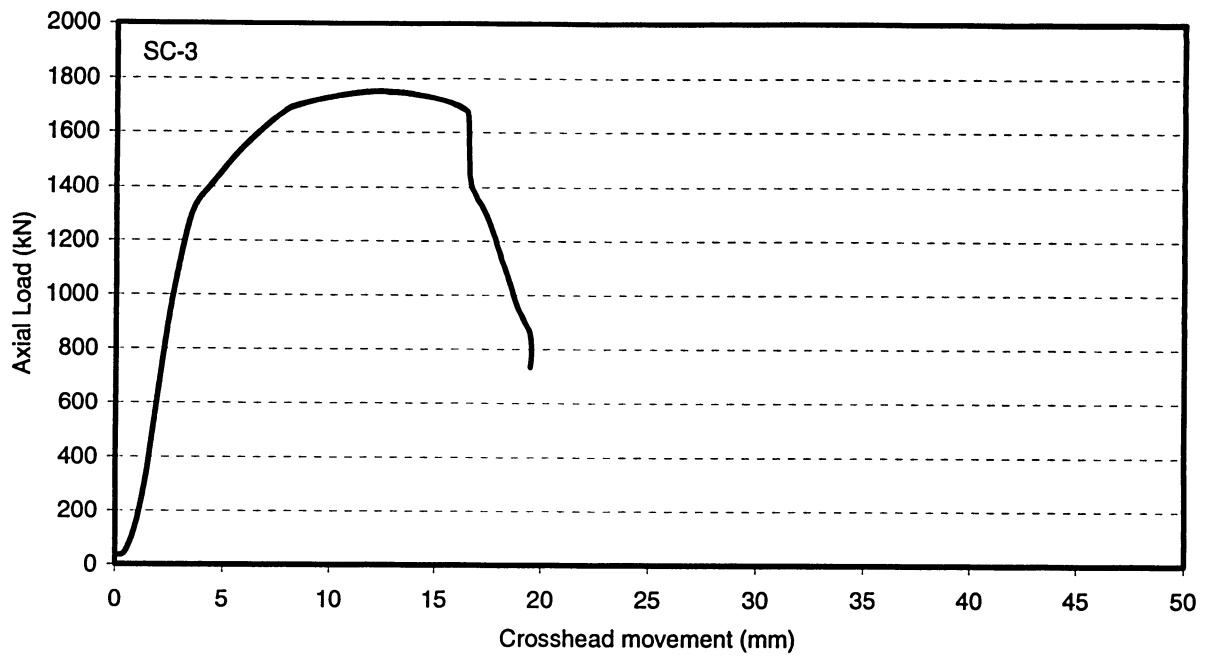


Figure 4.228 Load versus overall shortening curve for specimen SC-3

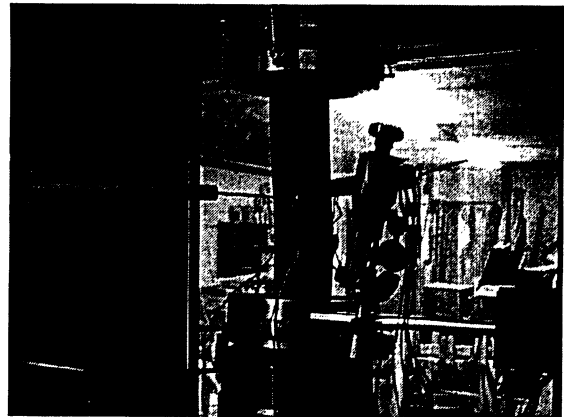
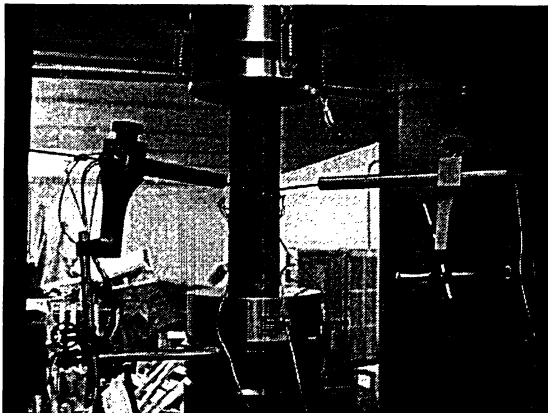


Figure 4.229 Views of specimen SC-4 before and after testing

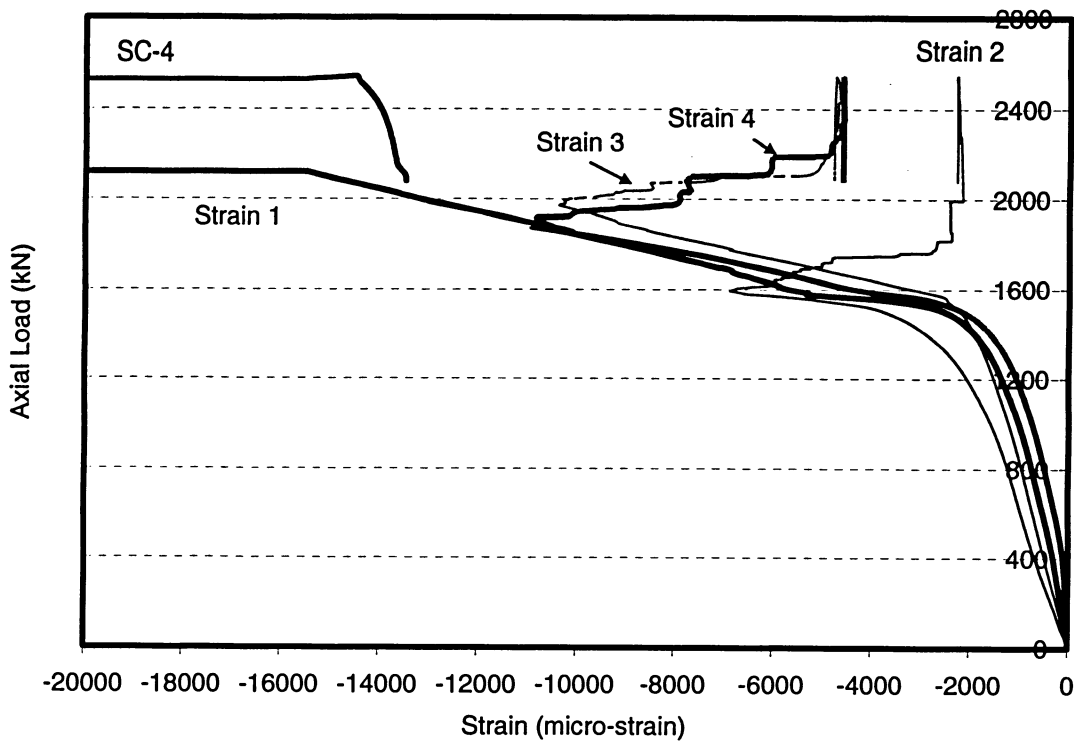


Figure 4.230 Axial load-strain relationships for specimen SC-4

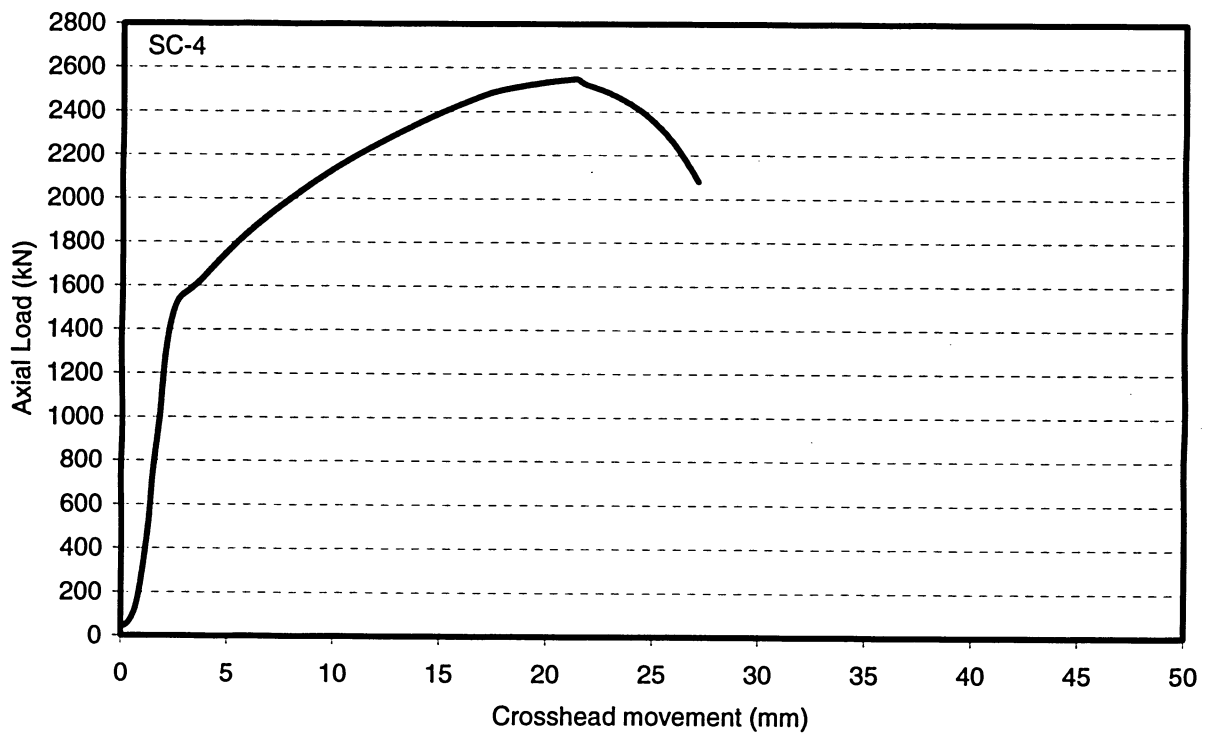


Figure 4.231 Load versus overall shortening curve for specimen SC-4

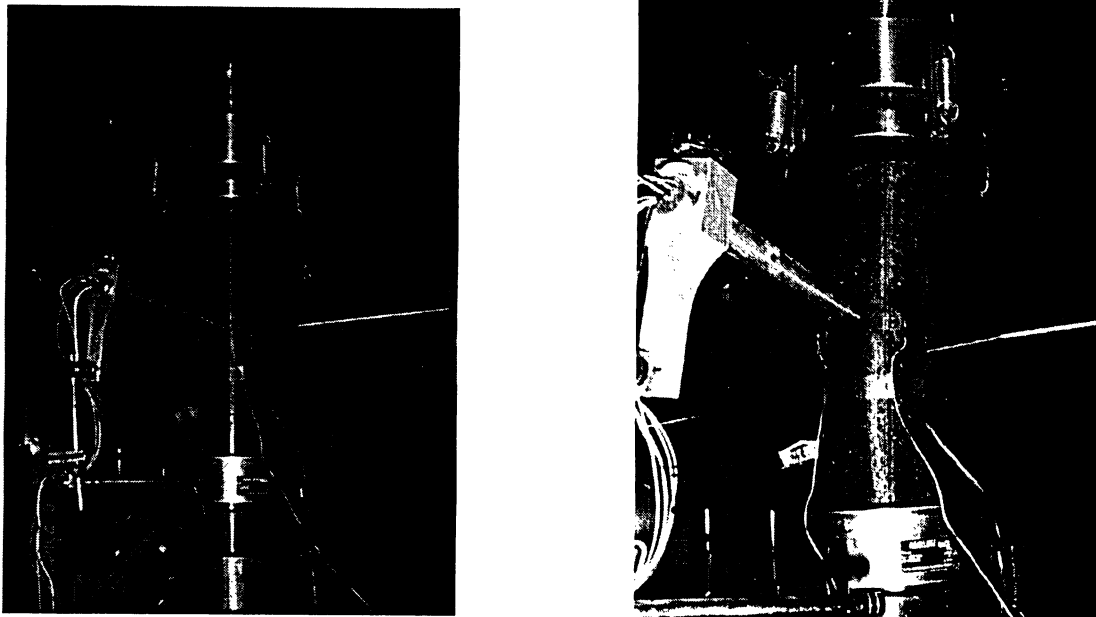


Figure 4.232 Views of specimen SC-5 before and after testing

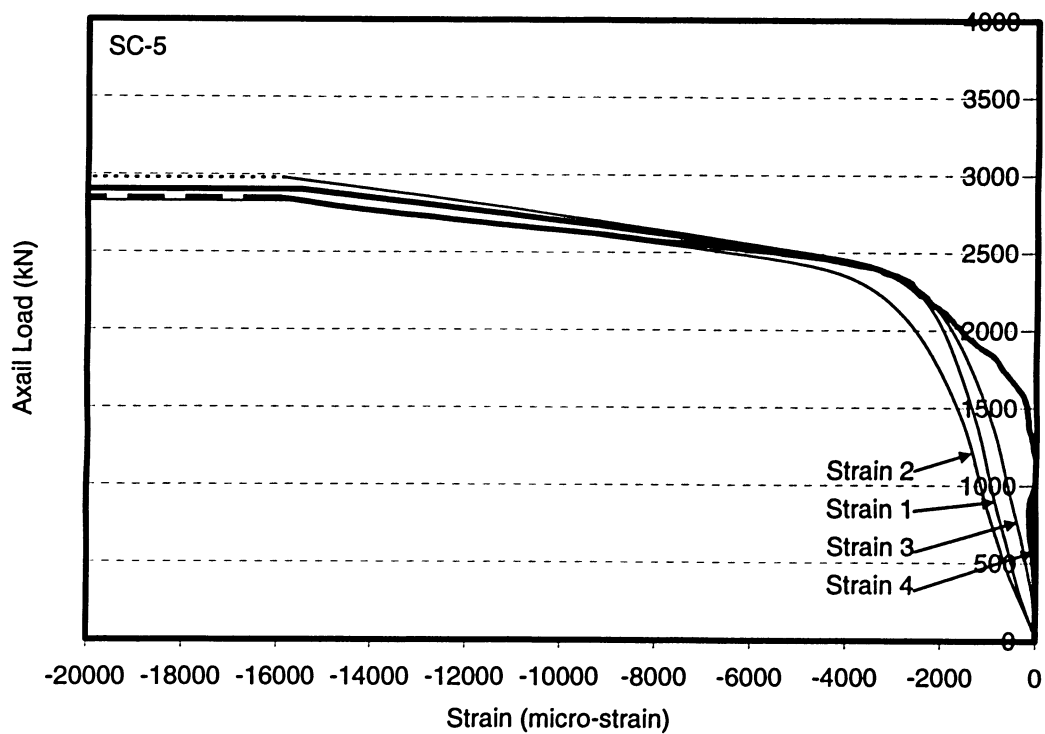


Figure 4.233 Axial load-strain relationships for specimen SC-5

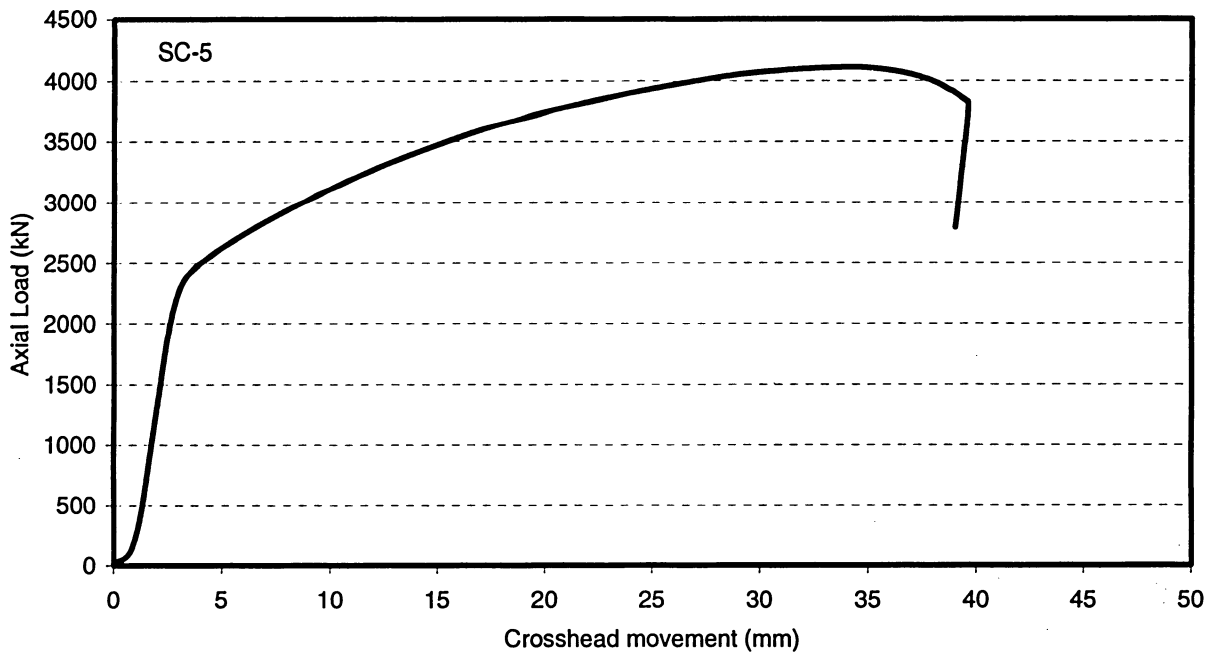


Figure 4.234 Load versus overall shortening curve for specimen SC-5

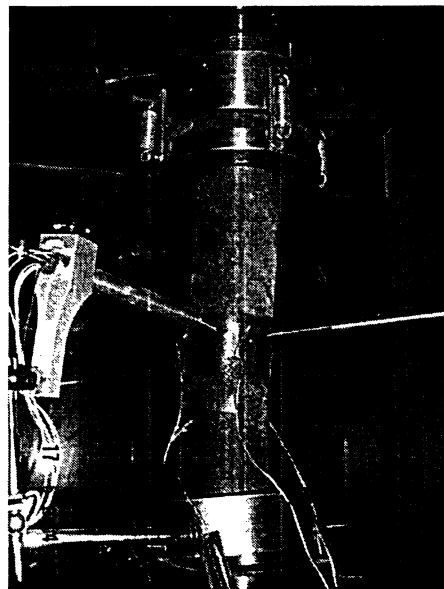
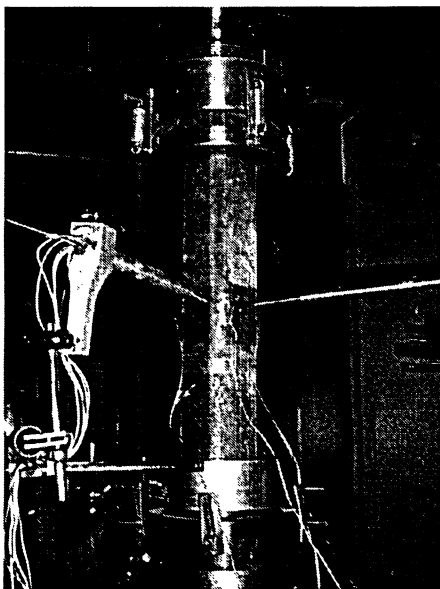


Figure 4.235 Views of specimen SC-6 before and after testing

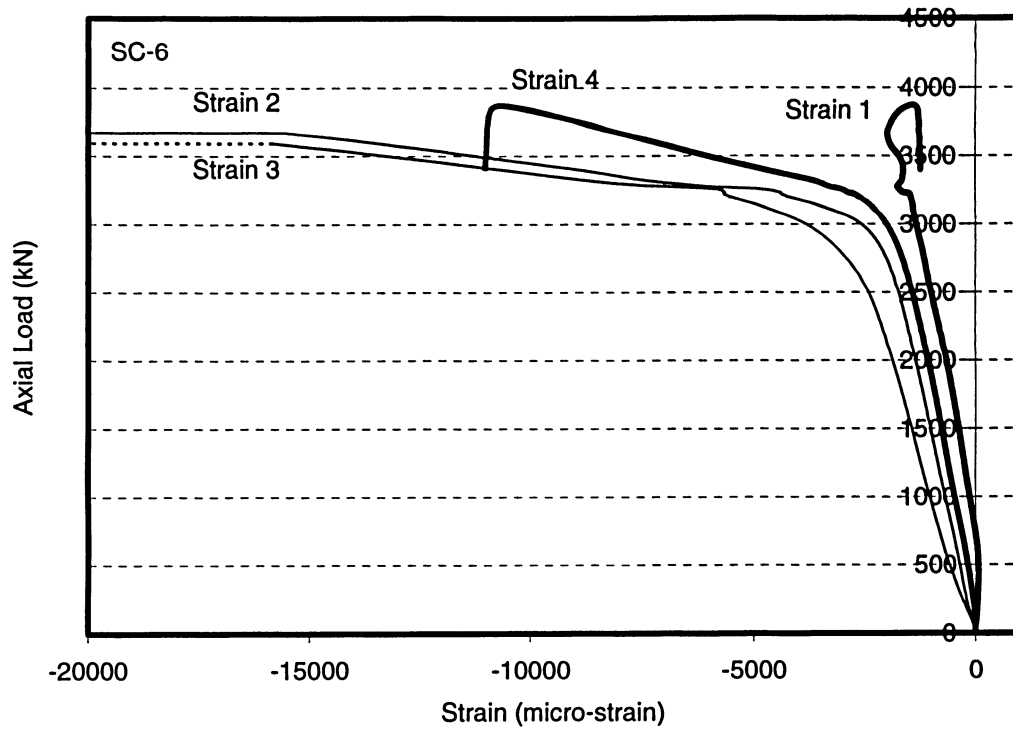


Figure 4.236 Axial load-strain relationships for specimen SC-6

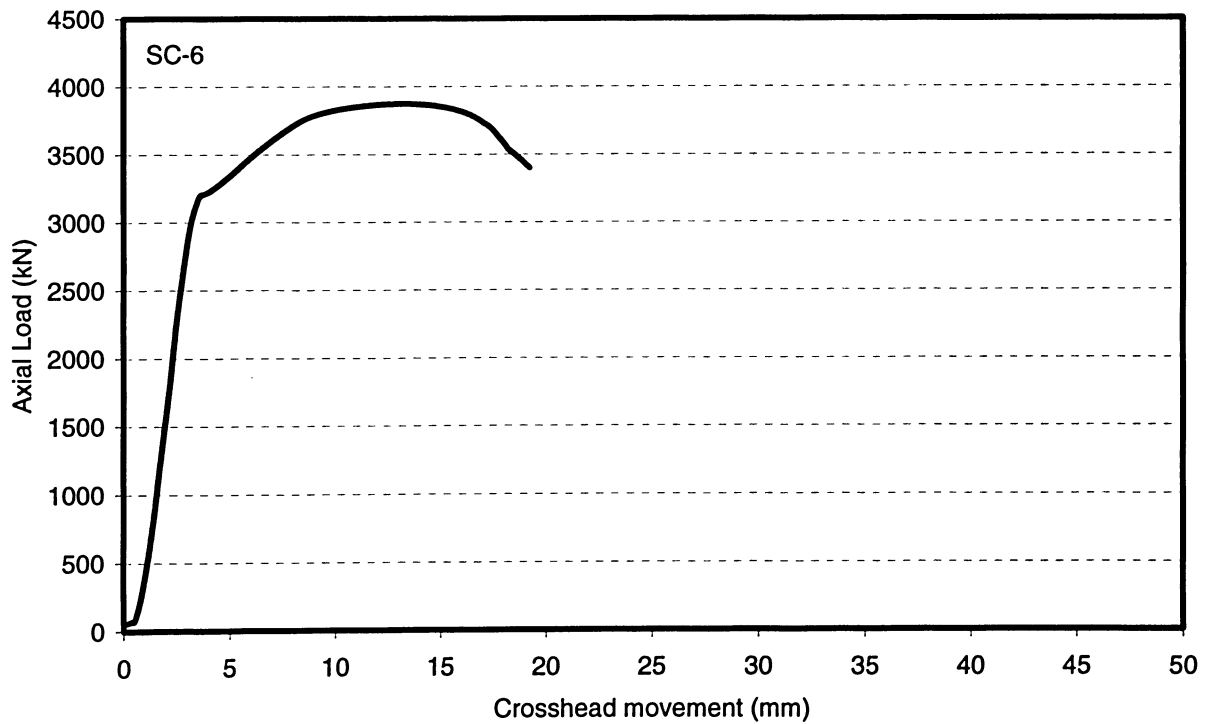


Figure 4.237 Load versus overall shortening curve for specimen SC-6

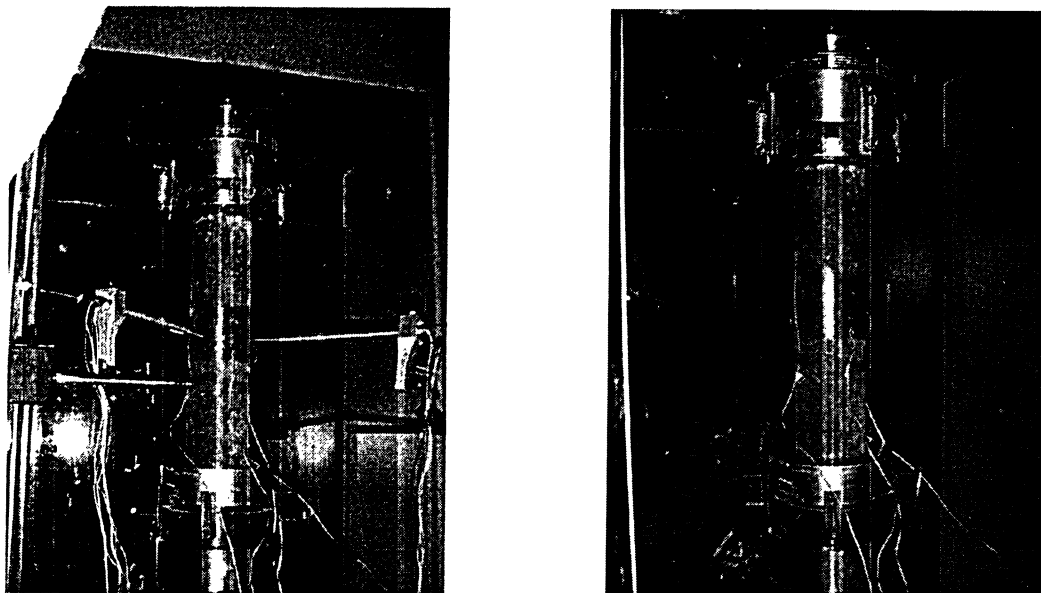


Figure 4.238 Views of specimen SC-7 before and after testing

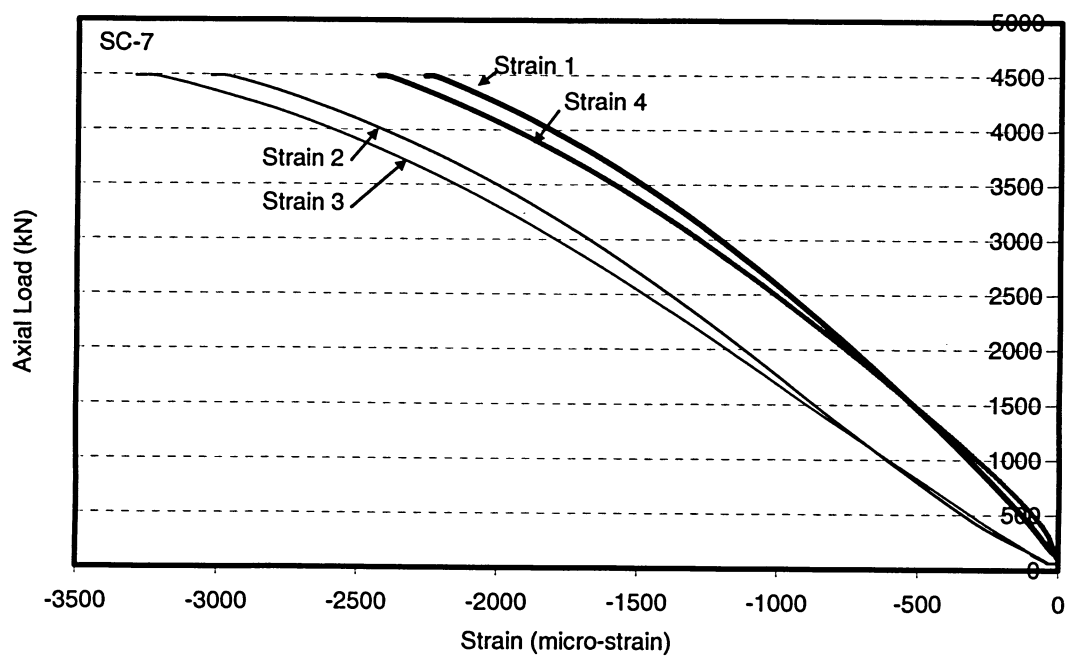


Figure 4.239 Axial load-strain relationships for specimen SC-7

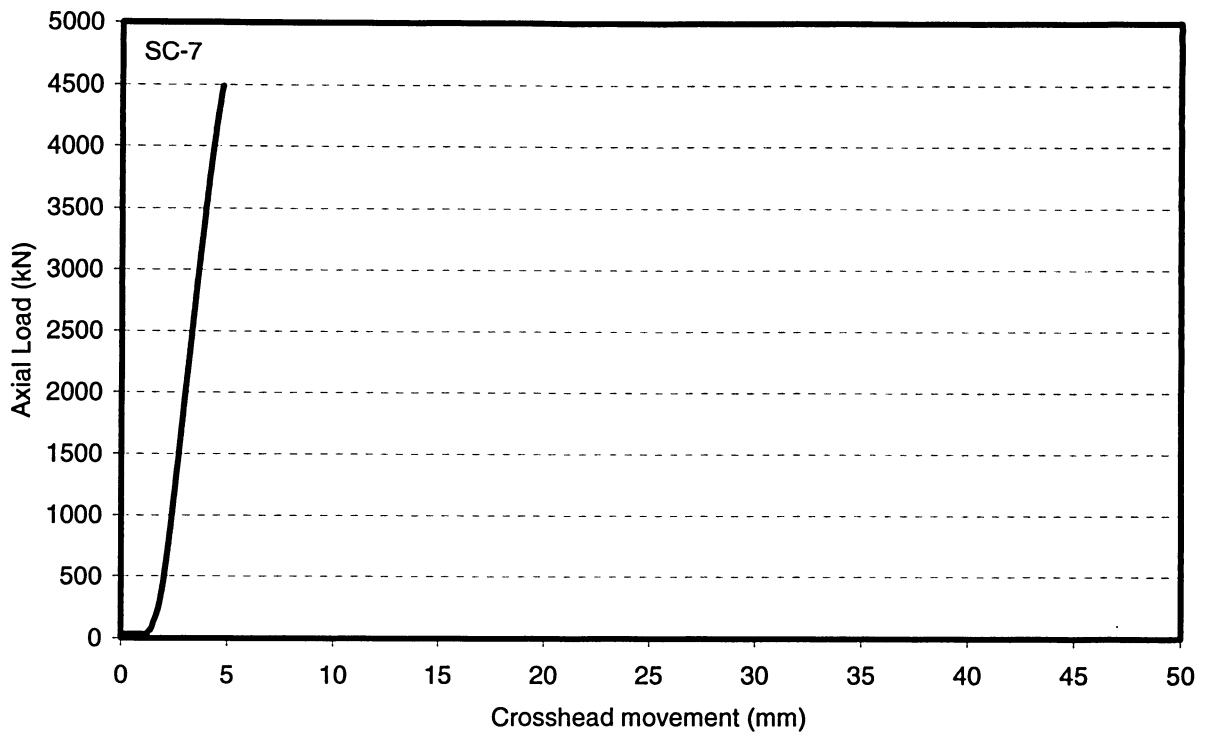


Figure 4.240 Load versus overall shortening curve for specimen SC-7